MITOCHONDRIAL AND PLASTIDIAL IRON-SULFUR CLUSTER BIOGENESIS IN PLANTS

by

TAMANNA AZAM

(Under the Direction of Michael K. Johnson)

ABSTRACT

The overall objectives of this research project were to investigate the properties and function of late-acting iron-sulfur cluster assembly proteins in plant mitochondria and plastids. To this end, proteins from *Arabidopsis thaliana* (*At*), namely mitochondrial monothiol GRXS15, ISCA1a/1b/2 and NFU4/5 and plastidial HCF101 and NFU2, were heterologously expressed in *E. coli* and purified to homogeneity. The combination of UV-visible absorption and circular dichroism, electron paramagnetic resonance and resonance Raman spectroscopy was used to elucidate the nature and properties of the iron-sulfur clusters assembled on these proteins and their interactions with physiological partner proteins. The results demonstrate that GRXS15 assembles one [2Fe-2S]$^{2+}$ cluster per homodimer and is an effective [2Fe-2S]$^{2+}$ cluster donor for maturation of mitochondrial apo ferredoxin. Co-expression of ISCA1a/2 resulted in samples with one [2Fe-2S]$^{2+}$ cluster per heterodimer, which can be converted to a form containing one [4Fe-4S]$^{2+}$ cluster per heterodimer by anaerobic Fe-S cluster reconstitution. Moreover, the [4Fe-4S]$^{2+}$ cluster-bound ISCA1a/2 heterodimer was formed via rapid [2Fe-2S]$^{2+}$ cluster transfer from [2Fe-2S]-GRXS15 to apo *At* ISCA1a/2, in the absence of exogenous glutathione or dithiotreitol. This result supports

the proposed role of ISCA1/2 heterodimers as effectors of $[2Fe\text{-}2S]^{2+}$ to $[4Fe\text{-}4S]^{2+}$ cluster conversions in mitochondrial Fe-S cluster biosynthesis. Both NFU4 and NFU5 were shown to assemble one $[4Fe\text{-}4S]^{2+}$ cluster per homodimer after cluster reconstitution. Moreover, ISCA1a/2, NFU4 and NFU5 were all found to be effective $[4Fe\text{-}4S]^{2+}$ cluster donors for maturation of apo mitochondrial aconitase, and ISCA1a/2 was found to be a competent and efficient $[4Fe\text{-}4S]^{2+}$ cluster donor for both NFU4 and NFU5. These cluster transfer processes are all rapid, unidirectional and quantitative, and demonstrate an Fe-S cluster trafficking shuttle involving GRXS15, ISCA1a/2 and NFU4 or NFU5 for the maturation of client [4Fe-4S] cluster-containing proteins in plants.

Plastidial HCF101 was shown to contain a sub-stoichiometric mixture of $[4Fe\text{-}4S]^{2+}$ and linear $[3Fe\text{-}4S]^{1+}$ cluster as purified under anaerobic conditions. However, as-purified HCF101 was converted to a form containing one $[4Fe\text{-}4S]^{2+}$ cluster per monomer after anaerobic Fe-S cluster reconstitution. Nevertheless, the high affinity of HCF101 for binding linear $[3Fe\text{-}4S]^{1+}$ clusters is evident by the observation that $[4Fe\text{-}4S]^{2+}$ cluster transfer from NFU2 to apo HCF101 is a very rapid and unidirectional process, resulting in transient [4Fe-4S]-HCF101, that gradually decays with time to yield linear $[3Fe\text{-}4S]^{1+}$ cluster-bound HCF101. These results, coupled with observation that linear $[3Fe\text{-}4S]^{1+}$ cluster-bound HCF101 is rapidly converted into [4Fe-4S]-HCF101 on addition of Fe^{2+} ions under anaerobic conditions, raise the possibility that both cluster-bound forms of HCF101 may be present in plastids under dark and light conditions.

INDEX WORDS: Iron-sulfur cluster, Fe-S cluster biogenesis, ISCA protein, NFU protein, monothiol glutaredoxin, ferredoxin, cluster trafficking, circular dichroism, electron paramagnetic resonance, resonance Raman

MITOCHONDRIAL AND PLASTIDIAL IRON-SULFUR CLUSTER BIOGENESIS IN PLANTS

by

TAMANNA AZAM

MS, University of Dhaka, Bangladesh, 2011

BS, University of Dhaka, Bangladesh, 2009

A Dissertation Submitted to the Graduate Faculty of The University of Georgia in Partial Fulfillment of the Requirements for the Degree

DOCTOR OF PHILOSOPHY

ATHENS, GEORGIA

2020

MITOCHONDRIAL AND PLASTIDIAL IRON-SULFUR CLUSTER BIOGENESIS IN PLANTS

by

TAMANNA AZAM

Major Professor:	Michael K. Johnson
Committee:	Michael W. W. Adams
	Robert Phillips

Electronic Version Approved:

Ron Walcott
Interim Dean of the Graduate School
The University of Georgia
May 2020

DEDICATION

To my loving parents

Tuhin Bin Azam and Papia Azam

And my brother

Taufiq Azam

ACKNOWLEDGEMENTS

I would like to express my appreciation to my advisor Dr. Michael K. Johnson for his continuous support and guidance during my entire Ph.D. study in UGA. He was a careful and close reader of my writing and his attention not only to how I sought to develop my ideas but express them in writing significantly shaped my revision of all the chapters. It would be impossible to accomplish this work without his guidance.

I would also like to thank my committee members, Dr. Michael Adams and Dr. Robert Phillips and our collaborator, Dr. Nicolas Rouhier for their investment of time and patience in my project

And finally, thanks to all members of Johnson lab, Ashley Holland and Soshawn Blair, for all those troubleshooting lessons, Sahel Mohebbi for showing how to become a positive person in difficult situations.

TABLE OF CONTENTS

Page

LIST OF TABLES

Page

LIST OF FIGURES

Page

CHAPTER 1

INTRODUCTION AND LITERATURE REVIEW

Background

Iron-sulfur (Fe-S) clusters are one of the most ancient and ubiquitous inorganic cofactors and are found in all kingdoms of life (1). Proteins utilizing iron-sulfur clusters participate in fundamental life processes, including energy production, respiration, photosynthesis, DNA maintenance, metabolic conversions, regulation of gene expression, protein translation, and antiviral response (1-3). In addition to one-electron transfer, Fe-S clusters also function in Lewis acid catalysis, sulfur atom transfer, mediating disulfide reduction and iron or Fe-S cluster storage (2,4-9). The maturation of Fe-S proteins in living cells is a complex process which requires several dedicated biogenesis pathways each comprising sets of highly conserved proteins. Research in molecular biology, genetics and cell biology over the past two decades have revealed three different Fe-S cluster biogenesis systems in bacteria, namely NIF (nitrogen fixation specific), SUF (sulfur mobilization) and ISC (iron-sulfur cluster assembly) (10). Plant chloroplasts inherited the SUF system from cyanobacteria, due to the SUF system's high tolerance for oxidative stress (11,12). Similarly, plant mitochondria inherited the ISC system from bacteria due to the ISC system's low tolerance for oxidative stress (12). In addition, two types of machinery specific to eukaryotes, the mitochondrial ISC export apparatus, and the CIA system (cytosolic iron-sulfur cluster assembly), have also been identified (12).

This literature review will begin with the phenotypes associated with 'Fe-S diseases' in humans followed by a brief introduction of general structures, properties, and physiological

functions of Fe-S clusters, and concluding with a discussion of current knowledge concerning Fe-S cluster biogenesis using the ISC and SUF machineries in plants. A summary of the research results presented in this work will be included at the end of this chapter.

Diseases and disorders associated with the impairment of Fe-S cluster biogenesis

Fe-S cluster biogenesis is an extremely complicated process involving the proper assembly and trafficking of Fe-S cluster followed by the insertion of the cluster in specific target apo-proteins. A growing number of human diseases and disorders have been attributed to the impaired biogenesis of Fe-S cluster. In particular, the genetic mutation or instability of the proteins involved in Fe-S cluster biogenesis can cause neurological, metabolic, systemic, and hematological diseases.

Friedreich's ataxia (FRDA) is a common neurodegenerative disease that causes impaired Fe-S cluster biogenesis (13,14). Cardiomyopathy is a clinical manifestation of FRDA; and other manifestations include Gait ataxia, Babinski signs, dysmetria of arms and legs, dysarthria, head titubation, atrophy and weakness of the distal extremities, absence of muscle stretch reflexes, loss of joint and vibratory senses, and superimposed stocking-and-glove type sensory neuropathy (13,15). In a typical FRDA case, a GAA-triplet expansion mutation in the first intron of the frataxin gene (*FXN*) interferes with transcription, resulting in frataxin protein levels decreased by 70% to 95% (16). Frataxin regulates the activity of the mitochondrial Fe-S cluster assembly complex and may provide a channel for delivery of Fe^{2+} ions. Deficiency of frataxin is considered to be the primary cause for all clinical and morphological manifestations of FRDA (15,16).

Other neurodegenerative diseases such as Parkinson's, Alzheimer's, and Huntington's are also associated with impaired Fe-S cluster biogenesis (17,18). For instance, Parkinson's disease is

mainly caused by mitochondrial dysfunction, iron accumulation, and oxidative stress. Mitochondrial dysfunction is likely to increase the production of reactive oxygen species, which in turn decreases the biosynthesis of hemes and Fe-S clusters, resulting in iron regulatory protein (IRP) activation and iron overload (18). Recently, GRX2, which is a member of the monothiol glutaredoxin family of Fe-S cluster trafficking proteins, was also implicated in the accumulation of iron in Parkinson's disease (19,20). In addition, misregulation of iron homeostasis by IRP, defects in ISC synthesis, and partial inhibition of complex 1 in the respiratory chain have been found in Parkinson's patients, all irregularities that affect the motor functions such as rigidity, resting tremor, and postural instability (20).

Hereditary myopathy with lactic acidosis (HML), a myopathy that results from a deficiency of the ISCU Fe-S cluster scaffolding protein, is a rare but recessively inherited disease characterized by lifelong exercise intolerance (21,22). ISCU deficiency is caused by the splice mutation in intron 4 of the *ISCU* gene (23,24). Fe-S clusters are assembled on ISCU in the mitochondrial ISC assembly complex (25,26). ISCU deficiency has several critical consequences, such as decreasing the activity of mitochondrial Fe-S cluster enzymes, increasing iron deposits, and impairing the steady-state protein levels of the desulfurase components (NFS1-ISD11) in the mitochondrial ISC assembly complex (23,27). FDX2 myopathy is another kind of mitochondrial myopathy found in patients and is caused by the disruption of the *FDX1L* gene (28). FDX2 functions as the electron donor for the mitochondrial ISC assembly complex. Disrupted ATG initiation code produced by the mutation (c.1A > T) lowers the levels of FDX2 in muscle and fibroblasts and decreases the activities of respiratory complex I-III and mitochondrial aconitase. Though their symptoms are similar, the symptoms of ISCU deficiency are more severe compared

to the symptoms of FDX2 deficiency and include severe exercise intolerance, weakness, and pain in active muscles (21,22).

Multiple mitochondrial dysfunction syndromes (MMDS) are also caused by the mutations of proteins involved in mitochondrial Fe-S cluster biogenesis. Four types of MMDS have been identified—MMDS1, MMDS2, MMDS3, and MMDS4—each caused by the mutation of a different Fe-S cluster assembly protein: NFU, BOLA3, IBA57, and ISCA2, respectively (29-32).

Infantile mitochondrial complex II/III deficiency is caused by the mutation of the cysteine desulfurase, NFS1, that is part of the mitochondrial Fe-S cluster assembly complex (33). ISD11 (human LYRM4) is required to stabilize NFS1 and mutation of ISD11 is likely to cause combined oxidative phosphorylation deficiency 19 (COXPD19) (34,35). Patients with ISD11 mutation exhibited further complications with deficiencies of complex I, II and III (34).

Cystic fibrosis has been found to be caused by the deficiency of mitoNEET RNA (36,37). MitoNEET, a mitochondrial outer membrane protein, controls lipid and glucose metabolism and overall mitochondrial bioenergetics by regulating Fe or Fe-S cluster homeostasis (38,39). Accordingly, mitoNEET has been considered as a target for drug development in treating cancer and diabetes. However, the specific involvement of the mitoNEET protein in Fe-S cluster biosynthesis is not well understood.

There are two forms of sideroblastic anemias associated with the defects of Fe-S cluster biogenesis. Mutations in the mitochondrial transporter protein ABCB7, which transports an unknown signal molecule into the cytosol in order to initiate the CIA Fe-S cluster assembly machinery, result in the misregulation of iron, which causes X-linked sideroblastic anemia (XLSA) (40). XLSA patients are characterized by ataxia, iron overload, cerebellar ataxia and ringed

sideroblasts (40,41). Another type of sideroblastic anemia, identified by microcytic anemia and severe iron overload, is caused by a homozygous mutation in the monothiol glutaredoxin *GRX5* gene that decreases its level of mRNA (42).

The connection between impaired Fe-S cluster biogenesis and neurodegenerative, hematological disorders and tumors highlights the importance of Fe-S clusters to human health. Moreover, understanding the mechanism of Fe-S cluster biogenesis, from the assembly of Fe-S clusters on scaffold proteins to the transfer and insertion of Fe-S clusters into specific apo target proteins, has the potential to identify opportunities for intervention and treatment.

General structures and properties of Fe-S clusters

Fe-S proteins were first discovered in 1960 by Helmut Beinert (43). They are most generally defined as proteins in which, non-heme iron is coordinated with cysteine sulfur and/or inorganic sulfur. While the majority of Fe-S clusters are attached to the polypeptide by cysteinyl sulfide-ligated Fe atoms, partial non-cysteinyl ligation involving His, Arg, Asp, Glu, and Ser Fe ligands has been identified, particularly in more complex Fe-S clusters (Figure 1.1 and 1.2).

The most common Fe-S centers employed in proteins are $Fe(SCys)_4$, $Fe_2(\mu_2\text{-}S)_2(SCys)_4$, $Fe_3(\mu_2\text{-}S)_3(\mu_3\text{-}S)(SCys)_3$, and $Fe_4(\mu_3\text{-}S)_4(SCys)_4$, as depicted in Figure 1.1. The electronic, vibrational, magnetic and redox properties of four Fe-S clusters are discussed in this section. In Fe-S clusters, the formal charge on the iron is 2+/ 3+/2.5+ depending on the extent of valance localization/delocalization and the formal charge on the bridging inorganic sulfur is 2− (shown in Figure 1.3). Fe-S clusters are represented by the stoichiometry of Fe and inorganic-S core in square brackets with the formal charge of the core indicated by superscripts, such as $[2Fe\text{-}2S]^{2+,1+}$, $[3Fe\text{-}4S]^{1+,0,2-}$, and $[4Fe\text{-}4S]^{3+,2+,1+,0}$. Understanding the extent of valance delocalization is important for

understanding the electronic, magnetic, and redox properties of Fe-S clusters, as valance-delocalized $Fe_2(\mu_2\text{-}S)_2$ fragments are the fundamental building blocks of all higher nuclearity clusters. Valance delocalization is also important for increasing the rates of redox reactions by minimizing reorganization energy(44,45). Ranges of midpoint potentials (mV vs. SHE) for the most common Fe-S centers in both complex and simple Fe-S proteins are summarized in Figure 1.4. The reduction potential of a specific center is dependent on a number of physicochemical factors, such as center type, cluster ligand, solvent exposure, backbone proximity and orientation, and side chain dipoles (46,47). For example, Rieske type $[2Fe\text{-}2S]^{2+,\,1+}$ centers, for example, have two histidyl ligands at the reducible Fe site, thereby producing higher midpoint potentials (E_m> -100 mV) than all cysteinyl ligated $[2Fe\text{-}2S]^{2+,1+}$ centers, (Figure 1.1).

Mononuclear Fe-S centers: Mononuclear Fe-S centers comprising high-spin Fe^{2+} or Fe^{3+}ligated by four cysteinyl-S in a distorted tetrahedral arrangement are the simplest type of Fe-S center. They are mainly found in rubredoxin (Rd) and desulforedoxin (Dx)(48). Rd centers are also found in two class of non-heme peroxidases, i.e., rubrerthrin and nigerythrin, together with an oxo-bridged dinuclear Fe center, and Dx centers are also found in 2Fe superoxide reductase (SORs) along with a mononuclear Fe active site (49). The mononuclear Fe-S centers in Rds, Dxs and 2Fe SOR have midpoint potentials in the range of +20 to -87 mV, whereas significantly higher potentials are observed for the mononuclear Fe-S centers in the peroxidases (rubrerthrin +281 mV and nigerythrin +213 mV) (50). Site-directed mutagenesis studies have shown that replacing a Cys with a Ser ligand in Rd type centers decreases the reduction potential by 100-200 mV, in accord with the ability of oxygenic ligands to stabilize the ferric state (51). The Fe sites in all Rds, including the Rd-type centers in non-heme peroxidases, are ligated by highly conserved Cys-X_2-Cys motifs near the C- and N-termini. However, one of the C-X_2-C motifs is replaced by a C-C

motif in Dx and the Dx-type center in 2Fe SOR, which results in a more axially distorted tetrahedral structure.

[2Fe-2S] clusters: [2Fe-2S] clusters are generally ligated by four cysteine residues. Figure 1.1A presents an all-cysteinyl ligated [2Fe-2S] cluster in ferredoxin (Fdx). Meanwhile, [2Fe-2S] clusters with two histidyl ligands at one Fe site (52), constitute a large group of [2Fe-2S] clusters called Rieske-type centers $[2Fe\text{-}2S]_R$, (Figure 1.1B). In addition, there are a few examples with one non-cysteinyl ligand, such as aspartate in succinate dehydrogenase (Asp) (53) and sulfide dehydrogenase (54), arginine in biotin synthase (55), and histidine in the mitoNEET protein (56-58). Different types of folds are present in [2Fe-2S]-cluster proteins or domains. For instance, the Fdx-fold containing a Cys-$X_{4/5}$-Cys-X_2-Cys-$X_{29–37}$-Cys motif is common to plant, hydroxylase- or mammalian-type, as well as Isc-type 2Fe Fdx (59). The thioredoxin (Trx)-fold containing a Cys-$X_{4/10/12}$-Cys-$X_{29–35}$-Cys-X_3-Cys motif, is common in NADH dehydrogenases and hydrogenases, and the thioredoxin-like class of 2Fe Fdxs (60). The Rieske-fold with a Cys-X-His-$X_{15–47}$-Cys-X_2-His motif, where the [2Fe-2S] is coordinated to the Cys and His residues, is common to all Rieske-type centers (52). Other unique coordination environments associated with [2Fe-2S] centers are present in biotin synthase (55) and members of the xanthine oxidase family of molybdoenzymes (61). In all cases, the overall [2Fe-2S] cluster core structure, the tetrahedral coordination at each Fe site, Fe-S bond lengths and Fe-S-Fe bond angles are essentially invariable.

The [2Fe-2S] clusters in proteins and numerous metalloenzymes undergo redox cycling between 2+ and 1+ core oxidation states, with a range of redox potentials spanning from +380 mV to -460 mV. The Rieske type centers generally have higher potential (+380 to -150 mV) than all-cysteinyl-ligated cluster centers (+100 to -460 mV), as shown in Figure 1.4. Site-directed mutagenesis studies have also revealed that individual substitution of Cys by Ser/Asp decreases

the redox potentials of $[2Fe\text{-}2S]^{2+,1+}$, indicating that this decrease corresponds with increasing ligand nucleophilicity (i.e., histidine>cysteinate>serinate~aspartate) (62,63). UV-visible absorption/circular dichroism (CD)/variable temperature magnetic circular dichroism (VTMCD), Mössbauer, nuclear magnetic resonance (NMR), electron paramagnetic resonance (EPR) and resonance Raman spectroscopies have been employed to provide a detailed characterization of the electronic, vibrational and magnetic properties of $[2Fe\text{-}2S]^{2+,+}$ clusters. An oxidized $[2Fe\text{-}2S]^{2+}$ cluster has a diamagnetic $S = 0$ ground state due to the antiferromagnetic coupling between the two ($S = 5/2$) Fe^{3+} centers. Whereas in the valance-localized reduced $[2Fe\text{-}2S]^{1+}$ form, ($S = 5/2$) Fe^{3+} and ($S = 2$) Fe^{2+} centers are antiferromagnetically coupled to give $S = 1/2$ ground state (64). However, there are two examples of valance-delocalized $[2Fe\text{-}2S]^{1+}$ centers in the equivalent Cys-to-Ser variants of the thioredoxin-type 2Fe Fdxs from *Clostridium pasteurianum* and *Aquifer aeolicus.* In variants where Cys56 and Cys60 are replaced with Ser, the two Fe sites in the $[2Fe\text{-}2S]^{1+}$ Fdx are ferromagnetically coupled. Ferromagnetic coupling enables the anti-parallel electron to switch between sites without undergoing a spin flip (65-69). Valance-delocalized $S = 9/2$ $[2Fe\text{-}2S]^{1+}$ fragments are found in all higher nuclearity Fe-S centers and facilitate rationalization of the ground and excited state magnetic and electronic properties (68-70).

[3Fe-4S] clusters: There are two types of [3Fe-4S] clusters, cubane-type Fe_3 (μ_3-S) (μ_2-S)$_3$ and linear Fe(μ_2-S)$_2$Fe(μ_2-S)$_2$Fe. Although both have been observed in biological systems, only the cubane-type has been demonstrated to be physiologically relevant thus far. The cubane-type [3Fe-4S] is structurally analogous to a cubane [4Fe-4S] cluster that is missing one Fe, as shown in Figure 1.1C. This similarity led to the speculation that cubane-type [3Fe-4S] clusters may all be artifacts of aerobic protein isolation procedures, as a result of oxidative loss of one Fe from an [4Fe-4S] cluster (71). This scenario was found to apply to several dehydratases, such as aconitase

and several Fdxs, particularly those containing [4Fe-4S] clusters with one unique Fe site ligated to a non-cysteinyl residue. However, based on the primary sequence, X-ray structure and spectroscopic evidence, cubane-type [3Fe-4S] clusters have been shown to be intrinsic prosthetic groups in 3Fe and 7Fe Fdxs, succinate dehydrogenase, fumarate reductase, nitrate reductase, NiFe-hydrogenase, arsenite oxidase, and Fdx- and NAD(P)H-dependent glutamate synthase (72). In contrast, linear $[3Fe\text{-}4S]^{1+}$ clusters have only been observed in alkaline or denatured forms of aconitase (73,74) and monothiol glutaredoxins (75).

Cubane-type [3Fe-4S] clusters have accessible 1+, 0, 2– redox states (76). $[3Fe\text{-}4S]^{1+,0}$ can participate in mediating biological electron transport with redox potentials ranging from +90 to –460 mV (Figure 1.4) (76). At pH 7, the midpoint potential of $[3Fe\text{-}4S]^{0,2-}$ redox couple is ~700 mV, and is strongly pH dependent. These characteristics have been interpreted in terms of the two-electron-reduction occurring with the uptake of three protons, most likely on the three doubly-bridged sulfides (77). X-ray crystal structures of cubane-type [3Fe-4S] centers with complete cysteine ligation have revealed that they have C_{3v} symmetry, indicating that the coordination geometry of each Fe site is approximately tetrahedral. The primary sequence arrangement of coordinating cysteines mainly involves two closely spaced and one remote cysteine, such as Cys-X_2-Cys (e.g., aconitase), Cys-X_5-Cys (e.g., 3Fe and 7Fe Fdxs, succinate hydrogenase, fumarate reductase, nitrate reductase), and Cys-X_7-Cys (e.g., some 3Fe and 7Fe Fds) (78). In bacterial Fds, [4Fe-4S] clusters are coordinated by a remote Cys and three closely spaced Cys, or two Cys and one Asp, in a Cys-X_2-Cys (or Asp)-X_2-Cys sequence that facilitates facile [3Fe-4S] ↔ [4Fe-4S] interconversion.

Absorption, VTMCD, EPR, ENDOR, NMR, saturation magnetization, Mössbauer and resonance Raman have been used to characterize the electronic, vibrational and magnetic

properties of [3Fe-4S] in their accessible redox states. Cubane-type $[3Fe\text{-}4S]^{1+}$ clusters have an S = 1/2 ground state due to the antiferromagnetically coupling of three S = 5/2 Fe^{3+} ions. For cubane-type $[3Fe\text{-}4S]^{1+}$ clusters, NMR and saturated magnetization studies have demonstrated that exchange interactions among the three Fe centers are nearly equivalent ($J_{12} \sim J_{13} \sim J_{23} \sim 300$ cm^{-1}) (79). Cubane-type $[3Fe\text{-}4S]^{0}$ clusters have an S = 2 ground state due to the antiferromagnetic interaction between a valance delocalized Fe^{2+}/Fe^{3+} pair (S = 9/2) and a valance trapped Fe^{3+} site (S = 5/2). However, linear $[3Fe\text{-}4S]^{1+}$ clusters with an S = 5/2 ground state exhibit asymmetric exchange interactions among the three Fe^{3+} ions ($J_{12} \sim J_{23} > 2J_{13}$) in accordance with the linear arrangement (73).

[4Fe-4S] clusters: Cubane [4Fe-4S] clusters with an $Fe_4(\mu_3\text{-}S)_4$ core are among the most common prosthetic groups in nature and one of the most pervasive electron transfer centers in biology (Figure 1.1D). Most [4Fe-4S] clusters have complete cysteinyl-S ligation involving three closely spaced Cys residues in either a Cys-X_2-Cys-X_2-Cys motif with one remote cysteine residue as observed in Fd-type proteins or a Cys-X_2-Cys-$X_{8\text{-}16}$-Cys-$X_{11\text{-}15}$-Cys motif as observed in high potential iron-sulfur proteins (HiPIPs) (80). There are also a few examples of [4Fe-4S] clusters with non-cysteinyl ligation at one Fe site such as histidine in NiFe- and Fe-hydrogenases (81,82), nitrate reductase (83), and aspartate in some ferredoxins (84). At the same time, [4Fe-4S] clusters with one non-cysteinyl ligand are also observed in aconitase, other (de)hydratases (85), and radical-S-adenosylmethionine (SAM) enzymes (86), which are involved in substrate binding and activation. Crystallographic studies of protein-bound [4Fe-4S] clusters revealed that they have approximately D_{2d} symmetry, a characteristic that indicates a tetragonally compressed conformation with four shorter Fe-S bonds (2.24 to 2.28 Å) and eight longer Fe-S bonds (2.29-2.31 Å) (87-91). In biology, [4Fe-4S] clusters have been characterized in the 3+, 2+, 1+, and 0

core oxidation states. Fd-type centers undergo redox cycling between the 2+ and 1+ core oxidation states with a midpoint potential between +80 and -715 mV, whereas HiPIP-type centers cycle between the 3+ and 2+ core oxidation states with a midpoint potential between +50 and +500 mV (Figure 1.4). The unique nitrogenase Fe protein which has a subunit bridging [4Fe-4S] cluster ligated by two Cys in each subunit can access three core oxidation states, i.e. 2+, 1+ and 0, thereby giving it the potential to act as a two-electron donor. The all ferrous $[4Fe\text{-}4S]^{0}$ center was prepared by reduction with Ti(III) citrate (92-94), and it was suggested that increased solvent exposure and NH---S hydrogen bonding stabilize all ferrous [4Fe-4S] forms (94). However, an $[4Fe\text{-}4S]^{1+,0}$ center may not be physiologically relevant due to its lower reduction potential (–790 mV) compared to that of an $[4Fe\text{-}4S]^{2+,1+}$couple (–350 mV) (95).

EPR, Mössbauer and VTMCD spectroscopies have been used to understand the magnetic and electronic properties of [4Fe-4S] centers. These spectroscopic studies have been interpreted in terms of antiferromagnetic coupling between ferromagnetically coupled diferric, diferrous and valence-delocalized [2Fe-2S] fragments (Figure 1.3). For example, (S = 1/2) $[4Fe\text{-}4S]^{3+}$ clusters result from the coupling of a (S = 5) Fe^{3+}/Fe^{3+} pair and a valance-delocalized (S = 9/2) Fe^{2+}/Fe^{3+} pair; (S = 0) $[4Fe\text{-}4S]^{2+}$ clusters result from the coupling of two valance-delocalized (S = 9/2) Fe^{2+}/Fe^{3+} pairs, (S = 1/2) $[4Fe\text{-}4S]^{1+}$ clusters result from the coupling of a (S = 4) Fe^{2+}/Fe^{2+} pair and a valance-delocalized (S = 9/2) Fe^{2+}/Fe^{3+} pair. In addition, more complicated coupling systems have been reported. The location of a valance-delocalized pair is dynamic on the NMR time scale as the cluster exists in rapid equilibrium in different forms (96,97). Some $[4Fe\text{-}4S]^{1+}$ clusters have S = 3/2 ground states or exist as mixtures of S = 1/2 and S = 3/2 ground states indicating a small energy difference between the S = 1/2 and S = 3/2 configurations (98-100). The S = 3/2 ground state is readily rationalized in terms of antiferromagnetic coupling of a (S = 4) Fe^{2+}/Fe^{2+} pair and

a valance-delocalized (S = 7/2) Fe^{2+}/Fe^{3+} pair. Based on EPR and Mössbauer studies, the ground state of the all ferrous $[4Fe\text{-}4S]^0$ cluster in a nitrogenase Fe protein has been shown to be S = 4. However, the details of this magnetic coupling scheme have yet to be fully elucidated. The coupling scheme seems to be quite different from the scheme characterized in the three higher oxidation states (101).

Functions of Biological Iron-Sulfur Centers

Fe-S clusters participate in a wide range of physiological functions such as electron transport, regulation of gene expression, enzyme activity, substrate binding and activation, disulfide reduction, radical generation, DNA damage recognition and repair, iron/electron/cluster storage, and sulfur donation. While each of these functions has been reviewed in-depth (2), a brief discussion of each is presented below.

Electron transport: Electron transfer chains containing one or more Fe-S centers play important roles in a wide variety of biological processes such as respiratory and photosynthetic energy conversion. In addition, many proteins (e.g., Fdxs, Rds, and HiPIPs) serve as either electron donors or acceptors, and they represent one of the largest groups of mobile electron transfer carriers. Fe-S centers are normally arranged in chains, so they can connect sites of catalysis and interprotein electron transfer. The close proximity of the clusters in these electron transfer chains enables them to tunnel electrons faster than substrate redox reactions. At the same time, the intra-cluster distances and the redox potentials and/or conformation of Fe-S centers in other oxidoreductases are modulated with external affecters, which facilitate rapid and thermally activated tunneling, as observed by MgATP in nitrogenase (102) and benzoyl-CoA reductase (103). There are many metalloenzymes where Fe-S clusters participate in coupled electron/proton

transfer reactions (e.g., NADH-quinone oxidoreductase, quinol-cytochrome *c* oxidoreductases, and nitrogenases). A few metalloenzymes have been reported in the literature where [4Fe-4S] clusters are directly attached to the substrate binding site via a bridging cysteinyl-S to facilitate rapid electron transfer to or from the substrate. Examples include the Fe-Fe-[4Fe-4S] center in Fe-hydrogenases (Figure 1.2C) (82,104), as well as the Ni-Ni-[4Fe-4S] center in acetyl-CoA synthase (Figure 1.2D) (105-107).

Substrate binding and activation: Fe-S clusters are involved in substrate binding and activation via one or more of the following: a) by having a unique ligation at a specific Fe site, b) by incorporating a heterometal into the cluster, and c) by attaching a metal site at a unique Fe site.

Non-redox enzymes: The largest classes of non-redox enzymes with substrate-binding Fe-S centers is the (de)hydratase family which includes aconitase, phosphogluconate dehydratase, maleate hydratase, lactyl-coenzyme A dehydratase, 2-hydroxyglutaryl-coenzyme A dehydratase, tartarate dehydratase, serine dehydratase, isopropylmalate isomerase, fumarase, and bacterial dihydroxy-acid dehydratase (108). These contain a $[4Fe\text{-}4S]^{2+}$ cluster with a unique, non–cysteine-ligated Fe site that binds to the substrate and facilitates reversible abstraction of the hydroxyl group and a proton from adjacent carbons on the substrate. The only exceptions are yeast and plant dihydroxy-acid dehydratases which contain a $[2Fe\text{-}2S]^{2+}$ cluster active site. The best characterized example is aconitase which catalyzes the dehydration and rehydration steps in the reversible interconversion of citrate to isocitrate via a cis-aconitate intermediate.

Redox enzymes: The radical-SAM superfamily is the largest group of Fe-S redox enzymes, containing more than 60 distinct enzymes (109). These enzymes share a common $C\text{-}X_3\text{-}C\text{-}X_2\text{-}C$ motif that coordinates an oxidative labile $[4Fe\text{-}4S]^{2+,1+}$ cluster that is responsible for the initiation

of the radical reaction. This reaction entails binding SAM at the unique Fe site of the cluster and transferring an electron to SAM to generate a transient 5'-deoxyadenosyl radical (55,110). The 5'-deoxyadenosyl is a highly reactive radical that generates a substrate or protein radical via hydrogen abstraction. Radical-SAM enzymes catalyze a wide variety of reactions including unusual methylations, isomerizations, sulfur insertions, ring formations, and protein radical generation. Notably, these reactions are the key steps in numerous DNA precursor, vitamin, cofactor, antibiotic, and herbicide biosynthetic pathways (4,6).

Regulation of gene expression and enzyme activity: Fe-S clusters are responsive to a variety of environmental stimuli, such as intracellular levels of certain essential ions and/or molecules. Fe-S clusters in gene regulatory proteins play important sensory roles as they can sense cellular levels of Fe-S clusters, O_2, NO, and reactive oxygen and nitrogen species. The two best-characterized examples of Fe-S clusters acting in sensory roles are the fumarate nitrate regulatory protein (FNR) and the SoxR protein. *E.coli* FNR is an oxygen sensitive protein that acts as a switch between aerobic and anaerobic respiration by regulating the expression of over 100 genes (111). The transcriptionally active DNA binding form of FNR is a homodimer containing one $[4Fe\text{-}4S]^{2+}$ cluster per subunit (112). When the active dimeric form of FNR is exposed to O_2, the FNR $[4Fe\text{-}4S]^{2+}$ cluster rapidly converts to a monomeric $[2Fe\text{-}2S]^{2+}$ cluster-bound form via an intermediate $[3Fe\text{-}4S]^{+}$ cluster. This process results in the loss of site-specific DNA binding and the inactivation of FNR as a transcriptional regulator (113,114). NO is also effective for the inactivation of FNR, with $[4Fe\text{-}4S]^{2+}$ cluster degradation occurring via the formation of monomeric and dimeric dinitrosyl-iron-dithiol species (115). SoxR functions as a redox-responsive switch to monitor and control oxidative stress in bacteria (116). The $[2Fe\text{-}2S]^{2+}$ cluster-bound SoxR activates *soxS* gene expression under oxidative stress conditions, which, in turn, enhances the expression of several

genes and results in the removal of superoxide and the repair of oxidative damage (116). In the absence of oxidative stress, reduced $[2Fe\text{-}2S]^{1+}$ cluster-bound SoxR binds to the *soxS* promoter DNA with the same affinity as the oxidized $[2Fe\text{-}2S]^{2+}$ cluster-bound SoxR (117). However, only the oxidized form is capable of activating *soxS* gene transcription (118,119).

IscR and iron regulatory proteins (IRP1) are two well characterized Fe-S cluster-containing regulatory proteins that use sensing mechanisms involving loss or gain of an Fe-S cluster. IscR is a transcriptional regulator of the Fe-S cluster biosynthesis operon (*iscRSUA-hscBA-fdx*). It contains an Fe-S cluster-binding domain involving a rigorously conserved $C\text{-}X_5\text{-}C\text{-}X_5\text{-}C\text{-}X_2\text{-}H$ motif located between two helix-turn-helix DNA-binding motifs (120). $[2Fe\text{-}2S]^{2+}$ cluster-bound IscR negatively represses of the entire *isc* operon, thereby providing feedback regulation to control the supply of Fe-S clusters generated by the ISC machinery. In addition, the apo form of IscR acts as a global regulator of several Fe-S protein genes. For example, it activates the transcription of the *suf* operon, which encodes the bacterial backup Fe-S cluster assembly system which operates under oxidative stress or iron starvation conditions (121). Apo IscR competes with other apo Fe-S proteins for $[2Fe\text{-}2S]^{2+}$ clusters assembled on IscU or IscA scaffold proteins during IscR-directed regulation (120,121). Prior research has demonstrated that the DNA-binding domain in IscR can recognize two different DNA sequences, a capacity suggesting that different types of DNA binding sites are used by the Fe-S cluster-bound and the Fe-S cluster-depleted forms of IscR (122).

The iron regulatory proteins, IRP1, found in both eukaryotic and prokaryotic cells, is involved in the translational regulation of iron in response to cellular iron availability and the level of oxidative stress (78,123). When starved for iron, IRP1 exists in an apo form. In this state, it inhibits the translation of ferritin mRNAs by binding to iron-responsive elements (IREs) in specific stem-loop RNA structures within untranslated regions (124,125). However, when iron is abundant,

IRP1 loses its ability to bind IREs by assembling a [4Fe-4S] cluster and the resulting protein has aconitase activity. The [4Fe–4S] clusters in both eukaryotic and prokaryotic IRPs respond to other stimuli associated with reactive oxygen and nitrogen species. This responsiveness enables IRPs to have both catalytic and regulatory roles in bacteria and eukaryotes (126-129).

A few enzymes have non-catalytic Fe-S clusters that have structural or regulatory roles. A well-studied enzyme is glutamine phosphoribosylpyrophosphate amidotransferase from *Bacillus subtilis* which catalyzes the first step in purine nucleotide biosynthesis (130). An oxygen sensitive [4Fe-4S] cluster acts as an O_2 sensor to regulate purine biosynthesis (131). Ferrochelatases catalyze the terminal step in heme biosynthesis, namely the insertion of Fe into protoporphyrin. While bacterial ferrochelatases generally do not contain Fe-S clusters, mammalian ferrochelatases invariably contain a [2Fe-2S] cluster (132,133), that does not have a specific catalytic role, but is essential for catalytic activity (134). Since the cluster is sensitive to NO-induced degradation, one possibility is that the cluster provide a means of locally shutting down heme biosynthesis as a defense mechanism against bacterial infections (135). However, the recent discovery of some bacterial ferrochelatases containing [2Fe-2S] clusters raises questions about this hypothesis (136). An alternative role for the [2Fe-2S] cluster-binding site in mammalian ferrochelatases is that it provides feedback regulation of heme biosynthesis by sensing the level of available Fe-S clusters (137).

Disulfide reduction: Typically, the biological disulfide reaction is catalyzed by FAD-containing pyridine nucleotide-disulfide oxidoreductases via an NADPH-dependent two-electron process. However, some $[4Fe\text{-}4S]^{2+}$ cluster-containing enzymes catalyze disulfide reduction in two sequential steps using novel site-specific cluster chemistry. For example, ferredoxin-thioredoxin reductase (FTR), found in plant chloroplasts, functions as the light-mediated activity regulator of

numerous oxygenic photosynthesis enzymes in plants. FTR is a disc-shaped αβ-heterodimer containing a highly conserved catalytic β-subunit with a [4Fe-4S] cluster close to a redox active cysteine disulfide (7,8). The proposed mechanism of FTR suggests that the [4Fe-4S] cluster reduces the disulfide of thioredoxin involving one-electron cluster oxidation of the $[4Fe\text{-}4S]^{2+}$ coupled with two-electron oxidation of the FTR disulfide. This reaction yields an intermediate comprising S =1/2 $[4Fe\text{-}4S]^{3+}$ with two cysteines ligated at a unique Fe (7,8,138). HypD, a NiFe-hydrogenase maturation protein, has a $[4Fe\text{-}4S]^{2+}$ cluster with an environment similar to that of FTR. Accordingly, HypD initiates a redox cascade of three disulfides similarly to release cyanide from a cysteine thiocyanate and, in turn, bring about the maturation of the NiFe-hydrogenase active site (139). Heterodisulfide reductase (HDR), the terminal enzyme in the disulfide respiratory chain of methanogenic archaea, catalyzes the reduction of CoM-S-S-CoB to Coenzyme M (CoM-SH) and Coenzyme B (CoB-SH) (140). Initial spectroscopic studies suggested a mechanism similar to FTR, except that the cluster interacts directly with the substrate. However, a recent crystal structure revealed the presence of two novel non-cubane [4Fe-4S] clusters composed of fused [3Fe-4S]-[2Fe-2S] fragments sharing 1 Fe and 1 S (141). Substrate soaking experiments indicated that the heterosulfide is positioned between the two clusters and homolytically cleaved to yield CoM and CoB bound to the same Fe in each cluster.

Iron, electron, and cluster storage: An iron/electron storage role for [4Fe-4S] clusters in 8Fe Fdxs containing two [4Fe-4S] was originally proposed by Thauer and co-workers (142). The discovery of polyferredoxins in methanogens containing 3 to 7 repeats of the 8Fe Fdx-like domains, thus hosting up to 14 [4Fe-4S] clusters, reinforced this hypothesis. Moreover, genes encoding polyferredoxins are found in operons encoding enzymes having a high demand for [4Fe-4S] clusters such as hydrogenase and formylmethanofuran dehydrogenase (9,143,144). Since Fe-

S clusters need to be assembled on scaffold proteins prior to their insertion into apo proteins, 8Fe Fdxs and polyferredoxins may act as storage sites for [4Fe-4S] clusters in biogenesis pathways.

DNA damage recognition and repair: Several Fe-S-containing DNA glycosylases (e.g., endonuclease III, MutY and thymine-DNA glycosylases) function in DNA repair(145,146). In addition, the structurally distinct enzymes of the family 4 uracil-DNA glycosylase family have been shown to contain a redox-active $[4Fe\text{-}4S]^{3+,\,2+}$ when bound to DNA (147). Consequently, this redox-active cluster is proposed to locate damaged DNA via DNA-mediated electron transport between cluster centers (145,146). Fe-S clusters in several DNA nucleotide excision repair helicases—XPD (xeroderma pigmentosum complementation group D), Rad3 in yeast, and FancJ (Fanconi J cross-link repair helicase)—have been suggested to have similar functions (148-150).

S donor: In radical-SAM enzymes, a second Fe-S cluster in addition to the [4Fe-4S] cluster can act as the immediate sulfur donor in a sulfur insertion reaction. The following clusters have been proposed to behave in this way: the [2Fe-2S] cluster in biotin synthase (BioB) (151,152), the [4Fe-4S] cluster in lipoic acid synthase (LipA) (153) and the [4Fe-4S] cluster in MiaB (154). In the case of BioB, the additional [2Fe-2S] cluster catalyzes a sulfur insertion reaction to form biotin from dethiobiotin in a single turnover reaction (152). Similarly the additional [4Fe-4S] cluster in LipA and MiaB, has been shown to act as the sulfur donor for lipoyl cofactor biosynthesis (153) and the thiomethylation of tRNA (154). On the other hand, the additional [4Fe-4S] cluster in MoaA/MOS1A does not catalyze a sulfur insertion reaction, but has been reported to play a crucial role in binding, positioning and activating the substrate for H-atom abstraction (155).

Cluster conversions

Fe-S cluster interconversions and degradations influence a wide variety of biological regulatory processes due to their contributions to protein structure (123). The following can degrade or convert Fe-S clusters into other structures: exposure to O_2 and NO, chemical oxidation or reduction, changes in pH, denaturants, and site-directed mutagenesis of specific residues. The most common type of cluster interconversions are between [4Fe-4S] and cubane-type [3Fe-4S] clusters and between [4Fe-4S] and [2Fe-2S] clusters. Figure 1.5 presents a summary of well-characterized Fe-S cluster transformations.

Aconitase is the most investigated enzyme for cluster transformations because it can accommodate multiple different types of clusters (78). The functional $[4Fe\text{-}4S]^{2+}$ form of aconitase transforms into an inactive cubane-type $[3Fe\text{-}4S]^{1+}$ form, upon exposure to air or aerobic isolation (156). The catalytically active $[4Fe\text{-}4S]^{2+}$ form can be restored under reducing conditions as the $[3Fe\text{-}4S]^{0}$ cluster can readily take up Fe^{2+} or incorporate other transition metal ions to form a heterometallic cubane cluster $[M\text{-}3Fe\text{-}4S]^{2+,1+}$ (M=Zn, Co, Ni, Cr, Mn, Cu, Cd, Ga, Tl) (157,158). This type of reversible cluster transformation between [4Fe-4S] and [3Fe-4S] clusters is most common in clusters containing one non-cysteinyl-ligated Fe atom, such as aconitase and some ferredoxins. Interestingly, many [4Fe-4S] clusters with complete cysteinyl ligation can also degrade to form $[3Fe\text{-}4S]^{1+}$, through this usually occurs under more extreme conditions, such as a prolonged exposure to air and/or a large excess of ferricyanide. The remarkable transformation from cubane-type $[3Fe\text{-}4S]^{1+}$ to linear $[3Fe\text{-}4S]^{1+}$ clusters is only observed in aconitase at pH > 9.5 or under partial denaturation conditions (e.g., in the presence of urea) (73,159). A major protein rearrangement is required during this transformation since only two of the original cysteine ligands to the cubane-type $[3Fe\text{-}4S]^{1+}$ are retained in the linear $[3Fe\text{-}4S]^{1+}$ cluster, and two more remote cysteines are recruited as cluster ligands (159). Notably, the linear $[3Fe\text{-}4S]^{1+}$ cluster-bound

aconitase can reform the active $[4Fe\text{-}4S]^{2+,1+}$ cluster on reduction in the presence of Fe^{2+}. During the denaturation of aconitase, the linear $[3Fe\text{-}4S]^{+}$ cluster is formed, along with some $[2Fe\text{-}2S]^{2+}$ clusters (73).

The O_2-induced $[4Fe\text{-}4S]^{2+}$ to $[2Fe\text{-}2S]^{2+}$ cluster conversion in FNR occurs with the loss of two Fe atoms and with oxidation of two sulfides to form a $[2Fe\text{-}2S]^{2+}$ cluster with two cysteine and two cysteine persulfide ligands (160). Moreover, this novel transformation is reversible in the presence of a dithiol reducing agent and Fe^{2+} in the absence of O_2. The facile reversibility of this cluster transformation makes FNR responsive to rapid changes in cellular O_2 levels (160). Preliminary evidence suggests that BioB undergoes the same reversible O_2-induced cluster conversion (160). Consequently, this cluster interconversion may afford a rapid repair mechanism for radical SAM enzymes degraded by O_2 exposure. Indeed, radical SAM enzymes are often purified with [2Fe-2S] clusters in place of the SAM-binding [4Fe-4S] cluster, unless rigorously purified under anaerobic conditions.

The nitrogenase Fe protein $[4Fe\text{-}4S]^{2+}$ cluster converts to a $[2Fe\text{-}2S]^{2+}$ cluster in the presence of Mg-ATP when exposed to iron chelators. In addition, crystallographic and spectroscopic studies looking at a mimic of the nucleotide-bound form of the nitrogenase Fe protein showed that in the presence of glycerol, the reduced [4Fe-4S] cluster is reversibly cleaved into two [2Fe-2S] fragments (161-163). The two [2Fe-2S] fragments in this example are separated by 5 Å, with glycerol serving as a bidentate ligand bridging the two fragments, and each of the fragments has one cysteinyl ligand at each Fe site (163). The reverse process is likely related to the reductive coupling of two $[2Fe\text{-}2S]^{2+}$ fragments to form a $[4Fe\text{-}4S]^{2+}$ cluster, a fundamental pathway for [4Fe-4S] assembly in Fe-S cluster biosynthesis. In addition, the reductive coupling of [2Fe-2S] clusters to form [4Fe-4S] clusters has also been observed in two primary scaffold

proteins, namely IscU and NifU (N-terminal domain) from *A. vinelandii* (164-166). The oxidative degradation of [4Fe-4S] to [2Fe-2S] clusters and the reductive coupling of [2Fe-2S] clusters to form [4Fe-4S] clusters can provide great insight into the biosynthesis and repair of Fe-S centers.

Biogenesis of biological Fe-S clusters

The most common type of Fe-S cluster is the cubane $[4Fe\text{-}4S]^{2+,1+}$ cluster; ancient cofactors that were almost certainly present under primordial conditions and used extensively in lifeforms under strictly anaerobic conditions during the first billion years of life on earth (167-169). However, they are not well suited for aerobic environments due their sensitivity to degradation by O_2, O_2^- and H_2O_2, compared to the more O_2-tolerant $[2Fe\text{-}2S]^{2+,1+}$ and cubane-type $[3Fe\text{-}4S]^{1+,0}$ clusters, which are stable in their all ferric states. Indeed, the oxygen sensitivity of $[4Fe\text{-}4S]^{2+,1+}$ clusters was likely to be a major determinant in the evolution of aerobic life forms, once cyanobacteria started to evolve O_2 more than 2.5 billion years ago (170). Nevertheless, aerobic organisms, including humans and plants, still rely heavily on O_2-sensitive [4Fe-4S] clusters for many crucial reactions, due to the evolution of repair mechanisms and enzymes such as superoxide dismutase/reductase and catalases. Due to the simple structure and composition of Fe-S clusters, an Fe-S cofactor can often be assembled on apo proteins *in vitro* via a simple chemical reconstitution procedure (171). However, Fe-S cluster biogenesis *in vivo* is a complex process due to the physiological toxicity of Fe^{2+} and S^{2-} in their free forms (172,173). In fact, over the past two decades, research has shown that biosynthesis of Fe-S is a complicated process undertaken by a subset of evolutionarily conserved proteins.

Based on existing genetic, molecular biology, and biochemical studies, three distinct bacterial Fe-S cluster assembly machineries have been identified, i.e., NIF (nitrogen fixation),

SUF (sulfur mobilization), and ISC (iron-sulfur cluster). The NIF system is generally specific for the maturation of Fe-S proteins associated with nitrogen fixation in nitrogen fixing organisms such as *Azotobacter vinelandii* (*Av*). The ISC system is the primary system for general Fe-S cluster biosynthesis in proteobacteria such as *Escherichia coli (Ec*) and *Av*. Moreover, along with a few additional components, the ISC system constitutes the eukaryotic mitochondrial machinery for Fe-S cluster biogenesis, which is in accord with the bacterial origin of this organelle in evolution. The SUF system plays a backup role in many proteobacteria, that it is operative only under conditions of iron limitation or oxidative stress. It is therefore not surprising that the bacterial SUF system also forms the basis of the Fe-S cluster biogenesis machinery in plant chloroplasts, an O_2-producing organelle with cyanobacterial evolutionary origins. The SUF system also appears to be the sole system for Fe-S cluster biogenesis in archaea, cyanobacteria, gram-positive and other pathogenic bacteria.

In plants, three Fe-S cluster assembly pathways, i.e., SUF, ISC, and CIA, are involved in the maturation of Fe-S proteins in plastids, mitochondria, and cytosol, respectively (Figure 1.6) (174). As discussed above, the ISC and SUF systems have been highly conserved throughout evolution. Despite their many differences, both ISC and SUF systems (in bacteria and eukaryotes) share a common biosynthetic theme: *de novo* Fe-S cluster assembly on the scaffold protein followed by the intact transfer of Fe-S clusters to cluster transfer proteins or apo target proteins. The mitochondrial ISC machinery is required not only for the biosynthesis of Fe-S clusters in mitochondrial proteins, but also for the maturation of cytosolic and nuclear Fe-S proteins (175). In eukaryotes, the mitochondrial ISC export system and CIA (cytosolic iron-sulfur assembly) are solely responsible for generating cytosolic and nuclear Fe-S proteins (12,175). As the research described in this thesis focuses on cluster assembly in plant plastidial and mitochondrial Fe-S

proteins, the remainder of this literature review will focus on the SUF and ISC systems in *Arabidopsis thaliana,* our model plant organism.

Mitochondrial ISC system in Arabidopsis thaliana: The mitochondrial ISC machinery is conserved in all eukaryotes and contains many of the same components found in the bacterial ISC machinery due to the evolutionary relationship between bacteria and mitochondria (Table 1.1) (174,176). The ISC machinery consists of more than 19 proteins, including iron and sulfur donors, scaffold proteins, and cluster transfer proteins (174). The mitochondrial ISC assembly pathway can be divided into four steps: 1) cysteine desulfurase-mediated assembly of a [2Fe-2S] cluster on an ISCU scaffold protein, 2) molecular chaperone-assisted [2Fe-2S] cluster transfer from ISCU to acceptor proteins, 3) synthesis of [4Fe-4S] clusters from [2Fe-2S] clusters, 4) intact [4Fe-4S] cluster transfer to acceptor proteins. The early steps of this machinery are believed to be involved in the assembly of [2Fe-2S] clusters, whereas the later steps are essential for the assembly of [4Fe-4S] clusters (177). Although most of the mitochondrial ISC components are known, many questions remain concerning how they interact and function at the molecular level. In particular, the molecular mechanism of [4Fe-4S] cluster assembly and insertion into target proteins is not well understood.

i. Cysteine desulfurase-mediated assembly of a [2Fe-2S] cluster on an ISU scaffold protein: Just as in bacteria, Fe-S cluster biogenesis in plant mitochondria starts with the *de novo* synthesis of a [2Fe-2S] cluster on the scaffold protein. In yeast, the scaffold role is performed by Isu1 (the bacterial IscU homolog), and in plants the scaffold protein in the ISC system is called the ISU protein. The *Arabidopsis* genome encodes three mitochondria-located ISU proteins (i.e., ISU1, ISU2, and ISU3) (178). The expression of *ISU1* is much higher than that of *ISU2* and *ISU3*, and is likely to encode the primary scaffold protein (179,180). However, the function of

ISCU2 and ISCU3 have yet to be investigated. The synthesis of an Fe-S cluster on scaffold protein ISU1 requires assistance from other ISC proteins. The key ISC enzyme is a PLP-dependent cysteine desulfurase, *At* NFS1, which converts cysteine-to-alanine and incorporates the released S as a cysteine persulfide on a flexible loop, which is subsequently transferred to form a cysteine persulfide on ISCU1 via a disulfide exchange mechanism (179). In *S. cerevisiae,* the cysteine desulfurase homolog, Nfs1 forms a complex with its partner proteins Isd11 and Acp1 (177,181). This Nfs1-Isd11-Acp1 complex is responsible for sulfur transfer to Isu1 in yeast. In *A. thaliana* the Isd11 ortholog has not been functionally characterized. However, an additional interacting protein of NFS1, *At* SUFE1, has been found (182). *At* SUFE1 functions as a sulfur transferase that activates plastidial (SUFS) and mitochondrial (NFS1) desulfurases in *Arabidopsis,* presumably by making the cysteine persulfide more accessible for transfer (182,183). While an overexpressed SUFE1-GFP fusion was found to be predominantly localized to plasmids, the observation that a plastidial-targeted SUFE1 is not sufficient for complementing the embryo lethality of the mutant supports a role in the mitochondrial ISC machinery. In addition to *At* SUFE1, Fe-S cluster synthesis on *At* ISU1 requires electrons, likely from the ferredoxin/ferredoxin reductase system, and iron, though the origin of iron has yet to be identified.

ii. Molecular chaperone-assisted [2Fe-2S] cluster transfer from ISU to acceptor proteins: Based on the studies of bacterial and yeast ISC systems (184-186), efficient transfer of the [2Fe-2S] cluster from *At* ISU1 scaffold protein is likely to require *At* HSCA1 and HSCB cochaperones in an ATP-dependent process. HSCB is proposed to bind and release the [2Fe-2S] cluster-bound ISU1 in the cluster assembly complex and escort it to HSCA1. HSCB binding greatly enhances the ATP hydrolysis activity of HSCA1 and the [2Fe-2S] cluster on ISU1 is transferred intact to an

apo acceptor protein bound to ISU1 in an ATP-dependent reaction involving HSCA1 binding the LPPVK motif on ISU1 that is adjacent to one of the cluster-bound cysteines. Yeast two-hybrid and bimolecular fluorescence studies showed that in *At* HSCB can interact with *At* ISU1 (187). In addition, HSCB can complement a yeast knockout strain involving the equivalent protein, Jac1. The involvement of the HSCA1 chaperone in plant mitochondria has yet to be investigated. However, the ATPase activity of *At* HSCA1 chaperon is stimulated *in vitro* by *At* HSCB (174,188) and studies in yeast have demonstrated that the Ssq1 homolog of HscA facilitates Fe-S cluster transfer from Isu1 to Grx5 via complex formation (186).

By analogy with the bacterial, human and yeast ISC systems, a monothiol GRX is likely to be the dedicated acceptor protein for [2Fe-2S] cluster on ISU1. GRXS15 is the only confirmed monothiol GRX in *Arabidopsis* mitochondria, and it has a 33% amino acid similarity with yeast and human mitochondrial monothiol glutaredoxins, see Figure 1.8 (189). A knockout mutant of *At* GRXS15 is embryo lethal, indicating an essential role in plant growth, and *At* GRXS15 can assemble an Fe-S cluster in the presence of glutathione (189). In addition, after a long debate about the importance of GRXS15 in the plant mitochondrial Fe-S cluster machinery, *At* GRXS15 has been shown to coordinate a [2Fe-2S] cluster in the presence of reduced glutathione (GSH) (189). Moreover, mutations of GRXS15 that weakens GSH and cluster binding diminish the ability of this protein to complement a yeast Δ*grx5* mutant, exhibit a dwarf phenotype and decrease aconitase activity by approximately 65%, indicating that the essential role of GRXS15 is involved with mitochondrial Fe-S cluster biogenesis (189).

The crystal structure of the human homolog of GRXS15, GLRX5 is in accord with GRXS15 acting as a [2Fe-2S] cluster transfer protein (190). The structure revealed a tetramer with [2Fe-2S] clusters bridging each dimer and each Fe ligated by the cysteinates of GSH and the

rigorously conserved CGFS motif that characterizes monothiol glutaredoxins, see Figure 1.9. Recently, a study suggested that the function of yeast homolog of *At* GRXS15, Grx5, can be bypassed to some extent (186), since the deletion of Grx5 in *S. cerevisiae* is not lethal (191,192). The trafficking role of Grx5 in yeast is mainly needed in an ambient or high-oxygen environment. Thus, under anaerobic conditions, Ssq1 and Jac1 (the yeast homologs of *At* HSCA1 and HSCB) can facilitate the release of clusters directly to target apo proteins rather than being mediated by Grx5 cluster trafficking protein. However, human diseases such as sideroblastic anemia and iron overload are associated with GLRX5 mutants, suggesting that higher eukaryotes need a Grx5-mediated trafficking reaction (42,193).

iii. Synthesis of a [4Fe-4S] cluster from [2Fe-2S] clusters: Studies of the yeast and human ISC systems have demonstrated that a complex composed of Isa1-Isa2-Iba57 is required for [4Fe-4S] cluster biosynthesis (194,195). Iba57 is a tetrahydrofolate-dependent protein of unknown function that appears to be required for cluster release (195). More specifically, this complex is essential for the maturation of [4Fe-4S] clusters in radical-*S*-adenosylmethionine (SAM) enzymes such as lipoic acid synthase and (de)hydratase enzymes such as aconitase (194,195). This complex does not react with early ISC machinery but rather depends on the delivery of [2Fe-2S] cluster species. Recently, there has been a debate about the molecular relationship between Iba57 and IscA proteins. *In vivo*, ISCA2 reacts with IBA57 but not with ISCA1 in humans, whereas in yeast both A-type proteins interact with Iba57. There are two Iba57 orthologs in *A. thaliana*, IBA57.1 localized in mitochondria and IBA57.2 localized in plastids (196).

The two ISC proteins belonging to the family of A-type carrier proteins are proposed to accept a [2Fe-2S] cluster from a monothiol GRX. A recent study demonstrated that two human GLRX5s can transfer [2Fe-2S] clusters to the ISCA1-ISCA2 heterodimeric complex without the

requirement of IBA57 to form a [4Fe-4S] cluster (197). Two-electron reductive coupling of two $[2Fe\text{-}2S]^{2+}$ clusters to form a [4Fe-4S] has been well established and rationalized for bacterial ^{Nif}IscA and IscU proteins using dithiothreitol (DTT) and dithionite (DT), respectively as the reducing agents (165,198,199). Hence, although reductive coupling is the likely mechanism for this cluster conversion, the physiological electron donor has not been established in any organism. The crystal structure of a [2Fe-2S]-bound IscA from *T. elongatus* indicated a unique asymmetric coordination of the [2Fe-2S] cluster, see Figure 1.11 (200). IscA is an asymmetric homodimeric protein with a partially solvent exposed [2Fe-2S] cluster, which is asymmetrically bound to the conserved three Cys residues from one monomer and one conserved Cys from another monomer (Figure 1.11(b)). Using human proteins, individual, ISCA1 or ISCA2 proteins do not form a [4Fe-4S] cluster from two [2Fe-2S]-GLRX5 donated clusters (201). Moreover, the heterodimeric ISCA1-ISCA2 complex is thermodynamically more favorable compared to the corresponding homodimers, indicating that the heterodimeric complex may be responsible for the assembly of a [4Fe-4S] cluster (201). This result also agrees with *in vivo* studies showing strong interaction between ISCA1 and ISCA2 proteins (202). Three mitochondrial A-type carrier proteins, i.e., ISCA1a, ISCA1b, and ISCA2 are present in *A. thaliana*, but they have yet to be investigated *in vitro.* The properties and function of these three A-type carrier proteins in *A. thaliana* (Figure 1.10) are investigated in this work.

iv. Intact [4Fe-4S] cluster transfer to acceptor proteins: In yeast and humans, two mitochondrial proteins Nfu1/NFU1 and Ind1/NUBPL help to insert [4Fe-4S] clusters into the following mitochondrial target proteins: aconitase, succinate dehydrogenase, lipoic acid synthase, and respiratory complexes I and II (201). In human mitochondria, target proteins could directly receive their [4Fe-4S] clusters from the ISCA1-ISCA2-IBA57 complex, or they could receive

them from NFU1/NUBPL following [4Fe-4S] cluster transfer from the ISCA1-ISCA2-IBA57 complex to NFU1/NUBPL. NFU1 can bind a [4Fe-4S] cluster (203), and functions as a late-acting factor in the maturation of lipoic acid synthase and subunits of respiratory complexes I and II (204,205). [4Fe-4S]-cluster-bound NUBPL is only required for the assembly of human respiratory complex I (206). Yeast Nfu1 binds a [4Fe-4S] cluster and has been shown to interact with Isa1 and Isa2 in the Isa1-Isa2-Iba57 complex and with mitochondrial [4Fe-4S] target proteins (207).

Very little functional information is available about maturation of [4Fe-4S] proteins in *Arabidopsis*. There are two NFU proteins in *A. thaliana* whose functions are unknown: NFU4 and NFU5. NFU4 is localized in mitochondria whereas the mitochondrial localization of NFU5 has yet to be confirmed. The mitochondrial Nfu proteins, i.e., *At* NFU4, *At* NFU5, *Hs* NFU1, and *Sc* Nfu1 all contain an N-terminal domain and a C-terminal domain with the CXXC motif involved in [4Fe-4S] cluster binding, see Figure 1.12 (208,209). The N-terminal domains may be involved with targeting specific acceptor proteins. However, gene knockouts studies indicate that the individual *At* NFU4 and NFU5 proteins have at least partially redundant functions in mitochondria but together they are essential for seedling development. Both *At* NFU proteins can rescue the growth development of a yeast *Δnfu1* mutant. To understand the roles of NFU4 and NFU5 in mitochondrial Fe-S cluster trafficking, Chapter 2 of this dissertation reports the purification of the *At* NFU4 and NFU5 proteins, as well as the assembly and spectroscopic characterization of an Fe-S cluster-bound forms of both proteins.

The plastidial SUF system in Arabidopsis thaliana: In bacteria, the SUF system generally plays a backup role only operative under the conditions of iron limitation or oxidative stress (210). However, it is the primary system in the more oxygen-rich cellular environments of cyanobacteria and plant chloroplasts (Table 1.2) (210,211). The SUF system can also be separated into two steps;

the first step is the assembly of an Fe-S cluster on a scaffold protein by cysteine desulfurase and sulfurtransferase. The second step is the transfer of Fe-S clusters from scaffold proteins to plastidial target proteins. In plant plastids, NFS2 (also called CpNifS) is a group II cysteine desulfurase and SUFE acts as sulfur-transferase to facilitate rapid S-transfer to the scaffold protein (212). There are three sulfur-transferases in plants: SUFE1, SUFE2, and SUFE3. *ΔsufE1* mutants are lethal because SUFE1 can interact with and activate both NFS2 and NFS1, making SUFE1 essential for Fe-S assembly in plastid and mitochondria (182,183). SUFE2 and SUFE3, however, are only targeted to plastids, but their specific roles have yet to be determined.

The cysteine persulfide from NFS2 is transferred to a scaffold complex comprised of three proteins—SUFB, SUFC, and SUFD—in a 1:2:1 (BC_2D) stoichiometry in which SUFB is the scaffold protein for cluster assembly (213,214). In *E. coli* both [4Fe-4S] and [2Fe-2S] clusters can be assembled on SufB *in vitro*. The expression of *At* SUFB and *At* SUFC can complement the growth defects of *E. coli ΔsufB* and *ΔsufC* mutants (215). The loss of SufC or both SufC and SufD reduced the *in vivo* formations of Fe-S clusters on SufB, indicating that SufC and SufD are both required for *in vivo* Fe-S cluster formation on SufB (213). In addition, while SufD participates in both embryogenesis and more general house-keeping role such as chlorophyll biosynthesis and chloroplast development, SufB and SufC only function in embryogenesis (216).

The Fe-S cluster formed on $SufBC_2D$ is delivered to target apo proteins directly or indirectly via carrier proteins (217,218). The mechanisms of cluster trafficking in SUF machinery are not well established compared to ISC machinery. In the bacterial SUF system, glutaredoxin 4 (Grx4), P-loop NTPase Mrp, Ygfz, ErpA, and NfuA are likely to play important roles for the late steps of Fe-S maturation, (see Table 1.2 for a list of plastidial Fe-S cluster assembly proteins in *Arabidopsis thaliana* and their bacterial relatives) (219). In plant chloroplasts, two GRX

orthologs— GrxS14 and GrxS16—can bind and transfer labile Fe-S clusters to acceptor proteins, which make them good candidates to serve as cluster transfer proteins (220). There are three isoforms of BOLA proteins in plant chloroplasts: BOLA, BOLA1, and BOLA4. Plastidial BOLA proteins can interact with [2Fe-2S] cluster-bound GRXS14 and GRXS16 to form heterodimers with bridging [2Fe-2S] clusters. The clusters are not essential for heterodimer stability as equivalent heterodimers are formed in the apo forms (221). Similar GRX-BOLA interactions been reported in bacteria, yeast, plants, and mammals and BOLA binding appears to play a role in stabilizing bound clusters with respect to oxidative stress and/or changing the acceptor protein specificity for [2Fe-2S] cluster transfer (222).

PSI is involved in electron transport in cyanobacteria, algae, and vascular plants during oxygenic photosynthesis (223). The reaction center of PSI contains three [4Fe-4S] clusters, which are the terminal electron acceptors denoted F_x, F_A, and F_B (224). Fx bridges the PsaA and PsaB subunits, while F_A and F_B are bound to a 9 kDa soluble protein, PsaC (225). F_A and F_B are necessary to transfer electrons from F_x to soluble ferredoxin or flavodoxin in the cytosol (226). PsaC is highly conserved among cyanobacteria, algae, and higher plants and it shares similarities with soluble 2[4Fe-4S] ferredoxins in terms of molecular mass and the presence of two [4Fe-4S] cluster binding motifs in its primary sequence (227,228). PsaC and the properties of its Fe-S clusters as a part of PSI, as well as the unbound (isolated) protein, have been studied over the last ten years. Unbound PsaC has broader EPR resonances, and peak positions are different from that of F_A and F_B bound to the PSI complex (226). Accordingly. PsaC undergoes a structural change upon binding with the PSI core, which affects the environment of the Fe-S cluster and alters its magnetic properties (229). Prior research has demonstrated that the UV-vis spectrum of reconstituted PsaC has a broad maximum at 390 nm and a broad shoulder at 320nm, features similar to typical 2[4Fe-4S]

ferredoxins (227). This EPR spectrum has similar g tensors for both clusters, in contrast to when PsaC is bound to the PSI core (230).

There are several genes that do not encode structural components of PSI but have been shown to be essential for the assembly of PSI (231). One of these is HCF101 (high chlorophyll fluorescence 101), the plastidial ortholog of Mrp, belongs to the ancient and ubiquitously distributed protein family of soluble Fe-S cluster containing NTPases (i.e., [4Fe-4S]-cluster-containing P-loop NTPases) (232). The chloroplast protein HCF101 is critical for the maturation of Photosystem I (PSI) and the soluble ferredoxin-thioredoxin reductase, both of which contain [4Fe-4S] clusters (232). Levels of PSI (three [4Fe-4S]) and FTR (one [4Fe-4S]) are significantly diminished in the HCF101 mutant, but the translation of PSI proteins is not affected(223). There are four classes of the P-loop NTPase family involved in Fe-S cluster biogenesis. They share a highly conserved protein signature and present in bacteria, plastid, mitochondria, and cytoplasm (233). The mature HCF101 contains an N-terminal DUF59 domain with eight cysteine residues along the sequence. Characteristic motifs, such as CXXC for Fe-S cluster binding, are present in N- and/or C-termini of cytosolic and mitochondrial proteins in eukaryotes and eubacteria, but they are absent in plastid HCF101 form (233). Research using Mössbauer and EPR spectroscopy has shown that chloroplast HCF101 binds a [4Fe-4S] cluster (233). Site-directed mutagenesis has found that three cysteine residues of HCF101 are essential for binding this cluster. Recent studies on PSI biogenesis have shown that the insertion of Fe-S clusters is the crucial step in the post-translational maturation of PSI (234). To understand the function of HCF101 in post-translational assembly of PSI, *in vitro* [4Fe-4S] cluster transfer from HCF101 to yeast apo-Leu1 as a model target protein has been tested, and the results suggested that HCF101 could transfer Fe-S clusters to apo-proteins in chloroplasts (233). However, it remains unknown whether HCF101 is involved

in binding and transferring Fe-S clusters or if it has acquired other functions in the course of evolution.

A-type carrier proteins play important roles in the maturation of Fe-S clusters in different organisms. SufA1 is the plastidial isoform among the bacterial SufA/ErpA/IscA family of ATC proteins found in plants, and IBA57.2 is the ortholog of Ygfz (235). As *ΔsufA1* mutants do not result in any defects in plant development, it is likely that SufA1 acts as a backup carrier for [2Fe-2S] clusters under stress conditions (236,237). There are two orthologs of IBA57 in plants, IBA57.1 targeted in mitochondria and IBA57.2 targeted to plastids (196). IBA57 cannot bind [4Fe-4S] clusters by themselves and their exact function is still unknown. Five members of the NFU family are present in plants, NFU1, NFU2, and NFU3 are in the plastid, and NFU4 and NFU5 are present in mitochondria (238). Plastidial proteins NFU2 and NFU3 are also required for the assembly of the Fe-S cluster in PSI (208). Plant NFU2 can accommodate both [2Fe-2S] and [4Fe-4S] clusters, and the [4Fe-4S] can be transferred rapidly and intact to a physiological relevant partner protein, adenosine 5-phosphosulfate reductase, APR1 (208). Even though *Arabidopsis nfu2* and *nfu3* mutants have a PSI defect, plants show a much milder phenotype than *hcf101* mutant plants (239). In contrast, *Arabidopsis nfu1* mutants exhibited no phenotype (239). *At* NFU2 and *At* HCF101 are both required for the maturation of Fe-S clusters in PSI, but their potential connection has not been investigated. Our working model for the SUF machinery in plastids is that NFU2 and NFU3 accept clusters from the scaffold $SUFBC_2D$ complex and then deliver them to HCF101 for the maturation of PsaC. Based on *in vivo* studies reporting that the *hcf101* mutant is lethal to seedlings and the double *nfu2* and *nfu3* mutant is lethal to embryos (240), it is likely that HCF101 acts downstream of the NFU proteins.

Summary of Presented Work

The objective of this dissertation is to investigate mitochondrial Fe-S cluster maturation processes in *Arabidopsis thaliana* involving monothiol glutaredoxin, A-type proteins, and NFU-type proteins. The results provide initial insights into a comprehensive model of late mitochondrial ISC machinery processes in plants. We also wanted to understand plant chloroplast Fe-S cluster trafficking involving HCF101; the NFU-type proteins, NFU2 and NFU3; and, PsaC. Fe-S-cluster-bound proteins were characterized using a combination of various spectroscopic techniques including absorption, circular dichroism (CD), resonance Raman (RR), and electron paramagnetic resonance (EPR), along with analytical methods such as gel filtration chromatography, protein/Fe determination, and enzyme activity assays. New and significant results have been found and will be presented and discussed in detail in Chapters 2 and 3.

The work in chapter 2, provides detailed spectroscopic characterization and interprotein cluster transfer studies involving the three major classes of mitochondrial carrier proteins in *At*, namely monothiol GRX, ISCA, and NFU proteins. The objective was to clarify the properties and function of the late-acting ISC proteins in the maturation of plant Fe-S proteins. The results show that i) ISCA1a/2 is able to accommodate either one $[2Fe\text{-}2S]^{2+}$ or one $[4Fe\text{-}4S]^{2+}$ cluster per heterodimer, ii) both NFU4 and NFU5 can assemble one $[4Fe\text{-}4S]^{2+}$ cluster per homodimer, iii) GRXS15 can assemble and efficiently transfer a $[2Fe\text{-}2S]^{2+}$ cluster to the mitochondrial *At* FDX1 protein, iv) $[2Fe\text{-}2S]^{2+}$ cluster-bound GRXS15 can assemble a $[4Fe\text{-}4S]^{2+}$ cluster on the ISCA1a/2 heterodimer, v) $[4Fe\text{-}4S]^{2+}$ cluster-bound ISCA1a/2 can efficiently transfer $[4Fe\text{-}4S]^{2+}$ clusters to NFU4 and NFU5, and vi) $[4Fe\text{-}4S]^{2+}$ cluster-bound ISCA1a/2, NFU4, and NFU5 are all competent tor maturation of apo ACO2.

At NFU2 and *At* HCF101 are both required for the maturation of Fe-S clusters in PSI, but their potential connection has not been investigated *in vitro*. Our working model for the SUF

machinery in plastids is that NFU2 accepts clusters from the $SUFBC_2D$ scaffold complex and then delivers them to HCF101 for the maturation of the three [4Fe-4S] clusters in PS1. Since relatively little has been reported about the properties of HCF101 in the literature, we first present spectroscopic characterization of HCF101, using UV-visible absorption/CD, resonance Raman and EPR, before demonstrating that NFU2 acts upstream of HCF101 for PSI [4Fe-4S] cluster assembly. Plastidial HCF101 was shown to contain a sub-stoichiometric mixture of $[4Fe\text{-}4S]^{2+}$ and linear $[3Fe\text{-}4S]^{1+}$ cluster as purified under anaerobic conditions. However, as-purified HCF101 was converted to a form containing one $[4Fe\text{-}4S]^{2+}$ cluster per monomer after anaerobic Fe-S cluster reconstitution. Nevertheless, the high affinity of HCF101 for binding linear $[3Fe\text{-}4S]^{1+}$ clusters is evident by the observation that $[4Fe\text{-}4S]^{2+}$ cluster transfer from NFU2 to apo HCF101 is a very rapid and unidirectional process, resulting in transient [4Fe-4S]-HCF101, that gradually decays with time to yield linear $[3Fe\text{-}4S]^{1+}$ cluster-bound HCF101. These results, coupled with observation that linear $[3Fe\text{-}4S]^{1+}$ cluster-bound HCF101 is rapidly converted into [4Fe-4S]-HCF101 on addition of Fe^{2+} ions under anaerobic conditions, raise the possibility that that both cluster-bound forms of HCF101 may be present in plastids under dark and light conditions.

Abbreviations

*A. thaliana, At, Arabidopsis thaliana; A. vinelandii., Av, Azotobater vinelandii; B. subtilis, Bs, Bacillus subtili**s;** E. coli, Ec, Escherichia coli; C. pasteurianum, Clostridium pasteurianum; H. sapiens, Hs, Homo sapiens; S. cerevisiae, Sc, Saccharomyces cerevisiae; S. pombe, Spo, Schizosaccharomyces pombe; T. elongatus, Thermosynechococcus elongatus; sp, Synechococcus*; Rd, rubredoxin; Fdx, ferredoxin; NAD(P)H, nicotinamide adenine dinucleotide phosphate (reduced); NHE, normal hydrogen electrode; HCF 101, high chlorophyll fluorescence 101; FRDA, Friedreich's ataxia; Fxn, frataxin gene; MMDS, mitochondrial dysfunction syndromes;

COXPD19, Combined oxidative phosphorylation deficiency 19; XLSA, X-linked sideroblastic anemia, LipA, APR, Adenosine 5'-phosphosulfate reductase; lipoic acid synthase; SDH2, succinate dehydrogenase; PDH, pyruvate dehydrogenase; KGDH, 2-ketoglutarate dehydrogenase; Dx, desulforedoxin; FNR, fumarate-nitrate reduction protein; FTR, ferredoxin–thioredoxin reductase; Grx, glutaredoxin; GSH, glutathione; HDR, heterodisulfide reductases; HiPIP, High potential iron-sulfur protein; IRE, iron-responsive element; IRP, iron regulatory proteins; Rd, rubredoxin; Trx, thioredoxin; WT, wild type; NIF, nitrogen fixation; ISC, iron-sulfur cluster; SUF, sulfur utilization factor; CIA, cytosolic iron sulfur cluster assembly; PSI, Photosystem I; DFT, density functional theory; DTT, dithiothreitol; FAS, ferrous ammonium sulfate; GSH, glutathione; IPTG, isopropyl β–D-1-thiolgalactopyranoside; PEI, Poly(ethyleneimine); PLP, pyridoxal phosphate; SAM, S-Adenosyl methionine; XAS, X-ray absorption spectroscopy; CD, circular dichroism; NMR, nuclear magnetic resonance; EPR, electron paramagnetic resonance; MCD, magnetic circular dichroism; VTMCD, variable temperature magnetic circular dichroism.

References

1. Beinert, H. (2000) Iron-sulfur proteins: Ancient structures, still full of surprises. *J. Biol. Inorg. Chem.* **5**, 2-15
2. Johnson, D. C., Dean, D. R., Smith, A. D., and Johnson, M. K. (2005) Structure, function, and formation of biological iron-sulfur clusters. *Annu. Rev. Biochem.* **74**, 247-281
3. Fuss, J. O., Tsai, C. L., Ishida, J. P., and Tainer, J. A. (2015) Emerging critical roles of Fe-S clusters in DNA replication and repair. *Biochim. Biophys. Acta* **1853**, 1253-1271
4. Jarrett, J. T. (2003) The generation of 5'-deoxyadenosyl radicals by adenosylmethionine-dependent radical enzymes. *Curr. Opin. Chem. Biol.* **7**, 174-182
5. Layer, G., Heinz, D. W., Jahn, D., and Schubert, W. D. (2004) Structure and function of radical SAM enzymes. *Curr. Opin. Chem. Biol.* **8**, 468-476
6. Marsh, E. N., Patwardhan, A., and Huhta, M. S. (2004) S-adenosylmethionine radical enzymes. *Bioorg. Chem.* **32**, 326-340
7. Dai, S., Schwendtmayer, C., Schurmann, P., Ramaswamy, S., and Eklund, H. (2000) Redox signaling in chloroplasts: Cleavage of disulfides by an iron-sulfur cluster. *Science* **287**, 655-658
8. Walters, E. M., and Johnson, M. K. (2004) Ferredoxin:thioredoxin reductase: Disulfide reduction catalyzed via novel site-specific [4Fe-4S] cluster chemistry. *Photosynth Res* **79**, 249-264

9. Hedderich, R., Albracht, S. P., Linder, D., Koch, J., and Thauer, R. K. (1992) Isolation and characterization of polyferredoxin from *Methanobacterium thermoautotrophicum*. The mvhB gene product of the methylviologen-reducing hydrogenase operon. *FEBS Lett.* **298**, 65-68

10. Bandyopadhyay, S., Chandramouli, K., and Johnson, M. K. (2008) Iron-sulfur cluster biosynthesis. *Biochem. Soc. Trans.* **36**, 1112-1119

11. Fontecave, M., Choudens, S. O., Py, B., and Barras, F. (2005) Mechanisms of iron-sulfur cluster assembly: The SUF machinery. *J. Biol. Inorg. Chem.* **10**, 713-721

12. Lill, R., and Muhlenhoff, U. (2006) Iron-sulfur protein biogenesis in eukaryotes: components and mechanisms. *Annu. Rev. Cell Dev. Biol.* **22**, 457-486

13. Koeppen, A. H. (2011) Friedreich's ataxia: Pathology, pathogenesis, and molecular genetics. *J. Neurol. Sci.* **303**, 1-12

14. Stamelou, M. (2016) Late-onset cerebellar ataxia: Do not forget Friedreich's. *Mov. Disord.* **31**, 7-8

15. Harding, A. E. (1981) Friedreich's ataxia: A clinical and genetic study of 90 families with an analysis of early diagnostic criteria and intrafamilial clustering of clinical features. *Brain* **104**, 589-620

16. Martelli, A., Napierala, M., and Puccio, H. (2012) Understanding the genetic and molecular pathogenesis of Friedreich's ataxia through animal and cellular models. *Dis. Model. Mech.* **5**, 165-176

17. Urrutia, P. J., Mena, N. P., and Nunez, M. T. (2014) The interplay between iron accumulation, mitochondrial dysfunction, and inflammation during the execution step of neurodegenerative disorders. *Front. Pharmacol.* **5**, 38

18. Horowitz, M. P., and Greenamyre, J. T. (2010) Mitochondrial iron metabolism and its role in neurodegeneration. *J. Alzheimers Dis.* **20 Suppl 2**, S551-568

19. Lee, D. W., Kaur, D., Chinta, S. J., Rajagopalan, S., and Andersen, J. K. (2009) A disruption in iron-sulfur center biogenesis via inhibition of mitochondrial dithiol glutaredoxin 2 may contribute to mitochondrial and cellular iron dysregulation in mammalian glutathione-depleted dopaminergic cells: Implications for Parkinson's disease. *Antioxid Redox Signal* **11**, 2083-2094

20. Munoz, Y., Carrasco, C. M., Campos, J. D., Aguirre, P., and Nunez, M. T. (2016) Parkinson's Disease: The Mitochondria-Iron Link. *Parkinsons Dis.* **2016**, 7049108

21. Maio, N., and Rouault, T. A. (2015) Iron-sulfur cluster biogenesis in mammalian cells: New insights into the molecular mechanisms of cluster delivery. *Biochim. Biophys. Acta* **1853**, 1493-1512

22. Stehling, O., Wilbrecht, C., and Lill, R. (2014) Mitochondrial iron–sulfur protein biogenesis and human disease. *Biochimie* **100**, 61-77

23. Mochel, F., Knight, M. A., Tong, W. H., Hernandez, D., Ayyad, K., Taivassalo, T., Andersen, P. M., Singleton, A., Rouault, T. A., Fischbeck, K. H., and Haller, R. G. (2008) Splice mutation in the iron-sulfur cluster scaffold protein ISCU causes myopathy with exercise intolerance. *Am. J. Hum. Genet.* **82**, 652-660

24. Olsson, A., Lind, L., Thornell, L. E., and Holmberg, M. (2008) Myopathy with lactic acidosis is linked to chromosome 12q23.3-24.11 and caused by an intron mutation in the ISCU gene resulting in a splicing defect. *Hum. Mol. Genet.* **17**, 1666-1672

25. Schmucker, S., Martelli, A., Colin, F., Page, A., Wattenhofer-Donze, M., Reutenauer, L., and Puccio, H. (2011) Mammalian frataxin: An essential function for cellular viability

through an interaction with a preformed ISCU/NFS1/ISD11 iron-sulfur assembly complex. *PLoS One* **6**, e16199

26. Tong, W. H., and Rouault, T. A. (2006) Functions of mitochondrial ISCU and cytosolic ISCU in mammalian iron-sulfur cluster biogenesis and iron homeostasis. *Cell Metab.* **3**, 199-210

27. Crooks, D. R., Jeong, S. Y., Tong, W. H., Ghosh, M. C., Olivierre, H., Haller, R. G., and Rouault, T. A. (2012) Tissue specificity of a human mitochondrial disease: differentiation-enhanced mis-splicing of the Fe-S scaffold gene ISCU renders patient cells more sensitive to oxidative stress in ISCU myopathy. *J. Biol. Chem.* **287**, 40119-40130

28. Spiegel, R., Saada, A., Halvardson, J., Soiferman, D., Shaag, A., Edvardson, S., Horovitz, Y., Khayat, M., Shalev, S. A., Feuk, L., and Elpeleg, O. (2014) Deleterious mutation in FDX1L gene is associated with a novel mitochondrial muscle myopathy. *Eur. J. Hum. Genet.* **22**, 902-906

29. Ahting, U., Mayr, J. A., Vanlander, A. V., Hardy, S. A., Santra, S., Makowski, C., Alston, C. L., Zimmermann, F. A., Abela, L., Plecko, B., Rohrbach, M., Spranger, S., Seneca, S., Rolinski, B., Hagendorff, A., Hempel, M., Sperl, W., Meitinger, T., Smet, J., Taylor, R. W., Van Coster, R., Freisinger, P., Prokisch, H., and Haack, T. B. (2015) Clinical, biochemical, and genetic spectrum of seven patients with NFU1 deficiency. *Front Genet* **6**, 123

30. Haack, T. B., Rolinski, B., Haberberger, B., Zimmermann, F., Schum, J., Strecker, V., Graf, E., Athing, U., Hoppen, T., Wittig, I., Sperl, W., Freisinger, P., Mayr, J. A., Strom, T. M., Meitinger, T., and Prokisch, H. (2013) Homozygous missense mutation in BOLA3

causes multiple mitochondrial dysfunctions syndrome in two siblings. *J. Inherit. Metab. Dis.* **36**, 55-62

31. Torraco, A., Ardissone, A., Invernizzi, F., Rizza, T., Fiermonte, G., Niceta, M., Zanetti, N., Martinelli, D., Vozza, A., Verrigni, D., Di Nottia, M., Lamantea, E., Diodato, D., Tartaglia, M., Dionisi-Vici, C., Moroni, I., Farina, L., Bertini, E., Ghezzi, D., and Carrozzo, R. (2017) Novel mutations in IBA57 are associated with leukodystrophy and variable clinical phenotypes. *J. Neurol.* **264**, 102-111

32. Al-Hassnan, Z. N., Al-Dosary, M., Alfadhel, M., Faqeih, E. A., Alsagob, M., Kenana, R., Almass, R., Al-Harazi, O. S., Al-Hindi, H., Malibari, O. I., Almutari, F. B., Tulbah, S., Alhadeq, F., Al-Sheddi, T., Alamro, R., AlAsmari, A., Almuntashri, M., Alshaalan, H., Al-Mohanna, F. A., Colak, D., and Kaya, N. (2015) ISCA2 mutation causes infantile neurodegenerative mitochondrial disorder. *J. Med. Genet.* **52**, 186-194

33. Farhan, S. M., Wang, J., Robinson, J. F., Lahiry, P., Siu, V. M., Prasad, C., Kronick, J. B., Ramsay, D. A., Rupar, C. A., and Hegele, R. A. (2014) Exome sequencing identifies NFS1 deficiency in a novel Fe-S cluster disease, infantile mitochondrial complex II/III deficiency. *Mol Genet Genomic Med* **2**, 73-80

34. Lim, S. C., Friemel, M., Marum, J. E., Tucker, E. J., Bruno, D. L., Riley, L. G., Christodoulou, J., Kirk, E. P., Boneh, A., DeGennaro, C. M., Springer, M., Mootha, V. K., Rouault, T. A., Leimkuhler, S., Thorburn, D. R., and Compton, A. G. (2013) Mutations in LYRM4, encoding iron-sulfur cluster biogenesis factor ISD11, cause deficiency of multiple respiratory chain complexes. *Hum. Mol. Genet.* **22**, 4460-4473

35. Saha, P. P., Srivastava, S., Kumar, S. K. P., Sinha, D., and D'Silva, P. (2015) Mapping key residues of ISD11 critical for NFS1-ISD11 subcomplex stability: Implications in the development of mitochondrial disorder, COXPD19. *J. Biol. Chem.* **290**, 25876-25890

36. Okatsu, K., Iemura, S., Koyano, F., Go, E., Kimura, M., Natsume, T., Tanaka, K., and Matsuda, N. (2012) Mitochondrial hexokinase HKI is a novel substrate of the Parkin ubiquitin ligase. *Biochem. Biophys. Res. Commun.* **428**, 197-202

37. Taminelli, G. L., Sotomayor, V., Valdivieso, A. G., Teiber, M. L., Marin, M. C., and Santa-Coloma, T. A. (2008) CISD1 codifies a mitochondrial protein upregulated by the CFTR channel. *Biochem. Biophys. Res. Commun.* **365**, 856-862

38. Tamir, S., Paddock, M. L., Darash-Yahana-Baram, M., Holt, S. H., Sohn, Y. S., Agranat, L., Michaeli, D., Stofleth, J. T., Lipper, C. H., Morcos, F., Cabantchik, I. Z., Onuchic, J. N., Jennings, P. A., Mittler, R., and Nechushtai, R. (2015) Structure-function analysis of NEET proteins uncovers their role as key regulators of iron and ROS homeostasis in health and disease. *Biochim. Biophys. Acta* **1853**, 1294-1315

39. Kusminski, C. M., Holland, W. L., Sun, K., Park, J., Spurgin, S. B., Lin, Y., Askew, G. R., Simcox, J. A., McClain, D. A., Li, C., and Scherer, P. E. (2012) MitoNEET, a key regulator of mitochondrial function and lipid homeostasis. *Nat. Med.* **18**, 1539-1549

40. Fujiwara, T., and Harigae, H. (2013) Pathophysiology and genetic mutations in congenital sideroblastic anemia. *Pediatr. Int.* **55**, 675-679

41. Sato, K., Torimoto, Y., Hosoki, T., Ikuta, K., Takahashi, H., Yamamoto, M., Ito, S., Okamura, N., Ichiki, K., Tanaka, H., Shindo, M., Hirai, K., Mizukami, Y., Otake, T., Fujiya, M., Sasaki, K., and Kohgo, Y. (2011) Loss of ABCB7 gene: Pathogenesis of

mitochondrial iron accumulation in erythroblasts in refractory anemia with ringed sideroblast with isodicentric (X)(q13). *Int. J. Hematol.* **93**, 311-318

42. Camaschella, C., Campanella, A., De Falco, L., Boschetto, L., Merlini, R., Silvestri, L., Levi, S., and Iolascon, A. (2007) The human counterpart of zebrafish shiraz shows sideroblastic-like microcytic anemia and iron overload. *Blood* **110**, 1353-1358

43. Cammack, R. (1992) Iron—sulfur clusters in enzymes: Themes and variations. In: *Adv. Inorg. Chem.*, Cammack, R. ed., Academic Press. pp 281-322.

44. Noodleman, L., and Case, D. A. (1992) Density-functional theory of spin polarization and spin coupling in iron—sulfur clusters. In: *Adv. Inorg. Chem.*, Cammack, R. ed., Academic Press. pp 423-470.

45. Dey, A., Glaser, T., Moura, J. J., Holm, R. H., Hedman, B., Hodgson, K. O., and Solomon, E. I. (2004) Ligand K-edge X-ray absorption spectroscopy and DFT calculations on $[Fe_3S_4]^{0,+}$ clusters: Delocalization, redox, and effect of the protein environment. *J. Am. Chem. Soc.* **126**, 16868-16878

46. Stephens, P. J., Jollie, D. R., and Warshel, A. (1996) Protein control of redox potentials of iron−sulfur proteins. *Chem. Rev.* **96**, 2491-2514

47. Chen, K., Bonagura, C. A., Tilley, G. J., McEvoy, J. P., Jung, Y. S., Armstrong, F. A., Stout, C. D., and Burgess, B. K. (2002) Crystal structures of ferredoxin variants exhibiting large changes in [Fe-S] reduction potential. *Nat. Struct. Biol.* **9**, 188-192

48. Romão, M.J. and Archer, M. (2008) Structural versatility of proteins containing rubredoxin-type centers. In: *Iron Metabolism*, G.C. Ferreira, J.J.G. Moura and R. Franco, eds., Wiley-VCH Verlag, pp 341-358

49. Kurtz, D. M., Jr. and Coulter, E.D. (2001) Bacterial nonheme iron proteins and oxidative stress. *Chemtracts, Inorg. Chem*, 407-435.

50. Johnson, M.K. and Smith, A.D. (2011) Iron–sulfur proteins. In: *Encyclopedia of Inorganic and Bioinorganic Chemistry*, R.A. Scott, ed., John Wiley and Sons.

51. Xiao, Z., Lavery, M. J., Ayhan, M., Scrofani, S. D. B., Wilce, M. C. J., Guss, J. M., Tregloan, P. A., George, G. N., and Wedd, A. G. (1998) The Rubredoxin from *Clostridium pasteurianum*: Mutation of the ion cysteinyl ligands to serine. Crystal and molecular structures of oxidized and dithionite-treated forms of the Cys42Ser mutant. *J. Am. Chem. Soc.* **120**, 4135-4150

52. Link, T. A. (1999) The structures of Rieske and Rieske-type proteins. In: *Advanced Inorganic Chemistry*, Sykes, A. G. ed., Academic Press. pp 83-157.

53. Yankovskaya, V., Horsefield, R., Tornroth, S., Luna-Chavez, C., Miyoshi, H., Leger, C., Byrne, B., Cecchini, G., and Iwata, S. (2003) Architecture of succinate dehydrogenase and reactive oxygen species generation. *Science* **299**, 700-704

54. Hagen, W. R., Silva, P. J., Amorim, M. A., Hagedoorn, P. L., Wassink, H., Haaker, H., and Robb, F. T. (2000) Novel structure and redox chemistry of the prosthetic groups of the iron-sulfur flavoprotein sulfide dehydrogenase from *Pyrococcus furiosus*; evidence for a [2Fe-2S] cluster with $Asp(Cys)_3$ ligands. *J. Biol. Inorg. Chem.* **5**, 527-534

55. Berkovitch, F., Nicolet, Y., Wan, J. T., Jarrett, J. T., and Drennan, C. L. (2004) Crystal structure of biotin synthase, an S-adenosylmethionine-dependent radical enzyme. *Science* **303**, 76-79

56. Hou, X., Liu, R., Ross, S., Smart, E. J., Zhu, H., and Gong, W. (2007) Crystallographic studies of human MitoNEET. *J. Biol. Chem.* **282**, 33242-33246

57. Lin, J., Zhou, T., Ye, K., and Wang, J. (2007) Crystal structure of human mitoNEET reveals distinct groups of iron sulfur proteins. *Proc. Natl. Acad. Sci. U. S. A.* **104**, 14640-14645

58. Paddock, M. L., Wiley, S. E., Axelrod, H. L., Cohen, A. E., Roy, M., Abresch, E. C., Capraro, D., Murphy, A. N., Nechushtai, R., Dixon, J. E., and Jennings, P. A. (2007) MitoNEET is a uniquely folded 2Fe-2S outer mitochondrial membrane protein stabilized by pioglitazone. *Proc. Natl. Acad. Sci. U. S. A.* **104**, 14342-14347

59. Fukuyama, K. (2004) Structure and function of plant-type ferredoxins. *Photosynth Res* **81**, 289-301

60. Meyer, J. (2001) Ferredoxins of the third kind. *FEBS Lett.* **509**, 1-5

61. Rom o, M. J., Archer, M., Moura, I., Moura, J. J. G., LeGall, J., Engh, R., Schneider, M., Hof, P., and Huber, R. (1995) Crystal structure of the xanthine oxidase-related aldehyde oxido-reductase from *D. gigas*. *Science* **270**, 1170-1176

62. Moulis, J. M., Davasse, V., Golinelli, M.-P., Meyer, J., and Quinkal, I. (1996) The coordination sphere of iron-sulfur clusters: lessons from site-directed mutagenesis experiments. *JBIC Journal of Biological Inorganic Chemistry* **1**, 2-14

63. Yeh, A. P., Ambroggio, X. I., Andrade, S. L., Einsle, O., Chatelet, C., Meyer, J., and Rees, D. C. (2002) High resolution crystal structures of the wild type and Cys-55-->Ser and Cys-59-->Ser variants of the thioredoxin-like [2Fe-2S] ferredoxin from *Aquifex aeolicus*. *J. Biol. Chem.* **277**, 34499-34507

64. Munck, E., and Kent, T. A. (1986) Structure and Magnetism of Iron-Sulfur Clusters in Proteins. *Hyperfine Interactions* **27**, 161-172

65. Achim, C., Golinelli, M.-P., Bominaar, E. L., Meyer, J., and Münck, E. (1996) Mössbauer study of Cys56Ser mutant 2Fe ferredoxin from *Clostridium Pasteurianum*: Evidence for double exchange in an $[Fe_2S_2]^+$ cluster. *J. Am. Chem. Soc.* **118**, 8168-8169

66. Breton, J. L., Duff, J. L., Butt, J. N., Armstrong, F. A., George, S. J., Petillot, Y., Forest, E., Schafer, G., and Thomson, A. J. (1995) Identification of the iron-sulfur clusters in a ferredoxin from the archaeon *Sulfolobus acidocaldarius*. Evidence for a reduced [3Fe-4S] cluster with pH-dependent electronic properties. *Eur. J. Biochem.* **233**, 937-946

67. Crouse, B. R., Meyer, J., and Johnson, M. K. (1995) Spectroscopic evidence for a reduced Fe_2S_2 cluster with a $S = 9/2$ ground state in mutant forms of *Clostridium pasteurianum* 2Fe ferredoxin. *J Am Chem Soc* **117**, 9612-9613

68. Subramanian, S., Duin, E. C., Fawcett, S. E., Armstrong, F. A., Meyer, J., and Johnson, M. K. (2015) Spectroscopic and redox studies of valence-delocalized [Fe2S2](+) centers in thioredoxin-like ferredoxins. *J. Am. Chem. Soc.* **137**, 4567-4580

69. Achim, C., Bominaar, E. L., Meyer, J., Peterson, J., and Münck, E. (1999) Observation and interpretation of temperature-dependent valence delocalization in the $[2Fe{-}2S]^+$ cluster of a ferredoxin from *Clostridium pasteurianum*. *J. Am. Chem. Soc.* **121**, 3704-3714

70. Johnson, M. K. D., E. C.; Crouse, B. R.; Golinelli, M.-P.; Meyer, J. . (1998) Valence-delocalized $[Fe_2S_2]^+$ clusters. In Spectroscopic methods in bioinorganic chemistry. in *American Chemical Society* (Solomon, E. I., Hodgson, K. O., Eds.;: Washington, D.C . ed.

71. Beinert, H., Emptage, M. H., Dreyer, J. L., Scott, R. A., Hahn, J. E., Hodgson, K. O., and Thomson, A. J. (1983) Iron-sulfur stoichiometry and structure of iron-sulfur clusters in three-iron proteins: evidence for [3Fe-4S] clusters. *Proc. Natl. Acad. Sci. U. S. A.* **80**, 393-396

72. Ellis, P. J., Conrads, T., Hille, R., and Kuhn, P. (2001) Crystal structure of the 100 kDa Arsenite Oxidase from *Alcaligenes faecalis* in two crystal forms at 1.64 Å and 2.03 Å. *Structure* **9**, 125-132

73. Kennedy, M. C., Kent, T. A., Emptage, M., Merkle, H., Beinert, H., and Munck, E. (1984) Evidence for the formation of a linear [3Fe-4S] cluster in partially unfolded aconitase. *J. Biol. Chem.* **259**, 14463-14471

74. Richards, A. J. M., Thomson, A. J., Holm, R. H., and Hagen, K. S. (1990) The magnetic circular dichroism spectra of the linear trinuclear clusters $[Fe_3S_4(SR)_4]^{3-}$ in purple aconitase and in a synthetic model. *Spectrochimica Acta Part A: Molecular Spectroscopy* **46**, 987-993

75. Zhang, B., Bandyopadhyay, S., Shakamuri, P., Naik, S. G., Huynh, B. H., Couturier, J., Rouhier, N., and Johnson, M. K. (2013) Monothiol glutaredoxins can bind linear $[Fe_3S_4]^{+}$ and $[Fe_4S_4]^{2+}$ clusters in addition to $[Fe_2S_2]^{2+}$ clusters: spectroscopic characterization and functional implications. *J. Am. Chem. Soc.* **135**, 15153-15164

76. Johnson, M. K., Duderstadt, R. E., and Duin, E. C. (1999) Biological and synthetic $[Fe_3S_4]$ clusters. in *Adv. Inorg. Chem.* (Sykes, A. G. ed.), Academic Press. pp 1-82

77. Duff, J. L. C., Breton, J. L. J., Butt, J. N., Armstrong, F. A., and Thomson, A. J. (1996) Novel redox chemistry of [3Fe−4S] clusters: Electrochemical characterization of the All-Fe(II) form of the [3Fe−4S] cluster generated reversibly in various proteins and its

spectroscopic investigation in *Sulfolobus acidocaldarius* ferredoxin. *J. Am. Chem. Soc.* **118**, 8593-8603

78. Beinert, H., Kennedy, M. C., and Stout, C. D. (1996) Aconitase as Iron−Sulfur Protein, Enzyme, and Iron-Regulatory Protein. *Chem. Rev.* **96**, 2335-2374

79. Sanakis, Y., Macedo, A. L., Moura, I., Moura, J. J. G., Papaefthymiou, V., and Münck, E. (2000) Evidence for antisymmetric exchange in cuboidal [3Fe−4S]$^{+}$ clusters. *J. Am. Chem. Soc.* **122**, 11855-11863

80. Sticht, H., and Rösch, P. (1998) The structure of iron–sulfur proteins. *Prog Biophys and Mol Bio*

70, 95-136

81. Volbeda, A., Charon, M. H., Piras, C., Hatchikian, E. C., Frey, M., and Fontecilla-Camps, J. C. (1995) Crystal structure of the nickel-iron hydrogenase from Desulfovibrio gigas. *Nature* **373**, 580-587

82. Peters, J. W. (1998) X-ray Crystal Structure of the Fe-Only Hydrogenase (CpI) from Clostridium pasteurianum to 1.8 Angstrom Resolution. *Science* **282**, 1853-1858

83. Bertero, M. G., Rothery, R. A., Palak, M., Hou, C., Lim, D., Blasco, F., Weiner, J. H., and Strynadka, N. C. (2003) Insights into the respiratory electron transfer pathway from the structure of nitrate reductase A. *Nat. Struct. Biol.* **10**, 681-687

84. Calzolai, L., Gorst, C. M., Zhao, Z. H., Teng, Q., Adams, M. W., and La Mar, G. N. (1995) 1H NMR investigation of the electronic and molecular structure of the four-iron cluster ferredoxin from the hyperthermophile *Pyrococcus furiosus.* Identification of Asp 14 as a cluster ligand in each of the four redox states. *Biochemistry* **34**, 11373-11384

85. Lauble, H., Kennedy, M. C., Beinert, H., and Stout, C. D. (1992) Crystal structures of aconitase with isocitrate and nitroisocitrate bound. *Biochemistry* **31**, 2735-2748

86. Layer, G., Moser, J., Heinz, D. W., Jahn, D., and Schubert, W. D. (2003) Crystal structure of coproporphyrinogen III oxidase reveals cofactor geometry of Radical SAM enzymes. *EMBO J.* **22**, 6214-6224

87. Dauter, Z., Wilson, K. S., Sieker, L. C., Meyer, J., and Moulis, J. M. (1997) Atomic resolution (0.94 A) structure of *Clostridium acidurici* ferredoxin. Detailed geometry of [4Fe-4S] clusters in a protein. *Biochemistry* **36**, 16065-16073

88. Fukuyama, K., Okada, T., Kakuta, Y., and Takahashi, Y. (2002) Atomic resolution structures of oxidized [4Fe-4S] ferredoxin from Bacillus thermoproteolyticus in two crystal forms: systematic distortion of [4Fe-4S] cluster in the protein. *J. Mol. Biol.* **315**, 1155-1166

89. Liu, L., Nogi, T., Kobayashi, M., Nozawa, T., and Miki, K. (2002) Ultrahigh-resolution structure of high-potential iron–sulfur protein from*Thermochromatium tepidum*. *Acta Crystallographica Section D Biological Crystallography* **58**, 1085-1091

90. Parisini, E., Capozzi, F., Lubini, P., Lamzin, V., Luchinat, C., and Sheldrick, G. M. (1999) Ab initio solution and refinement of two high-potential iron protein structures at atomic resolution. *Acta Crystallographica Section D-Biological Crystallography* **55**, 1773-1784

91. Stout, C. D., Stura, E. A., and McRee, D. E. (1998) Structure of Azotobacter vinelandii 7Fe ferredoxin at 1.35 A resolution and determination of the [Fe-S] bonds with 0.01 A accuracy. *J. Mol. Biol.* **278**, 629-639

92. Watt, G. D., and Reddy, K. R. N. (1994) Formation of an all ferrous Fe_4S_4 cluster in the iron protein component of *Azotobacter vinelandii* nitrogenase. *J. Inorg. Biochem.* **53**, 281-294

93. Angove, H. C., Yoo, S. J., Burgess, B. K., and Münck, E. (1997) Mössbauer and EPR evidence for an all-ferrous Fe_4S_4 cluster with $S = 4$ in the Fe protein of nitrogenase. *J. Am. Chem. Soc.* **119**, 8730-8731

94. Torres, R. A., Lovell, T., Noodleman, L., and Case, D. A. (2003) Density functional and reduction potential calculations of Fe4S4 clusters. *J. Am. Chem. Soc.* **125**, 1923-1936

95. Guo, M., Sulc, F., Ribbe, M. W., Farmer, P. J., and Burgess, B. K. (2002) Direct assessment of the reduction potential of the $[4Fe\text{-}4S]^{1+/0}$ couple of the Fe protein from *Azotobacter vinelandii*. *J. Am. Chem. Soc.* **124**, 12100-12101

96. Belinskiy, M., Bertini, I., Galas, O., and Luchinat, C. (1996) An exchange coupling model for the $Fe_4S_4^{3+}$ polymetallic center present in high potential iron-sulfur proteins. *Inorg. Chim. Acta.* **243**, 91-99

97. Noodleman, L., Case, D. A., Mouesca, J. M., and Lamotte, B. (1996) Valence electron delocalization in polynuclear iron-sulfur clusters. *JBIC Journal of Biological Inorganic Chemistry* **1**, 177-182

98. Arendsen, A. F., Hadden, J., Card, G., McAlpine, A. S., Bailey, S., Zaitsev, V., Duke, E. H. M., Lindley, P. F., Kröckel, M., Trautwein, A. X., Feiters, M. C., Charnock, J. M., Garner, C. D., Marritt, S. J., Thomson, A. J., Kooter, I. M., Johnson, M. K., van den Berg, W. A. M., van Dongen, W. M. A. M., and Hagen, W. R. (1998) The "prismane" protein resolved: X-ray structure at 1.7 Å and multiple spectroscopy of two novel 4Fe clusters. *JBIC Journal of Biological Inorganic Chemistry* **3**, 81-95

99. Duderstadt, R. E., Brereton, P. S., Adams, M. W. W., and Johnson, M. K. (1999) A pure *S*=3/2 $[Fe_4S_4]^+$ cluster in the A33Y variant of *Pyrococcus furiosus* ferredoxin. *FEBS Lett.* **454**, 21-26

100. Koehler, B. P., Mukund, S., Conover, R. C., Dhawan, I. K., Roy, R., Adams, M. W. W., and Johnson, M. K. (1996) Spectroscopic characterization of the tungsten and iron centers in aldehyde ferredoxin oxidoreductases from two hyperthermophilic archaea. *J. Am. Chem. Soc.* **118**, 12391-12405

101. Yoo, S. J., Angove, H. C., Burgess, B. K., Hendrich, M. P., and Münck, E. (1999) Mössbauer and integer-spin EPR studies and spin-coupling analysis of the $[4Fe\text{-}4S]^0$ cluster of the Fe protein from *Azotobacter vinelandii* nitrogenase. *J. Am. Chem. Soc.* **121**, 2534-2545

102. Schindelin, H., Kisker, C., Schlessman, J. L., Howard, J. B., and Rees, D. C. (1997) Structure of ADP x AIF4(-)-stabilized nitrogenase complex and its implications for signal transduction. *Nature* **387**, 370-376

103. Mobitz, H., Friedrich, T., and Boll, M. (2004) Substrate binding and reduction of benzoyl-CoA reductase: evidence for nucleotide-dependent conformational changes. *Biochemistry* **43**, 1376-1385

104. Nicolet, Y., Cavazza, C., and Fontecilla-Camps, J. C. (2002) Fe-only hydrogenases: structure, function and evolution. *J. Inorg. Biochem.* **91**, 1-8

105. Doukov, T. I., Iverson, T. M., Seravalli, J., Ragsdale, S. W., and Drennan, C. L. (2002) A Ni-Fe-Cu center in a bifunctional carbon monoxide dehydrogenase/acetyl-CoA synthase. *Science* **298**, 567-572

106. Darnault, C., Volbeda, A., Kim, E. J., Legrand, P., Vernede, X., Lindahl, P. A., and Fontecilla-Camps, J. C. (2003) Ni-Zn-[Fe4-S4] and Ni-Ni-[Fe4-S4] clusters in closed and open subunits of acetyl-CoA synthase/carbon monoxide dehydrogenase. *Nat. Struct. Biol.* **10**, 271-279

107. Svetlitchnyi, V., Dobbek, H., Meyer-Klaucke, W., Meins, T., Thiele, B., Romer, P., Huber, R., and Meyer, O. (2004) A functional Ni-Ni-[4Fe-4S] cluster in the monomeric acetyl-CoA synthase from *Carboxydothermus hydrogenoformans*. *Proc. Natl. Acad. Sci. U. S. A.* **101**, 446-451

108. Flint, D. H., and Allen, R. M. (1996) Iron-sulfur proteins with nonredox functions. *Chem. Rev.* **96**, 2315-2334

109. Sofia, H. J., Chen, G., Hetzler, B. G., Reyes-Spindola, J. F., and Miller, N. E. (2001) Radical SAM, a novel protein superfamily linking unresolved steps in familiar biosynthetic pathways with radical mechanisms: functional characterization using new analysis and information visualization methods. *Nucleic Acids Res.* **29**, 1097-1106

110. Walsby, C. J., Hong, W., Broderick, W. E., Cheek, J., Ortillo, D., Broderick, J. B., and Hoffman, B. M. (2002) Electron-nuclear double resonance spectroscopic evidence that S-Adenosylmethionine binds in contact with the catalytically active $[4Fe{-}4S]^{+}$ cluster of pyruvate formate-lyase activating enzyme. *J. Am. Chem. Soc.* **124**, 3143-3151

111. Kiley, P. J., and Beinert, H. (1998) Oxygen sensing by the global regulator, FNR: the role of the iron-sulfur cluster. *FEMS Microbiol. Rev.* **22**, 341-352

112. Bates, D. M., Popescu, C. V., Khoroshilova, N., Vogt, K., Beinert, H., Munck, E., and Kiley, P. J. (2000) Substitution of leucine 28 with histidine in the *Escherichia coli*

transcription factor FNR results in increased stability of the [4Fe-4S]$^{2+}$ cluster to oxygen. *J. Biol. Chem.* **275**, 6234-6240

113. Popescu, C. V., Bates, D. M., Beinert, H., Münck, E., and Kiley, P. J. (1998) Mössbauer spectroscopy as a tool for the study of activation/inactivation of the transcription regulator FNR in whole cells of Escherichia coli. *Proc. Natl. Acad. Sci. U. S. A.* **95**, 13431-13435

114. Crack, J. C., Green, J., Le Brun, N. E., and Thomson, A. J. (2006) Detection of sulfide release from the oxygen-sensing [4Fe-4S] cluster of FNR. *J. Biol. Chem.* **281**, 18909-18913

115. Cruz-Ramos, H., Crack, J., Wu, G., Hughes, M. N., Scott, C., Thomson, A. J., Green, J., and Poole, R. K. (2002) NO sensing by FNR: Regulation of the *Escherichia coli* NO-detoxifying flavohaemoglobin, Hmp. *EMBO J.* **21**, 3235-3244

116. Demple, B., Ding, H., and Jorgensen, M. (2002) [35] *Escherichia coli* SoxR protein: Sensor/transducer of oxidative stress and nitric oxide. in *Methods Enzymol.* (Sies, H., and Packer, L. eds.), Academic Press. pp 355-364

117. Gaudu, P., and Weiss, B. (1996) SoxR, a [2Fe-2S] transcription factor, is active only in its oxidized form. *Proc. Natl. Acad. Sci. U. S. A.* **93**, 10094-10098

118. Ding, H., and Demple, B. (1997) *In vivo* kinetics of a redox-regulated transcriptional switch. *Proc. Natl. Acad. Sci. U. S. A.* **94**, 8445-8449

119. Ding, H., and Demple, B. (2000) Direct nitric oxide signal transduction via nitrosylation of iron-sulfur centers in the SoxR transcription activator. *Proc. Natl. Acad. Sci. U. S. A.* **97**, 5146-5150

120. Schwartz, C. J., Giel, J. L., Patschkowski, T., Luther, C., Ruzicka, F. J., Beinert, H., and Kiley, P. J. (2001) IscR, an Fe-S cluster-containing transcription factor, represses expression of *Escherichia coli* genes encoding Fe-S cluster assembly proteins. *Proc. Natl. Acad. Sci. U. S. A.* **98**, 14895-14900

121. Yeo, W. S., Lee, J. H., Lee, K. C., and Roe, J. H. (2006) IscR acts as an activator in response to oxidative stress for the suf operon encoding Fe-S assembly proteins. *Mol. Microbiol.* **61**, 206-218

122. Giel, J. L., Rodionov, D., Liu, M., Blattner, F. R., and Kiley, P. J. (2006) IscR-dependent gene expression links iron-sulphur cluster assembly to the control of O2-regulated genes in Escherichia coli. *Mol. Microbiol.* **60**, 1058-1075

123. Kiley, P. J., and Beinert, H. (2003) The role of Fe–S proteins in sensing and regulation in bacteria. *Curr. Opin. Microbiol.* **6**, 181-185

124. Walden, W. E., Selezneva, A. I., Dupuy, J., Volbeda, A., Fontecilla-Camps, J. C., Theil, E. C., and Volz, K. (2006) Structure of dual function iron regulatory protein 1 complexed with ferritin IRE-RNA. *Science* **314**, 1903-1908

125. Wallander, M. L., Leibold, E. A., and Eisenstein, R. S. (2006) Molecular control of vertebrate iron homeostasis by iron regulatory proteins. *Biochim. Biophys. Acta* **1763**, 668-689

126. Alen, C., and Sonenshein, A. L. (1999) *Bacillus subtilis* aconitase is an RNA-binding protein. *Proc. Natl. Acad. Sci. U. S. A.* **96**, 10412-10417

127. Tang, Y., and Guest, J. R. (1999) Direct evidence for mRNA binding and post-transcriptional regulation by Escherichia coli aconitases. *Microbiology* **145 (Pt 11)**, 3069-3079

128. Tang, Y., Quail, M. A., Artymiuk, P. J., Guest, J. R., and Green, J. (2002) Escherichia coli aconitases and oxidative stress: post-transcriptional regulation of sodA expression. *Microbiology* **148**, 1027-1037

129. Tang, Y., Guest, J. R., Artymiuk, P. J., Read, R. C., and Green, J. (2004) Post-transcriptional regulation of bacterial motility by aconitase proteins. *Mol. Microbiol.* **51**, 1817-1826

130. Smith, J. L., Zaluzec, E. J., Wery, J. P., Niu, L., Switzer, R. L., Zalkin, H., and Satow, Y. (1994) Structure of the allosteric regulatory enzyme of purine biosynthesis. *Science* **264**, 1427-1433

131. Grandoni, J. A., Switzer, R. L., Makaroff, C. A., and Zalkin, H. (1989) Evidence that the iron-sulfur cluster of *Bacillus subtilis* glutamine phosphoribosylpyrophosphate amidotransferase determines stability of the enzyme to degradation *in vivo*. *J. Biol. Chem.* **264**, 6058-6064

132. Sellers, V. M., Johnson, M. K., and Dailey, H. A. (1996) Function of the [2FE-2S] cluster in mammalian ferrochelatase: a possible role as a nitric oxide sensor. *Biochemistry* **35**, 2699-2704

133. Dailey, H. A., Finnegan, M. G., and Johnson, M. K. (1994) Human ferrochelatase is an iron-sulfur protein. *Biochemistry* **33**, 403-407

134. Ferreira, G. C., Franco, R., Lloyd, S. G., Pereira, A. S., Moura, I., Moura, J. J., and Huynh, B. H. (1994) Mammalian ferrochelatase, a new addition to the metalloenzyme family. *J. Biol. Chem.* **269**, 7062-7065

135. Wu, C. K., Dailey, H. A., Rose, J. P., Burden, A., Sellers, V. M., and Wang, B. C. (2001) The 2.0 A structure of human ferrochelatase, the terminal enzyme of heme biosynthesis. *Nat. Struct. Biol.* **8**, 156-160

136. Dailey, T. A., and Dailey, H. A. (2002) Identification of [2Fe-2S] clusters in microbial ferrochelatases. *J. Bacteriol.* **184**, 2460-2464

137. Albetel, A. N. (2012) Role and spectroscopic characterization of [2Fe-2S] centers in perrochelatases. *Ph. D.Thesis*

138. Walters, E. M., Garcia-Serres, R., Jameson, G. N., Glauser, D. A., Bourquin, F., Manieri, W., Schurmann, P., Johnson, M. K., and Huynh, B. H. (2005) Spectroscopic characterization of site-specific [Fe(4)S(4)] cluster chemistry in ferredoxin:thioredoxin reductase: implications for the catalytic mechanism. *J. Am. Chem. Soc.* **127**, 9612-9624

139. Watanabe, S., Matsumi, R., Arai, T., Atomi, H., Imanaka, T., and Miki, K. (2007) Crystal structures of [NiFe] hydrogenase maturation proteins HypC, HypD, and HypE: insights into cyanation reaction by thiol redox signaling. *Mol. Cell* **27**, 29-40

140. Duin, E. C., Madadi-Kahkesh, S., Hedderich, R., Clay, M. D., and Johnson, M. K. (2002) Heterodisulfide reductase from Methanothermobacter marburgensis contains an active-site [4Fe-4S] cluster that is directly involved in mediating heterodisulfide reduction. *FEBS Lett.* **512**, 263-268

141. Wagner, T., Koch, J., Ermler, U., and Shima, S. (2017) Methanogenic heterodisulfide reductase (HdrABC-MvhAGD) uses two noncubane [4Fe-4S] clusters for reduction. *Science* **357**, 699-703

142. Thauer, R. K. S., P. (1982) Iron-sulfur complexes of ferredoxin as a storage form of iron in Clostridium pasteurianum. In Iron-Sulfur Proteins, Spiro, T. G., Ed.; . *Wiley: New York*, 329-341

143. Reeve, J. N., Beckler, G. S., Cram, D. S., Hamilton, P. T., Brown, J. W., Krzycki, J. A., Kolodziej, A. F., Alex, L., Orme-Johnson, W. H., and Walsh, C. T. (1989) A hydrogenase-linked gene in *Methanobacterium thermoautotrophicum* strain delta H encodes a polyferredoxin. *Proc. Natl. Acad. Sci. U. S. A.* **86**, 3031-3035

144. Vorholt, J. A., Vaupel, M., and Thauer, R. K. (1996) A polyferredoxin with eight [4Fe-4S] clusters as a subunit of molybdenum formylmethanofuran dehydrogenase from *Methanosarcina barkeri*. *Eur. J. Biochem.* **236**, 309-317

145. Boal, A. K., Yavin, E., and Barton, J. K. (2007) DNA repair glycosylases with a [4Fe-4S] cluster: A redox cofactor for DNA-mediated charge transport? *J. Inorg. Biochem.* **101**, 1913-1921

146. Boal, A. K., Genereux, J. C., Sontz, P. A., Gralnick, J. A., Newman, D. K., and Barton, J. K. (2009) Redox signaling between DNA repair proteins for efficient lesion detection. *Proc. Natl. Acad. Sci. U. S. A.* **106**, 15237-15242

147. Hinks, J. A., Evans, M. C., De Miguel, Y., Sartori, A. A., Jiricny, J., and Pearl, L. H. (2002) An iron-sulfur cluster in the family 4 uracil-DNA glycosylases. *J. Biol. Chem.* **277**, 16936-16940

148. White, M. F. (2003) Archaeal DNA repair: Paradigms and puzzles. *Biochem. Soc. Trans.* **31**, 690-693

149. Rudolf, J., Makrantoni, V., Ingledew, W. J., Stark, M. J., and White, M. F. (2006) The DNA repair helicases XPD and FancJ have essential iron-sulfur domains. *Mol. Cell* **23**, 801-808

150. White, M. F. (2009) Structure, function and evolution of the XPD family of iron-sulfur-containing 5'-->3' DNA helicases. *Biochem. Soc. Trans.* **37**, 547-551

151. Tse Sum Bui, B., Florentin, D., Fournier, F., Ploux, O., Méjean, A., and Marquet, A. (1998) Biotin synthase mechanism: On the origin of sulphur. *FEBS Lett.* **440**, 226-230

152. Jameson, G. N., Cosper, M. M., Hernandez, H. L., Johnson, M. K., and Huynh, B. H. (2004) Role of the [2Fe-2S] cluster in recombinant *Escherichia coli* biotin synthase. *Biochemistry* **43**, 2022-2031

153. Cicchillo, R. M., Lee, K. H., Baleanu-Gogonea, C., Nesbitt, N. M., Krebs, C., and Booker, S. J. (2004) *Escherichia coli* lipoyl synthase binds two distinct [4Fe-4S] clusters per polypeptide. *Biochemistry* **43**, 11770-11781

154. Hernandez, H. L., Pierrel, F., Elleingand, E., Garcia-Serres, R., Huynh, B. H., Johnson, M. K., Fontecave, M., and Atta, M. (2007) MiaB, a bifunctional radical-S-adenosylmethionine enzyme involved in the thiolation and methylation of tRNA, contains two essential [4Fe-4S] clusters. *Biochemistry* **46**, 5140-5147

155. Hanzelmann, P., Hernandez, H. L., Menzel, C., Garcia-Serres, R., Huynh, B. H., Johnson, M. K., Mendel, R. R., and Schindelin, H. (2004) Characterization of MOCS1A, an oxygen-sensitive iron-sulfur protein involved in human molybdenum cofactor biosynthesis. *J. Biol. Chem.* **279**, 34721-34732

156. Kent, T. A., Dreyer, J. L., Kennedy, M. C., Huynh, B. H., Emptage, M. H., Beinert, H., and Munck, E. (1982) Mossbauer studies of beef heart aconitase: evidence for facile interconversions of iron-sulfur clusters. *Proc. Natl. Acad. Sci. U. S. A.* **79**, 1096-1100

157. Butt, J. N., Armstrong, F. A., Breton, J., George, S. J., Thomson, A. J., and Hatchikian, E. C. (1991) Investigation of metal ion uptake reactivities of [3Fe-4S] clusters in proteins: voltammetry of co-adsorbed ferredoxin-aminocyclitol films at graphite electrodes and spectroscopic identification of transformed clusters. *J. Am. Chem. Soc.* **113**, 6663-6670

158. Finnegan, M. G., Conover, R. C., Park, J.-B., Zhou, Z. H., Adams, M. W. W., and Johnson, M. K. (1995) Electronic, magnetic, redox, and ligand-binding properties of [MFe_3S_4] clusters (M = Zn, Co, Mn) in *Pyrococcus furiosus* ferredoxin. *Inorg. Chem.* **34**, 5358-5369

159. Plank, D. W., Kennedy, M. C., Beinert, H., and Howard, J. B. (1989) Cysteine labeling studies of beef heart aconitase containing a 4Fe, a cubane 3Fe, or a linear 3Fe cluster. *J. Biol. Chem.* **264**, 20385-20393

160. Zhang, B., Crack, J. C., Subramanian, S., Green, J., Thomson, A. J., Le Brun, N. E., and Johnson, M. K. (2012) Reversible cycling between cysteine persulfide-ligated [2Fe-2S] and cysteine-ligated [4Fe-4S] clusters in the FNR regulatory protein. *Proc. Natl. Acad. Sci. U. S. A.* **109**, 15734-15739

161. Anderson, G. L., and Howard, J. B. (1984) Reactions with the oxidized iron protein of *Azotobacter vinelandii* nitrogenase: formation of a 2Fe center. *Biochemistry* **23**, 2118-2122

162. Ryle, M. J., Lanzilotta, W. N., Seefeldt, L. C., Scarrow, R. C., and Jensen, G. M. (1996) Circular dichroism and x-ray spectroscopies of Azotobacter vinelandii nitrogenase iron protein. MgATP and MgADP induced protein conformational changes affecting the [4Fe-4S] cluster and characterization of a [2Fe-2S] form. *J. Biol. Chem.* **271**, 1551-1557

163. Sen, S., Igarashi, R., Smith, A., Johnson, M. K., Seefeldt, L. C., and Peters, J. W. (2004) A conformational mimic of the MgATP-bound "on state" of the nitrogenase iron protein. *Biochemistry* **43**, 1787-1797

164. Agar, J. N., Krebs, C., Frazzon, J., Huynh, B. H., Dean, D. R., and Johnson, M. K. (2000) IscU as a scaffold for iron−sulfur cluster biosynthesis: Sequential assembly of [2Fe-2S] and [4Fe-4S] clusters in IscU†. *Biochemistry* **39**, 7856-7862

165. Chandramouli, K., Unciuleac, M. C., Naik, S., Dean, D. R., Huynh, B. H., and Johnson, M. K. (2007) Formation and properties of [4Fe-4S] clusters on the IscU scaffold protein. *Biochemistry* **46**, 6804-6811

166. Smith, A. D., Jameson, G. N., Dos Santos, P. C., Agar, J. N., Naik, S., Krebs, C., Frazzon, J., Dean, D. R., Huynh, B. H., and Johnson, M. K. (2005) NifS-mediated assembly of [4Fe-4S] clusters in the N- and C-terminal domains of the NifU scaffold protein. *Biochemistry* **44**, 12955-12969

167. Wächtershäuser, G. (1992) Groundworks for an evolutionary biochemistry: The iron-sulphur world. *Prog. Biophys. Mol. Biol.* **58**, 85-201

168. Huber, C., and Wachtershauser, G. (1997) Activated acetic acid by carbon fixation on (Fe,Ni)S under primordial conditions. *Science* **276**, 245-247

169. Huber, C., and Wachtershauser, G. (1998) Peptides by activation of amino acids with CO on (Ni,Fe)S surfaces: implications for the origin of life. *Science* **281**, 670-672

170. Imlay, J. A. (2006) Iron-sulphur clusters and the problem with oxygen. *Mol. Microbiol.* **59**, 1073-1082

171. Malkin, R., and Rabinowitz, J. C. (1966) The reconstitution of clostridial ferredoxin. *Biochem. Biophys. Res. Commun.* **23**, 822-827

172. Munday, R. (1989) Toxicity of thiols and disulphides: involvement of free-radical species. *Free Radic. Biol. Med.* **7**, 659-673

173. Müller, C., Kuki, K. N., Pinheiro, D. T., de Souza, L. R., Siqueira Silva, A. I., Loureiro, M. E., Oliva, M. A., and Almeida, A. M. (2015) Differential physiological responses in rice upon exposure to excess distinct iron forms. *Plant and Soil* **391**, 123-138

174. Couturier, J., Touraine, B., Briat, J. F., Gaymard, F., and Rouhier, N. (2013) The iron-sulfur cluster assembly machineries in plants: current knowledge and open questions. *Front Plant Sci* **4**, 259

175. Lill, R., and Muhlenhoff, U. (2008) Maturation of iron-sulfur proteins in eukaryotes: mechanisms, connected processes, and diseases. *Annu. Rev. Biochem.* **77**, 669-700

176. Lill, R., Hoffmann, B., Molik, S., Pierik, A. J., Rietzschel, N., Stehling, O., Uzarska, M. A., Webert, H., Wilbrecht, C., and Muhlenhoff, U. (2012) The role of mitochondria in cellular iron-sulfur protein biogenesis and iron metabolism. *Biochim. Biophys. Acta* **1823**, 1491-1508

177. Braymer, J. J., and Lill, R. (2017) Iron-sulfur cluster biogenesis and trafficking in mitochondria. *J. Biol. Chem.* **292**, 12754-12763

178. Balk, J., and Schaedler, T. A. (2014) Iron cofactor assembly in plants. *Annu. Rev. Plant Biol.* **65**, 125-153

179. Frazzon, A. P., Ramirez, M. V., Warek, U., Balk, J., Frazzon, J., Dean, D. R., and Winkel, B. S. (2007) Functional analysis of *Arabidopsis* genes involved in mitochondrial iron-sulfur cluster assembly. *Plant Mol. Biol.* **64**, 225-240

180. Leon, S., Touraine, B., Briat, J. F., and Lobreaux, S. (2005) Mitochondrial localization of *Arabidopsis thaliana* Isu Fe-S scaffold proteins. *FEBS Lett.* **579**, 1930-1934

181. Van Vranken, J. G., Jeong, M. Y., Wei, P., Chen, Y. C., Gygi, S. P., Winge, D. R., and Rutter, J. (2016) The mitochondrial acyl carrier protein (ACP) coordinates mitochondrial fatty acid synthesis with iron sulfur cluster biogenesis. *eLife* **5**, e17828

182. Xu, X. M., and Moller, S. G. (2006) AtSufE is an essential activator of plastidic and mitochondrial desulfurases in Arabidopsis. *EMBO J.* **25**, 900-909

183. Ye, H., Abdel-Ghany, S. E., Anderson, T. D., Pilon-Smits, E. A., and Pilon, M. (2006) CpSufE activates the cysteine desulfurase CpNifS for chloroplastic Fe-S cluster formation. *J. Biol. Chem.* **281**, 8958-8969

184. Chandramouli, K., and Johnson, M. K. (2006) HscA and HscB stimulate [2Fe-2S] cluster transfer from IscU to apoferredoxin in an ATP-dependent reaction. *Biochemistry* **45**, 11087-11095

185. Shakamuri, P., Zhang, B., and Johnson, M. K. (2012) Monothiol glutaredoxins function in storing and transporting [Fe2S2] clusters assembled on IscU scaffold proteins. *J. Am. Chem. Soc.* **134**, 15213-15216

186. Uzarska, M. A., Dutkiewicz, R., Freibert, S. A., Lill, R., and Muhlenhoff, U. (2013) The mitochondrial Hsp70 chaperone Ssq1 facilitates Fe/S cluster transfer from Isu1 to Grx5 by complex formation. *Mol. Biol. Cell* **24**, 1830-1841

187. Xu, X. M., Lin, H., Latijnhouwers, M., and Moller, S. G. (2009) Dual localized AtHscB involved in iron sulfur protein biogenesis in *Arabidopsis*. *PLoS One* **4**, e7662

188. Heazlewood, J. L., Tonti-Filippini, J. S., Gout, A. M., Day, D. A., Whelan, J., and Millar, A. H. (2004) Experimental analysis of the *Arabidopsis* mitochondrial proteome highlights signaling and regulatory components, provides assessment of targeting prediction programs, and indicates plant-specific mitochondrial proteins. *Plant Cell* **16**, 241-256

189. Moseler, A., Aller, I., Wagner, S., Nietzel, T., Przybyla-Toscano, J., Muhlenhoff, U., Lill, R., Berndt, C., Rouhier, N., Schwarzlander, M., and Meyer, A. J. (2015) The mitochondrial monothiol glutaredoxin S15 is essential for iron-sulfur protein maturation in Arabidopsis thaliana. *Proc. Natl. Acad. Sci. U. S. A.* **112**, 13735-13740

190. Johansson, C., Roos, A. K., Montano, S. J., Sengupta, R., Filippakopoulos, P., Guo, K., von Delft, F., Holmgren, A., Oppermann, U., and Kavanagh, K. L. (2011) The crystal structure of human GLRX5: iron-sulfur cluster co-ordination, tetrameric assembly and monomer activity. *Biochem. J.* **433**, 303-311

191. Rodriguez-Manzaneque, M. T., Tamarit, J., Belli, G., Ros, J., and Herrero, E. (2002) Grx5 is a mitochondrial glutaredoxin required for the activity of iron/sulfur enzymes. *Mol. Biol. Cell* **13**, 1109-1121

192. Rodriguez-Manzaneque, M. T., Ros, J., Cabiscol, E., Sorribas, A., and Herrero, E. (1999) Grx5 glutaredoxin plays a central role in protection against protein oxidative damage in Saccharomyces cerevisiae. *Mol. Cell. Biol.* **19**, 8180-8190

193. Ye, H., Jeong, S. Y., Ghosh, M. C., Kovtunovych, G., Silvestri, L., Ortillo, D., Uchida, N., Tisdale, J., Camaschella, C., and Rouault, T. A. (2010) Glutaredoxin 5 deficiency

causes sideroblastic anemia by specifically impairing heme biosynthesis and depleting cytosolic iron in human erythroblasts. *J. Clin. Invest.* **120**, 1749-1761

194. Sheftel, A. D., Wilbrecht, C., Stehling, O., Niggemeyer, B., Elsasser, H. P., Muhlenhoff, U., and Lill, R. (2012) The human mitochondrial ISCA1, ISCA2, and IBA57 proteins are required for [4Fe-4S] protein maturation. *Mol. Biol. Cell* **23**, 1157-1166

195. Gelling, C., Dawes, I. W., Richhardt, N., Lill, R., and Muhlenhoff, U. (2008) Mitochondrial Iba57p is required for Fe/S cluster formation on aconitase and activation of radical SAM enzymes. *Mol. Cell. Biol.* **28**, 1851-1861

196. Waller, J. C., Ellens, K. W., Alvarez, S., Loizeau, K., Ravanel, S., and Hanson, A. D. (2012) Mitochondrial and plastidial COG0354 proteins have folate-dependent functions in iron-sulphur cluster metabolism. *J Exp Bot* **63**, 403-411

197. Brancaccio, D., Gallo, A., Mikolajczyk, M., Zovo, K., Palumaa, P., Novellino, E., Piccioli, M., Ciofi-Baffoni, S., and Banci, L. (2014) Formation of [4Fe-4S] clusters in the mitochondrial iron-sulfur cluster assembly machinery. *J. Am. Chem. Soc.* **136**, 16240-16250

198. Mapolelo, D. T., Zhang, B., Naik, S. G., Huynh, B. H., and Johnson, M. K. (2012) Spectroscopic and functional characterization of iron-sulfur cluster-bound forms of Azotobacter vinelandii (Nif)IscA. *Biochemistry* **51**, 8071-8084

199. Agar, J. N., Yuvaniyama, P., Jack, R. F., Cash, V. L., Smith, A. D., Dean, D. R., and Johnson, M. K. (2000) Modular organization and identification of a mononuclear iron-binding site within the NifU protein. *JBIC Journal of Biological Inorganic Chemistry* **5**, 167-177

200. Morimoto, K., Yamashita, E., Kondou, Y., Lee, S. J., Arisaka, F., Tsukihara, T., and Nakai, M. (2006) The asymmetric IscA homodimer with an exposed [2Fe-2S] cluster suggests the structural basis of the Fe-S cluster biosynthetic scaffold. *J. Mol. Biol.* **360**, 117-132

201. Ciofi-Baffoni, S., Nasta, V., and Banci, L. (2018) Protein networks in the maturation of human iron-sulfur proteins. *Metallomics* **10**, 49-72

202. Beilschmidt, L. K., Ollagnier de Choudens, S., Fournier, M., Sanakis, I., Hograindleur, M. A., Clemancey, M., Blondin, G., Schmucker, S., Eisenmann, A., Weiss, A., Koebel, P., Messaddeq, N., Puccio, H., and Martelli, A. (2017) ISCA1 is essential for mitochondrial Fe4S4 biogenesis in vivo. *Nat Commun* **8**, 15124

203. Tong, W. H., Jameson, G. N., Huynh, B. H., and Rouault, T. A. (2003) Subcellular compartmentalization of human Nfu, an iron-sulfur cluster scaffold protein, and its ability to assemble a [4Fe-4S] cluster. *Proc. Natl. Acad. Sci. U. S. A.* **100**, 9762-9767

204. Navarro-Sastre, A., Tort, F., Stehling, O., Uzarska, M. A., Arranz, J. A., Del Toro, M., Labayru, M. T., Landa, J., Font, A., Garcia-Villoria, J., Merinero, B., Ugarte, M., Gutierrez-Solana, L. G., Campistol, J., Garcia-Cazorla, A., Vaquerizo, J., Riudor, E., Briones, P., Elpeleg, O., Ribes, A., and Lill, R. (2011) A fatal mitochondrial disease is associated with defective NFU1 function in the maturation of a subset of mitochondrial Fe-S proteins. *Am. J. Hum. Genet.* **89**, 656-667

205. Cameron, J. M., Janer, A., Levandovskiy, V., Mackay, N., Rouault, T. A., Tong, W. H., Ogilvie, I., Shoubridge, E. A., and Robinson, B. H. (2011) Mutations in iron-sulfur cluster scaffold genes NFU1 and BOLA3 cause a fatal deficiency of multiple respiratory chain and 2-oxoacid dehydrogenase enzymes. *Am. J. Hum. Genet.* **89**, 486-495

206. Bych, K., Kerscher, S., Netz, D. J., Pierik, A. J., Zwicker, K., Huynen, M. A., Lill, R., Brandt, U., and Balk, J. (2008) The iron-sulphur protein Ind1 is required for effective complex I assembly. *EMBO J.* **27**, 1736-1746

207. Melber, A., Na, U., Vashisht, A., Weiler, B. D., Lill, R., Wohlschlegel, J. A., and Winge, D. R. (2016) Role of Nfu1 and Bol3 in iron-sulfur cluster transfer to mitochondrial clients. *Elife* **5**, e15991

208. Gao, H., Subramanian, S., Couturier, J., Naik, S. G., Kim, S. K., Leustek, T., Knaff, D. B., Wu, H. C., Vignols, F., Huynh, B. H., Rouhier, N., and Johnson, M. K. (2013) *Arabidopsis thaliana* Nfu2 accommodates [2Fe-2S] or [4Fe-4S] clusters and is competent for *in vitro* maturation of chloroplast [2Fe-2S] and [4Fe-4S] cluster-containing proteins. *Biochemistry* **52**, 6633-6645

209. Cai, K., Liu, G., Frederick, R. O., Xiao, R., Montelione, G. T., and Markley, J. L. (2016) Structural/functional properties of human NFU1, an intermediate [4Fe-4S] carrier in human mitochondrial iron-sulfur cluster biogenesis. *Structure* **24**, 2080-2091

210. Takahashi, Y., and Tokumoto, U. (2002) A third bacterial system for the assembly of iron-sulfur clusters with homologs in archaea and plastids. *J. Biol. Chem.* **277**, 28380-28383

211. Balk, J., and Lobreaux, S. (2005) Biogenesis of iron-sulfur proteins in plants. *Trends Plant Sci* **10**, 324-331

212. Pilon-Smits, E. A., Garifullina, G. F., Abdel-Ghany, S., Kato, S., Mihara, H., Hale, K. L., Burkhead, J. L., Esaki, N., Kurihara, T., and Pilon, M. (2002) Characterization of a NifS-like chloroplast protein from *Arabidopsis*. Implications for its role in sulfur and selenium metabolism. *Plant Physiol.* **130**, 1309-1318

213. Hu, X., Kato, Y., Sumida, A., Tanaka, A., and Tanaka, R. (2017) The SUFBC2 D complex is required for the biogenesis of all major classes of plastid Fe-S proteins. *Plant J.* **90**, 235-248

214. Xu, X. M., Adams, S., Chua, N. H., and Moller, S. G. (2005) AtNAP1 represents an atypical SufB protein in *Arabidopsis* plastids. *J. Biol. Chem.* **280**, 6648-6654

215. Nagane, T., Tanaka, A., and Tanaka, R. (2010) Involvement of AtNAP1 in the regulation of chlorophyll degradation in *Arabidopsis thaliana*. *Planta* **231**, 939-949

216. Hjorth, E., Hadfi, K., Zauner, S., and Maier, U. G. (2005) Unique genetic compartmentalization of the SUF system in cryptophytes and characterization of a SufD mutant in *Arabidopsis thaliana*. *FEBS Lett.* **579**, 1129-1135

217. Marinoni, E. N., de Oliveira, J. S., Nicolet, Y., Raulfs, E. C., Amara, P., Dean, D. R., and Fontecilla-Camps, J. C. (2012) $(IscS\text{-}IscU)_2$ complex structures provide insights into Fe_2S_2 biogenesis and transfer. *Angew. Chem. Int. Ed. Engl.* **51**, 5439-5442

218. Chahal, H. K., Dai, Y., Saini, A., Ayala-Castro, C., and Outten, F. W. (2009) The SufBCD Fe-S scaffold complex interacts with SufA for Fe-S cluster transfer. *Biochemistry* **48**, 10644-10653

219. Roche, B., Aussel, L., Ezraty, B., Mandin, P., Py, B., and Barras, F. (2013) Iron/sulfur proteins biogenesis in prokaryotes: formation, regulation and diversity. *Biochim. Biophys. Acta* **1827**, 455-469

220. Bandyopadhyay, S., Gama, F., Molina-Navarro, M. M., Gualberto, J. M., Claxton, R., Naik, S. G., Huynh, B. H., Herrero, E., Jacquot, J. P., Johnson, M. K., and Rouhier, N. (2008) Chloroplast monothiol glutaredoxins as scaffold proteins for the assembly and delivery of [2Fe-2S] clusters. *EMBO J.* **27**, 1122-1133

221. Roret, T., Tsan, P., Couturier, J., Zhang, B., Johnson, M. K., Rouhier, N., and Didierjean, C. (2014) Structural and spectroscopic insights into BolA-glutaredoxin complexes. *J. Biol. Chem.* **289**, 24588-24598

222. Li, H., and Outten, C. E. (2012) Monothiol CGFS glutaredoxins and BolA-like proteins: [2Fe-2S] binding partners in iron homeostasis. *Biochemistry* **51**, 4377-4389

223. Lezhneva, L., Amann, K., and Meurer, J. (2004) The universally conserved HCF101 protein is involved in assembly of [4Fe-4S]-cluster-containing complexes in *Arabidopsis thaliana* chloroplasts. *Plant J.* **37**, 174-185

224. Chitnis, P. R. (2001) PHOTOSYSTEM I: Function and Physiology. *Annu. Rev. Plant Physiol. Plant Mol. Biol.* **52**, 593-626

225. Antonkine, M. L., Koay, M. S., Epel, B., Breitenstein, C., Gopta, O., Gartner, W., Bill, E., and Lubitz, W. (2009) Synthesis and characterization of de novo designed peptides modelling the binding sites of [4Fe-4S] clusters in photosystem I. *Biochim. Biophys. Acta* **1787**, 995-1008

226. Vassiliev, I. R., Antonkine, M. L., and Golbeck, J. H. (2001) Iron–sulfur clusters in type I reaction centers. *Biochim. Biophys. Acta* **1507**, 139-160

227. Bentrop, D., Bertini, I., Luchinat, C., Nitschke, W., and Muhlenhoff, U. (1997) Characterization of the unbound 2[Fe_4S_4]-ferredoxin-like photosystem I subunit PsaC from the Cyanobacterium *Synechococcus elongatus*. *Biochemistry* **36**, 13629-13637

228. Golbeck, J. H. (1994) Photosystem I in Cyanobacteria. 319-360

229. Antonkine, M. L., Liu, G., Bentrop, D., Bryant, D. A., Bertini, I., Luchinat, C., Golbeck, J. H., and Stehlik, D. (2002) Solution structure of the unbound, oxidized Photosystem I

subunit PsaC, containing [4Fe-4S] clusters F(A) and F(B): A conformational change occurs upon binding to photosystem I. *J. Biol. Inorg. Chem.* **7**, 461-472

230. Li, N., Zhao, J., Warren, P. V., Warden, J. T., Bryant, D. A., and Golbeck, J. H. (1991) PsaD is required for the stable binding of PsaC to the photosystem I core protein of Synechococcus sp. PCC 6301. *Biochemistry* **30**, 7863-7872

231. Boudreau, E., Takahashi, Y., Lemieux, C., Turmel, M., and Rochaix, J. D. (1997) The chloroplast ycf3 and ycf4 open reading frames of Chlamydomonas reinhardtii are required for the accumulation of the photosystem I complex. *EMBO J.* **16**, 6095-6104

232. Schwenkert, S., Netz, D. J., Frazzon, J., Pierik, A. J., Bill, E., Gross, J., Lill, R., and Meurer, J. (2009) Chloroplast HCF101 is a scaffold protein for [4Fe-4S] cluster assembly. *Biochem. J.* **425**, 207-214

233. Schwenkert, S., Netz, D. J., Frazzon, J., Pierik, A. J., Bill, E., Gross, J., Lill, R., and Meurer, J. (2010) Chloroplast HCF101 is a scaffold protein for [4Fe-4S] cluster assembly. *Biochem. J.* **425**, 207-214

234. Shen, G., Zhao, J., Reimer, S. K., Antonkine, M. L., Cai, Q., Weiland, S. M., Golbeck, J. H., and Bryant, D. A. (2002) Assembly of photosystem I. I. Inactivation of the rubA gene encoding a membrane-associated rubredoxin in the cyanobacterium Synechococcus sp. PCC 7002 causes a loss of photosystem I activity. *J. Biol. Chem.* **277**, 20343-20354

235. Waller, J. C., Ellens, K. W., Hasnain, G., Alvarez, S., Rocca, J. R., and Hanson, A. D. (2012) Evidence that the folate-dependent proteins YgfZ and MnmEG have opposing effects on growth and on activity of the iron-sulfur enzyme MiaB. *J. Bacteriol.* **194**, 362-367

236. Lu, Y. (2018) Assembly and Transfer of Iron-Sulfur Clusters in the Plastid. *Front Plant Sci* **9**, 336

237. Yabe, T., Morimoto, K., Kikuchi, S., Nishio, K., Terashima, I., and Nakai, M. (2004) The *Arabidopsis* chloroplastic NifU-like protein CnfU, which can act as an iron-sulfur cluster scaffold protein, is required for biogenesis of ferredoxin and photosystem I. *Plant Cell* **16**, 993-1007

238. Leon, S., Touraine, B., Ribot, C., Briat, J. F., and Lobreaux, S. (2003) Iron-sulphur cluster assembly in plants: distinct NFU proteins in mitochondria and plastids from Arabidopsis thaliana. *Biochem. J.* **371**, 823-830

239. Touraine, B., Boutin, J. P., Marion-Poll, A., Briat, J. F., Peltier, G., and Lobreaux, S. (2004) Nfu2:A scaffold protein required for [4Fe-4S] and ferredoxin iron-sulphur cluster assembly in *Arabidopsis* chloroplasts. *Plant J.* **40**, 101-111

240. Touraine, B., Vignols, F., Przybyla-Toscano, J., Ischebeck, T., Dhalleine, T., Wu, H. C., Magno, C., Berger, N., Couturier, J., Dubos, C., Feussner, I., Caffarri, S., Havaux, M., Rouhier, N., and Gaymard, F. (2019) Iron-sulfur protein NFU2 is required for branched-chain amino acid synthesis in Arabidopsis roots. *J Exp Bot* **70**, 1875-1889

241. Johnson, M. K., Duin, E. C., Crouse, B. R., Golinelli, M. P., and Meyer, J. (1998) Valence-delocalized $[Fe_2S_2]^+$ clusters. in *Spectroscopic Methods in Bioinorganic Chemistry*, American Chemical Society. pp 286-301

242. Surerus, K. K., Munck, E., Moura, I., Moura, J. J. G., and LeGall, J. (1987) Evidence for the formation of a $ZnFe_3S_4$ cluster in *Desulfovibrio gigas* ferredoxin II. *J. Am. Chem. Soc.* **109**, 3805-3807

243. Johnson, M. K. a. S., A. D. (2011) Iron–Sulfur Proteins. in *Encyclopedia of Inorganic and Bioinorganic Chemistry*. pp

244. Mapolelo, D. T. (2010) Characterization of roles of A-type proteins and monothiol CGFS glutaredoxins in iron sulfur cluster biogenesis. . *Ph. D.Thesis*

245. Rouhier, N., Couturier, J., Johnson, M. K., and Jacquot, J. P. (2010) Glutaredoxins: roles in iron homeostasis. *Trends Biochem. Sci.* **35**, 43-52

Table 1.1: Mitochondrial proteins from *Arabidopsis thaliana* and their bacterial, yeast and human homologs

Plant protein name	**Human homolog**	**Yeast homolog**	**Bacterial relative**	**Function**
NFS1	NFS1	Nfs1	IscS	Cysteine desulfurase: Sulfur donor
ISD11	ISD11	Isd11	-	NFS1 stability
ISU1 ISU2 ISU3	ISCU	Isu1 Isu2	IscU	Fe-S scaffold protein
GRXS15	GLRX5	Grx5	GrxD	Fe-S cluster transfer
ISCA1a ISCA1b ISCA2	ISCA1 ISCA2	Isa1 Isa2	IscA ErpA	Specific targeting of Fe-S clusters Specific targeting of Fe-S clusters
IBA57.2	IBA57	Iba57	-	Specific targeting of Fe-S clusters
NFU4 NFU5	NFU1	Nfu1	NifU NfuA	Specific targeting of Fe-S clusters

Table 1.2: Plastidial proteins from *Arabidopsis thaliana* and their bacterial relatives

Plant protein names	**Bacterial relative**	**Function**
NFS2	SufS	Cysteine desulfurase: Sulfur donor
SUFE1 SUFE2 SUFE3	SufE	Activator for cysteine desulfurase
SUFB SUFC SUFD	SufB SufC SufD	$SUFBC_2D$ acts as a scaffold complex
SUFA1	SufA	assumed as Fe-S cluster transfer protein
NFU1 NFU2 NFU3	NfuA	Specific targeting of Fe-S clusters
HCF101	Mrp	Specific targeting of Fe-S clusters
IBA57.2	Ygfz	Specific targeting of Fe-S clusters
GRXS14 GRXS16	Grx4	Fe-S cluster transfer proteins

Figure 1.1: Structures of different types of Fe-S clusters which function primarily in mediating electron transfer, as determined by X-ray crystallography. Structures are taken from coordinates deposited in the Protein Data Bank. (A) Fe Rd, rubredoxin (Rd) Fe center from *Desulfovibrio vulgaris*, PDB ID# 8RXN; (B) [2Fe-2S], ferredoxin (Fd) from *Anabaena pcc7120*, PDB ID# 1FRD; (C) $[2Fe\text{-}2S]_R$, Rieske protein from *Sulfolobus acidocaldarius*, PDB ID#1JM1; (D) [3Fe-4S], cubane [3Fe-4S] cluster from *A. vinelandii* FdI, PDB ID# 6FDR; (E) [4Fe-4S], *A. vinelandii* FdI, PDB ID# 6FDR; (F) $[8Fe\text{-}7S]^N$, dithionite-reduced MoFe protein from *A. vinelandii*, PDB ID# 1M1N; (G) $[8Fe\text{-}7S]^{OX}$, thionine-oxidized MoFe protein from *A. vinelandii*, PDB ID# 2MIN. Color code: magenta, Fe; yellow, S; gray, C; red, O. Unlabeled S atoms correspond to bridging sulfides. Adapted from reference (2)

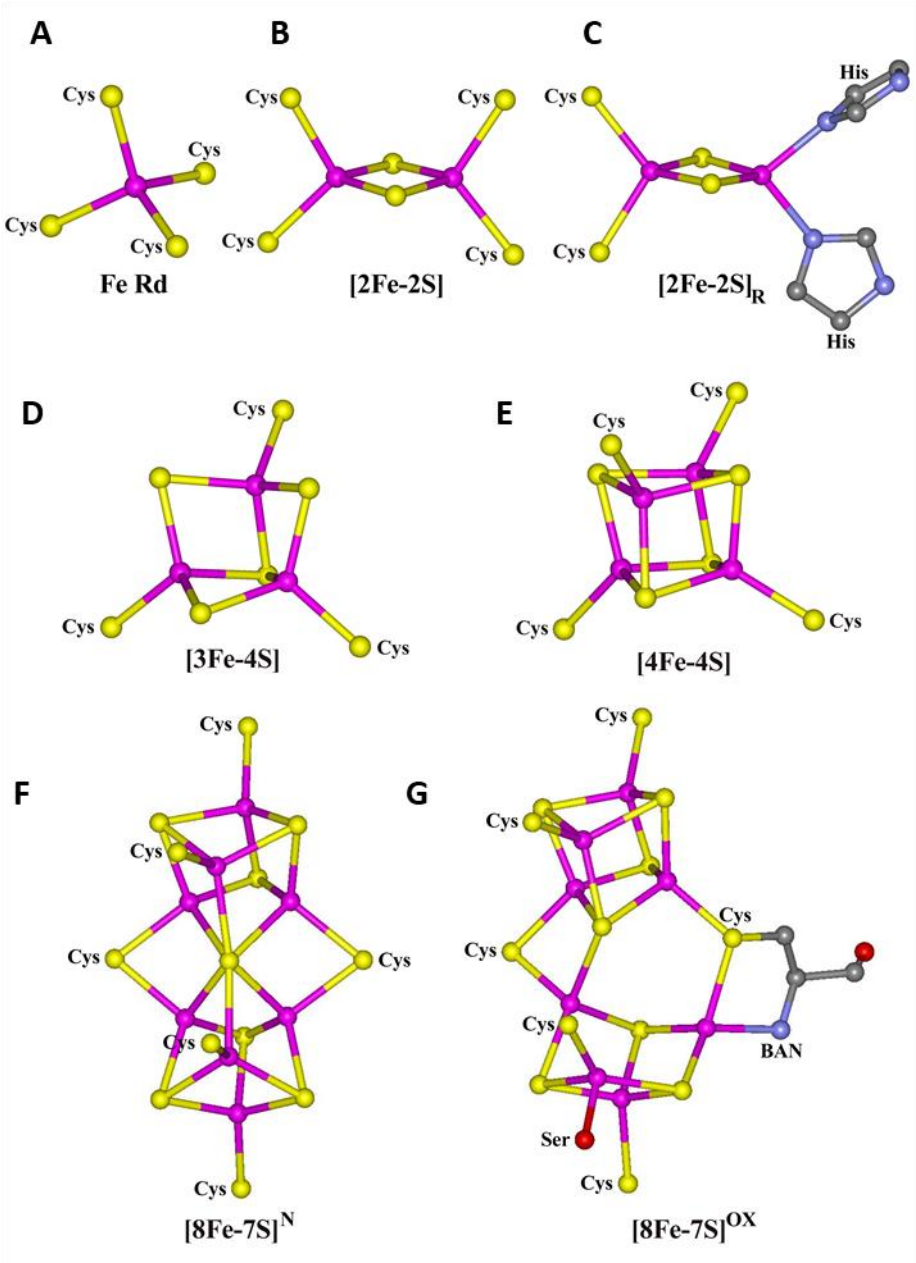
A
Cys
Cys
Cys
Cys
Fe Rd
B
Cys
Cys
Cys
Cys
[2Fe-2S]
C
His
Cys
Cys
His
[2Fe-2S]R
D
Cys
Cys
Cys
[3Fe-4S]
E
Cys
Cys
Cys
Cys
[4Fe-4S]
F
Cys
Cys
Cys
Cys
Cys
Cys
[8Fe-7S]N
G
Cys
Cys
Cys
Cys
Cys
BAN
Ser
Cys
[8Fe-7S]OX

Figure 1.2: Schematic representations of structures of different types of Fe-S centers primarily involved in substrate binding and activation, as determined by X-ray crystallography. They are taken from coordinates deposited in the Protein Data Bank: (A) [4Fe-4S] + isocitrate, isocitrate-bound form of porcine heart aconitase, PDB ID#7ACN; (B) [4Fe-4S] + SAM, SAM-bound form of HemN from *E. coli*, PDB ID# 1OLT; (C) siroheme-[4Fe-4S], sulfite-bound form of sulfite reductase from E. coli, PDB ID # 2GEP (D) [Mo-7Fe-9S-X], *A. vinelandii* MoFe protein, PDB ID# 1M1N; (E) [Ni-4Fe-5S], reduced CO dehydrogenase II from *Carboxydothermus hydrogenoformans*, PDB ID# 1SU8 (D) Ni-Ni-[4Fe-4S], acetyl-CoA synthase from *Carboxydothermus hydrogenoformans*, PDB ID# 1RU3. Color code: magenta, Fe; yellow S; gray, C; red, O; green, Ni; gold, Mo; black, unknown low Z atom (O/C/N). Unlabeled S atoms (2)

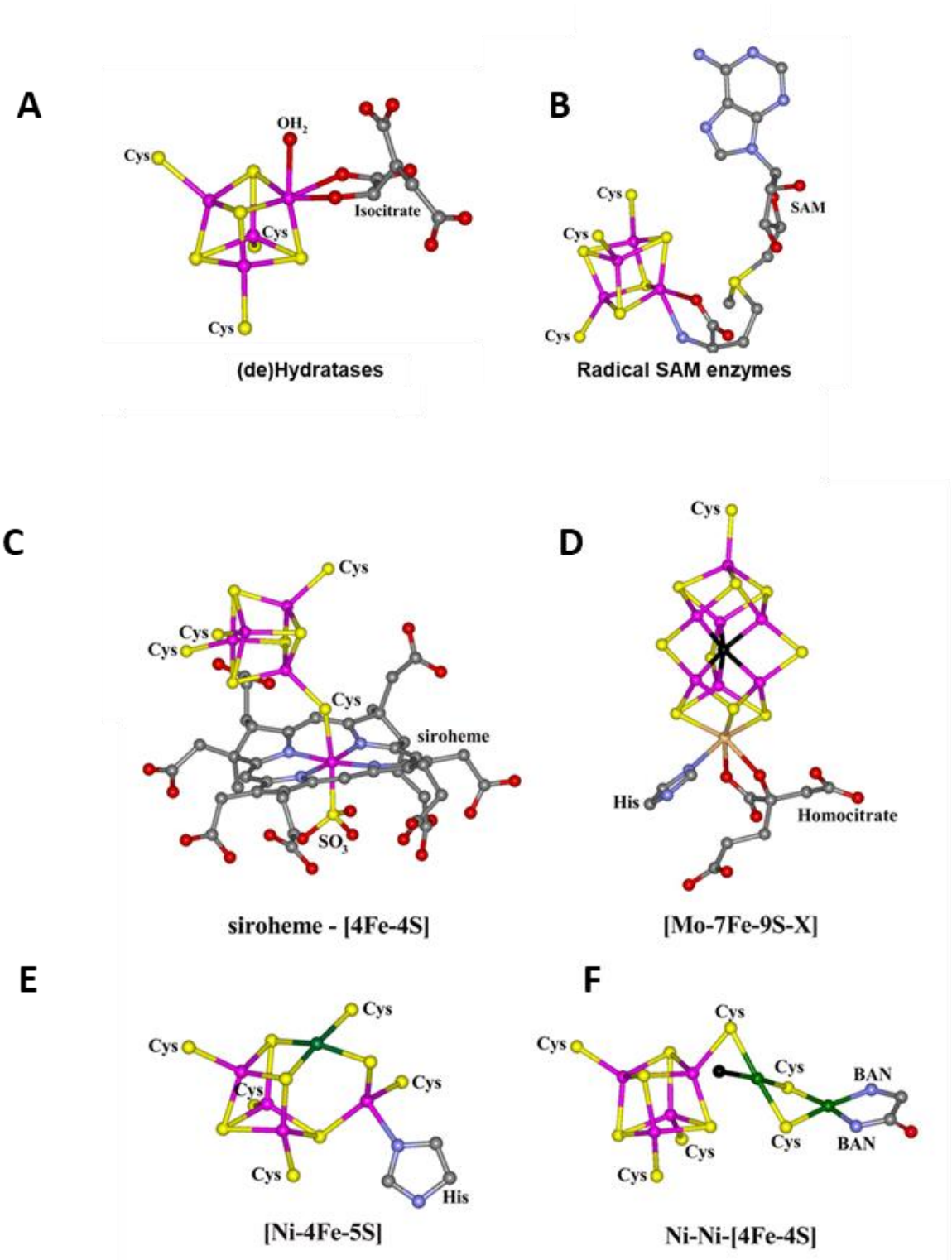
A
OH2
Cys
Isocitrate
Cys
Cys
(de)Hydratases
B
Cys
SAM
Cys
Cys
Radical SAM enzymes
C
Cys
Cys
Cys
Cys
siroheme
SO3
siroheme - [4Fe-4S]
D
Cys
His
Homocitrate
[Mo-7Fe-9S-X]
E
Cys
Cys
Cys
Cys
Cys
His
[Ni-4Fe-5S]
F
Cys
Cys
Cys
BAN
Cys
Cys
BAN
Cys
Ni-Ni-[4Fe-4S]

Figure 1.3: Ground state spin (*S*) and valence-delocalization schemes for major types of Fe-S centers with the core oxidation state of Fe-S centers. Valence-delocalized $[2Fe\text{-}2S]^{+}$ cluster (S = 9/2) has only been observed in C56S and C60S variants of *Clostridium pasteurianum* 2Fe Fd (65,67,241). $[3Fe\text{-}4S]^{-}$ shown in parenthesis here have never been observed in any protein clusters. However, they are only identified as fragments in heterometallic cubane clusters (242). Reduction of $[3Fe\text{-}4S]^{+}$ centers result in $[3Fe\text{-}4S]^{2-}$ clusters with concomitant addition of three protons (66). Color code: red, Fe^{3+}; blue, Fe^{2+}; green, $Fe^{2.5+}$, valance-delocalized; yellow, S; grey, O. Adapted from reference (2)

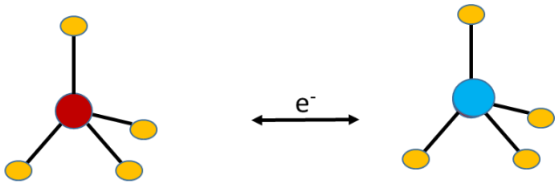

Fe^{3+} (S=5/2) Fe^{2+} (S=5/2)

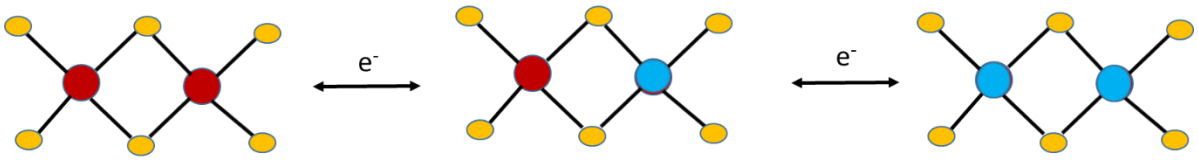

$[2Fe\text{-}2S]^{2+}$ (S=0) $[2Fe\text{-}2S]^{1+}$ (S=1/2) $[2Fe\text{-}2S]$ (S=0)

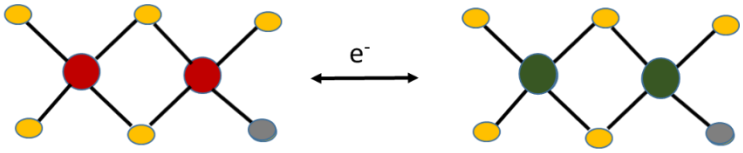

$[2Fe\text{-}2S]^{2+}$ (S=0) $[2Fe\text{-}2S]^{1+}$ (S=9/2)

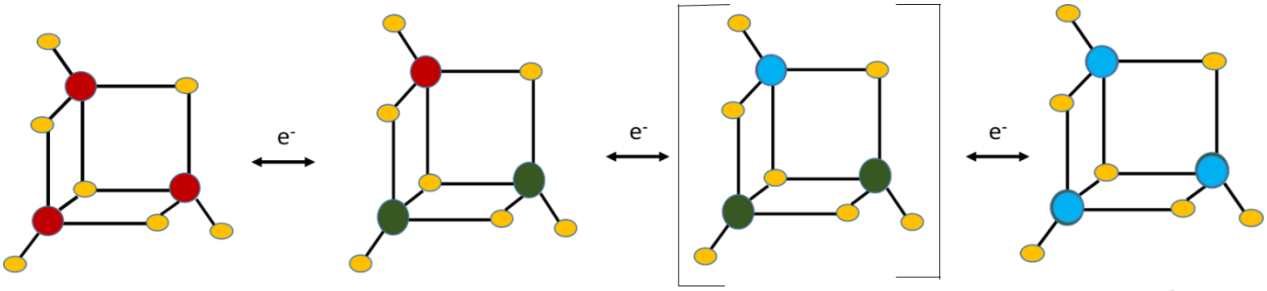

$[3Fe\text{-}4S]^{+}$ (S=1/2) $[3Fe\text{-}4S]^{0}$(S=2) $[3Fe\text{-}4S]^{-}$ (S=5/2) $[3Fe\text{-}4S]^{2-}$(S=?)

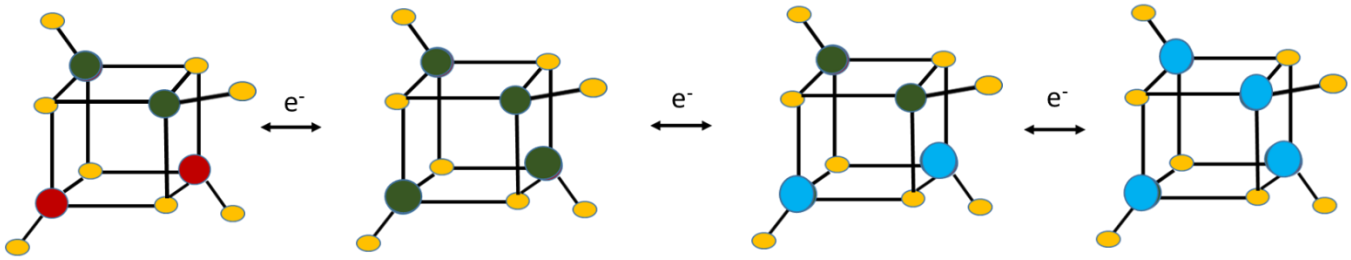

$[4Fe\text{-}4S]^{3+}$ (S=1/2) $[4Fe\text{-}4S]^{2+}$ (S=0) $[4Fe\text{-}4S]^{+}$ (S=1/2 or 3/2) $[4Fe\text{-}4S]^{0}$ (S=4)

Figure 1.4: Ranges of midpoint potentials (mV vs. NHE) for different types of biological Fe-S centers in their most common accessible redox states. Color code: purple, Fe^{3+}; blue, Fe^{2+}; green, $Fe^{2.5+}$, valance-delocalized; yellow, S; grey C. Adapted from reference (243)

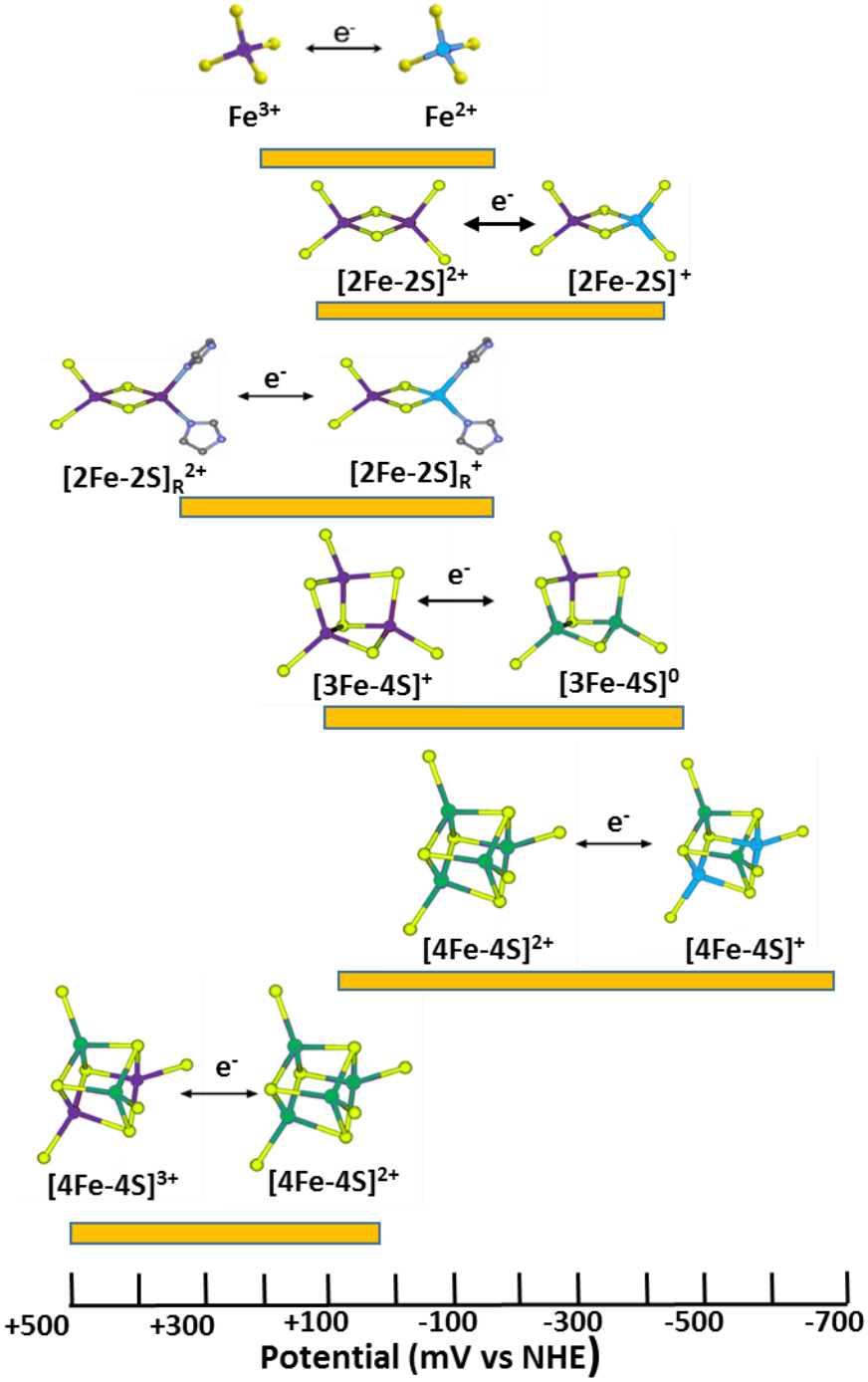
e-
Fe3+
Fe2+
e-
[2Fe-2S]2+
[2Fe-2S]+
e-
[2Fe-2S]R2+
[2Fe-2S]R+
e-
[3Fe-4S]+
[3Fe-4S]0
e-
[4Fe-4S]2+
[4Fe-4S]+
e-
[4Fe-4S]3+
[4Fe-4S]2+
+500
+300
+100
-100
-300
-500
-700
Potential (mV vs NHE)

Figure 1.5: Different types of Fe-S cluster interconversions observed in Fe-S proteins. M^{2+} = Cr^{2+}, Mn^{2+}, Co^{2+}, Ni^{2+}, Zn^{2+}, Cd^{2+}, Pb^{2+} ; M^{+} = Cu^{+} and Tl^{+} . The cluster center in dashed box represent two $[2Fe\text{-}2S]^{2+}$ centers located on two adjacent subunits as in the case of IscU (165) and IscA (244). Adapted from reference (243).

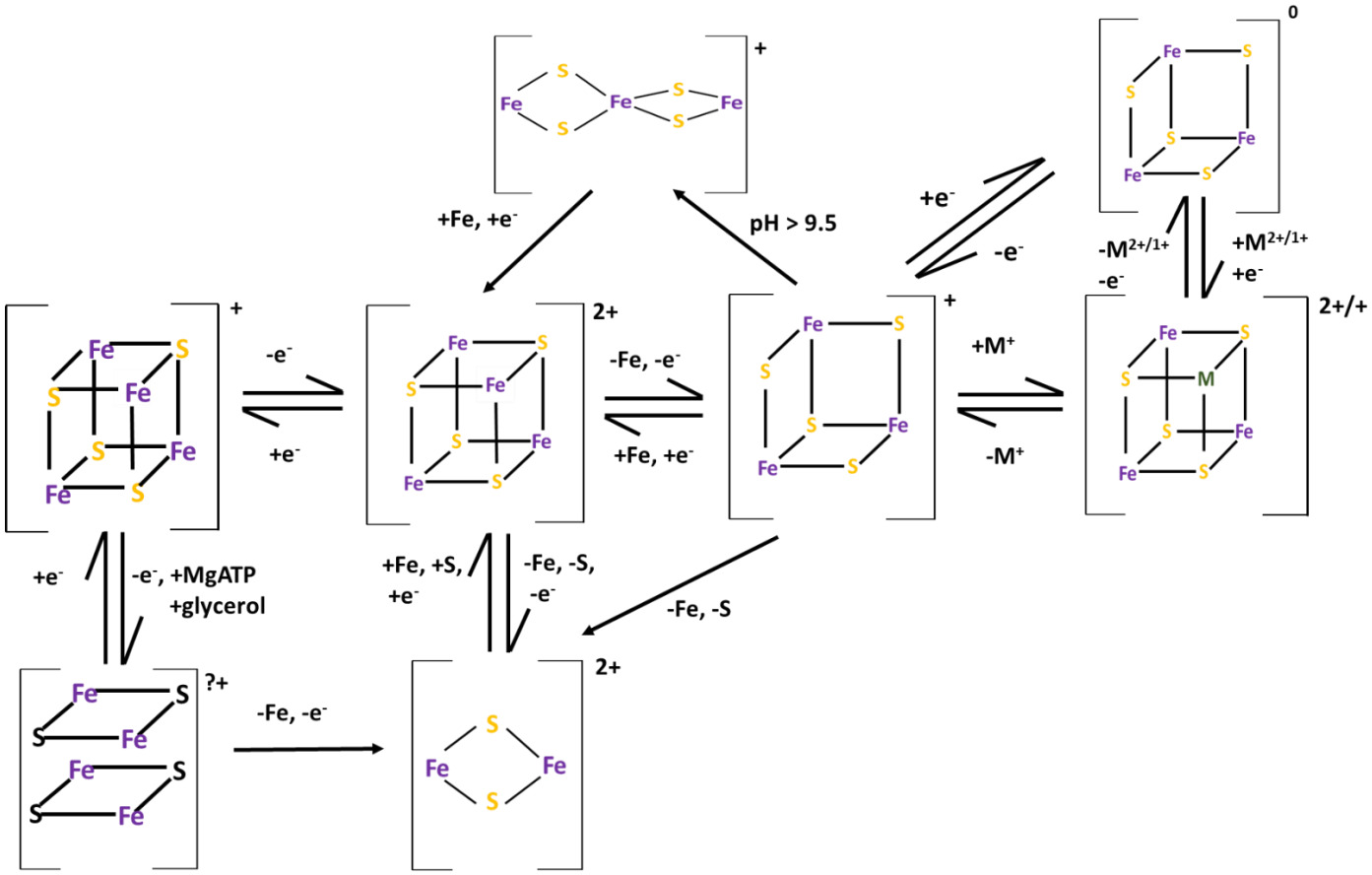
+
+Fe, +e-
pH > 9.5
+e-
-e-
0
-M2+/1+
-e-
+M2+/1+
+e-
2+/+
+
-e-
+e-
2+
-Fe, -e-
+Fe, +e-
+M+
-M+
+e-
-e-, +MgATP
+glycerol
+Fe, +S,
+e-
-Fe, -S,
-e-
-Fe, -S
?+
-Fe, -e-
2+

Figure 1.6: Schematic representation of Fe-S machineries in eukaryotic cells (plants). Eukaryotes contain Fe-S proteins in mitochondria, the cytosol, and the nucleus. The SUF machinery of plastids and ISC machinery of mitochondria were inherited from photosynthetic bacteria and α-proteobacteria respectively via endosymbiosis (12). Mitochondrial ISC assembly machinery, a mitochondrial ISC export system, and CIA machinery are required for the maturation of cytosolic and nuclear Fe-S proteins. Adapted from reference (12)

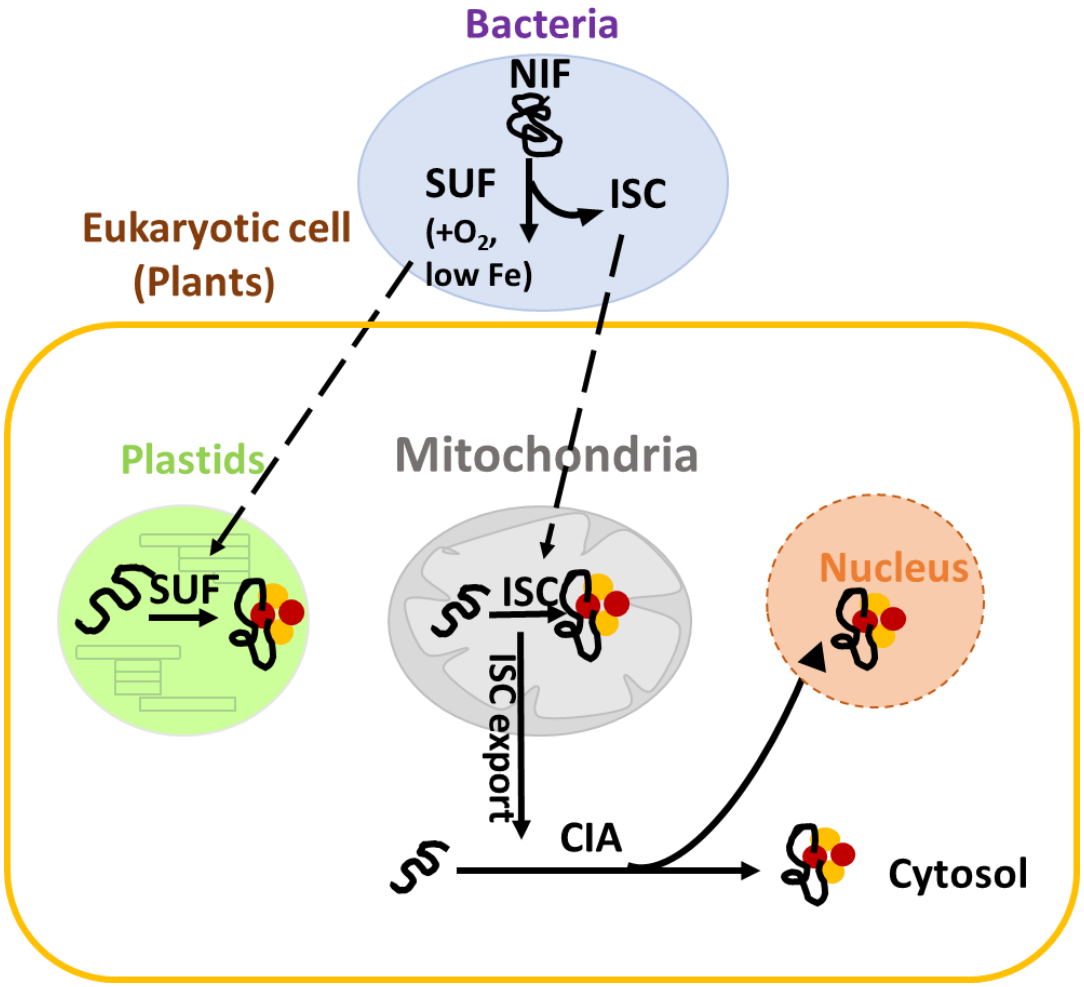
Bacteria
NIF
SUF
(+O2,
low Fe)
ISC
Eukaryotic cell
(Plants)
Plastids
Mitochondria
SUF
ISC
Nucleus
ISC export
CIA
Cytosol

Figure 1.7: Schematic representation of the domain structures of different Grx-type proteins. Grxs present in all photosynthetic organisms are included in classes I and II. Class I Grxs have a single domain, whereas class II Grxs has variable domain organization. All Grx domains for class I and class II are respectively colored green and blue with active site motifs labeled accordingly. The orange box represents the N-terminal extension specific to GrxS16 and additional thioredoxin-like modules are shown in yellow. Domain lengths are not drawn to scale (245).

Class I

(Plant GrxC1 toC5, S12, *Hs* Grx1 and 2,

Ec Grx1 and 3, *Sc* Grx1, 2, 6, 7)

Class II

(Plant GRXS14 and S15, *Sc* Grx5, *Ec* Grx4)

GrxS16 (specific to plants only)

GrxS17 (lower plants, algae)

GrxS17 (higher plants)

Sc Grx3p, *Sc* Grx4p

Figure 1.8: Primary sequence alignments of *At* GRXS15, *Sc* Grx5 and *Hs* GLRX5. *At* GRXS15, *A. thaliana*; *Sc* Grx5, *S. cerevisiae*; *Hs* GLRX5, *H. sapiens.* The sequence alignment was performed with MUSCLE. Conserved amino acids are highlighted in blue.

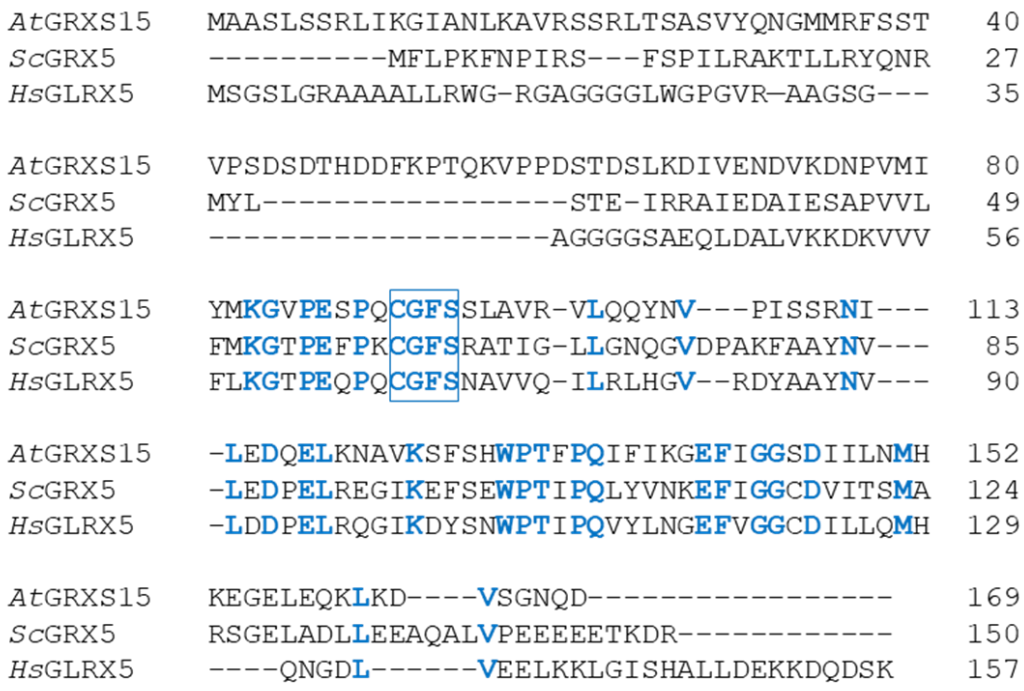
AtGRXS15 MAASLSSRLIKGIANLKAVRSSRLTSASVYQNGMMRFSST 40
ScGRX5 ----------MFLPKFNPIRS---FSPILRAKTLLRYQNR 27
HsGLRX5 MSGSLGRAAAALLRWG-RGAGGGGLWGPGVR-AAGSG--- 35
AtGRXS15 VPSDSDTHDDFKPTQKVPPDSTDSLKDIVENDVKDNPVMI 80
ScGRX5 MYL-----------------STE-IRRAIEDAIESAPVVL 49
HsGLRX5 -------------------AGGGGSAEQLDALVKKDKVVV 56
AtGRXS15 YMKGVPESPQCGFSSLAVR-VLQQYNV---PISSRNI--- 113
ScGRX5 FMKGTPEFPKCGFSRATIG-LLGNQGVDPAKFAAYNV--- 85
HsGLRX5 FLKGTPEQPQCGFSNAVVQ-ILRLHGV--RDYAAYNV--- 90
AtGRXS15 -LEDQELKNAVKSFSHWPTFPQIFIKGEFIGGSDIILNMH 152
ScGRX5 -LEDPELREGIKEFSEWPTIPQLYVNKEFIGGCDVITSMA 124
HsGLRX5 -LDDPELRQGIKDYSNWPTIPQVYLNGEFVGGCDILLQMH 129
AtGRXS15 KEGELEQKLKD----VSGNQD---------- 169
ScGRX5 RSGELADLLEEAQALVPEEEEETKDR---------- 150
HsGLRX5 ----QNGDL------VEELKKLGISHALLDEKKDQDSK 157

Figure 1.9: The 2.4-Å crystal structure of [2Fe-2S] cluster-bound human GLRX5 (190). Structures are taken from coordinates deposited in the Protein Data Bank, PDB ID# 2WUL. Orange and yellow spheres represent iron and sulfur respectively in [2Fe-2S] cluster and GSH is shown in sticks. Color code: blue, N; red, oxygen; grey C.

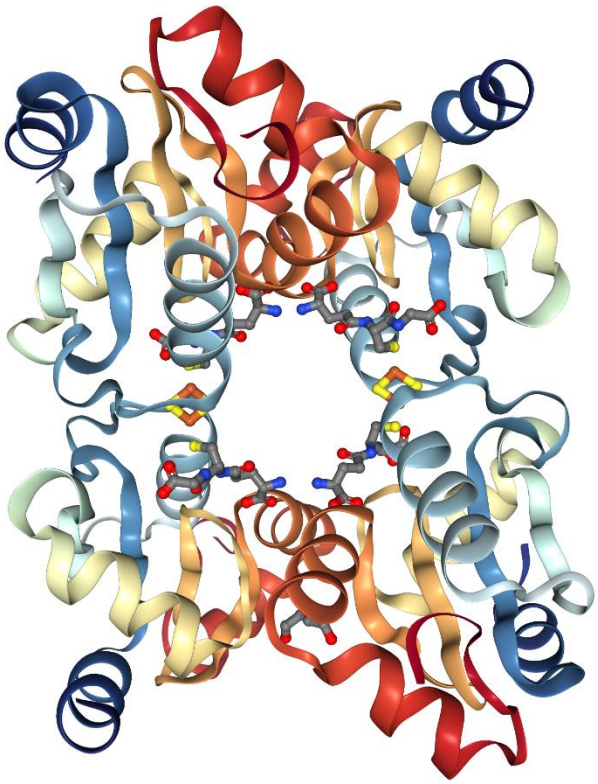

Figure 1.10: Amino acid sequence alignment of ISCA proteins from plant, yeast and human. *At* stands for *A. thaliana*, *Sc* for *S. cerevisiae* and *Hs* for *H. sapiens*. The sequence alignment was performed with MUSCLE. Conserved amino acid positions are highlighted in blue and cysteines required for the Fe-S cluster incorporation are indicated by asterisks. Adapted from reference (200)

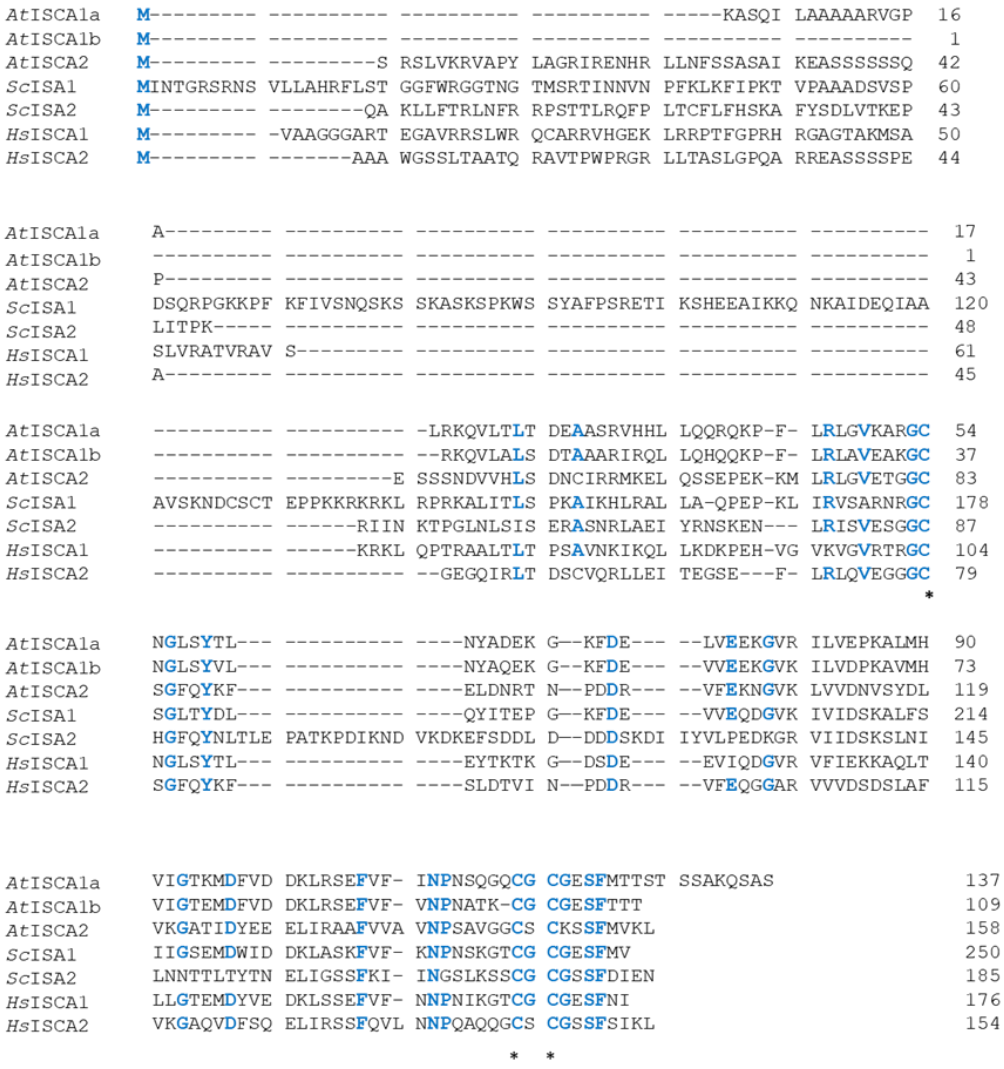
AtISCA1a M--------- ---------- ---------- ---------- -----KASQI LAAAAARVGP 16
AtISCA1b M--------- ---------- ---------- ---------- ---------- ---------- 1
AtISCA2 M--------- ---------S RSLVKRVAPY LAGRIRENHR LLNFSSASAI KEASSSSSSQ 42
ScISA1 MINTGRSRNS VLLAHRFLST GGFWRGGTNG TMSRTINNVN PFKLKFIPKT VPAAADSVSP 60
ScISA2 M--------- --------QA KLLFTRLNFR RPSTTLRQFP LTCFLFHSKA FYSDLVTKEP 43
HsISCA1 M--------- -VAAGGGART EGAVRRSLWR QCARRVHGEK LRRPTFGPRH RGAGTAKMSA 50
HsISCA2 M--------- -------AAA WGSSLTAATQ RAVTPWPRGR LLTASLGPQA RREASSSSPE 44
AtISCA1a A--------- ---------- ---------- ---------- ---------- ---------- 17
AtISCA1b ---------- ---------- ---------- ---------- ---------- ---------- 1
AtISCA2 P--------- ---------- ---------- ---------- ---------- ---------- 43
ScISA1 DSQRPGKKPF KFIVSNQSKS SKASKSPKWS SYAFPSRETI KSHEEAIKKQ NKAIDEQIAA 120
ScISA2 LITPK----- ---------- ---------- ---------- ---------- ---------- 48
HsISCA1 SLVRATVRAV S--------- ---------- ---------- ---------- ---------- 61
HsISCA2 A--------- ---------- ---------- ---------- ---------- ---------- 45
AtISCA1a ---------- ---------- -LRKQVLTLT DEAASRVHHL LQQRQKP-F- LRLGVKARGC 54
AtISCA1b ---------- ---------- --RKQVLALS DTAAARIRQL LQHQQKP-F- LRLAVEAKGC 37
AtISCA2 ---------- ---------E SSSNDVVHLS DNCIRRMKEL QSSEPEK-KM LRLGVETGGC 83
ScISA1 AVSKNDCSCT EPPKKRKRKL RPRKALITLS PKAIKHLRAL LA-QPEP-KL IRVSARNRGC 178
ScISA2 ---------- ------RIIN KTPGLNLSIS ERASNRLAEI YRNSKEN--- LRISVESGGC 87
HsISCA1 ---------- ------KRKL QPTRAALTLT PSAVNKIKQL LKDKPEH-VG VKVGVRTRGC 104
HsISCA2 ---------- ---------- --GEGQIRLT DSCVQRLLEI TEGSE---F- LRLQVEGGGC 79
*
AtISCA1a NGLSYTL--- ---------- ----NYADEK G--KFDE--- --LVEEKGVR ILVEPKALMH 90
AtISCA1b NGLSYVL--- ---------- ----NYAQEK G--KFDE--- --VVEEKGVK ILVDPKAVMH 73
AtISCA2 SGFQYKF--- ---------- ----ELDNRT N--PDDR--- --VFEKNGVK LVVDNVSYDL 119
ScISA1 SGLTYDL--- ---------- ----QYITEP G--KFDE--- --VVEQDGVK IVIDSKALFS 214
ScISA2 HGFQYNLTLE PATKPDIKND VKDKEFSDDL D--DDDSKDI IYVLPEDKGR VIIDSKSLNI 145
HsISCA1 NGLSYTL--- ---------- ----EYTKTK G--DSDE--- --EVIQDGVR VFIEKKAQLT 140
HsISCA2 SGFQYKF--- ---------- ----SLDTVI N--PDDR--- --VFEQGGAR VVVDSDSLAF 115
AtISCA1a VIGTKMDFVD DKLRSEFVF- INPNSQGQCG CGESFMTTST SSAKQSAS 137
AtISCA1b VIGTEMDFVD DKLRSEFVF- VNPNATK-CG CGESFTTT 109
AtISCA2 VKGATIDYEE ELIRAAFVVA VNPSAVGGCS CKSSFMVKL 158
ScISA1 IIGSEMDWID DKLASKFVF- KNPNSKGTCG CGESFMV 250
ScISA2 LNNTTLTYTN ELIGSSFKI- INGSLKSSCG CGSSFDIEN 185
HsISCA1 LLGTEMDYVE DKLSSEFVF- NNPNIKGTCG CGESFNI 176
HsISCA2 VKGAQVDFSQ ELIRSSFQVL NNPQAQQGCS CGSSFSIKL 154
* *

Figure 1.11: (a) The 2.5-Å crystal structure of [2Fe-2S] cluster-bound IscA from *Thermosynechococcus elongatus* (200). Structures are taken from coordinates deposited in the Protein Data Bank, PDB ID# 1X0Z. Orange and yellow spheres represent iron and sulfur respectively in [2Fe-2S] cluster. (b) Partially exposed $[2Fe\text{-}2S]^{2+}$ cluster of IscA, which is asymmetrically coordinated with (Cys37, Cys101, and Cys103) from the α protomer and Cys103 from the β protomer. Red and yellow spheres represent iron and sulfur respectively in [2Fe-2S] cluster (200).

(a)

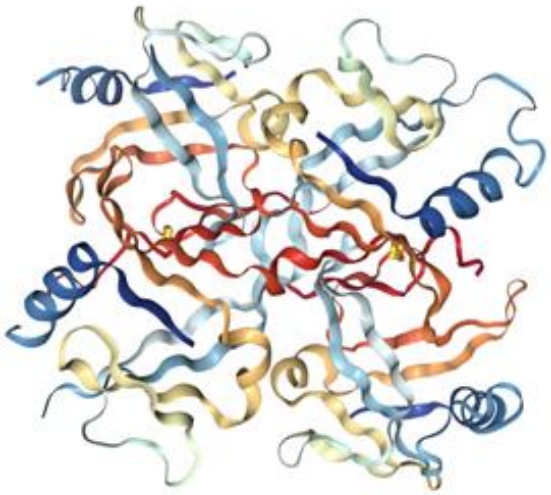

(b)

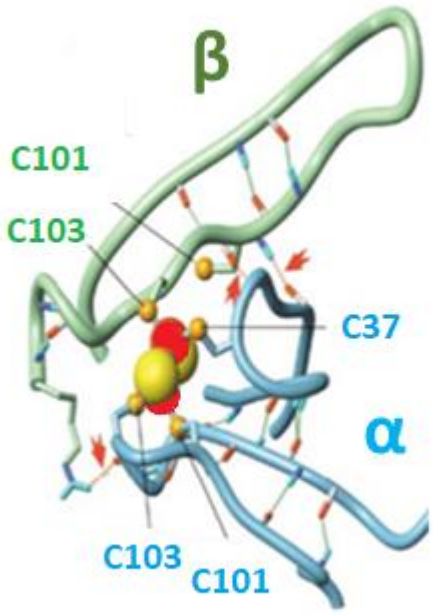

Figure 1.12: Schematic representations of domain structures of different Nfu-type and U type proteins from different organisms. IscU domains, with three conserved cysteine residues are presented by dark pink boxes, Nfu domains with the CXXC motif are shown by teal boxes and Fdx-like domain specific to *Av* NifU is presented by light blue box. Bacterial NfuA-type proteins have an N-terminal A-type carrier domain without the conserved cluster-binding cysteine residues that is shown by a green box. Eukaryotic mitochondrial, nuclear and cytosolic Nfu type proteins also have a unique N terminal domain shown by a brown box. Chloroplastic-type Nfu proteins have the extra C-terminal Nfu-type domain lacking the active site cysteine residues that is shown by a purple box. The red and grey bars represent the mitochondrial and chloroplastic targeting sequences, respectively. Domain lengths are not drawn to scale. *Av*, *Azotobacter vinelandii*; *Ec*, *Escherichia coli*; *Sy*, *Synechocystis*; *At*, *Arabidopsis thaliana*; *Sc*, *Saccharomyces cerevisiae*; *Hs*, *Homo sapiens*. Adapted from reference (208).

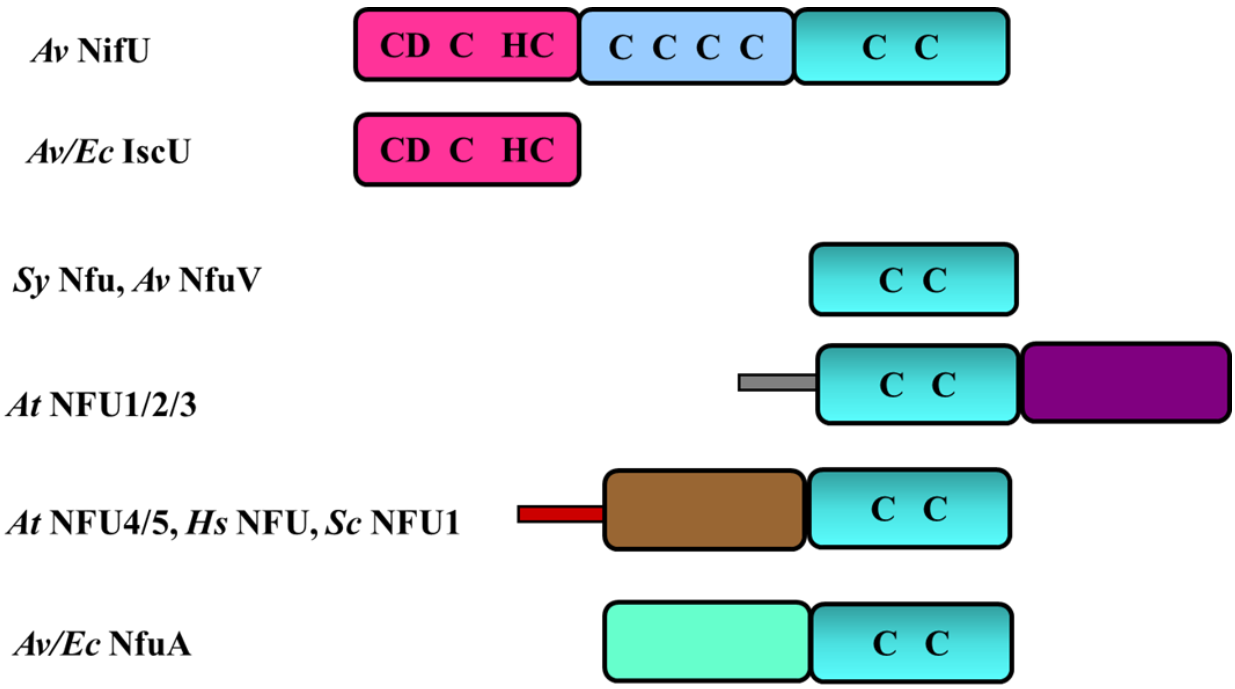
Av NifU
CD C HC
C C C C
C C
Av/Ec IscU
CD C HC
Sy Nfu, *Av* NfuV
C C
At NFU1/2/3
C C
At NFU4/5, *Hs* NFU, *Sc* NFU1
C C
Av/Ec NfuA
C C

CHAPTER 2

MITOCHONDRIAL Fe-S CLUSTER ASSEMBLY IN PLANTS: *IN VITRO* CHARACTERIZATION OF THE PROPERTIES AND ROLES OF *ARABIDOPSIS THALIANA* GRX, ISCA AND NFU PROTEINS

Tamanna Azam,[1] Jonathan Przybyla-Toscano,[2] Jérémy Couturier[2], Nicolas Rouhier[2], and Michael K. Johnson[1, *] *to be submitted to Journal of Biological Chemistry*

[1]Department of Chemistry and Center for Metalloenzyme Studies, University of Georgia, Athens, Georgia, 30602, USA and [2]UMR1136 Interactions Arbres-Microorganismes, Université de Lorraine/INRA, Faculté des Sciences et Technologies, 54500 Vandoeuvre-lès-Nancy, France

Abbreviations: *At*, *Arabidopsis thaliana*; *Hs*, *Homo sapiens*; ISC, iron-sulfur cluster assembly; Fe-S cluster, Iron-sulfur cluster; ATC, A-type carrier; CD, circular dichroism; RR, resonance Raman; EPR, electron paramagnetic resonance; DTT, dithiothreitol; DT, dithionite; GSH, glutathione; IPTG, isopropyl 1-thio-β-D-galactopyranoside; FAS, ferrous ammonium sulfate; PMSF, phenylmethanesulfonyl fluoride; SDS-PAGE, dodecyl sulfate polyacrylamide gel electrophoresis; TCA, trichloroacetoc acid; FDX1, ferredoxin 1; FDX2, ferredoxin 2, ACO2, aconitase 2.

.

Abstract

The molecular mechanism of $[4Fe\text{-}4S]^{2+}$ cluster assembly and insertion into target proteins by late-acting mitochondrial Fe-S cluster assembly proteins is not well understood. Here we report detailed characterization of the four late-acting mitochondrial Fe-S cluster carrier proteins from *Arabidopsis thaliana* (*At*), GRXS15, ISCA1a/2, and NFU4/5, using UV-visible absorption/CD, resonance Raman, EPR, and analytical studies. Co-expression of ISCA1a/2 resulted in samples with one $[2Fe\text{-}2S]^{2+}$ cluster per heterodimer. Cluster reconstitution using as purified [2Fe-2S]-ISCA1a/2 resulted in the $[4Fe\text{-}4S]^{2+}$ cluster-bound heterodimer. NFU4 and NFU5 were both purified as apo proteins but assembled one $[4Fe\text{-}4S]^{2+}$ cluster per homodimer after cluster reconstitution. Cluster transfer reactions monitored by UV-visible absorption and CD spectroscopy or enzyme activity were used to investigate the roles of these proteins in Fe-S cluster trafficking and maturation of client target proteins. [2Fe-2S]-GRXS15 was found to mediate $[2Fe\text{-}2S]^{2+}$ cluster assembly on mitochondrial ferredoxin and $[4Fe\text{-}4S]^{2+}$ cluster assembly on the ISCA1a/2 heterodimer, suggesting that ISCA1a/2 is an assembler of $[4Fe\text{-}4S]^{2+}$ clusters, via two-electron reductive coupling of two $[2Fe\text{-}2S]^{2+}$ clusters. ISCA1a/2, NFU4 and NFU5 were all found to be effective $[4Fe\text{-}4S]^{2+}$ cluster donors for maturation of apo *At* mitochondrial aconitase, and ISCA1a/2 is a competent and efficient $[4Fe\text{-}4S]^{2+}$ cluster donor for both NFU4 and NFU5. These cluster transfer processes are all rapid, unidirectional and quantitative and demonstrate a cluster trafficking shuttle involving GRXS15, ISCA1a/2 and NFU4 or NFU5 for the maturation of client [4Fe-4S] cluster-containing proteins.

Introduction

Iron-sulfur proteins constitute one of the largest classes of proteins and are found in all kingdoms of life. These proteins are involved in fundamental biological processes, ranging from electron transfer and catalyzing metabolic reactions to small molecule sensing, DNA repair and regulating gene expression (1-3). Synthetic and biological Fe-S clusters can generally be assembled via spontaneous self-assembly using excess iron and sulfide ions. However, the presence of excess iron and sulfide ions are toxic to cells, due to the redox reactions of Fe^{3+} and Fe^{2+} ions that generate reactive oxygen species and the ability of S^{2-} ions to precipitate metals ions. Therefore, cells use complex biosynthetic pathways to ensure the correct assembly and trafficking of Fe-S clusters (1,4,5).

The mitochondrial ISC machinery is highly conserved in all eukaryotes and contains many of the same components found in the bacterial ISC machinery due to the evolutionary relationship between bacteria and mitochondria (6,7). Moreover, the ISC machinery is required not only for the biosynthesis of Fe-S clusters in mitochondrial proteins, but also for the maturation of cytosolic and nuclear Fe-S proteins (8). Mitochondrial Fe-S cluster biogenesis can be divided into four steps: i) cysteine desulfurase-mediated assembly of a $[2Fe\text{-}2S]^{2+}$ cluster on an ISU scaffold protein, ii) molecular chaperone-assisted $[2Fe\text{-}2S]^{2+}$ cluster transfer from ISU to acceptor proteins, iii) synthesis of $[4Fe\text{-}4S]^{2+}$ clusters from $[2Fe\text{-}2S]^{2+}$ clusters, and iv) intact $[4Fe\text{-}4S]^{2+}$ cluster transfer to acceptor proteins. Early ISC machinery is considered to be consisting of steps (i) and (ii) whereas late ISC machinery consists of steps (iii) and (iv) (5).

Based on yeast and human studies, a basic model of the mitochondrial ISC machinery has been proposed, but uncertainties concerning the mechanistic pathways of late-acting steps still

persist. Moreover, the proteins involved with late-acting plant mitochondrial ISC machinery have yet to be purified and characterized *in vitro*. The lack of research into the plant ISC machinery may be due to the inherent complexity which arises from the presence of multiple copies of several key proteins, e.g. three ISC machinery scaffold proteins (ISU1/2/3), two ferredoxins (FDX1/2), two sets of chaperones (MGE1a/b, HSCA1/2), two NFU-type cluster transfer proteins (NFU4/5) and three ISCA-type cluster transfer proteins (ISCA1a/1b/2) (6).

The early steps of mitochondrial ISC machinery mainly involve biosynthesis and trafficking of $[2Fe\text{-}2S]^{2+}$ clusters (5). In yeast, the biosynthesis proteins include Nfs1, Isd11, acyl carrier protein (Acp), scaffold protein Isu1/2, ferredoxin (Fdx), and frataxin (Fxn). Yeast deletion mutant studies have been beneficial in characterizing the roles of the corresponding plant proteins involved in early ISC machinery. Just as in yeast, Fe-S cluster biogenesis in plant mitochondria starts with the *de novo* synthesis of a $[2Fe\text{-}2S]^{2+}$ cluster on a scaffold protein. In yeast, the scaffold role is performed by Isu1 (the bacterial IscU homolog), and in plants the scaffold protein in the ISC system is called the ISU protein. The *Arabidopsis* genome encodes three mitochondrial-located ISU proteins (i.e., ISU1, ISU2, and ISU3) (9,10) and ISU1 is likely to be the primary scaffold protein (11). A PLP-dependent cysteine desulfurase, Nfs1 in yeast, converts cysteine to alanine and incorporates the released S as a cysteine persulfide on a flexible loop, which is subsequently transferred to form a cysteine persulfide on Isu1, via a disulfide exchange mechanism (10). Maturation of $[2Fe\text{-}2S]^{2+}$ clusters on Isu1 occurs in a complex that involves Nfs1, Isd11, Acp1 and Isu1 as core proteins and Fdx and/or Fxn as transient participants (5,12). The same proteins are present in plant mitochondria, although the components of the core assembly complex has yet to be established.

In yeast, the co-chaperones Ssq1 and Jac1 work together to efficiently transfer $[2Fe\text{-}2S]^{2+}$ clusters from Isu1 to monothiol glutaredoxin Grx5 (5). *At* HSCA1 and *At* HSCB can complement yeast knockout strains involving the equivalent proteins, Ssq1 and Jac1 respectively (13). Based on the studies of bacterial and yeast ISC systems (14-16), $[2Fe\text{-}2S]^{2+}$ cluster transfer from the *At* ISCU1 scaffold protein is likely to require *At* HSCA1 and HSCB co-chaperones in an ATP-dependent process. It is proposed that *At* HSCB can bind and release the $[2Fe\text{-}2S]^{2+}$ cluster-bound ISU1 in the cluster assembly complex and escort it to *At* HSCA1 (13). HSCB binding greatly enhances the ATP hydrolysis activity of HSCA1, which facilitates intact transfer of the $[2Fe\text{-}2S]^{2+}$ cluster on ISU1 to a bound apo acceptor protein.

While the early ISC machinery appears to provide the $[2Fe\text{-}2S]^{2+}$ cluster building block for $[4Fe\text{-}4S]^{2+}$ cluster biogenesis, the molecular mechanisms of $[4Fe\text{-}4S]^{2+}$ cluster assembly, trafficking, and insertion into target proteins are not well understood. The existing body of research has led to two hypotheses regarding $[4Fe\text{-}4S]^{2+}$ cluster assembly. The evidence for facile reductive coupling of two $[2Fe\text{-}2S]^{2+}$ clusters to form a $[4Fe\text{-}4S]^{2+}$ cluster at the subunit interface of bacterial IscU dimers (17), raises the possibility that $[4Fe\text{-}4S]^{2+}$ clusters are assembled on U-type scaffold proteins and transferred directly to $[4Fe\text{-}4S]^{2+}$ cluster trafficking or acceptor proteins. The second hypothesis is that $[4Fe\text{-}4S]^{2+}$ clusters are formed on A-type carrier (ATC) proteins instead of U-type proteins. This was originally proposed based on the observation of facile and reversible $[2Fe\text{-}2S]^{2+} \leftrightarrow [4Fe\text{-}4S]^{2+}$ cluster interconversions on ^{Nif}IscA (18). Additional support for this proposal was provided by the observation that two human GLRX5 homodimers donate $[2Fe\text{-}2S]^{2+}$ clusters to form a $[4Fe\text{-}4S]^{2+}$ cluster on the ISCA1-ISCA2 heterodimeric complex (19).

By analogy with the bacterial and yeast ISC systems (15,16), a monothiol GRX is likely to be the dedicated acceptor protein for $[2Fe\text{-}2S]^{2+}$ clusters assembled on ISU1 in plants. GRXS15 is

the only confirmed monothiol GRX in *Arabidopsis* mitochondria, and it has a 33% amino acid similarity with yeast and human mitochondrial monothiol glutaredoxins, see Figure 2.1. The involvement of Grx5 and its homologs in mitochondrial Fe-S cluster assembly has been established in yeast and vertebrates but has only recently been investigated in plants. *grxs15* null mutants were found to be embryo lethal in *Arabidopsis* indicating an essential role in plant growth and GRXS15 was found to assemble a Fe-S cluster *in vitro* in the presence of glutathione (20). Targeted mutagenesis studies of *At* GRXS15 resulted in variants with diminished glutathione and Fe-S cluster content. Using these variants for complementing plant *Δgrxs15* strains led to a dwarf phenotype and a 65% decrease in aconitase activity (20). These findings show that *At* GRXS15 is an essential protein that is involved with mitochondrial Fe-S cluster biogenesis. In addition, cluster transfer studies monitored by UV-visible absorption and CD were interpreted in terms of [2Fe-2S]$^{2+}$ cluster-bound *At* GRXS15 functioning as a donor for maturation of the [2Fe-2S]$^{2+}$ cluster on the mitochondrial ferredoxin (20).

Studies of the yeast and human ISC systems have demonstrated that a complex composed of Isa1-Isa2-Iba57 is required for [4Fe-4S]$^{2+}$ cluster biosynthesis (21,22). Iba57 is a tetrahydrofolate-dependent protein of unknown function that appears to be required for cluster release. This complex does not react with early ISC machinery but rather depends on the delivery of [2Fe-2S]$^{2+}$ cluster species. Recently, there has been a debate about the molecular relationship between Iba57 and IscA proteins. *In vivo* and *in vitro* studies have shown that *Hs* ISCA2 reacts with *Hs* IBA57, but not with *Hs* ISCA1(23,24); whereas in yeast both ATC proteins interact with Iba57 (25). However, *in vitro* studies reported that *Hs* IBA57 is not required for the assembly of [4Fe-4S]$^{2+}$ clusters on ISCA proteins (19). The deletion of IBA57, *Hs* ISCA1 (*Sc* Isa1), or *Hs* ISCA2 (*Sc* Isa2) from yeast and human cell lines causes defects in the assembly of the respiratory

complex, the biosynthesis of lipoic acid, and the maturation of aconitase, homoaconitase, and glutamate synthase (21,22,25,26). These results suggest that IBA57 may be involved in other functions other than [4Fe-4S] cluster assembly. Using human proteins, individual ISCA1 or ISCA2 proteins do not form a $[4Fe\text{-}4S]^{2+}$ cluster from two $[2Fe\text{-}2S]^{2+}$-GLRX5 donated clusters (27). Moreover, the heterodimeric ISCA1-ISCA2 complex is thermodynamically more favorable compared to the corresponding homodimers, indicating that the heterodimeric complex may be responsible for the assembly of a $[4Fe\text{-}4S]^{2+}$ cluster (27). This result also agrees with *in vivo* studies showing strong interaction between ISCA1 and ISCA2 proteins (26). *Arabidopsis* has four ATC proteins: SUFA1 is localized in plastids (28), while the other three are predicted to be present in mitochondria. Three mitochondrial ATC proteins, i.e., ISCA1a, ISCA1b, and ISCA2 are present in *At*, but they have yet to be investigated *in vitro*. These three are named based on their homologs in eukaryotic model organisms (29). For example, *At* ISCA1a and *At* ISCA1b are grouped with yeast Isa1 and human ISCA1 (30), and *At* ISCA2 is grouped with yeast Isa2 and human ISCA2. The three conserved cysteines responsible for the ligation of Fe-S cluster are present in all ATC proteins, Figure 2.2.

ISC targeting factors (e.g., Nfu1, INDH, and Bol1/3) help to transfer the assembled clusters to target apo proteins. In human mitochondria, target proteins could directly receive their $[4Fe\text{-}4S]^{2+}$ clusters from the ISCA1-ISCA2-IBA57 complex, or they could receive them from NFU1/NUBPL following $[4Fe\text{-}4S]^{2+}$ cluster transfer from the ISCA1-ISCA2-IBA57 complex to NFU1/NUBPL. *In vivo* and *in vitro* studies have shown that yeast Nfu1 can bind a $[4Fe\text{-}4S]^{2+}$ cluster via a CXXC motif similar to human and plant homologs (31-33). In yeast and human cells, the deletion of Nfu1 only partially affects aconitase, lipoic acid synthase, and succinate dehydrogenase activity, suggesting a non-essential role for Nfu1 as a $[4Fe\text{-}4S]^{2+}$ cluster targeting

protein (34,35). There are five NFU-type proteins in *Arabidopsis,* and based on their localization, they are divided into two classes (36). NFU1-3 are located in plastids and share a similar sequence identity with cyanobacterial *Sy* Nfu. NFU4 and NFU5 are predicted to be in mitochondria and have a similar sequence and structural organization to *Hs* NFU1 and *Sc* Nfu1, see Figure 2-3 (36). All Nfu-type proteins have a conserved CXXC motif; however, NFU4 and NFU5 have a unique N-terminal domain, which is specific to eukaryotic mitochondrial, cytosolic, and nuclear Nfu proteins, Figure 2.3 (33). *At* NFU4, *At* NFU5, *Hs* NFU1, and *Sc* Nfu1, all contain an N-terminal domain and a C-terminal domain with a CXXC motif involved in $[4Fe\text{-}4S]^{2+}$ cluster binding, Figure 2.3 (31,33). The N-terminal domains may be involved with targeting specific acceptor proteins. However, gene knockout studies indicate that the individual *At* NFU4 and *At* NFU5 proteins have at least partially redundant functions in mitochondria, but together they are essential for seedling development. Both *At* NFU proteins can rescue the growth defect of a yeast *Δnfu1* mutant (30). Recent complementation studies performed with *At* NFU4/5 and ISCA1/2 and the corresponding yeast deletion mutants showed that *At* NFU4/5 can interact with the physiological partners of *Saccharomyces cerevisiae* (*Sc*) Nfu1 and can perform similar functions to yeast Nfu1 (30,35,37). These complementation studies also reported that the heterodimeric complex *At* ISCA1a/2 can functionally substitute for a yeast *isa1/2* mutant, while *At* ISCA1a or *At* ISCA2 homodimers cannot. These observations suggest that the heterodimeric ISCA1a/2 complex is the functional unit in the mitochondrial ISC machinery, which agrees with the *in vitro* studies of human proteins (19). However, spectroscopic characterization and potential functions of *Arabidopsis* ISCA proteins in late-stage ISC machinery have yet to be investigated *in vitro*.

This work provides detailed spectroscopic characterization and interprotein cluster transfer studies involving the three major classes of mitochondrial carrier proteins in *At,* namely monothiol

GRX, ISCA, and NFU proteins. The objective was to clarify the properties and function of the late-acting ISC proteins in the maturation of plant Fe-S proteins. The results show that i) ISCA1a/2 is able to accommodate either one $[2Fe\text{-}2S]^{2+}$ or one $[4Fe\text{-}4S]^{2+}$ cluster per heterodimer, ii) both NFU4 and NFU5 can assemble one $[4Fe\text{-}4S]^{2+}$ cluster per homodimer, iii) GRXS15 can assemble and efficiently transfer a $[2Fe\text{-}2S]^{2+}$ cluster to the mitochondrial *At* FDX1 protein, iv) $[2Fe\text{-}2S]^{2+}$ cluster-bound GRXS15 can assemble a $[4Fe\text{-}4S]^{2+}$ cluster on the ISCA1a/2 heterodimer, v) $[4Fe\text{-}4S]^{2+}$ cluster-bound ISCA1a/2 can efficiently transfer $[4Fe\text{-}4S]^{2+}$ clusters to NFU4 and NFU5, and vi) $[4Fe\text{-}4S]^{2+}$ cluster-bound ISCA1a/2, NFU4, and NFU5 are all competent tor maturation of apo ACO2.

Experimental procedures

All the chemicals and materials were purchased from commercial suppliers (Fisher Scientific, Sigma-Aldrich Chemical Co, and GE Healthcare/Invitrogen) and were used without any further treatment unless otherwise stated. The plasmids for overexpression of *At* GRXS15, FDX1, ISCA1a/2, NFU4, and NFU5 were provided by Dr. Nicolas Rouhier (Université de Lorraine, Nancy, France). Nucleotide sequence of these proteins were performed by the University of Georgia Genomics Facility.

Analytical and spectroscopic methods: Protein concentrations were determined by the DC protein assay (Bio-Rad) using bovine serum albumin (Roche) as standard. Iron concentrations were determined colorimetrically using bathophenanthroline under reducing conditions after digesting proteins in 0.8% $KMnO_4$/0.2 M HCl. A calibration curve was constructed from a series of dilutions of a 1000 ppm atomic absorption iron standard.

The preparation and handling of anaerobic samples for spectroscopic studies and cluster transfer experiments were carried out inside a Vacuum Atmosphere glove box under argon atmosphere at an oxygen level of 2 ppm or below. UV-visible absorption spectra were recorded in sealed quartz cuvettes at room temperature using a Shimadzu-3101PC spectrophotometer. CD spectra were recorded in sealed quartz cuvettes using a Jasco J-715 spectropolarimeter. Resonance Raman samples were prepared under strictly anaerobic conditions and comprised 18-μL frozen droplets of protein solutions (~2 mM in Fe-S clusters) mounted on the cold finger of an Air Products Displex Model CSA-202E closed cycle refrigerator (Air Products, Allentown, PA). Resonance Raman spectra were recorded at 17 K using an Instrument SA Ramanor U1000 scanning spectrometer coupled with a Coherent Sabre argon ion laser. Spectra were recorded by photon counting for 1 s every 0.5 cm^{-1}, using 7 cm^{-1} resolution, and each spectrum is the sum of 80-120 scans. X-band (~9.6 GHz) EPR spectra were recorded using a Bruker ESP-300E EPR spectrometer equipped with a dual-mode ER-4116 cavity and an Oxford Instruments ESR-9 flow cryostat.

Overexpression, anaerobic purification and Fe-S cluster reconstitution of At GRXS15: *At* GRXS15 was heterologously expressed in *E. coli* BL21 (DE3) and co-transformed with the recombinant plasmid and the pSBET plasmid. One colony was grown overnight at 37°C in 100 mL LB media containing 100 μg/mL ampicillin and 30 μg/mL kanamycin. 1 L of the same media was inoculated by adding 20 mL of the culture grown overnight and then incubated at 37°C until an exponential growth phase was attained. Protein expression was induced by adding Isopropyl 1-thio-β-D-galactopyranoside (IPTG) to a final concentration of 100 μg/mL. The cells were allowed to grow for an additional 5 hours at 34°C before harvesting by centrifugation at 6690 × g and storing at –80°C for later use.

For the aerobic purification of *At* GRXS15, 20 g of cell paste were resuspended in 50 mL of buffer A (100 mM Tris-HCl, pH 7.8) containing 150 µg/mL PMSF, 2 mU/mL DNase (Roche), and 0.5 µg/mL RNase (Roche) with an additional 2 mM GSH and lysed by intermittent aerobic sonication on ice. After breaking the cells, the soluble and the insoluble fractions were separated by centrifugation at 39800 × g at 4°C for 1 hour. The soluble fraction was subjected to a 40% ammonium sulfate cut, and the precipitate was removed by centrifugation at 39800 × g for another 30 minutes. The supernatant containing *At* GRXS15 was loaded onto a phenyl sepharose column equilibrated with buffer A containing 2 mM GSH and 1.0 M ammonium sulfate and eluted by a decreasing linear gradient of 1.0 to 0 M ammonium sulfate. Based on gel electrophoresis, fractions containing GRXS15 were concentrated using Amicon ultrafiltration with a YM10 membrane. The concentrated fraction was loaded onto a 25 mL Q Sepharose anion exchange column, previously equilibrated with buffer A, and eluted with an increasing linear gradient of 0 to 1.0 M sodium chloride. Apo GRXS15 was prepared by incubating as-isolated samples with a 50-fold excess of EDTA and a 20-fold excess of potassium ferricyanide for 60 minutes. Apo GRXS15 was then purified with a 15 mL desalting column to remove residual iron and sulfide under anaerobic conditions. The as-isolated apo samples, estimated by SDS-PAGE to be >90% pure, were used in spectroscopic studies and for *in vitro* reconstitution studies.

Reconstitution of Fe-S clusters on apo GRXS15 was carried out under anaerobic conditions inside the glove box. In the presence of 5 mM GSH, apo GRXS15 was incubated with 12-fold excess of ferrous ammonium sulfate (FAS), 12-fold excess of L-cysteine and catalytic amounts of IscS, for approximately 2 hours in a strictly anaerobic environment. The cluster-bound GRXS15 was loaded on to a 5 mL Mono-Q column to remove excess reagents with an increasing

salt gradient of 0-1 M NaCl. The Mono-Q column was able to separate Fe-S cluster-bound GRXS15 into two different colored fractions.

Overexpression and aerobic purification of His-tagged At FDX1: Recombinant FDX1 was expressed in an *E. coli* BL21 (DE3) strain. Colonies containing FDX1 were grown in LB media at 37°C, and exponential protein overexpression was induced with IPTG to a final concentration of 100 μg/mL. The bacterial culture was further allowed to cultivate at 37°C for 5-6 hours. The dark reddish-brown cells were harvested by centrifugation at 6690 × g at 4°C and stored at –80°C for later use.

For the aerobic purification of FDX1, 20 g of cell paste were thawed and resuspended in 50 mL of buffer A and lysed by intermittent aerobic sonication on ice. After breaking the cells, the soluble and the insoluble fractions were separated by centrifugation at 39800 × g at 4°C for 2 hours. The dark reddish-brown soluble fraction containing *At* FDX1 was then loaded onto a 25 mL His-Trap HP column previously equilibrated with binding buffer (100 mM Tris-HCl, pH 7.8, containing 0.5 M NaCl and 20 mM imidazole). The column was washed with 10 column volumes of binding buffer before the protein of interest was eluted with a 20–500 mM imidazole gradient. The purest fractions containing holo *At* FDX1 were collected, and imidazole was removed by loading FDX1 onto a 25 mL desalting column. Based on Fe and protein determinations, UV-visible absorption, and CD studies, holo *At* FDX1 was found to contain 1.0 ± 0.1 $[2Fe\text{-}2S]^{2+}$ cluster/monomer. Apo *At* FDX1 was prepared by acid precipitation with 10% trichloroacetic acid (TCA). The pelleted protein was isolated and resuspended in buffer A. FDX1 was buffer-washed 4-5 times by ultrafiltration dialysis using a YM10 membrane with 100 mM Tris-HCl, pH 7.8. The apo *At* FDX1 used for spectroscopic studies was >95% pure, based on SDS-PAGE gels.

Overexpression, anaerobic purification, and Fe-S cluster reconstitution of His-tagged At ISCA1a/2: Recombinant *At* ISCA1a/2 was expressed in an *E. coli* BL21 (DE3) strain. Cells harboring ISCA1a/2 plasmids were cultivated overnight at 37°C in LB media containing 100 μg/mL spectinomycin, and 20 mL of the culture grown overnight were used to inoculate 1 L of the same media. Protein expression was induced with IPTG to a final concentration of 100 μg/mL when OD_{600} was between 0.6-0.8. The cells were allowed to grow for an additional 5 hours at 34°C before harvesting by centrifugation at 6690 × g and storing at –80°C for later use.

The procedure used to purify ISCA1a/2 is very similar to the purification procedure of FDX1, except that sonication and all chromatographic processes were carried out in the glove box under anaerobic condition (O_2 < 2 ppm). The buffers used in the purification procedure were rigorously degassed to remove oxygen. For the purification of ISCA1a/2, 18 g of reddish cell pellets were thawed and resuspended in 30 mL of buffer A containing 150 μg/mL PMSF, 2 mU/mL DNase (Roche) and 0.5 μg/mL RNase (Roche), and lysed by intermittent anaerobic sonication on ice. After breaking the cells, the soluble and the insoluble fractions were separated by centrifugation at 39800 × g at 4°C for 1.5 hours. The reddish-brown soluble fraction containing *At* ISCA1a/2 was loaded onto a 25 mL His-Trap HP column, which was pre-equilibrated with binding buffer. The column was washed with 10 column volumes of binding buffer before the protein of interest was eluted with a 20–500 mM imidazole gradient. The purest fraction containing holo $[2Fe\text{-}2S]^{2+}$ cluster-bound heterodimeric *At* ISCA1a/2 was collected, and imidazole was removed by loading the concentrated ISCA1a/2 fraction onto a 25 mL desalting column. Apo ISCA1a/2 was prepared by treating the holo protein with a 50-fold excess of EDTA and a 20-fold excess of potassium ferricyanide under anaerobic conditions and removing the excess reagents by ultrafiltration dialysis using a YM10 membrane to remove excess iron and sulfide.

Reconstitution of Fe-S clusters on as purified ISCA1a/2 was carried out under anaerobic conditions in the presence of 2 mM DTT. As purified ISCA1a/2 was incubated with a 12-fold excess of FAS, 12-fold excess of L-cysteine, and catalytic amounts of IscS, for approximately 5 hours in a strictly anaerobic environment. The reconstitution mixture was loaded on to a 10 mL Hitrap Q-Sepharose column (GE Healthcare), and the protein was eluted with an increasing salt gradient of 0–1 M NaCl. A single colored fraction containing predominantly $[4Fe\text{-}4S]^{2+}$ cluster-bound ISCA1a/2 was eluted under an increasing NaCl gradient.

Overexpression, purification and IscS-mediated reconstitution of NFU4 and NFU5: Purified apo forms of *At* NFU4 and *At* NFU5 were supplied by Dr. Nicholas Rouhier. NFU4 and NFU5 were chemically reconstituted by incubating with a 12-fold excess of FAS, a 12-fold excess of L-cysteine and a catalytic amount of IscS in the presence of 2 mM DTT for approximately 50 minutes under strictly anaerobic conditions. The reconstitution was monitored using UV-visible absorption and CD spectroscopy. After purifying with a 10 mL Hitrap Q-Sepharose column, a single fraction containing $[4Fe\text{-}4S]^{2+}$ cluster-bound NFU4 or NFU5 was eluted with an increasing NaCl gradient.

Protocol for donor-to-acceptor cluster transfer studies monitored by UV-visible CD spectroscopy: The time course of the cluster transfer from the cluster-bound donor to apo acceptor were monitored at room temperature, under anaerobic conditions in 1-cm cuvettes using CD spectroscopy. In all cases, the apo protein acceptor was incubated with 2 mM DTT for 30 min and repurified (DTT pretreatment), prior to initiation of the reaction by the addition of apo protein to the donor protein solution. The CD spectrum was monitored until no further change was observed. Peek-to-trough or fixed wavelength changes in CD intensity were used to assess the extent of cluster transfer as a function of time. The data were fitted to second order kinetics using the

Kinetiscope chemical kinetics simulator software package (IBM), based on the initial concentration of Fe-S clusters on the donor protein and the concentration of the apo protein acceptor. The directionality of cluster transfer was assessed by repeating the reaction with cluster-bound acceptor as the donor and the apo donor as the acceptor. The lability of the Fe-S center in the donor in the reaction mixture was assessed by monitoring the UV-visible absorption or CD spectrum of the donor, in the absence of the acceptor, over the time course of the reaction. The specific conditions for each cluster transfer reported in this work are given in the results section and in the figure legends.

Activation of apo At mitochondrial aconitase, ACO2, using Fe-S cluster-loaded forms of ISCA1a/2, NFU4 and NFU5: Non-His tagged *At* ACO2 was overexpressed in *E. coli* BL21 (DE3) strain, aerobically purified and was made apo by incubating as purified *At* ACO2 with EDTA and potassium ferricyanide as described previously (17,38). Activation mixtures contained 2.4 µM apo *At* ACO2 and [4Fe-4S] cluster-containing ISCA1a/2, NFU4 or NFU5, each 7.4 µM in $[4Fe\text{-}4S]^{2+}$ clusters, in 100 mM Tris-HCl buffer, pH 7.8, with 1 mM DTT. $[4Fe\text{-}4S]^{2+}$ cluster concentrations on ISCA1a/2, NFU4 and NFU5 were assessed based on a molar extinction coefficient of ε_{400} = 15.0 $mM^{-1}cm^{-1}$. The same procedure was used in attempts to activate *At* ACO2 (2.4 µM) using [2Fe-2S] cluster-containing ISCA1a/2 (14.5 µM in $[2Fe\text{-}2S]^{2+}$ clusters). The $[2Fe\text{-}2S]^{2+}$ cluster concentration on ISCA1a/2 was assessed using a molar extinction coefficient of ε_{420} = 7.5 $mM^{-1}cm^{-1}$ per $[2Fe\text{-}2S]^{2+}$cluster. Activation mixtures were incubated at room temperature under anaerobic conditions, and 10 µL samples were withdrawn at different times and assayed for aconitase activity. This activity was measured spectrophotometrically at 240 nm by following the formation of *cis*-aconitate from citrate or isocitrate, using a molar absorption coefficient ε_{240} = 3400 $mM^{-1}cm^{-1}$ for *cis*-aconitate (39,40). Anaerobically reconstituted samples of *A. thaliana*

ACO2 containing one [4Fe-4S] cluster per protein monomer were used to establish maximal specific activity.

Results

Nature and properties of Fe-S clusters assembled on At GRXS15 and At FDX1: Aerobic purification of *At* GRXS15 in the presence of GSH resulted in a brown fraction with weak visible absorption characteristic of trace amounts of a $[2Fe\text{-}2S]^{2+}$ cluster (data not shown). Consequently, samples of cluster-bound *At* GRXS15 for spectroscopic characterization and cluster transfer studies were prepared by reconstituting apo GRXS15 under anaerobic conditions. No Fe-S clusters were assembled in samples reconstituted in the absence of GSH, either after pretreatment with DTT or in the presence of 5 mM DTT. This is in contrast to *Sc* Grx5, which reconstituted $[4Fe\text{-}4S]^{2+}$ clusters in the presence of 5 mM DTT (41). However, *in vitro* IscS-mediated reconstitution of apo GRXS15 in the presence of 5 mM GSH, resulted in samples containing a mixture of $[2Fe\text{-}2S]^{2+}$ and linear $[3Fe\text{-}4S]^{1+}$ clusters, based on comparison of UV-visible absorption and CD spectra with published data for other cluster-bound monothiol glutaredoxins (41). Purification of the reconstitution mixture using a Mono-Q column removed excess reagents and separated the homogeneous $[2Fe\text{-}2S]^{2+}$ cluster-bound form of GRXS15 from the linear $[3Fe\text{-}4S]^{1+}$ cluster-bound form. The UV-visible absorption and CD spectra of one fraction are very similar to those of the $[2Fe\text{-}2S]^{2+}$-bound *At* GRXS16 and *Sc* Grx3(42-44), indicating homogenous $[2Fe\text{-}2S]^{2+}$ cluster-bound GRXS15 (Figure 2.4). Moreover, Fe and protein concentrations indicate 2.1 ± 0.2 Fe/dimer, in accord with one $[2Fe\text{-}2S]^{2+}$ cluster per dimer. The UV-visible absorption and CD spectra of the other fraction, notably the general increase in absorption intensity and appearance of pronounced bands at 518 nm and 570 nm, coupled with the appearance of a positive CD band at 550 nm, are indicative of the presence of linear $[3Fe\text{-}4S]^{1+}$ clusters (41,45), see Figure 2.4 The UV-visible

absorption and CD spectra of this fraction are best interpreted as containing a mixture of [2Fe-2S]$^{2+}$ and linear [3Fe-4S]$^{1+}$ clusters. In this work, only the fraction containing homogenous [2Fe-2S]$^{2+}$ cluster was used for in further studies.

FDX1 purified under aerobic conditions was dark reddish-brown in color and exhibited UV-visible absorption and CD spectra characteristics of a [2Fe-2S]$^{2+}$ protein. The spectra shown in Figure 2.5 are also very similar to those of purified human ferredoxins, *Hs* Fdx1 and *Hs* Fdx2 (46). Fe and protein concentrations indicate 1.98 ± 0.2 Fe/monomer, in accord with one [2Fe-2S]$^{2+}$ cluster per monomer.

Purification and spectroscopic characterization of Fe-S clusters assembled on At ISCA1a/2: Anaerobic purification of *At* ISCA1a/2 under strictly anaerobic conditions resulted in a reddish-brown [2Fe-2S]$^{2+}$ cluster-bound form of ISCA1a/2. The samples contained approximately equal amounts of ISCA1a and ISCA2 and were >95% pure as judged by gel electrophoresis, see Figure 2.6. The UV-visible absorption spectrum of anaerobically purified ISCA1a/2 is dominated in the 300–600 nm region by bands centered at 320 nm and 425 nm, and in the CD spectrum, the positive bands are centered at 359 nm and 543 nm and the negative bands are centered at 304 nm, 453 nm, and 606 nm. The UV-visible absorption and CD spectra of anaerobically purified ISCA1a/2 are shown in Figure 2.7 (black lines) and both are characteristic of [2Fe-2S]$^{2+}$ clusters in ATC proteins (18). Protein and iron analysis indicated 0.83 ±0.10 [2Fe-2S]$^{2+}$ clusters per heterodimeric ISCA1a/2. Since [2Fe-2S]$^{2+}$ clusters typically have ε_{425} values between 7 and 11 $mM^{-1}cm^{-1}$ and the UV-visible absorption spectrum of ISCA1a/2 indicated ε_{425}=7.2 ± 0.2 $mM^{-1}cm^{-1}$, this result also indicates that as purified co-expressed ISCA1a/2 contains one [2Fe-2S]$^{2+}$ cluster per heterodimer.

The vibrational properties of the $[2Fe\text{-}2S]^{2+}$ center in ISCA1a/2 were characterized by resonance Raman spectroscopy, which provides information on cluster type and ligand environment. Resonance Raman spectra of as purified $[2Fe\text{-}2S]^{2+}$ cluster-bound ISCA1a/2 in the Fe-S stretching region (240-450 cm^{-1}), obtained using 458 and 488 nm laser excitation, showed an intense band at 288 cm^{-1} and additional major bands at 334 cm^{-1}, 352 cm^{-1}, 398 cm^{-1}, and 421 cm^{-1} (Figure 2.8). The Fe-S stretching frequencies for the $[2Fe\text{-}2S]^{2+}$ cluster in ISCA1a/2 are very similar to those of the all-cysteine ligated $[2Fe\text{-}2S]^{2+}$ centers in ferredoxins, which suggests a similar cluster environment in ISCA1a/2 (47,48). The frequencies are readily assigned to the stretching modes of the $Fe_2S^b{}_2S^t{}_4$ center (S^b = bridging S and S^t = terminal or cysteinyl S), under idealized D_{2h} symmetry, based on published normal mode calculations and $^{34}S^b/^{32}S^b$ isotope shifts for synthetic and biological $[2Fe\text{-}2S]^{2+}$ clusters (18,47), see Table 2.1 .

The $[4Fe\text{-}4S]^{2+}$ cluster-containing form of homodimeric *Azotobacter vinelandii* ^{Nif}IscA can be generated by incubating the subunit-bridging $[2Fe\text{-}2S]^{2+}$ cluster-containing form with DTT for 15 minutes under anaerobic conditions (18). A dissociative mechanism involving two-electron reductive coupling of two $[2Fe\text{-}2S]^{2+}$ clusters at the subunit interface of ^{Nif}IscA monomers was proposed for the formation of a subunit bridging $[4Fe\text{-}4S]^{2+}$ cluster. Subsequent exposure to O_2 resulted in oxidative cleavage of the $[4Fe\text{-}4S]^{2+}$ cluster-bound form of homodimeric ^{Nif}IscA, to form the original $[2Fe\text{-}2S]^{2+}$ cluster-bound form. This suggested that rapid and reversible interconversion between two $[2Fe\text{-}2S]^{2+}$ clusters and one $[4Fe\text{-}4S]^{2+}$ cluster can occur on ^{Nif}IscA in a dithiol reducing medium, with the reaction direction determined by the level of oxidative stress (18). However, unlike the $[2Fe\text{-}2S]^{2+}$ cluster-bound ^{Nif}IscA homodimer, $[2Fe\text{-}2S]^{2+}$ cluster bound ISCA1a/2 heterodimer did not undergo conversion to a $[4Fe\text{-}4S]^{2+}$ cluster-bound form upon

anaerobic incubation with 5 mM DTT for 30 min as judged by no change in the absorption and CD spectra (data not shown).

Anaerobic IscS-mediated reconstitution of as purified $[2Fe\text{-}2S]^{2+}$ cluster-bound ISCA1a/2 heterodimer, in the presence of excess FAS and L-cysteine, resulted in a predominantly $[4Fe\text{-}4S]^{2+}$ cluster-bound form of the ISCA1a/2 heterodimer (Figure 2.7). The UV-visible absorption spectrum of reconstituted ISCA1a/2 showed broad shoulders centered near 320 and 400 nm (Figure 2.7), which are indicative of a $[4Fe\text{-}4S]^{2+}$ cluster. Protein and iron analyses revealed 3.6 ±0.4 Fe per heterodimer and the extinction coefficients based on the protein heterodimer, ε_{280} = 32 $mM^{-1}cm^{-1}$ and ε_{420} = 15 $mM^{-1}cm^{-1}$, both indicate one $[4Fe\text{-}4S]^{2+}$ cluster per heterodimer. As for the $[4Fe\text{-}4S]^{2+}$ cluster-bound ^{Nif}IscA homodimer (18), $[4Fe\text{-}4S]^{2+}$ cluster-bound ISCA1a/2 has negligible visible CD intensity and the observed CD clearly results from residual $[2Fe\text{-}2S]^{2+}$ cluster-bound ISCA1a/2. Gel electrophoresis indicates that the $[4Fe\text{-}4S]^{2+}$ cluster-bound form of ISCA1a/2 retains approximately equal amounts of ISCA1a and ISCA2, see Figure 2.6.

Nature and properties of cluster-bound forms of At NFU4 and NFU5: The nature of Fe-S clusters assembled on *At* NFU4 and *At* NFU5 were determined through spectroscopic and analytical studies of reconstituted samples. Aerobically purified *At* NFU4 and NFU5 have no visible absorption, indicating that they were purified as apo proteins (Figure 2.9). Anaerobic cysteine desulfurase-mediated cluster reconstitution experiments were conducted in the presence of DTT to address the ability of *At* NFU4 and NFU5 to incorporate Fe-S clusters. Reconstituted NFU4 and NFU5 eluted from the Q-Sepharose column as a single brown fraction. The UV-visible absorption spectra of reconstituted NFU4 and NFU5 are very similar, comprising broad shoulders centered near 320 and 410 nm which are characteristic of $[4Fe\text{-}4S]^{2+}$ clusters (Figure 2.9, blue lines). The UV-visible CD spectra of reconstituted NFU4 and NFU5 are also very similar with

intense positive and negative bands at 310 and 350 nm, respectively, and weaker positive bands at 440 and 510 nm. The CD spectra are very similar to the reconstituted $[4Fe\text{-}4S]^{2+}$ cluster-bound form of chloroplast *At* NFU1 (49), but quite different to the reconstituted $[4Fe\text{-}4S]^{2+}$ cluster-bound form of chloroplast *At* NFU2 (31), suggesting at least two distinct classes of plant NFU proteins. Protein and iron analyses indicated 2.2 ±0.3 Fe per NFU4/5 monomer, suggesting that the reconstituted samples contained approximately one $[4Fe\text{-}4S]^{2+}$ cluster per NFU4 and NFU5 homodimer. Moreover, the broad shoulder in the absorption spectra centered at 400 nm (A_{400}/A_{280} = 0.28 ± 0.2) with a molar extinction coefficient ε_{400} = 7.5 ±0.5 $mM^{-1}cm^{-1}$, based on NFU monomer concentration, is indicative of approximately one $[4Fe\text{-}4S]^{2+}$ cluster per NFU4 and NFU5 dimer (17,40,50).

The vibrational properties of the $[4Fe\text{-}4S]^{2+}$ cluster in *At* NFU4 and NFU5 were investigated by low temperature resonance Raman spectroscopy. The resonance Raman spectra of NFU4 and NFU5, shown in Figure 2.10, uniquely characteristic of a $[4Fe\text{-}4S]^{2+}$ cluster. The spectra are similar in terms of Fe-S stretching frequencies and relative intensities to those reported for all-cysteinyl-ligated $[4Fe\text{-}4S]^{2+}$ clusters in ferredoxins and the nitrogenase Fe protein, see Table 2.2. The $[4Fe\text{-}4S]^{2+}$ clusters in NFU4/5 and the nitrogenase Fe protein are both ligated at the subunit interface via CXXC motifs in each subunit. The Fe-S stretching modes are readily assigned, based on normal mode calculations and $^{34}S^{b}/^{32}S^{b}$ isotope shifts reported for cubane $[Fe_4S^{b}_4]S^{t}_4$ units in ferredoxins and appropriate analog complexes, under idealized T_d symmetry, see Table 2.2 (40,51,52). The most intense bands in the spectra of NFU4 and NFU5 are the totally symmetric (A_1) breathing modes of the cubane $[Fe_4S^{b}_4]$ core, which are both observed at 338 cm^{-1}. This is in accord with all cysteinyl ligation (frequency range 333–339 cm^{-}

^{1}), whereas replacement of one ligated cysteine by hydroxide, serinate, or aspartate generally results in higher frequencies (frequency range 340–343 cm^{-1})(53).

Reduction of $[4Fe\text{-}4S]^{2+}$ cluster-containing NFU4 and NFU5 by incubation with a 10-fold excess of dithionite for 10 min resulted in complete cluster degradation based on UV-visible absorption and EPR studies. This indicates that the reduced $[4Fe\text{-}4S]^{1+}$ clusters are not stable in NFU4 and NFU5 and are unlikely to be physiologically relevant. This conclusion is supported by the observation of EPR signals indicative of a reduced $[4Fe\text{-}4S]^{1+}$ cluster in samples of reconstituted NFU4 and NFU5 reduced with one equivalent of dithionite and frozen within 3 s in liquid nitrogen, see Figure 2.11. Identical, near-axial, fast-relaxing $S = 1/2$ EPR signals with $g_{\|} = 2.03$ and $g_{\perp} = 1.93$, maximally accounting for 0.35 spins per NFU dimer, were observed for both NFU4 and NFU5. These resonances were only observable without broadening below 30 K indicating fast relaxation, which is characteristic of $[4Fe\text{-}4S]^{1+}$ clusters. The low $S = 1/2$ spin quantification does not result from mixed spin $[4Fe\text{-}4S]^{1+}$ clusters, since low-field resonances around $g = 5$ indicative of $S = 3/2$ $[4Fe\text{-}4S]^{1+}$ clusters were not observed. Rather, the low spin quantification appears to a consequence of the $[4Fe\text{-}4S]^{1+}$ cluster being a transient intermediate in the reductive cluster degradation pathway, as increasing the reaction time before freezing resulted in progressively decreasing spin quantification.

In vitro cluster transfer from $[2Fe\text{-}2S]^{2+}$-GRXS15 to apo mitochondrial FDX1: Previous studies have reported that monothiol glutaredoxins, i.e., chloroplastic GrxS14 and GrxS16, can donate $[2Fe\text{-}2S]^{2+}$ clusters to apo chloroplastic ferredoxin(43,54). Ferredoxin acts as a multifunctional electron carrier in chloroplasts and can accept clusters from different proteins (55). Mitochondrial *At* FDX1, which binds a $[2Fe\text{-}2S]^{2+}$ cluster, was used to assess the ability of *At* GRXS15 as a cluster transfer protein, since the holo forms of both proteins have major differences

in their CD spectra, see Figure 2.12A. Anaerobic cluster transfer from $[2Fe\text{-}2S]^{2+}$-GRXS15 to DTT-pretreated apo FDX1 with a 1:1 donor:acceptor ratio was 90% complete after 22 min and shows one set of isodichroic points, indicating intact cluster transfer, see Figure 2.12A. Percent cluster transfer was assessed by CD intensity at 550 nm (black circles) and simulated with a second-order rate constant of 1.1×10^4 $M^{-1}min^{-1}$ based on initial 40 μM concentrations for donor and acceptor, see Figure 2.12B. Control studies showed no reaction for the reverse cluster transfer indicating a unidirectional reaction and no degradation of the $[2Fe\text{-}2S]^{2+}$ cluster on GRXS15 in the absence of apo FDX1, over the time course of the reaction, indicating intact cluster transfer. Clearly, GRXS15 is an effective $[2Fe\text{-}2S]^{2+}$ cluster donor for rapid and quantitative maturation apo FDX1.

Incorporation of an Fe-S cluster on apo At ISCA1a/2 via cluster transfer from At [2Fe-2S]$^{2+}$-GRXS15: Anaerobic cluster transfer from *At* $[2Fe\text{-}2S]^{2+}$-GRXS15 to DTT-pretreated apo *At* ISCA1a/2 with a 1:2 donor:acceptor ratio was complete after <1 min based on the loss of the intense CD spectrum of $[2Fe\text{-}2S]^{2+}$-GRXS15, see Figure 2.13A. Kinetic simulations indicate a very rapid reaction with an apparent second-order rate constant > 4.0×10^4 $M^{-1}min^{-1}$ based on the initial concentrations for donor (30 μM in $[2Fe\text{-}2S]^{2+}$ clusters) and acceptor (60 μM in apo *At* ISCA1a/2). The resultant CD spectrum corresponds to $[2Fe\text{-}2S]^{2+}$-ISCA1a/2, but the CD intensity indicates that only 20% of the original $[2Fe\text{-}2S]^{2+}$ clusters are present as $[2Fe\text{-}2S]^{2+}$-ISCA1a/2, Figures 2.7 and 2.13A. Since $[4Fe\text{-}4S]^{2+}$-ISCA1a/2 has a negligible CD spectrum and the UV-visible absorption spectra of the $[4Fe\text{-}4S]^{2+}$ and $[2Fe\text{-}2S]^{2+}$ cluster-bound forms of ISCA1a/2 are quite distinct, see above and Figure 2.7, absorption can be used to monitor formation of $[4Fe\text{-}4S]^{2+}$-ISCA1a/2, see Figure 2.13B. As for the CD spectra, no further change in the absorption spectra is observed after the first minute of reaction and the absorption spectrum quantitatively

shows that the remaining 80% of the original $[2Fe\text{-}2S]^{2+}$ clusters are now present as $[4Fe\text{-}4S]^{2+}$-ISCA1a/2. We conclude that $[2Fe\text{-}2S]^{2+}$ cluster transfer from $[2Fe\text{-}2S]^{2+}$-GRXS15 to apo ISCA1a/2 is a very rapid reaction that results in 80:20 mixture of $[4Fe\text{-}4S]^{2+}$ and $[2Fe\text{-}2S]^{2+}$ cluster-bound ISCA1a/2.

Incorporation of clusters on At NFU4 and At NFU5 via cluster transfer from At ISCA1a/2 and GRXS15: Cluster transfer experiments involving *At* $[2Fe\text{-}2S]^{2+}$-GRXS15 and both $[2Fe\text{-}2S]^{2+}$ and $[4Fe\text{-}4S]^{2+}$ cluster-bound *At* ISCA1a/2 were carried out to assess the cluster donor for *At* NFU4 and NFU5. No cluster transfer was observed using either $[2Fe\text{-}2S]^{2+}$-ISCA1a/2 or $[2Fe\text{-}2S]^{2+}$-GRXS15 as cluster donors for apo NFU4/5, as evidenced by no change in the $[2Fe\text{-}2S]^{2+}$-ISCA1a/2 or $[2Fe\text{-}2S]^{2+}$-GRXS15 CD spectra for 30 min after addition of a two-fold excess of apo NFU4 or NFU5. In contrast, $[4Fe\text{-}4S]^{2+}$ cluster transfer from ISCA1a/2 was shown to be effective for incorporating $[4Fe\text{-}4S]^{2+}$ clusters in both NFU4 and NFU5, see Figures 2.14 and 2.15. Similar cluster transfer data was observed with NFU4 and NFU5. Reconstituted ISCA1a/2 containing 25% $[2Fe\text{-}2S]^{2+}$-ISCA1a/2 and % $[4Fe\text{-}4S]^{2+}$-ISCA1a/2 was used as the donor. Since $[4Fe\text{-}4S]^{2+}$-ISCA1a/2 exhibits negligible visible CD, the CD spectrum of the donor arises solely from $[2Fe\text{-}2S]^{2+}$-ISCA1a/2, which will remain unchanged during $[4Fe\text{-}4S]^{2+}$ cluster transfer, as the above results show that the $[2Fe\text{-}2S]^{2+}$ cluster on ISCA1a/2 cannot be transferred to NFU4 or NFU5. Anaerobic $[4Fe\text{-}4S]^{2+}$ cluster transfer from reconstituted ISCA1a/2 to DTT-pretreated apo NFU4 and NFU5 with a 1:1 donor:acceptor ratio was 80-90% complete after 20 min, see Figure 2.14A and 2.15A. Percent cluster transfer was assessed by the difference in CD intensity at 326 and 362 nm (corrected for the contribution from $[2Fe\text{-}2S]^{2+}$-ISCA1a/2). Kinetic simulation for second-order kinetics yielded a rate constant of 9.1×10^3 $M^{-1}min^{-1}$ for NFU4 and 7.0×10^3 $M^{-1}min^{-1}$ for NFU5, based on the initial concentrations of $[4Fe\text{-}4S]^{2+}$ clusters on ISCA1a/2 and the apo NFU4

and NFU5 dimers, see Figures 2.14B and 2.15B. Control studies showed no reaction for the reverse cluster transfer indicating a unidirectional reaction and absorption studies showed no degradation of the $[4Fe\text{-}4S]^{2+}$ cluster on ISCA1a/2 in the absence of NFU4 or NFU5, over the time course of the reaction, indicating intact cluster transfer.

In summary, we conclude that the rapid, quantitative, and unidirectional cluster transfer from $[4Fe\text{-}4S]^{2+}$-ISCA1a/2 to NFU4 and NFU5 is likely to be a physiologically relevant pathway in plants. In addition, the results indicate that ISCA1a/2 and not NFU4 or NFU5 are responsible for $[2Fe\text{-}2S]^{2+} \rightarrow [4Fe\text{-}4S]^{2+}$ cluster conversions in late stage mitochondrial Fe-S cluster biogenesis and suggest that NFU4 and NFU5 are obligate $[4Fe\text{-}4S]^{2+}$ cluster trafficking proteins.

Activation of At ACO2 using cluster-loaded forms of At ISCA1a/2, NFU4 and NFU5: The ability of [4Fe-4S] cluster-loaded forms of ISCA1a/2, NFU4 and NFU5 and [2Fe-2S] cluster-loaded ISCA1a/2 to effect maturation of apo mitochondrial aconitase, ACO2, was assessed by monitoring aconitase activity as a function of time, after addition of a 3-fold excess of $[4Fe\text{-}4S]^{2+}$ clusters or a 6-fold excess of $[2Fe\text{-}2S]^{2+}$ clusters, see Figure 2.16. Very similar results were observed for [4Fe-4S]-NFU4 and [4Fe-4S]-NFU5 and only the NFU5 data is shown in Figure 2.16. Only the potential [4Fe-4S] cluster donors were effective in rapid restoration of aconitase activity, with second order rate constants of $3.0 \times 10^4\ M^{-1}min^{-1}$ for [4Fe-4S] cluster transfer from ISCA1a/2 and $1.2 \times 10^4\ M^{-1}min^{-1}$ for [4Fe-4S] cluster transfer from NFU4 and NFU5. Both reactions are at least 5 times faster than those observed under the same conditions with equivalent amounts of Fe^{2+} and S^{2-} ions, indicating that both are a consequence of intact cluster transfer rather than cluster degradation and reassembly on ACO2. The negligible rate of restoration of aconitase activity using [2Fe-2S]-ISCA1a/2 indicates that consecutive $[2Fe\text{-}2S]^{2+}$ cluster transfers followed by *in situ* 2-

electron reductive coupling is not a viable mechanism for maturation of the aconitase [4Fe-4S] cluster.

Discussion

The *in vitro* results presented above provide new insights into the function and properties *At* GRXS15, ISCA1a/2 and NFU4/5, which constitute the three major classes of late acting Fe-S cluster carrier proteins in plant mitochondria. In particular, the results show the type of clusters that can be incorporated and a scheme for interprotein cluster trafficking that incorporates a mechanism for reductive $[2Fe\text{-}2S]^{2+}$ to $[4Fe\text{-}4S]^{2+}$ cluster conversion, see Figure 2.17.

In vivo and *in vitro* studies have identified mitochondrial and bacterial monothiol glutaredoxins as primary or sole acceptors of $[2Fe\text{-}2S]^{2+}$ clusters assembled on U-type scaffold proteins(15,16,56). In accord with this hypothesis, *At* GRXS15 plays a central role in plant mitochondrial Fe-S cluster biogenesis and has recently been shown to be essential for plant growth (20). Δ*grxs15* mutants were found to be embryo lethal in *Arabidopsis* and targeted mutations in GRXS15 that diminished GSH and Fe-S cluster binding showed lower aconitase activity and a dwarf phenotype. Interestingly, poplar *grxs15* failed to complement the yeast Δ*grx5* mutant (43) and *At grxs15* only partially complements the yeast Δ*grx5* mutant (20). This suggests significant structural differences in the mitochondrial monothiol glutaredoxins in plants compared to those in yeast and humans and is consistent with the low amino acid similarity (33%) with yeast and human mitochondrial monothiol glutaredoxins, see primary sequence comparisons in Figure 2.1. One noteworthy primary sequence difference is the lack of second partially conserved cysteine in *At* GRXS15. This cysteine forms a disulfide with the active site CGFS cysteine in apo yeast Grx5 (57) and is required for $[4Fe\text{-}4S]^{2+}$ cluster binding by yeast Grx5 in the absence of GSH (41). This

provides rationalization of the observed inability of *At* GRXS15 to reconstitute an Fe-S cluster in the absence of GSH, both in the presence of DTT or in samples pretreated with DTT.

Fe-S cluster reconstitution of apo *At* GRXS15 in the presence of GSH resulted in samples containing a mixture of $[2Fe\text{-}2S]^{2+}$ and linear $[3Fe\text{-}4S]^{1+}$ clusters. As noted previously, such cluster mixtures are commonly found in as purified and reconstituted samples of monothiol glutaredoxins (41). However, reconstituted *At* GRXS15 could be resolved into a pure $[2Fe\text{-}2S]^{2+}$ cluster-containing fraction and a mixed $[2Fe\text{-}2S]^{2+}$ and linear $[3Fe\text{-}4S]^{1+}$ cluster-containing fraction using a Mono-Q column. This facilitated quantitative, CD-monitored cluster transfer studies between [2Fe-2S]-GRXS16 and apo FDX1 which revealed a complete, intact and unidirectional $[2Fe\text{-}2S]^{2+}$ cluster transfer with a second order rate constant of 1.1×10^4 $M^{-1}min^{-1}$ at room temperature. Hence, *At* GRXS15 is shown to be effective in [2Fe-2S] cluster trafficking and the maturation of [2Fe-2S] cluster-containing proteins. This cluster transfer had been reported in a previous study using native gels and CD spectroscopy (20). However, only qualitative data are reported in the previous work and the observation that the CD spectrum of the cluster donor does not correspond to $[2Fe\text{-}2S]^{2+}$ or linear $[3Fe\text{-}4S]^{1+}$ cluster-bound forms of *At* GRXS15 is major concern.

Mitochondrial ATC proteins in yeast (Isa1 and Isa2), human (ISCA1 and ISCA2), and plant (ISCA1a, ISCA1b, ISCA2) function in the maturation of $[4Fe\text{-}4S]^{2+}$ cluster-containing proteins (8,19,21,25,26). However, the role of the plant ATC proteins is solely based on yeast complementation studies, which showed that *At* ISCA1a or ISCA1b rescued the growth defects of *Sc* Δ*Isa1* cells and that *At* ISCA2 rescued the growth defects of *Sc* Δ*Isa2* cells, but not vice-versa. Indeed, plant ATC proteins have never been purified and characterized prior to the work presented herein. Co-expressed *At* ISCA1a/2 purified as a stable heterodimer containing one $[2Fe\text{-}2S]^{2+}$ cluster, which can be converted to a form containing one $[4Fe\text{-}4S]^{2+}$ cluster per heterodimer by

anaerobic Fe-S cluster reconstitution. Moreover, the $[4Fe\text{-}4S]^{2+}$ cluster-bound *At* ISCA1a/2 heterodimer was also formed via rapid $[2Fe\text{-}2S]^{2+}$ cluster transfer from *At* [2Fe-2S]-GRXS15 to apo *At* ISCA1a/2, in the absence of exogenous GSH or DTT. Since GRXS15 cannot bind a $[4Fe\text{-}4S]^{2+}$ cluster, $[4Fe\text{-}4S]^{2+}$ cluster formation must involve the ISCA1a/2 heterodimer acting as a $[4Fe\text{-}4S]^{2+}$ cluster assembler complex. The observation that cluster transfer product is a 80:20 mixture of [4Fe-4S]-ISCA1a/2 and [2Fe-2S]-ISCA1a/2 heterodimers suggests that the first step involves intact $[2Fe\text{-}2S]^{2+}$ cluster transfer from GRXS15 to form a [2Fe-2S]-ISCA1a/2 heterodimer. The second step is likely to involve binding of [2Fe-2S]-GRXS15 to [2Fe-2S]-ISCA1a/2 resulting in two $[2Fe\text{-}2S]^{2+}$ clusters in close enough proximity for two-electron reductive coupling, mediated by disulfide formation involving released cysteine or GSH ligands. Two-electron reductive coupling of two $[2Fe\text{-}2S]^{2+}$ clusters to form a $[4Fe\text{-}4S]^{2+}$ has been well established and rationalized for bacterial ^{Nif}IscA and IscU proteins using DTT and dithionite, respectively as exogenous reducing agents (17,18). In addition, cluster transfer from human [2Fe-2S]-GRX5 to the apo human ISCA1/2 heterodimer also resulted in the formation of [4Fe-4S]-ISCA1/2 in the presence of excess DTT and/or GSH, as assessed by the combination NMR, MS and UV-visible absorption data (19). Hence, the results presented in this work add further support to the proposed role of ISCA1/2 heterodimers as effectors of $[2Fe\text{-}2S]^{2+}$ to $[4Fe\text{-}4S]^{2+}$ cluster conversions in mitochondrial Fe-S cluster biosynthesis.

Individually, NFU4 and NFU5 are redundant in plant mitochondria, but together they are essential for seedling development (58). In addition, they both can rescue the growth defects of the yeast *nfu1* mutant. NFU1 in yeast and human cells has been shown to be important for the maturation of lipoic acid synthase and subunits of respiratory complex I and II (34,59,60). In general, NFU proteins have emerged as a major class of Fe-S cluster carrier proteins capable of

binding and trafficking $[2Fe\text{-}2S]^{2+}$ or $[4Fe\text{-}4S]^{2+}$ clusters that are bound by conserved CXXC motifs at the subunit interface of a homodimer. This is well illustrated by our previous work on chloroplastic *At* NFU2, which purifies as a $[2Fe\text{-}2S]^{2+}$ cluster-containing recombinant protein when expressed in *E. coli*, and can be obtained in either a $[2Fe\text{-}2S]^{2+}$ or $[4Fe\text{-}4S]^{2+}$ cluster-bound form via anaerobic reconstitution of the apo protein (31). [2Fe-2S]-NFU2 has been shown to be a competent $[2Fe\text{-}2S]^{2+}$ cluster donor for GRXS16 and chloroplast ferredoxin (31,61), and [4Fe-4S]-NFU2 was shown to be the likely physiological $[4Fe\text{-}4S]^{2+}$ cluster donor for adenosine 5′-phosphosulfate reductase (31). However, as discussed below, [2Fe-2S] trafficking by NFU proteins may be confined to the SUF systems for Fe-S cluster assembly in bacteria and plastids, which function under higher levels of O_2.

The human and yeast mitochondrial NFU proteins involved with the ISC system for Fe-S cluster assembly have been proposed to function exclusively as $[4Fe\text{-}4S]^{2+}$ cluster carrier proteins based on both *in vivo* and *in vitro* evidence (5,32-35). This hypothesis has recently been challenged in a series of five publications by Cowan and coworkers, which claim that human mitochondrial NFU1 is a $[2Fe\text{-}2S]^{2+}$ cluster carrier protein, based on inconclusive UV-visible absorption/CD and EPR data (62-66). However, this interpretation is incorrect, based on our characterization of the homologous mitochondrial *At* NFU4 and NFU5 as $[4Fe\text{-}4S]^{2+}$ cluster-carrier proteins. The UV-visible absorption and CD of reconstituted *At* NFU4 and NFU5 are essentially the same as those reported for reconstituted human NFU1 (62). However, the resonance Raman spectra of reconstituted *At* NFU4 and NFU5 and the EPR spectra of reduced samples, unambiguously demonstrate that these absorption and CD attributes are indicative of a $[4Fe\text{-}4S]^{2+}$ cluster, not a $[2Fe\text{-}2S]^{2+}$ cluster. Moreover, Mössbauer and NMR studies have also demonstrated that reconstituted human NFU1 exclusively contains a $[4Fe\text{-}4S]^{2+}$ cluster (32,33). This reinterpretation

necessitates a major reevaluation of the results and conclusions of Cowan and coworkers studies of human NFU1 (62-66). The discovery that both NFU4 and NFU5 are $[4Fe\text{-}4S]^{2+}$ cluster-binding proteins, coupled with our inability to assemble a $[2Fe\text{-}2S]^{2+}$ cluster on *At* NFU4 and NFU5, either by reconstitution or cluster transfer from *At* [2Fe-2S]-ISCA1a/2 or *At* [2Fe-2S]-GRXS15, is in accord with the hypothesis that mitochondrial NFU proteins function in $[4Fe\text{-}4S]^{2+}$ cluster trafficking. Nevertheless, we cannot rule out the possibility that $[4Fe\text{-}4S]^{2+}$ cluster assembly on NFU4/5 in plants can also occur via $[2Fe\text{-}2S]^{2+}$ cluster transfer from a GRXS15/BOLA complex, as recently proposed for the formation of human mitochondrial [4Fe-4S]-NFU1 via $[2Fe\text{-}2S]^{2+}$ clusters provided by a GLRX5/BOLA3 complex (67).

Cluster transfer studies also implicate [4Fe-4S]-ISCA1a/2 as a viable and unidirectional donor for incorporating $[4Fe\text{-}4S]^{2+}$ clusters on NFU4 and NFU5. The second order rate constants for intact $[4Fe\text{-}4S]^{2+}$ cluster transfer from [4Fe-4S]-ISCA1a/2 to NFU4 and NFU5, 9.1×10^3 $M^{-1}min^{-1}$ and 7.0×10^3 $M^{-1}min^{-1}$, respectively, are potentially physiologically relevant. However, these cluster transfers were performed in the absence of mitochondrial *At* IBA57.1. IBA57 has been shown to form an essential functional complex with ISCA1/2 in yeast and human mitochondria (21,25) and *At* IBA57.1 complements the *Sc ΔIba57* mutant. While previous results (19), and the results presented herein, argue against IBA57 playing a role in $[4Fe\text{-}4S]^{2+}$ cluster assembly on ISCA1/2 heterodimers, IBA57 may be required for preventing oxidative degradation of the assembled $[4Fe\text{-}4S]^{2+}$ cluster and/or facilitating $[4Fe\text{-}4S]^{2+}$ cluster transfer to client proteins. Unfortunately, our inability to express *At* IBA57.1 as soluble protein has precluded *in vitro* experiments to establish the function of *At* IBA57.1.

Do ISCA1a/2 heterodimers function solely as $[4Fe\text{-}4S]^{2+}$ cluster assembler proteins that supply downstream $[4Fe\text{-}4S]^{2+}$ cluster-carrier proteins such as NFU4/5 or do they also function in

terminal $[4Fe\text{-}4S]^{2+}$ cluster delivery to a subset of client enzymes? The *in vitro* cluster transfer results presented in this work suggest that the latter is correct, based on the ability of [4Fe-4S]-ISCA1a/2 to effect rapid maturation of *At* ACO2 via intact cluster transfer (second order rate constant of 3.0×10^4 $M^{-1}min^{-1}$), even in the absence of IBA57.1. In addition, [4Fe-4S]-NFU4 and [4Fe-4S]-NFU5 are shown to be viable alternative $[4Fe\text{-}4S]^{2+}$ cluster donors for *At* ACO2, albeit with slightly lower rates of cluster transfer (second order rate constants of ~1.2×10^4 $M^{-1}min^{-1}$). This is consistent with the non-essential role of NFU1 in yeast and human mitochondria, as evidenced by partially defective Fe-S enzymes aconitase, succinate dehydrogenase, and lipoic acid synthase, in cells lacking NFU1 (34,35,68). Our cluster transfer studies also support mitochondrial aconitase maturation via intact $[4Fe\text{-}4S]^{2+}$ cluster transfer, rather than a mechanism involving sequential transfer of two $[2Fe\text{-}2S]^{2+}$ clusters followed by *in situ* reductive coupling, as recently proposed by Cowan and coworkers for human mitochondrial and cytosolic aconitase (66).

Acknowledgements

This work was supported by a grant from the National Institutes of Health (R37GM62524 to M.K.J).

References

1. Johnson, D. C., Dean, D. R., Smith, A. D., and Johnson, M. K. (2005) Structure, function, and formation of biological iron-sulfur clusters. *Annu. Rev. Biochem.* **74**, 247-281
2. Fuss, J. O., Tsai, C. L., Ishida, J. P., and Tainer, J. A. (2015) Emerging critical roles of Fe-S clusters in DNA replication and repair. *Biochim. Biophys. Acta* **1853**, 1253-1271
3. Crack, J. C., and Le Brun, N. E. (2018) Redox-Sensing Iron-Sulfur Cluster Regulators. *Antioxid. Redox. Signal.* **29**, 1809-1829
4. Dong, G., Witcher, S., Outten, F. W., and Pilon, M. (2017). The Suf system in archaea, bacteria, and eukaryotic organelles. In: Metalloprotein Active Site Assembly, M. K. Johnson and R. A. Scott, eds., Chichester, UK: John Wiley and Sons, pp 37-52.
5. Braymer, J. J., and Lill, R. (2017) Iron-sulfur cluster biogenesis and trafficking in mitochondria. *J. Biol. Chem.* **292**, 12754-12763
6. Couturier, J., Touraine, B., Briat, J. F., Gaymard, F., and Rouhier, N. (2013) The iron-sulfur cluster assembly machineries in plants: current knowledge and open questions. *Front Plant Sci* **4**, 259
7. Lill, R., Hoffmann, B., Molik, S., Pierik, A. J., Rietzschel, N., Stehling, O., Uzarska, M. A., Webert, H., Wilbrecht, C., and Muhlenhoff, U. (2012) The role of mitochondria in cellular iron-sulfur protein biogenesis and iron metabolism. *Biochim. Biophys. Acta* **1823**, 1491-1508

8. Lill, R., and Muhlenhoff, U. (2008) Maturation of iron-sulfur proteins in eukaryotes: Mechanisms, connected processes, and diseases. *Annu. Rev. Biochem.* **77**, 669-700

9. Balk, J., and Schaedler, T. A. (2014) Iron cofactor assembly in plants. *Annu. Rev. Plant Biol.* **65**, 125-153

10. Frazzon, A. P., Ramirez, M. V., Warek, U., Balk, J., Frazzon, J., Dean, D. R., and Winkel, B. S. (2007) Functional analysis of *Arabidopsis* genes involved in mitochondrial iron-sulfur cluster assembly. *Plant Mol. Biol.* **64**, 225-240

11. Leon, S., Touraine, B., Briat, J. F., and Lobreaux, S. (2005) Mitochondrial localization of *Arabidopsis thaliana* Isu Fe-S scaffold proteins. *FEBS Lett.* **579**, 1930-1934

12. Van Vranken, J. G., Jeong, M. Y., Wei, P., Chen, Y. C., Gygi, S. P., Winge, D. R., and Rutter, J. (2016) The mitochondrial acyl carrier protein (ACP) coordinates mitochondrial fatty acid synthesis with iron sulfur cluster biogenesis. *eLife* **5**, e17828

13. Xu, X. M., Lin, H., Latijnhouwers, M., and Moller, S. G. (2009) Dual localized AtHscB involved in iron sulfur protein biogenesis in *Arabidopsis*. *PLoS One* **4**, e7662

14. Chandramouli, K., and Johnson, M. K. (2006) HscA and HscB stimulate [2Fe-2S] cluster transfer from IscU to apoferredoxin in an ATP-dependent reaction. *Biochemistry* **45**, 11087-11095

15. Shakamuri, P., Zhang, B., and Johnson, M. K. (2012) Monothiol glutaredoxins function in storing and transporting [Fe_2S_2] clusters assembled on IscU scaffold proteins. *J. Am. Chem. Soc.* **134**, 15213-15216

16. Uzarska, M. A., Dutkiewicz, R., Freibert, S. A., Lill, R., and Mühlenhoff, U. (2013) The mitochondrial Hsp70 chaperone Ssq1 facilitates Fe/S cluster transfer from Isu1 to Grx5 by complex formation. *Mol. Biol. Cell* **24**, 1830-1841

17. Chandramouli, K., Unciuleac, M. C., Naik, S., Dean, D. R., Huynh, B. H., and Johnson, M. K. (2007) Formation and properties of [4Fe-4S] clusters on the IscU scaffold protein. *Biochemistry* **46**, 6804-6811

18. Mapolelo, D. T., Zhang, B., Naik, S. G., Huynh, B. H., and Johnson, M. K. (2012) Spectroscopic and functional characterization of iron-sulfur cluster-bound forms of *Azotobacter vinelandii* ^{Nif}IscA. *Biochemistry* **51**, 8071-8084

19. Brancaccio, D., Gallo, A., Mikolajczyk, M., Zovo, K., Palumaa, P., Novellino, E., Piccioli, M., Ciofi-Baffoni, S., and Banci, L. (2014) Formation of [4Fe-4S] clusters in the mitochondrial iron-sulfur cluster assembly machinery. *J. Am. Chem. Soc.* **136**, 16240-16250

20. Moseler, A., Aller, I., Wagner, S., Nietzel, T., Przybyla-Toscano, J., Muhlenhoff, U., Lill, R., Berndt, C., Rouhier, N., Schwarzlander, M., and Meyer, A. J. (2015) The mitochondrial monothiol glutaredoxin S15 is essential for iron-sulfur protein maturation in *Arabidopsis thaliana*. *Proc. Natl. Acad. Sci. U. S. A.* **112**, 13735-13740

21. Sheftel, A. D., Wilbrecht, C., Stehling, O., Niggemeyer, B., Elsasser, H. P., Muhlenhoff, U., and Lill, R. (2012) The human mitochondrial ISCA1, ISCA2, and IBA57 proteins are required for [4Fe-4S] protein maturation. *Mol. Biol. Cell* **23**, 1157-1166

22. Gelling, C., Dawes, I. W., Richhardt, N., Lill, R., and Mühlenhoff, U. (2008) Mitochondrial Iba57p is required for Fe/S cluster formation on aconitase and activation of radical SAM enzymes. *Mol. Cell. Biol.* **28**, 1851-1861

23. Gourdoupis, S., Nasta, V., Calderone, V., Ciofi-Baffoni, S., and Banci, L. (2018) IBA57 Recruits ISCA2 to Form a [2Fe-2S] Cluster-Mediated Complex. *J. Am. Chem. Soc.* **140**, 14401-14412

24. Nasta, V., Da Vela, S., Gourdoupis, S., Ciofi-Baffoni, S., Svergun, D. I., and Banci, L. (2019) Structural properties of [2Fe-2S] ISCA2-IBA57: a complex of the mitochondrial iron-sulfur cluster assembly machinery. *Sci. Rep.* **9**, 18986

25. Mühlenhoff, U., Richter, N., Pines, O., Pierik, A. J., and Lill, R. (2011) Specialized function of yeast Isa1 and Isa2 proteins in the maturation of mitochondrial [4Fe-4S] proteins. *J. Biol. Chem.* **286**, 41205-41216

26. Beilschmidt, L. K., Ollagnier de Choudens, S., Fournier, M., Sanakis, I., Hograindleur, M. A., Clemancey, M., Blondin, G., Schmucker, S., Eisenmann, A., Weiss, A., Koebel, P., Messaddeq, N., Puccio, H., and Martelli, A. (2017) ISCA1 is essential for mitochondrial Fe_4S_4 biogenesis *in vivo*. *Nat Commun* **8**, 15124

27. Ciofi-Baffoni, S., Nasta, V., and Banci, L. (2018) Protein networks in the maturation of human iron-sulfur proteins. *Metallomics* **10**, 49-72

28. Abdel-Ghany, S. E., Ye, H., Garifullina, G. F., Zhang, L., Pilon-Smits, E. A., and Pilon, M. (2005) Iron-sulfur cluster biogenesis in chloroplasts. Involvement of the scaffold protein CpIscA. *Plant Physiol.* **138**, 161-172

29. Vinella, D., Brochier-Armanet, C., Loiseau, L., Talla, E., and Barras, F. (2009) Iron-sulfur (Fe/S) protein biogenesis: phylogenomic and genetic studies of A-type carriers. *PLoS Genet.* **5**, e1000497

30. Uzarska, M. A., Przybyla-Toscano, J., Spantgar, F., Zannini, F., Lill, R., Mühlenhoff, U., and Rouhier, N. (2018) Conserved functions of *Arabidopsis* mitochondrial late-acting maturation factors in the trafficking of ironsulfur clusters. *Biochim Biophys Acta Mol Cell Res* **1865**, 1250-1259

31. Gao, H., Subramanian, S., Couturier, J., Naik, S. G., Kim, S. K., Leustek, T., Knaff, D. B., Wu, H. C., Vignols, F., Huynh, B. H., Rouhier, N., and Johnson, M. K. (2013) *Arabidopsis thaliana* Nfu2 accommodates [2Fe-2S] or [4Fe-4S] clusters and is competent for *in vitro* maturation of chloroplast [2Fe-2S] and [4Fe-4S] cluster-containing proteins. *Biochemistry* **52**, 6633-6645

32. Tong, W. H., Jameson, G. N., Huynh, B. H., and Rouault, T. A. (2003) Subcellular compartmentalization of human Nfu, an iron-sulfur cluster scaffold protein, and its ability to assemble a [4Fe-4S] cluster. *Proc. Natl. Acad. Sci. U. S. A.* **100**, 9762-9767

33. Cai, K., Liu, G., Frederick, R. O., Xiao, R., Montelione, G. T., and Markley, J. L. (2016) Structural/functional properties of human NFU1, an intermediate [4Fe-4S] carrier in human mitochondrial iron-sulfur cluster biogenesis. *Structure* **24**, 2080-2091

34. Navarro-Sastre, A., Tort, F., Stehling, O., Uzarska, M. A., Arranz, J. A., Del Toro, M., Labayru, M. T., Landa, J., Font, A., Garcia-Villoria, J., Merinero, B., Ugarte, M., Gutierrez-Solana, L. G., Campistol, J., Garcia-Cazorla, A., Vaquerizo, J., Riudor, E., Briones, P., Elpeleg, O., Ribes, A., and Lill, R. (2011) A fatal mitochondrial disease is associated with defective NFU1 function in the maturation of a subset of mitochondrial Fe-S proteins. *Am. J. Hum. Genet.* **89**, 656-667

35. Melber, A., Na, U., Vashisht, A., Weiler, B. D., Lill, R., Wohlschlegel, J. A., and Winge, D. R. (2016) Role of Nfu1 and Bol3 in iron-sulfur cluster transfer to mitochondrial clients. *Elife* **5**, e15991

36. Leon, S., Touraine, B., Ribot, C., Briat, J. F., and Lobreaux, S. (2003) Iron-sulphur cluster assembly in plants: distinct NFU proteins in mitochondria and plastids from *Arabidopsis thaliana*. *Biochem. J.* **371**, 823-830

37. Benz, C., Kovarova, J., Kralova-Hromadova, I., Pierik, A. J., and Lukes, J. (2016) Roles of the Nfu Fe-S targeting factors in the trypanosome mitochondrion. *Int. J. Parasitol.* **46**, 641-651

38. Kennedy, M. C., and Beinert, H. (1988) The state of cluster SH^- and S^{2-} of aconitase during cluster interconversions and removal. A convenient preparation of apoenzyme. *J. Biol. Chem.* **263**, 8194-8198

39. Unciuleac, M. C., Chandramouli, K., Naik, S., Mayer, S., Huynh, B. H., Johnson, M. K., and Dean, D. R. (2007) *In vitro* activation of apo-aconitase using a [4Fe-4S] cluster-loaded form of the IscU [Fe-S] cluster scaffolding protein. *Biochemistry* **46**, 6812-6821

40. Bandyopadhyay, S., Naik, S. G., O'Carroll, I. P., Huynh, B. H., Dean, D. R., Johnson, M. K., and Dos Santos, P. C. (2008) A proposed role for the *Azotobacter vinelandii* NfuA protein as an intermediate iron-sulfur cluster carrier. *J. Biol. Chem.* **283**, 14092-14099

41. Zhang, B., Bandyopadhyay, S., Shakamuri, P., Naik, S. G., Huynh, B. H., Couturier, J., Rouhier, N., and Johnson, M. K. (2013) Monothiol glutaredoxins can bind linear $[Fe_3S_4]^+$ and $[Fe_4S_4]^{2+}$ clusters in addition to $[Fe_2S_2]^{2+}$ clusters: spectroscopic characterization and functional implications. *J. Am. Chem. Soc.* **135**, 15153-15164

42. Li, H., Mapolelo, D. T., Dingra, N. N., Naik, S. G., Lees, N. S., Hoffman, B. M., Riggs-Gelasco, P. J., Huynh, B. H., Johnson, M. K., and Outten, C. E. (2009) The yeast iron regulatory proteins Grx3/4 and Fra2 form heterodimeric complexes containing a [2Fe-2S] cluster with cysteinyl and histidyl ligation. *Biochemistry* **48**, 9569-9581

43. Bandyopadhyay, S., Gama, F., Molina-Navarro, M. M., Gualberto, J. M., Claxton, R., Naik, S. G., Huynh, B. H., Herrero, E., Jacquot, J. P., Johnson, M. K., and Rouhier, N.

(2008) Chloroplast monothiol glutaredoxins as scaffold proteins for the assembly and delivery of [2Fe-2S] clusters. *EMBO J.* **27**, 1122-1133

44. Mapolelo, D. T., Zhang, B., Randeniya, S., Albetel, A. N., Li, H., Couturier, J., Outten, C. E., Rouhier, N., and Johnson, M. K. (2013) Monothiol glutaredoxins and A-type proteins: Partners in Fe-S cluster trafficking. *Dalton Trans* **42**, 3107-3115

45. Kennedy, M. C., Kent, T. A., Emptage, M., Merkle, H., Beinert, H., and Munck, E. (1984) Evidence for the formation of a linear [3Fe-4S] cluster in partially unfolded aconitase. *J. Biol. Chem.* **259**, 14463-14471

46. Sheftel, A. D., Stehling, O., Pierik, A. J., Elsasser, H. P., Mühlenhoff, U., Webert, H., Hobler, A., Hannemann, F., Bernhardt, R., and Lill, R. (2010) Humans possess two mitochondrial ferredoxins, Fdx1 and Fdx2, with distinct roles in steroidogenesis, heme, and Fe/S cluster biosynthesis. *Proc. Natl. Acad. Sci. U. S. A.* **107**, 11775-11780

47. Fu, W., Drozdzewski, P. M., Davies, M. D., Sligar, S. G., and Johnson, M. K. (1992) Resonance Raman and magnetic circular dichroism studies of reduced [2Fe-2S] proteins. *J. Biol. Chem.* **267**, 15502-15510

48. Han, S., Czernuszewicz, R. S., Kimura, T., Adams, M. W. W., and Spiro, T. G. (1989) Fe_2S_2 protein resonance Raman spectra revisited: structural variations among adrenodoxin, ferredoxin, and red paramagnetic protein. *J. Am. Chem. Soc.* **111**, 3505-3511

49. Roland, M., Przybyla-Toscano, J., Vignols, F., Berger, N., Azam, T., Christ, L., Santoni, V., Wu, H. C., Dhalleine, T., Johnson, M. K., Dubos, C., Couturier, J., and Rouhier, N. (2020) The plastidial *Arabidopsis thaliana* NFU1 protein binds and delivers [4Fe-4S] clusters to specific client proteins. *J. Biol. Chem.*, 10.1074/jbc.RA1119.011034

50. Agar, J. N., Krebs, C., Frazzon, J., Huynh, B. H., Dean, D. R., and Johnson, M. K. (2000) IscU as a scaffold for iron-sulfur cluster biosynthesis: sequential assembly of [2Fe-2S] and [4Fe-4S] clusters in IscU. *Biochemistry* **39**, 7856-7862

51. Zhang, B., Crack, J. C., Subramanian, S., Green, J., Thomson, A. J., Le Brun, N. E., and Johnson, M. K. (2012) Reversible cycling between cysteine persulfide-ligated [2Fe-2S] and cysteine-ligated [4Fe-4S] clusters in the FNR regulatory protein. *Proc. Natl. Acad. Sci. U. S. A.* **109**, 15734-15739

52. Czernuszewicz, R. S., Macor, K. A., Johnson, M. K., Gewirth, A., and Spiro, T. G. (1987) Vibrational mode structure and symmetry in proteins and analogs containing Fe_4S_4 clusters: Resonance Raman evidence that HiPIP is tetrahedral while ferredoxin undergoes a D_{2d} distortion. *J. Am. Chem. Soc.* **109**, 7178-7187

53. Brereton, P. S., Duderstadt, R. E., Staples, C. R., Johnson, M. K., and Adams, M. W. (1999) Effect of serinate ligation at each of the iron sites of the [Fe_4S_4] cluster of *Pyrococcus furiosus* ferredoxin on the redox, spectroscopic, and biological properties. *Biochemistry* **38**, 10594-10605

54. Subramanian, S. (2010) Characterization of the properties and roles of Fe-S centers in ferredoxins, glutaredoxins and radical S-adenosyl methionine enzymes. *Ph.D. Thesis, University of Georgia*

55. Sticht, H., and Rösch, P. (1998) The structure of iron–sulfur proteins. *Prog Biophys Mol Bio* **70**, 95-136

56. Mühlenhoff, U., Gerber, J., Richhardt, N., and Lill, R. (2003) Components involved in assembly and dislocation of iron-sulfur clusters on the scaffold protein Isu1p. *EMBO J.* **22**, 4815-4825

57. Tamarit, J., Belli, G., Cabiscol, E., Herrero, E., and Ros, J. (2003) Biochemical characterization of yeast mitochondrial Grx5 monothiol glutaredoxin. *J. Biol. Chem.* **278**, 25745-25751

58. Maclean, A. E. (2017) The function of respiratory complex I in plants and in human disease. *Ph. D.Thesis, University of East Anglia*

59. Cameron, J. M., Janer, A., Levandovskiy, V., Mackay, N., Rouault, T. A., Tong, W. H., Ogilvie, I., Shoubridge, E. A., and Robinson, B. H. (2011) Mutations in iron-sulfur cluster scaffold genes NFU1 and BOLA3 cause a fatal deficiency of multiple respiratory chain and 2-oxoacid dehydrogenase enzymes. *Am. J. Hum. Genet.* **89**, 486-495

60. McCarthy, E. L., and Booker, S. J. (2017) Destruction and reformation of an iron-sulfur cluster during catalysis by lipoyl synthase. *Science* **358**, 373-377

61. Nishio, K., and Nakai, M. (2000) Transfer of iron-sulfur cluster from NifU to apoferredoxin. *J. Biol. Chem.* **275**, 22615-22618

62. Wachnowsky, C., Fidai, I., and Cowan, J. A. (2016) Iron-sulfur cluster exchange reactions mediated by the human Nfu protein. *J. Biol. Inorg. Chem.* **21**, 825-836

63. Wesley, N. A., Wachnowsky, C., Fidai, I., and Cowan, J. A. (2017) Understanding the molecular basis for multiple mitochondrial dysfunctions syndrome 1 (MMDS1): impact of a disease-causing Gly189Arg substitution on NFU1. *FEBS J* **284**, 3838-3848

64. Wesley, N. A., Wachnowsky, C., Fidai, I., and Cowan, J. A. (2017) Analysis of NFU-1 metallocofactor binding-site substitutions-impacts on iron-sulfur cluster coordination and protein structure and function. *FEBS J* **284**, 3817-3837

65. Wachnowsky, C., Liu, Y., Yoon, T., and Cowan, J. A. (2018) Regulation of human Nfu activity in Fe-S cluster delivery-characterization of the interaction between Nfu and the HSPA9/Hsc20 chaperone complex. *FEBS J* **285**, 391-410

66. Wachnowsky, C., Hendricks, A. L., Wesley, N. A., Ferguson, C., Fidai, I., and Cowan, J. A. (2019) Understanding the mechanism of [4Fe-4S] cluster assembly on eukaryotic mitochondrial and cytosolic aconitase. *Inorg. Chem.* **58**, 13686-13695

67. Nasta, V., Suraci, D., Gourdoupis, S., Ciofi-Baffoni, S., and Banci, L. (2019) A pathway for assembling $[4Fe\text{-}4S]^{2+}$ clusters in mitochondrial iron-sulfur protein biogenesis. *FEBS J*, 10.1111/febs.15140

68. Uzarska, M. A., Nasta, V., Weiler, B. D., Spantgar, F., Ciofi-Baffoni, S., Saviello, M. R., Gonnelli, L., Mühlenhoff, U., Banci, L., and Lill, R. (2016) Mitochondrial Bol1 and Bol3 function as assembly factors for specific iron-sulfur proteins. *eLife* **5**, e16673

69. Fu, W. G., Morgan, T. V., Mortenson, L. E., and Johnson, M. K. (1991) Resonance Raman studies of the [4Fe-4S] to [2Fe-2S] cluster conversion in the iron protein of nitrogenase. *FEBS Lett.* **284**, 165-168

Table 2.1: Fe-S stretching frequencies (cm^{-1}) and vibrational assignments for the $[2Fe\text{-}2S]^{2+}$ clusters in *A. thaliana* ISCA1a/2, *A. vinelandii* ^{Nif}IscA and *S. oleracea* ferredoxin

Assignments under D_{2h} symmetry[a]	*S. oleracea* 2Fe Ferredoxin[b]	*A. vinelandii* ^{Nif}IscA[b]	*At thaliana* ISCA1a/2
$B_{2u}{}^{b}$	427	421	421
$A_g{}^{b}$	395	396	398
$B_{3u}{}^{b}$	367	358	368
$B_{1u}{}^{t}$, $B_{2g}{}^{t}$	357	345	352
$A_g{}^{t}$	338	338	334
$B_{1g}{}^{b}$	329	325	~324
$B_{3u}{}^{t}$	283	290	288

[a]Symmetry labels assuming idealized T_d symmetry for the $Fe_2S_2{}^{b}S_4{}^{t}$ core, where Fe-S^{b} and Fe-S^{t} indicate bridging and terminal stretching, respectively. [b]Taken from Ref (18).

Table 2.2: Fe-S stretching frequencies (cm^{-1}) and vibrational assignments for the $[4Fe\text{-}4S]^{2+}$ centers in *C. pasterianum* 8Fe Fd, *C. pasterianum* N_2ase Fe-protein, *A. thaliana* NFU4, and *A. thaliana* NFU5

Assignments under T_d symmetry[a]	*C. pasterianum* 8Fe Ferredoxin[b]	*C. pasterianum* N_2ase Fe-protein[c]	*A. thaliana* NFU4	*A. thaliana* NFU5
Mainly Terminal $\nu(Fe\text{-}S^t)$				
A_1	395	391	409 or 388	405 or 387
T_2	363, 351	356	358	358
Mainly Bridging $\nu(Fe\text{-}S^b)$				
T_2	380	391	388	387
A_1	338	335	338	338
E	298, 276	281	299, 288	299. 288
T_1	276, 266	265	288, 277	288, 274
T_2	251	248	252	252

[a]Symmetry labels assuming idealized T_d symmetry for the $Fe_4S_4{}^bS_4{}^t$ core, where $Fe\text{-}S^b$ and $Fe\text{-}S^t$ indicate bridging and terminal stretching, respectively.

[b]Taken from Ref. (52)

[c]Taken from Ref. (69)

Figure 2.1: Primary sequence alignments of monothiol glutaredoxins from plant, yeast and human: *At* GRXS15; *Sc* Grx5; *Hs* GLRX5. The sequence alignment was performed with MUSCLE. Conserved amino acids are highlighted in blue.

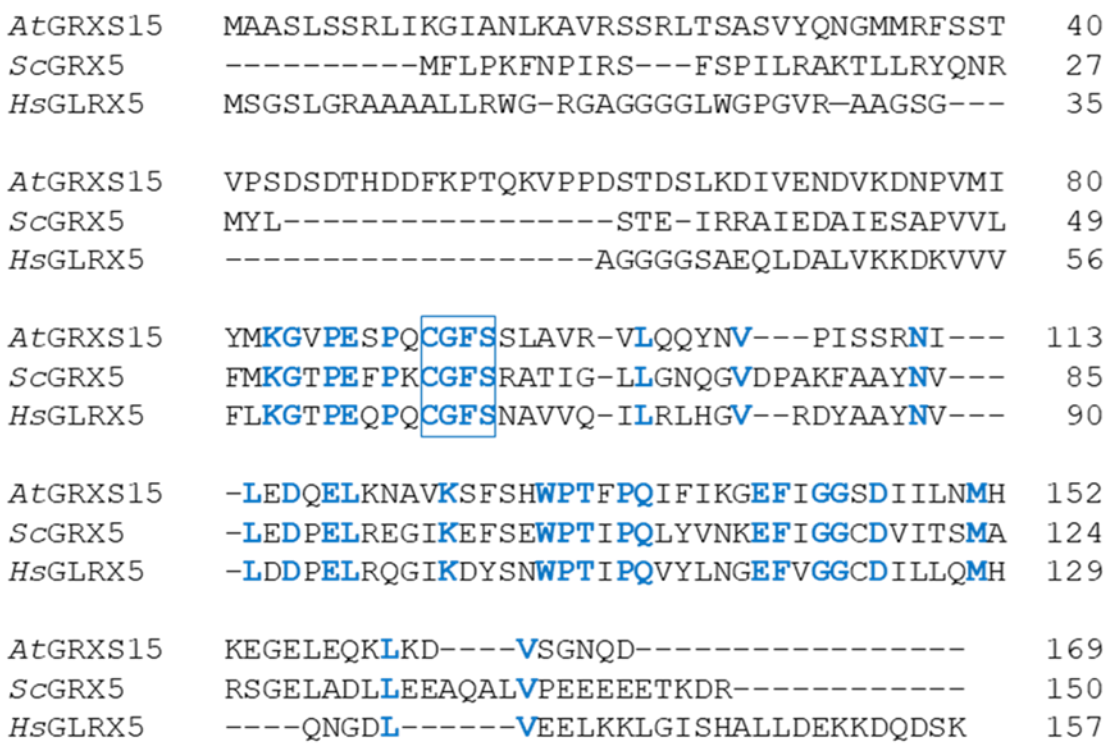
AtGRXS15 MAASLSSRLIKGIANLKAVRSSRLTSASVYQNGMMRFSST 40
ScGRX5 ----------MFLPKFNPIRS---FSPILRAKTLLRYQNR 27
HsGLRX5 MSGSLGRAAAALLRWG-RGAGGGGLWGPGVR—AAGSG--- 35
AtGRXS15 VPSDSDTHDDFKPTQKVPPDSTDSLKDIVENDVKDNPVMI 80
ScGRX5 MYL----------STE-IRRAIEDAIESAPVVL 49
HsGLRX5 ----------AGGGGSAEQLDALVKKDKVVV 56
AtGRXS15 YMKGVPESPQCGFSSLAVR-VLQQYNV---PISSRNI--- 113
ScGRX5 FMKGTPEFPKCGFSRATIG-LLGNQGVDPAKFAAYNV--- 85
HsGLRX5 FLKGTPEQPQCGFSNAVVQ-ILRLHGV--RDYAAYNV--- 90
AtGRXS15 -LEDQELKNAVKSFSHWPTFPQIFIKGEFIGGSDIILNMH 152
ScGRX5 -LEDPELREGIKEFSEWPTIPQLYVNKEFIGGCDVITSMA 124
HsGLRX5 -LDDPELRQGIKDYSNWPTIPQVYLNGEFVGGCDILLQMH 129
AtGRXS15 KEGELEQKLKD----VSGNQD---------- 169
ScGRX5 RSGELADLLEEAQALVPEEEEETKDR---------- 150
HsGLRX5 ----QNGDL------VEELKKLGISHALLDEKKDQDSK 157

Figure 2.2: Amino acid sequence alignment of ISCA1a, ISCA1b, and ISCA2 from *A. thaliana*, Isa1 and Isa2 from *S. cerevisiae*, and ISCA1 and ISCA2 from *H. sapiens*. Conserved amino acid positions are highlighted in blue and cysteines required for the Fe-S cluster incorporation are indicated by asterisks.

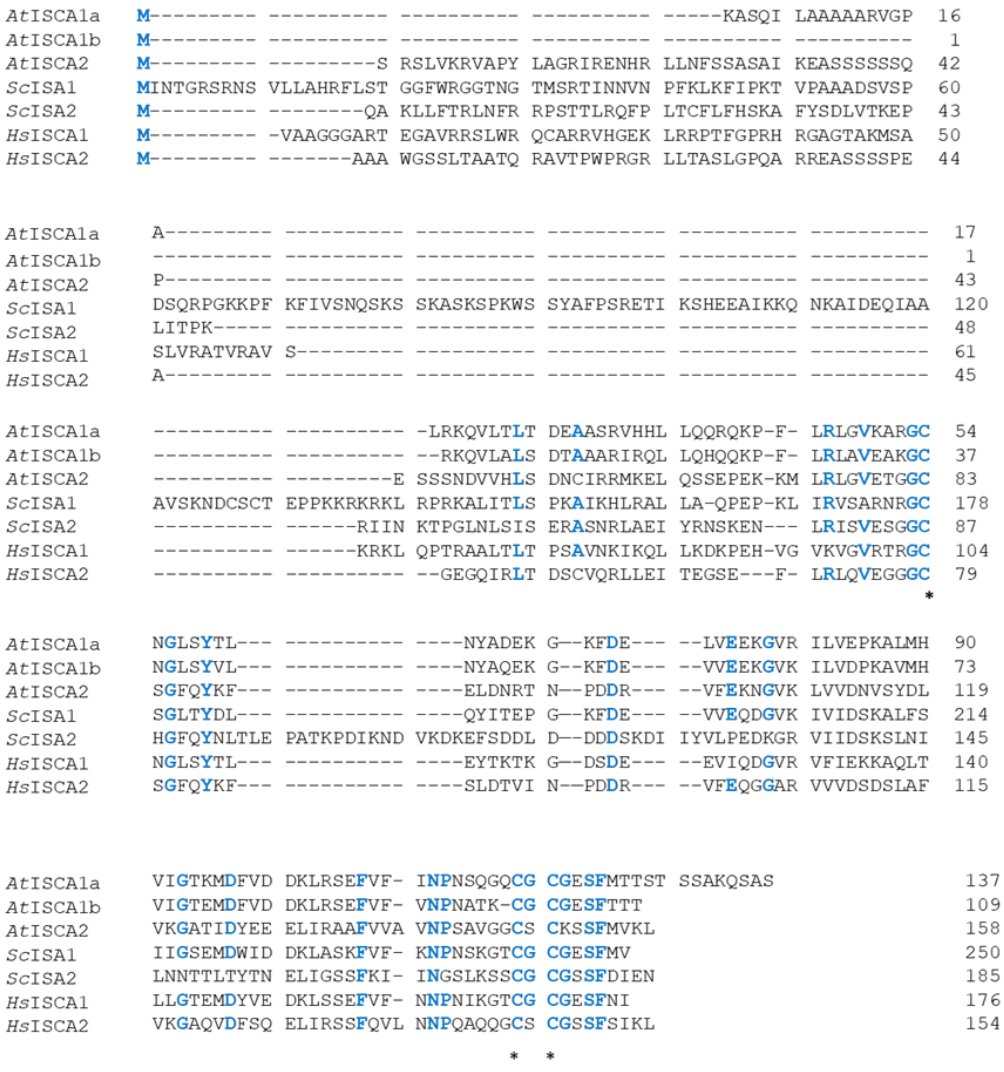
AtISCA1a M--------- ---------- ---------- ---------- -----KASQI LAAAAARVGP 16
AtISCA1b M--------- ---------- ---------- ---------- ---------- ---------- 1
AtISCA2 M--------- ---------S RSLVKRVAPY LAGRIRENHR LLNFSSASAI KEASSSSSSQ 42
ScISA1 MINTGRSRNS VLLAHRFLST GGFWRGGTNG TMSRTINNVN PFKLKFIPKT VPAAADSVSP 60
ScISA2 M--------- --------QA KLLFTRLNFR RPSTTLRQFP LTCFLFHSKA FYSDLVTKEP 43
HsISCA1 M--------- -VAAGGGART EGAVRRSLWR QCARRVHGEK LRRPTFGPRH RGAGTAKMSA 50
HsISCA2 M--------- -------AAA WGSSLTAATQ RAVTPWPRGR LLTASLGPQA RREASSSSPE 44
AtISCA1a A--------- ---------- ---------- ---------- ---------- ---------- 17
AtISCA1b ---------- ---------- ---------- ---------- ---------- ---------- 1
AtISCA2 P--------- ---------- ---------- ---------- ---------- ---------- 43
ScISA1 DSQRPGKKPF KFIVSNQSKS SKASKSPKWS SYAFPSRETI KSHEEAIKKQ NKAIDEQIAA 120
ScISA2 LITPK----- ---------- ---------- ---------- ---------- ---------- 48
HsISCA1 SLVRATVRAV S--------- ---------- ---------- ---------- ---------- 61
HsISCA2 A--------- ---------- ---------- ---------- ---------- ---------- 45
AtISCA1a ---------- ---------- -LRKQVLTLT DEAASRVHHL LQQRQKP-F- LRLGVKARGC 54
AtISCA1b ---------- ---------- --RKQVLALS DTAAARIRQL LQHQQKP-F- LRLAVEAKGC 37
AtISCA2 ---------- ---------E SSSNDVVHLS DNCIRRMKEL QSSEPEK-KM LRLGVETGGC 83
ScISA1 AVSKNDCSCT EPPKKRKRKL RPRKALITLS PKAIKHLRAL LA-QPEP-KL IRVSARNRGC 178
ScISA2 ---------- ------RIIN KTPGLNLSIS ERASNRLAEI YRNSKEN--- LRISVESGGC 87
HsISCA1 ---------- ------KRKL QPTRAALTLT PSAVNKIKQL LKDKPEH-VG VKVGVRTRGC 104
HsISCA2 ---------- ---------- --GEGQIRLT DSCVQRLLEI TEGSE---F- LRLQVEGGGC 79
*
AtISCA1a NGLSYTL--- ---------- ----NYADEK G--KFDE--- --LVEEKGVR ILVEPKALMH 90
AtISCA1b NGLSYVL--- ---------- ----NYAQEK G--KFDE--- --VVEEKGVK ILVDPKAVMH 73
AtISCA2 SGFQYKF--- ---------- ----ELDNRT N--PDDR--- --VFEKNGVK LVVDNVSYDL 119
ScISA1 SGLTYDL--- ---------- ----QYITEP G--KFDE--- --VVEQDGVK IVIDSKALFS 214
ScISA2 HGFQYNLTLE PATKPDIKND VKDKEFSDDL D--DDDSKDI IYVLPEDKGR VIIDSKSLNI 145
HsISCA1 NGLSYTL--- ---------- ----EYTKTK G--DSDE--- --EVIQDGVR VFIEKKAQLT 140
HsISCA2 SGFQYKF--- ---------- ----SLDTVI N--PDDR--- --VFEQGGAR VVVDSDSLAF 115
AtISCA1a VIGTKMDFVD DKLRSEFVF- INPNSQGQCG CGESFMTTST SSAKQSAS 137
AtISCA1b VIGTEMDFVD DKLRSEFVF- VNPNATK-CG CGESFTTT 109
AtISCA2 VKGATIDYEE ELIRAAFVVA VNPSAVGGCS CKSSFMVKL 158
ScISA1 IIGSEMDWID DKLASKFVF- KNPNSKGTCG CGESFMV 250
ScISA2 LNNTTLTYTN ELIGSSFKI- INGSLKSSCG CGSSFDIEN 185
HsISCA1 LLGTEMDYVE DKLSSEFVF- NNPNIKGTCG CGESFNI 176
HsISCA2 VKGAQVDFSQ ELIRSSFQVL NNPQAQQGCS CGSSFSIKL 154
* *

Figure 2.3: Schematic representations of domain structures of Nfu-type and IscU type proteins from different organisms. IscU domains, with three conserved cysteine residues are presented by dark pink boxes, Nfu domains with the CXXC motif are shown by teal boxes and 75is presented by light blue box. Bacterial NfuA-type proteins have an N-terminal A-type carrier domain without the conserved cluster-binding cysteine residues that is shown by a green box. Eukaryotic mitochondrial, nuclear and cytosolic Nfu type proteins also have a unique N-terminal domain shown by a brown box. Chloroplastic-type Nfu proteins have the extra C-terminal Nfu-type domain lacking the active site cysteine residues that is shown by a purple box. The red and grey bars represent mitochondrial and chloroplastic targeting sequences, respectively. Domain lengths are not drawn to scale. *Av*, *Azotobacter vinelandii*; *Ec*, *Escherichia coli*; *Sy*, *Synechocystis*; *At*, *Arabidopsis thaliana*; *Sc*, *Saccharomyces cerevisiae*; *Hs*, *Homo sapiens*. Adapted from reference (16).

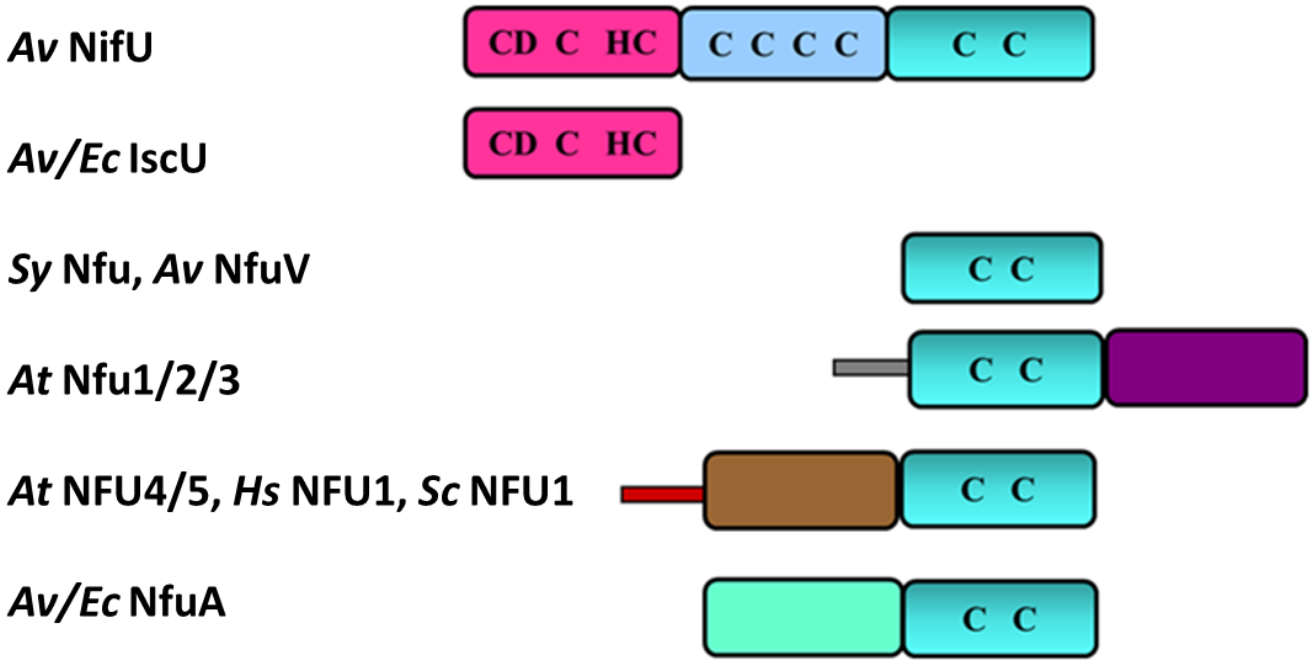
Av NifU
CD C HC
C C C C
C C
Av/Ec IscU
CD C HC
Sy Nfu, *Av* NfuV
C C
At Nfu1/2/3
C C
At NFU4/5, *Hs* NFU1, *Sc* NFU1
C C
Av/Ec NfuA
C C

Figure 2.4: UV-visible absorption and CD spectra of Fraction 1 (black line) and Fraction 2 (blue line) of reconstituted *At* GRXS15 after purification using a Mono-Q column. Spectra were recorded under anaerobic conditions in sealed 0.1 cm cuvettes in 100 mM Tris-HCl buffer with 5 mM GSH at pH 7.5. The ε and Δε values are based on concentration of *At* GRXS15 dimer.

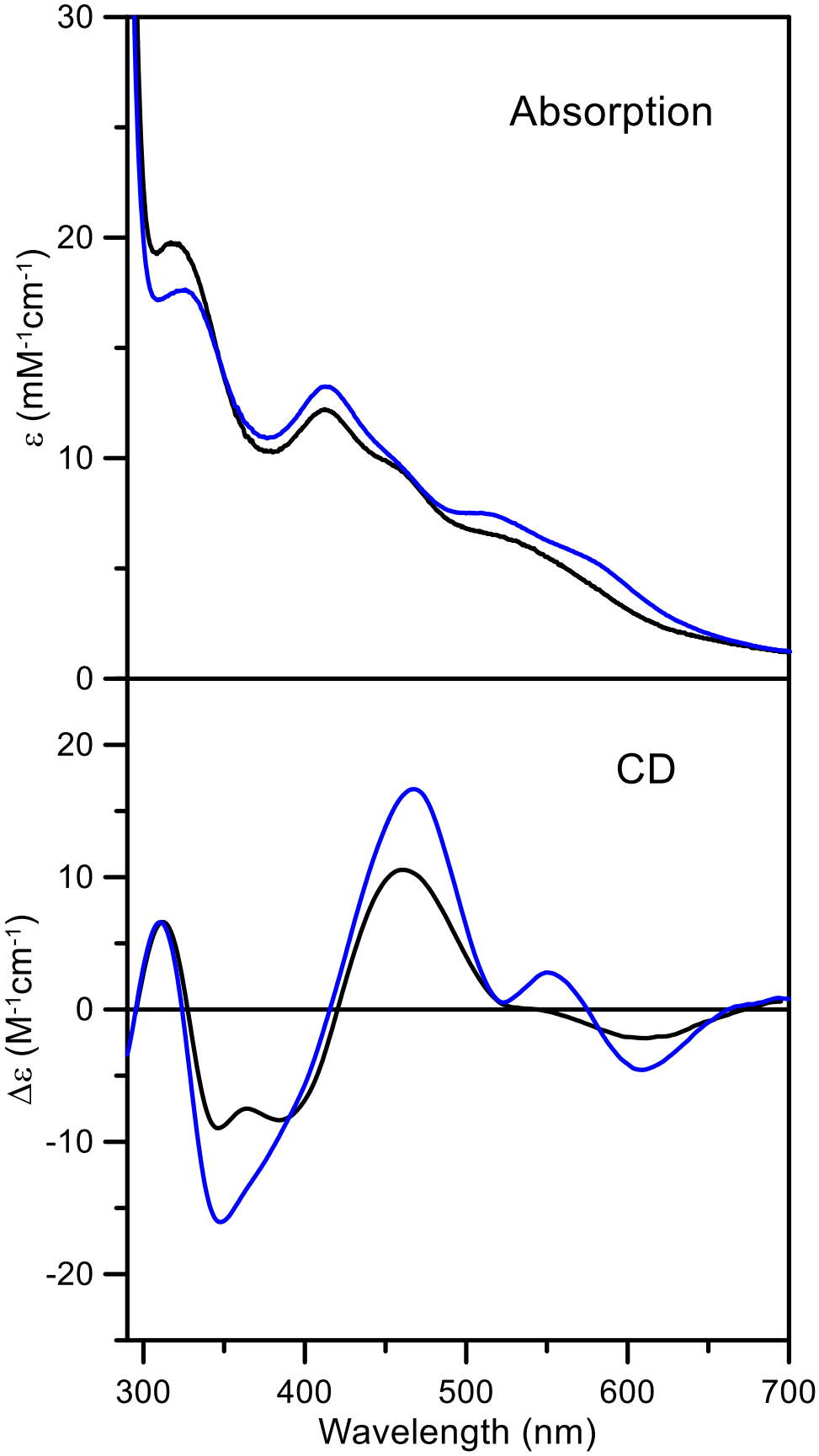
Absorption
ε (mM-1cm-1)
30
20
10
0
CD
Δε (M-1cm-1)
20
10
0
-10
-20
300
400
500
600
700
Wavelength (nm)

Figure 2.5: Room temperature UV-visible absorption and CD spectra of $[2Fe\text{-}2S]^{2+}$ cluster-bound as isolated *At* FDX1. All ε and Δε values were calculated based on the cluster concentrations.

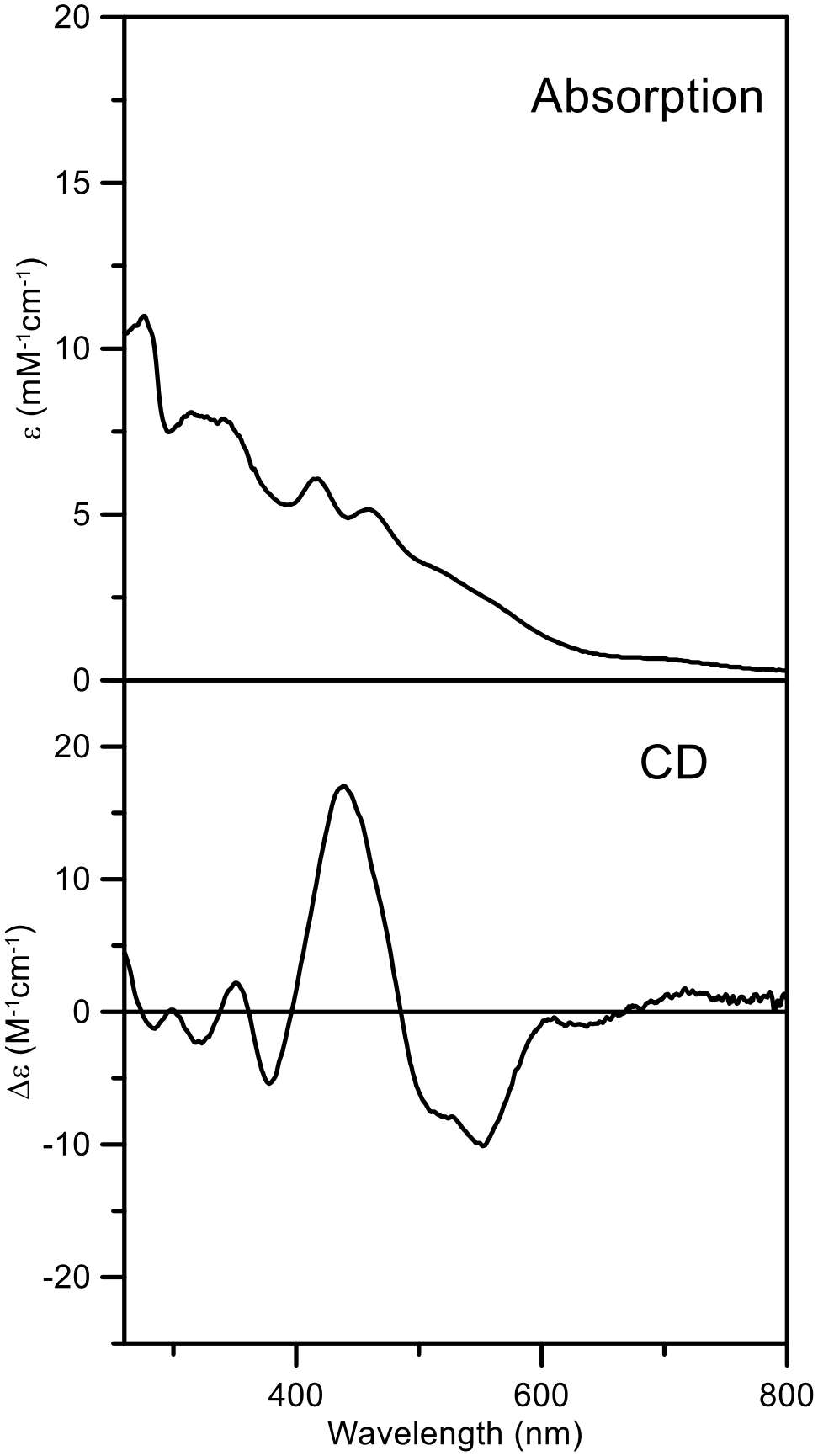
Absorption
ε (mM-1cm-1)
20
15
10
5
0
CD
Δε (M-1cm-1)
20
10
0
-10
-20
400
600
800
Wavelength (nm)

Figure 2.6: Gel electrophoresis of as purified, apo and reconstituted ISCA1a/2 samples. Proteins were separated by 20 % SDS-PAGE and stained with Coomasie Brilliant blue. Lane M, molecular mass standards, Lane 1, apo ISCA1a/2, Lane 2, as purified ISCA1a, Lane 3, , as purified ISCA2, Lane 4, as purified [2Fe-2S] cluster-bound ISCA1a/2, Lane 5, reconstituted [4Fe-4S] cluster bound ISCA1a/2

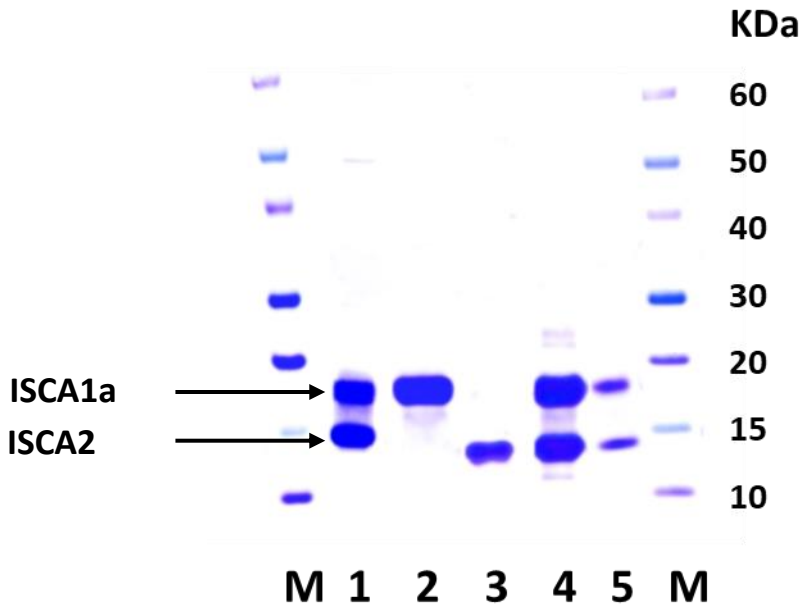
KDa
60
50
40
30
20
15
10
ISCA1a
ISCA2
M 1 2 3 4 5 M

Figure 2.7: Room temperature UV-visible absorption and CD spectra of $[2Fe\text{-}2S]^{2+}$ cluster-bound as isolated *At* ISCA1a/2 (black lines) and $[4Fe\text{-}4S]^{2+}$ cluster-bound reconstituted *At* ISCA1a/2 (blue lines). All ε and Δε values are based on ISCA1a/2 heterodimer concentration.

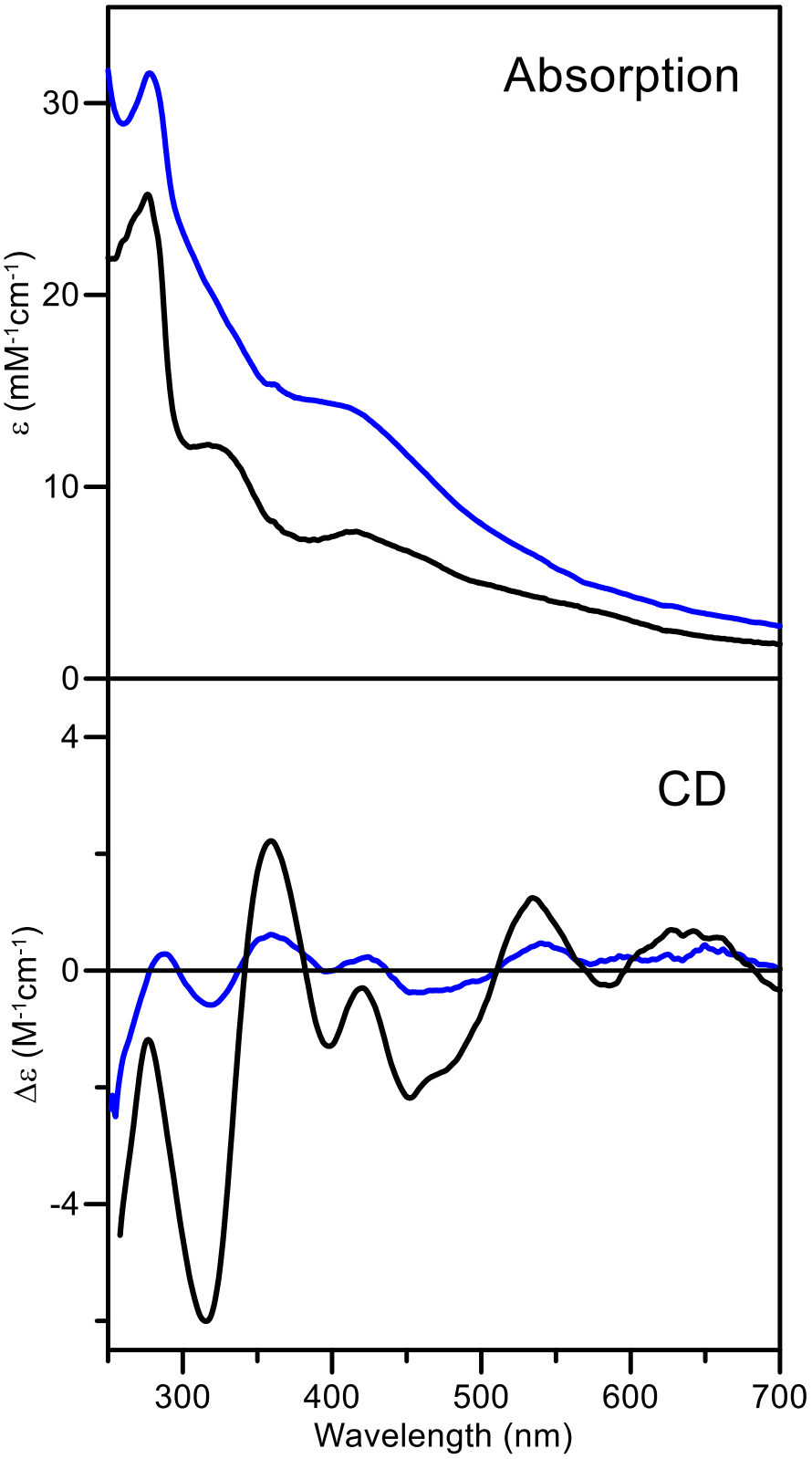
Absorption
30
20
10
0
ε (mM-1cm-1)
CD
4
0
-4
Δε (M-1cm-1)
300
400
500
600
700
Wavelength (nm)

Figure 2.8: Resonance Raman spectra of $[2Fe\text{-}2S]^{2+}$ cluster-bound as isolated *At* ISCA1a/2 using 458-nm and 488-nm laser excitation. The sample (~2 mM $[2Fe\text{-}2S]^{2+}$ clusters) in 100 mM Tris-HCl buffer at pH 7.8 and was in the form of a frozen droplet at 17 K. The spectrum is the sum of 100 individual scans with each scan involving photon counting for 1 s at 0.5 cm^{-1} increments with 7 cm^{-1} spectral resolution. Bands due to lattice modes of the frozen buffer solution have been subtracted from both spectra.

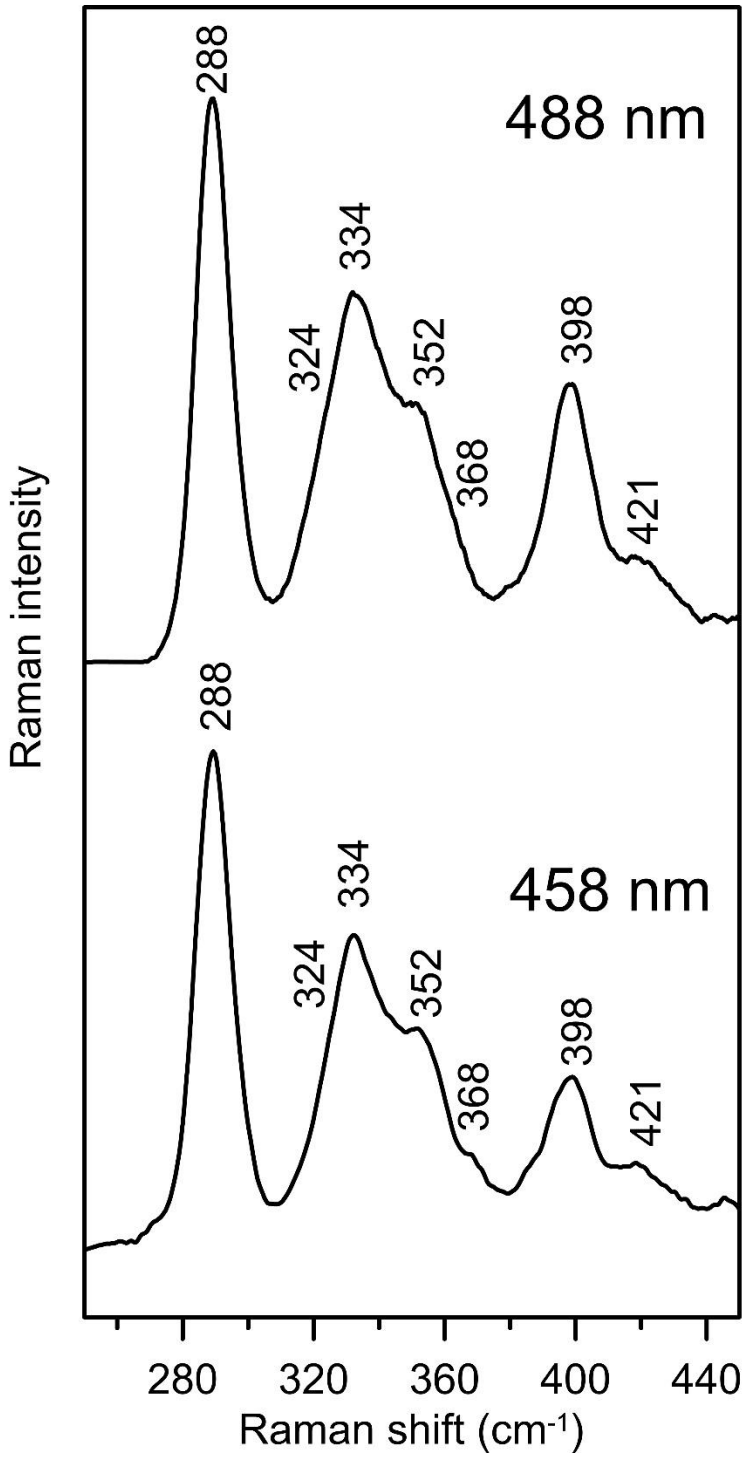
488 nm
458 nm
288
324
334
352
368
398
421
Raman intensity
280
320
360
400
440
Raman shift (cm-1)

Figure 2.9: Room temperature UV-visible absorption spectra and CD spectra of *At* NFU4 (A) and *At* NFU5 (B). Apo as purified *At* NFU4 and *At* NFU5 are shown as black lines and reconstituted *At* NFU4 and *At* NFU5 are shown as blue lines). All ε and Δε values are based on NFU4 and NFU5 protein monomer concentration.

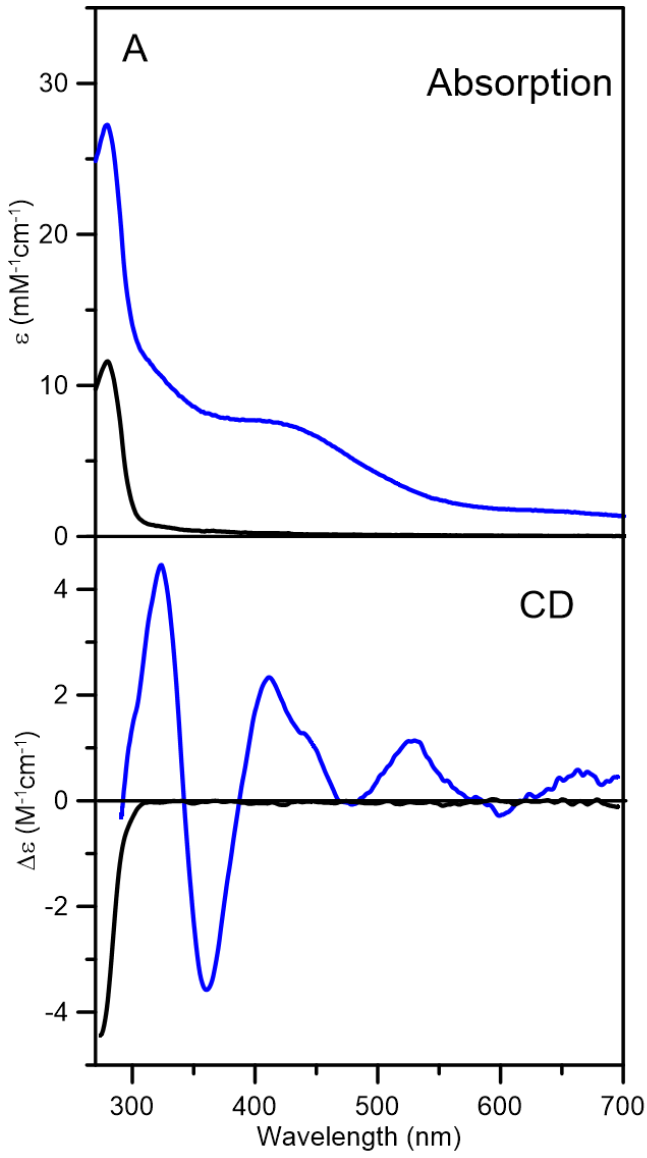
A
Absorption
ε (mM-1cm-1)
30
20
10
0
CD
Δε (M-1cm-1)
4
2
0
-2
-4
300
400
500
600
700
Wavelength (nm)

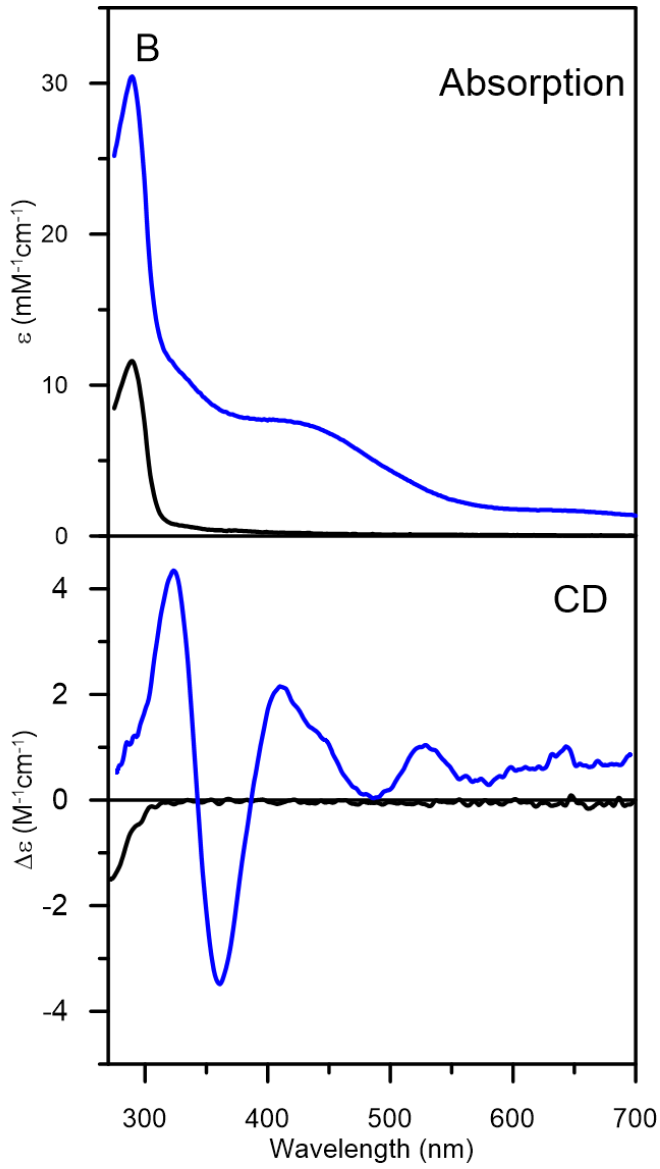
B
Absorption
ε (mM-1cm-1)
30
20
10
0
CD
Δε (M-1cm-1)
4
2
0
-2
-4
300
400
500
600
700
Wavelength (nm)

Figure 2.10: Comparison of the resonance Raman spectra of reconstituted *At* NFU4 and *At* NFU5 recorded at 17 K with 457.9-nm excitation. Each spectrum is the sum of 100 individual scans, with each scan involving photon counting for 1 s at 0.5 cm^{-1} increments, with 7 cm^{-1} spectral resolution. Bands due to frozen buffer solution have been subtracted from both spectra.

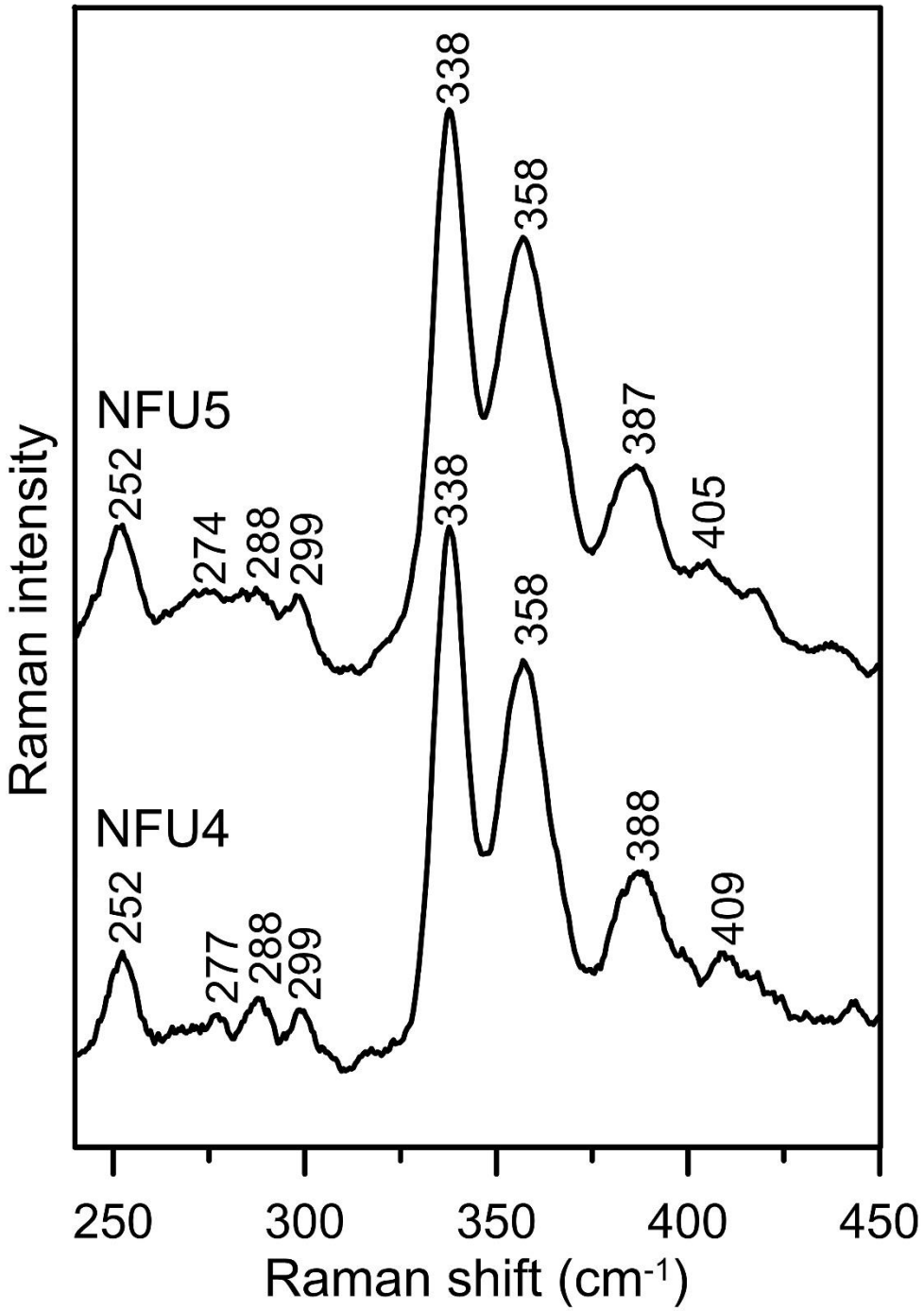
NFU5
252
274
288
299
338
358
387
405
NFU4
252
277
288
299
338
358
388
409
Raman intensity
250
300
350
400
450
Raman shift (cm-1)

Figure 2.11: The X-band EPR spectrum of reconstituted *At* NFU4 reduced with one reducing equivalent of dithionite. The sample was reduced under anaerobic conditions by the addition of one reducing equivalent of sodium dithionite, followed by rapid freezing in liquid nitrogen. EPR conditions: microwave frequency, 9.60 GHz; microwave power, 10 mW; modulation amplitude, 0.63 mT; temperature, 10 K.

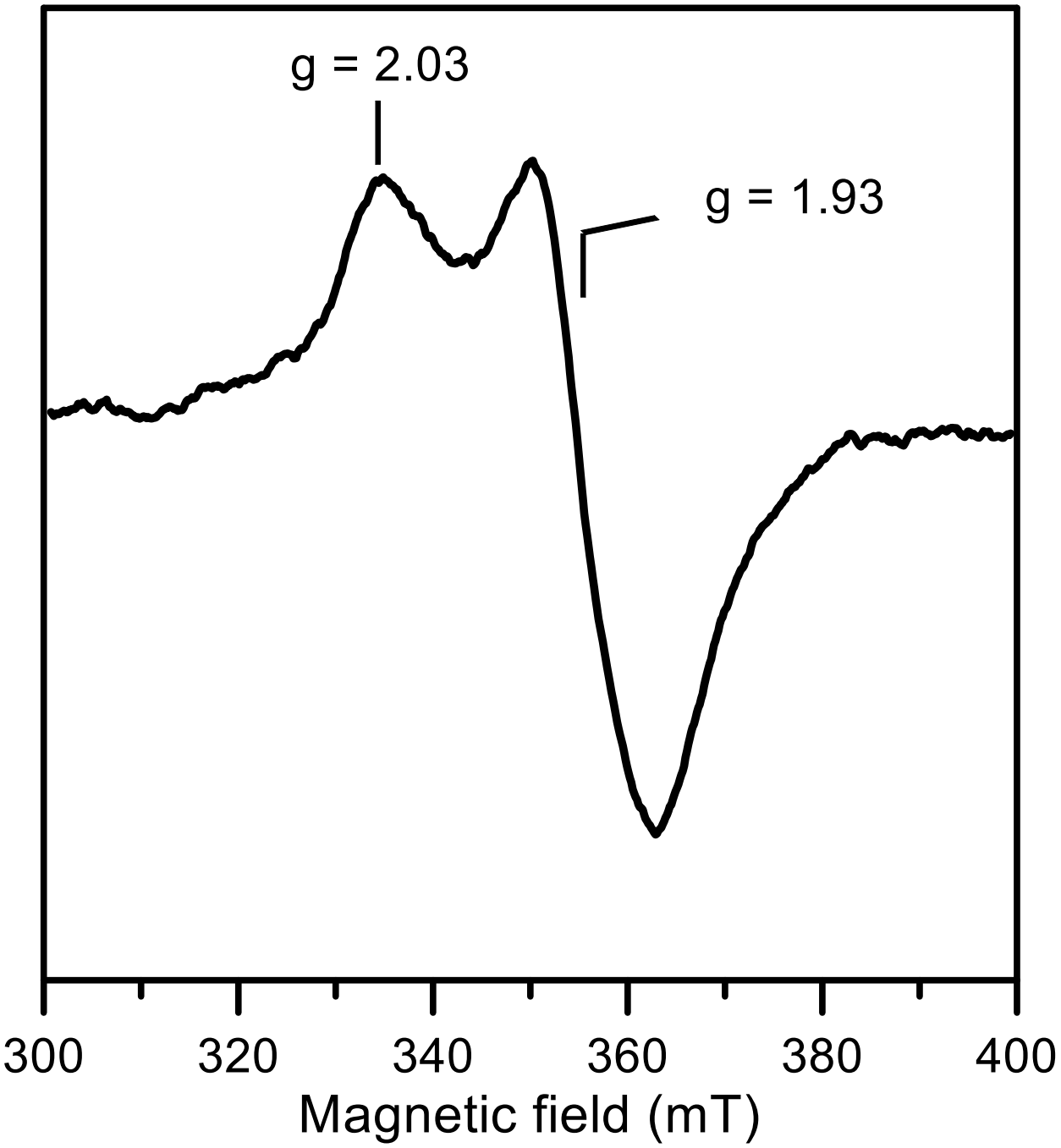
g = 2.03
g = 1.93
300
320
340
360
380
400
Magnetic field (mT)

Figure 2.12: Cluster transfer from *At* $[2Fe\text{-}2S]^{2+}$-GRXS15 to apo *At* FDX1 monitored by CD spectroscopy as a function of time. (A) CD spectra of the cluster transfer reaction mixture that was initially 40 µM in GRXS15 $[2Fe\text{-}2S]^{2+}$ clusters and 40 µM in apo FDX1. The thick red line corresponds to $[2Fe\text{-}2S]^{2+}$-GRXS15 recorded before addition of apo FDX1. The thin grey lines correspond to CD spectra recorded at 1, 3, 5, 8, 10, 13, 15, 17, 20, 22, 25, 27, 30, 32, 34, 37, 40, 45, 50, 56, 60, 69, 75, 86, 95, 101, 105, 110 and 120 min after the addition of apo FDX1. The thick blue line corresponds to complete $[2Fe\text{-}2S]^{2+}$ cluster transfer to FDX1. The arrows indicate the direction of intensity change with increasing time at selected wavelengths and $\Delta\varepsilon$ values were calculated based on the initial concentration of $[2Fe\text{-}2S]^{2+}$ clusters. The cluster transfer reaction was carried out under anaerobic conditions at room temperature in 100 mM Tris-HCl buffer at pH 7.8. (B) Kinetic simulation of cluster transfer from $[2Fe\text{-}2S]^{2+}$-GRXS15 to apo FDX1 based on second-order kinetics and the initial concentrations of $[2Fe\text{-}2S]^{2+}$ clusters on $[2Fe\text{-}2S]^{2+}$-GRXS15 and of apo FDX1. Percent cluster transfer was assessed by CD intensity at 550 nm (black circles) and simulated with a second-order rate constant of $1.1 \times 10^4\ M^{-1}min^{-1}$.

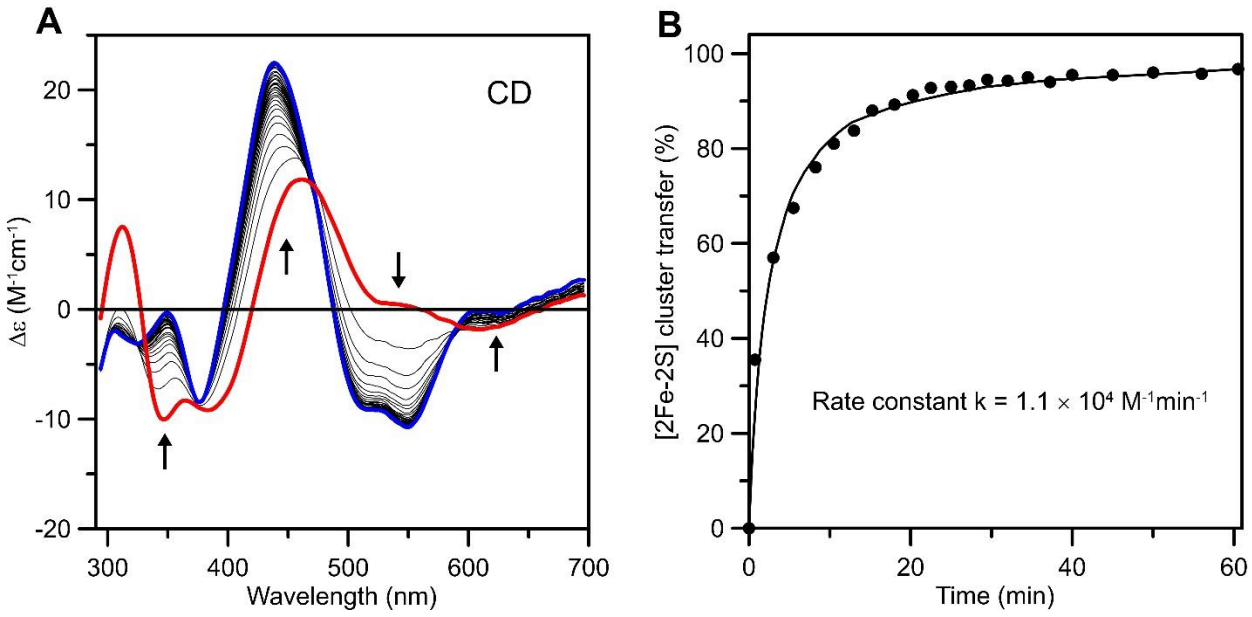
A
CD
Δε (M-1cm-1)
Wavelength (nm)
B
[2Fe-2S] cluster transfer (%)
Time (min)
Rate constant k = 1.1 × 10⁴ M-1min-1

Figure 2.13: Cluster transfer from *At* $[2Fe\text{-}2S]^{2+}$-GRXS15 to apo *At* ISCA1a/2 monitored by UV-visible absorption and CD spectroscopy as a function of time. A. The thick red line is the CD spectrum of $[2Fe\text{-}2S]^{2+}$ cluster-bound GRXS15 before addition of apo *At* ISCA1a/2 to the reaction mixture. The thin grey lines are CD spectra of the reaction mixture, GRXS15 (30 μM in $[2Fe\text{-}2S]^{2+}$ clusters) mixed with DTT-pretreated apo ISCA1a/2 (60 μM), recorded at 1, 3, 5, 17, 20, 25, 28, 30, and 34 min after addition of apo ISCA1a/2. The thick blue line corresponds to the final CD spectra after 60 min. The arrows indicate the direction of change in CD intensity with time at selected wavelengths and Δε values are based on the initial concentration of $[2Fe\text{-}2S]^{2+}$ clusters in the reaction mixture. B. The thick red line is the absorption spectrum of $[2Fe\text{-}2S]^{2+}$ cluster-bound GRXS15 before addition of apo *At* ISCA1a/2 to the reaction mixture. The thick blue line corresponds to the final absorption spectrum, 60 min after addition of apo *At* ISCA1a/2 to the reaction mixture. ε values are based on the initial concentration of $[2Fe\text{-}2S]^{2+}$ clusters in the reaction mixture.

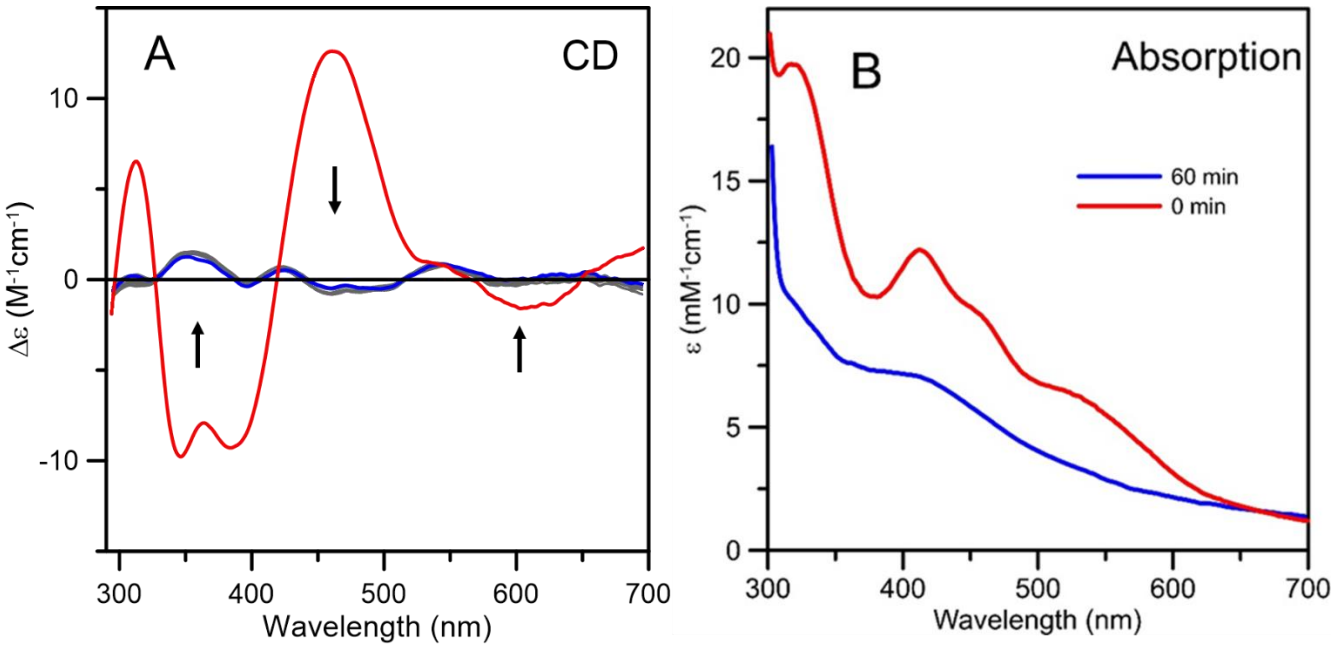
A
CD
10
0
-10
Δε (M-1cm-1)
300
400
500
600
700
Wavelength (nm)
B
Absorption
20
15
10
5
0
ε (mM-1cm-1)
60 min
0 min
300
400
500
600
700
Wavelength (nm)

Figure 2.14: Cluster transfer from *At* $[4Fe\text{-}4S]^{2+}$-ISCA1a/2 to apo *At* apo NFU4 monitored by CD spectroscopy as a function of time. (A) CD spectra of the cluster transfer reaction mixture that was initially 30 μM in ISCA1a/2 $[4Fe\text{-}4S]^{2+}$ clusters and 60 μM in DTT-pretreated apo NFU4 monomer. The thick red line corresponds to $[4Fe\text{-}4S]^{2+}$-ISCA1a/2 recorded before addition of apo NFU4 to the reaction mixture. The thin grey lines correspond to CD spectra recorded at 4, 7, 11, 20, 36, 40, 45, and 50 min after the addition of apo NFU4. The thick blue line corresponds to complete $[4Fe\text{-}4S]^{2+}$ cluster transfer to NFU4. The arrows indicate the direction of intensity change with increasing time at selected wavelengths and Δε values were calculated based on the initial concentration of $[4Fe\text{-}4S]^{2+}$ clusters in the reaction mixture. The cluster transfer reaction was carried out under anaerobic conditions at room temperature in 100 mM Tris-HCl buffer at pH 7.8. (B) Kinetic simulation of cluster transfer from $[4Fe\text{-}4S]^{2+}$-ISCA1a/2 to apo NFU4 based on second-order kinetics and the initial concentrations of $[4Fe\text{-}4S]^{2+}$ clusters on $[4Fe\text{-}4S]^{2+}$-ISCA1a/2 and of apo NFU4. Percent cluster transfer was assessed by the difference in CD intensity at 326 and 362 nm (black circles) and simulated with a second-order rate constant of 9.1×10^3 $M^{-1}min^{-1}$ (black line). The residual $[2Fe\text{-}2S]^{2+}$-ISCA1a/2 peak-to-trough CD intensity at 362 and 326 nm at zero time was added on to each data point as there is no evidence for any $[2Fe\text{-}2S]^{2+}$ cluster transfer.

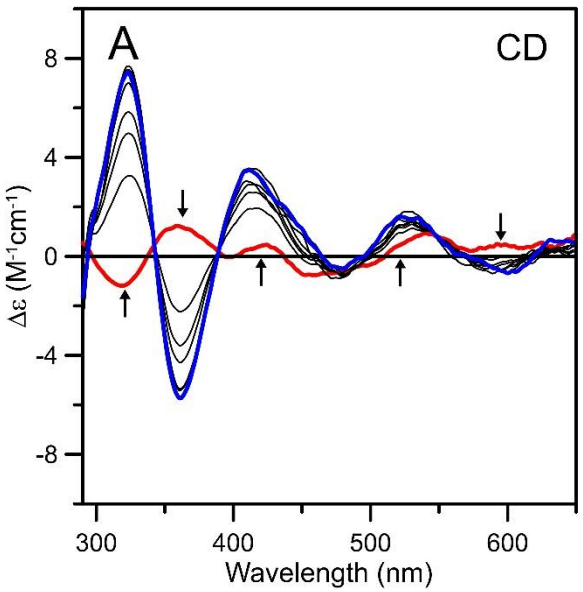
A
CD
8
4
0
-4
-8
Δε (M-1cm-1)
300
400
500
600
Wavelength (nm)

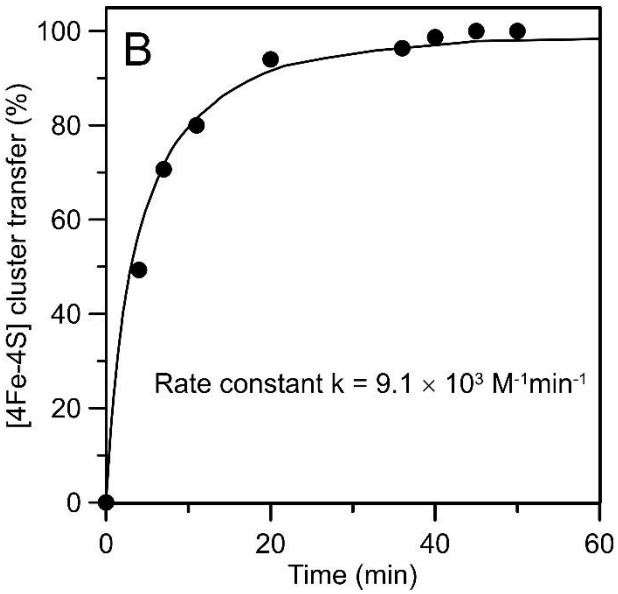
B
100
80
60
40
20
0
[4Fe-4S] cluster transfer (%)
Rate constant k = 9.1 × 10³ M-1min-1
0
20
40
60
Time (min)

Figure 2.15: Cluster transfer from *At* $[4Fe\text{-}4S]^{2+}$-ISCA1a/2 to apo *At* apo NFU5 monitored by CD spectroscopy as a function of time. (A) CD spectra of the cluster transfer reaction mixture that was initially 40 μM in ISCA1a/2 $[4Fe\text{-}4S]^{2+}$ clusters and 80 μM in DTT-pretreated apo NFU5 monomer. The thick red line corresponds to $[4Fe\text{-}4S]^{2+}$-ISCA1a/2 recorded before addition of apo NFU5 to the reaction mixture. The thin grey lines correspond to CD spectra recorded at 5, 9, 13, 18, 27, 40, and 60 min after the addition of apo NFU5. The thick blue line corresponds to complete $[4Fe\text{-}4S]^{2+}$ cluster transfer to NFU5. The arrows indicate the direction of intensity change with increasing time at selected wavelengths and Δε values were calculated based on the initial concentration of $[4Fe\text{-}4S]^{2+}$ clusters in the reaction mixture. The cluster transfer reaction was carried out under anaerobic conditions at room temperature in 100 mM Tris-HCl buffer at pH 7.8. (B) Kinetic simulation of cluster transfer from $[4Fe\text{-}4S]^{2+}$-ISCA1a/2 to apo NFU5 based on second-order kinetics and the initial concentrations of $[4Fe\text{-}4S]^{2+}$ clusters on $[4Fe\text{-}4S]^{2+}$-ISCA1a/2 and of apo NFU5. Percent cluster transfer was assessed by the difference in CD intensity at 326 and 362 nm (black circles) and simulated with a second-order rate constant of 7.0×10^3 $M^{-1}min^{-1}$ (black dots). The residual $[2Fe\text{-}2S]^{2+}$-ISCA1a/2 peak-to-trough CD intensity at 362 and 326 nm at zero time was added on to each data point, as there is no evidence for any $[2Fe\text{-}2S]^{2+}$ cluster transfer.

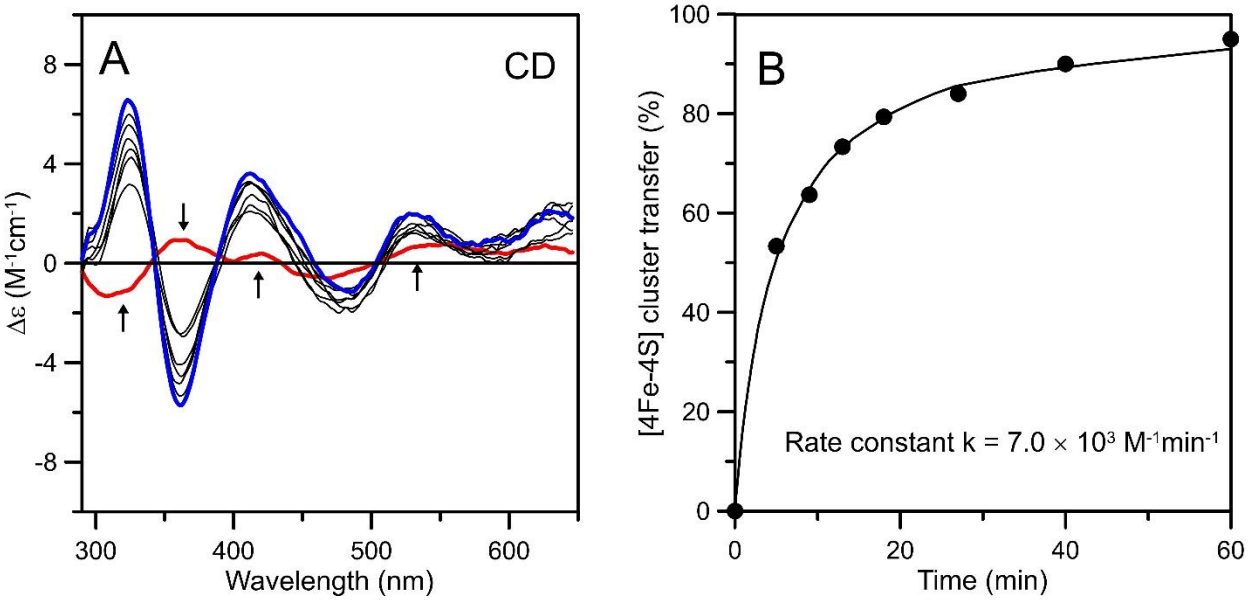
A
CD
8
4
0
-4
-8
Δε (M-1cm-1)
300
400
500
600
Wavelength (nm)
B
100
80
60
40
20
0
[4Fe-4S] cluster transfer (%)
Rate constant k = 7.0 × 10³ M-1min-1
0
20
40
60
Time (min)

Figure 2.16: Activation of apo ACO2 using [4Fe-4S] cluster-bound ISCA1a/2 (red data), [4Fe-4S] cluster-bound NFU5 (black data), and [2Fe-2S] cluster-bound ISCA1a/2 (blue data). Apo ACO2 (2.4 μM) was incubated with [4Fe-4S] cluster loaded ISCa1a/2 or NFU5 (both 7.4 μM in [4Fe-4S] clusters) and [2Fe-2S] cluster-loaded ISCA1a/2 (14.5 μM in $[2Fe\text{-}2S]^{2+}$ clusters) at room temperature under anaerobic conditions. 10 μL aliquots of the reaction mixture were removed at selected time points and assayed immediately for aconitase activity. Residual 2.1aconitase activity of apo ACO2, in the absence of a cluster donor, was assessed and subtracted from all measured activities. Aconitase specific activity as a function of incubation time with the cluster donor are expressed as a percentage of the maximal specific activity of $[4Fe\text{-}4S]^{2+}$ cluster-replete ACO2. Solid lines are best fits to second order kinetics, with the indicated rate constants, k, based on the initial concentrations of apo ACO2 and $[4Fe\text{-}4S]^{2+}$ clusters on ISCA1a/2 or NFU5 and half the initial $[2Fe\text{-}2S]^{2+}$ cluster concentration of [2Fe-2S]- ISCA1a/2.

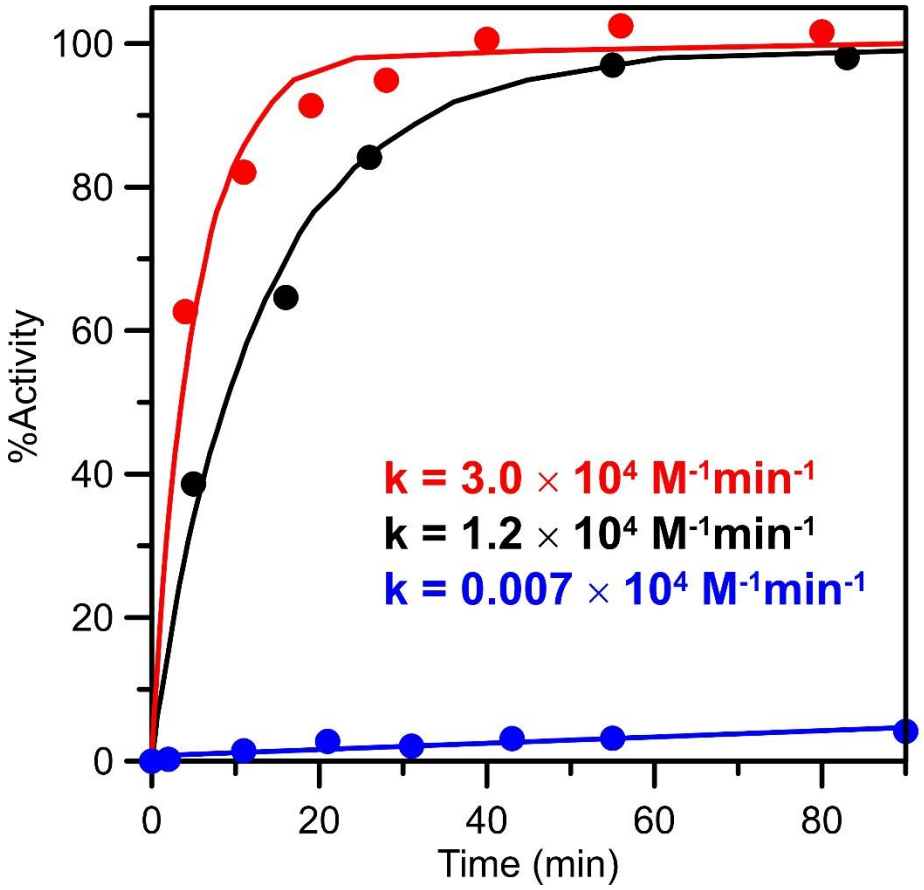
100
80
60
40
20
0
%Activity
0
20
40
60
80
Time (min)
k = 3.0 × 10⁴ M⁻¹min⁻¹
k = 1.2 × 10⁴ M⁻¹min⁻¹
k = 0.007 × 10⁴ M⁻¹min⁻¹

Figure 2.17: Proposed scheme for interprotein cluster trafficking in the late steps of mitochondrial ISC machinery based on the results presented in this work.

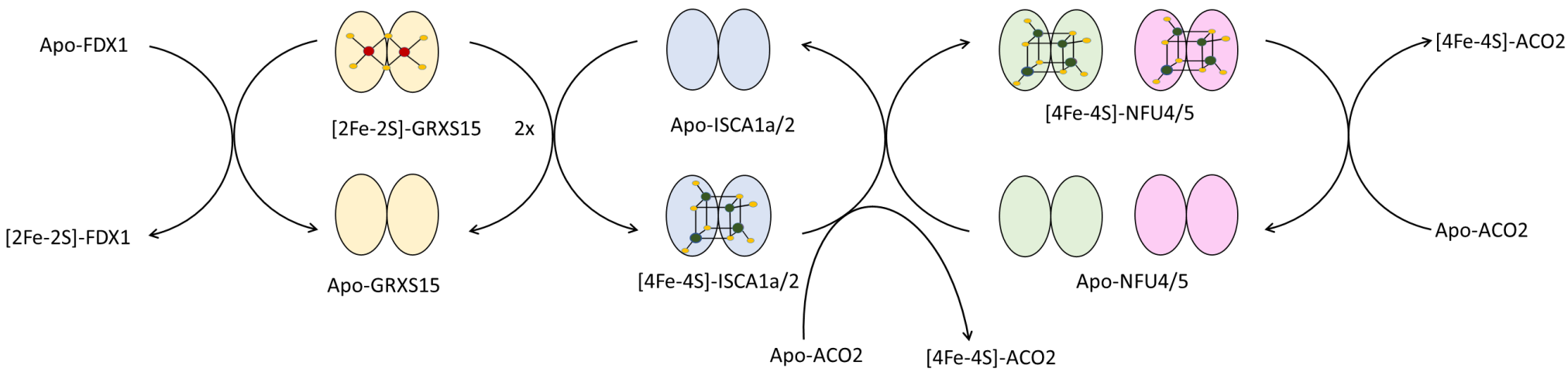
Apo-FDX1
[2Fe-2S]-FDX1
[2Fe-2S]-GRXS15
Apo-GRXS15
2x
Apo-ISCA1a/2
[4Fe-4S]-ISCA1a/2
Apo-ACO2
[4Fe-4S]-ACO2
[4Fe-4S]-NFU4/5
Apo-NFU4/5
[4Fe-4S]-ACO2
Apo-ACO2

CHAPTER 3

PLASTIDIAL Fe-S CLUSTER ASSEMBLY IN *ARABIDOPSIS THALIANA*: *IN VITRO* CHARACTERIZATION OF THE PROPERTIES AND ROLES OF NFU2, HCF101, AND PSAC PROTEINS

Tamanna Azam,[1] Jonathan Przybyla-Toscano,[2] Jérémy Couturier[2], Nicolas Rouhier[2], and Michael K. Johnson[1,*] *to be submitted to the Journal of Inorganic Biochemistry*

[1]Department of Chemistry and Center for Metalloenzyme Studies, University of Georgia, Athens, Georgia, 30602, USA and [2]UMR1136 Interactions Arbres-Microorganismes, Université de Lorraine/INRA, Faculté des Sciences et Technologies, 54500 Vandoeuvre-lès-Nancy, France

Abbreviations: *At*, *Arabidopsis thaliana*; *Av*, *Azotobacter vinelandii*; *Syn*, *Synechococcus;* PSI, photosystem I; HCF101, high chlorophyll fluorescence; Grx, glutaredoxin; FTR, ferredoxin thioredoxin reductase; SAM, radical-S-adenosylmethionine; Fdx, ferredoxin; APR, adenosine 5'-phosphosulfate reductase; NIR, nitrite reductase; Fe-S clusters, iron-sulfur clusters; CD, circular dichroism; RR, resonance Raman; EPR, electron paramagnetic resonance, DTT, dithiothreitol; IPTG, isopropyl 1-thio-β-D-galactopyranoside; FAS, ferrous ammonium sulfate; PMSF, phenylmethanesulfonyl fluoride; GSH, reduced glutathione; EDTA, ethylenediaminetetraacetic acid disodium salt; SDS-PAGE, dodecyl sulfate polyacrylamide gel electrophoresis

Abstract

Maturation of Fe-S cluster containing proteins in plastids depends on a complex machinery, named the SUF (Sulfur Utilization Factor) system, which is utilized in the oxygen-rich cellular environments of cyanobacteria and plant chloroplasts. The SUF system uses NFU1, NFU2, NFU3 and HCF101 as late acting proteins for the maturation of [4Fe-4S] clusters in PSI. However, the mechanisms of [4Fe-4S] cluster trafficking and insertion into target plastidial proteins are currently unknown. This work focused on investigating cluster transfer interactions involving NFU2, HCF101, and PSAC. Since relatively little has been reported about the properties of HCF101 in the literature, we first present spectroscopic characterization of HCF101, using UV-visible absorption/CD, resonance Raman and EPR, before demonstrating that NFU2 acts upstream of HCF101 for PSI [4Fe-4S] cluster assembly. Plastidial HCF101 was shown to contain a sub-stoichiometric mixture of $[4Fe\text{-}4S]^{2+}$ and linear $[3Fe\text{-}4S]^{1+}$ cluster as purified under anaerobic conditions. However, as-purified HCF101 was converted to a form containing one $[4Fe\text{-}4S]^{2+}$ cluster per monomer after anaerobic Fe-S cluster reconstitution. Nevertheless, the high affinity of HCF101 for binding linear $[3Fe\text{-}4S]^{1+}$ clusters is evident by the observation that $[4Fe\text{-}4S]^{2+}$ cluster transfer from NFU2 to apo HCF101 is a very rapid and unidirectional process, resulting in transient [4Fe-4S]-HCF101, that gradually decays with time to yield linear $[3Fe\text{-}4S]^{1+}$ cluster-bound HCF101. These results, coupled with observation that linear $[3Fe\text{-}4S]^{1+}$ cluster-bound HCF101 is rapidly converted into [4Fe-4S]-HCF101 on addition of Fe^{2+} ions under anaerobic conditions, raise the possibility that that both cluster-bound forms of HCF101 may be present in plastids under dark and light conditions.

Introduction

In plants, iron is present in prosthetic groups, such as heme or iron-sulfur (Fe-S) clusters. Essential metabolic processes in cells, such as photosynthesis and respiration, rely heavily on Fe-S clusters. Other metabolic and cellular pathways in the chloroplast, specifically nitrogen and sulfur assimilation, carbon fixation, chlorophyll catabolism, tRNA thio-modification, lipoic acid synthesis, and thiamine synthesis, also depend on Fe-S proteins (1-3). There are three machineries in plants required for the maturation of plastidial, mitochondrial, and cytosolic/nuclear Fe-S proteins, namely the SUF (sulfur utilization factor), ISC (iron sulfur cluster assembly), and CIA (cytosolic iron-sulfur cluster assembly), respectively (4). In bacteria, the SUF system generally plays a backup role only operative under the conditions of iron limitation or oxidative stress (5,6). However, it is the primary system in the more oxygen-rich cellular environments of cyanobacteria and plant chloroplasts (5,7). The SUF machinery in plant plastids has been inherited from bacteria, and the *E. coli* SUF system has been extensively studied. Consequently, analogies to the *E. coli* SUF system are used below to understand the plastidial SUF system.

The SUF system can be separated into two steps; the first step is the assembly of a Fe-S cluster on a scaffold complex by cysteine desulfurase and sulfurtransferase (8). The second step is the delivery of that cluster to plastidial target apo proteins with the help of transfer/carrier proteins. Prior research has established the $SUFBC_2D$ complex as the scaffold for Fe-S cluster assembly in the plastidial SUF system (9,10). To assemble a Fe-S cluster on the scaffold $SUFBC_2D$ complex, S is extracted from cysteine by pyridoxal-L-phosphate (PLP) dependent cysteine desulfurase NFS2, an ortholog of bacterial cysteine desulfurase SufS (11). The released sulfane S (S^0) forms a persulfide group on the catalytic cysteine of cysteine desulfurase (12). The transfer of sulfane (S^0) to scaffold proteins is impeded by the presence of a β-hairpin near the catalytic cysteine, which

limits the accessibility of the persulfide group (13,14). Therefore, an additional protein functions as a sulfurtransferase, to accept sulfane (S^0) from cysteine desulfurase before transferring it to a cysteine on the scaffold complex. In *Arabidopsis thaliana,* there are three sulfurtransferase proteins: SUFE1, SUFE2, and SUFE3 (15). The reason behind the existence of three isoforms of SUFE is likely to be their different expression patterns, as SUFE2 is expressed in pollen while SUFE1 and SUFE3 are expressed in vegetative tissues (15). The presence of two different domains in SUFE1 and SUFE3 might be another reason for the presence of three SUFE isoforms. SUFE2 and SUFE3 are only targeted to plastids, but their specific roles have yet to be determined. SUFE1 targeted to both plastids and mitochondria, has a C-terminal BOLA domain (16,17) and recent *in vivo* and *in vitro* studies have shown that the BOLA domain helps SUFE1 interact with monothiol glutaredoxin (GRXs) (18). Knock out studies of *At* SUFE1 concluded that SUFE1 is essential for embryo development (16,17). Furthermore, *in vitro* studies have demonstrated that *At* SUFE1 can activate plastid-targeted NFS2 and mitochondria-targeted NFS1, findings that prove the necessity of SUFE1 for Fe-S cluster assembly in plastids and mitochondria (16,17). SUFE3 has a C-terminal quinolinate synthase (NadA domain) in addition to a SUFE domain, and SUFE2 only has a SUFE domain (15). While the phenotypes of Δ*sufE2* have not been reported yet, Δ*sufE3* mutants are embryo lethal, indicating that SUFE3 is also an essential protein (15).

In *E. coli* and in *A. thaliana,* the scaffold complex is composed of three proteins, SUFB, SUFC, and SUFD in a 1:2:1 stoichiometry ($SUFBC_2D$) (9,19). Fe-S cluster formation occurs on SUFB, but all three proteins are required for Fe-S cluster assembly *in vivo* (10). In *E. coli*, both [4Fe-4S] and [2Fe-2S] clusters can be assembled on SufB *in vitro.* The expression of *At* SUFB and *At* SUFC can complement the growth defects of *E. coli ΔsufB* and *ΔsufC* mutants (20). The loss of SufC or both SufC and SufD reduced the *in vivo* formation of Fe-S clusters on SufB, indicating

that SufC and SufD are both required for *in vivo* Fe-S cluster formation on SufB (9). In addition, while SufD participates in both embryogenesis and more general house-keeping role such as chlorophyll biosynthesis and chloroplast development, SufB and SufC only function in embryogenesis (21). The $SUFBC_2D$ complex is purified with a reduced flavin-adenine dinucleotide ($FADH_2$) molecule, and it is now believed that $FADH_2$ plays an important role in Fe-S cluster assembly by producing reducing equivalents for the reduction of ferric iron (10,22). The source of iron for SUF machinery, however, is still unknown. Initially it was believed that ferritin is the Fe donor, but no phenotype was observed in ferritin mutants, suggesting that ferritin is not the Fe source (23). Recently, it has been reported that frataxin (FH) is not only located in mitochondria, but also targeted to plastids, raising the possibility that FH is a candidate for Fe delivery (24). FH-deficient plants show decreased levels of chlorophyll and heme content, as well as lower nitrite reductase (NIR) activity, conditions that point to FH as a likely Fe donor (25). However, more evidence is needed to support this hypothesis.

The Fe-S cluster formed on $SufBC_2D$ is delivered to target apo proteins directly or indirectly via carrier proteins (26,27). The mechanisms of cluster trafficking in SUF machinery are not well established compared to ISC machinery. In the bacterial SUF system, glutaredoxin 4 (Grx4), Mrp (member of the Fe-S cluster-containing p-loop NTPase superfamily), Ygfz (IBA57 homolog) , ErpA, and NfuA are likely to play important roles for the late steps of Fe-S maturation, (see Table 3.1 for a list of plastidial Fe-S cluster assembly proteins in *Arabidopsis thaliana* and their bacterial relatives) (28). Mitochondrial *At* GRXS15, the primary transfer protein, receives a [2Fe-2S] cluster from scaffold ISCU proteins (29). [2Fe-2S]-GRXS15 directly transfers the [2Fe-2S] cluster or converts it into a [4Fe-4S] cluster on heterodimeric ISCA-type proteins. This step is followed by the insertion of a [4Fe-4S] cluster into target apo proteins (discussed in chapter 2)

with the help of NFU, BOLA, or IND1/INDH proteins. IND1 and INDH are members of the Fe-S cluster-containing p-loop NTPases superfamily. GRXS14 and GRXS16 are localized in plant plastids, and both GRXs can complement the yeast *Δgrx5* mutant (30). *Δgrxs14* mutants and *Δgrxs16* mutants separately, do not have any phenotypes under standard conditions (31); however, deletion of GRXS14 and GRXS16 together causes retarded plant growth, indicating the non-essential roles of GRXS14 and GRXS16. GRXS14 binds a [2Fe-2S] cluster at the subunit interface of a homodimer and can transfer intact [2Fe-2S] clusters to apo ferredoxin (30) and also to SUFA1 (32) at a rapid rate. The unidirectional cluster transfer from GRXS14 to SUFA1 suggests that GRXS14 might act upstream of SUFA1 in [2Fe-2S] cluster trafficking *in vivo.* (33). It has been shown that GRXS16 can bind [2Fe-2S] and [4Fe-4S] clusters, and [4Fe-4S] cluster-bound GRXS16 can transfer a [4Fe-4S] cluster to apo NFU2 (S. Subramanian and M.K. Johnson, unpublished results). This unidirectional cluster transfer suggests that GRXS16 might be involved with [4Fe-4S] cluster trafficking in plastids.

A-type carrier proteins play important roles in the maturation of Fe-S clusters in different organisms. A-type proteins (e.g., IscA, SufA, and ErpA) in bacteria and ISCA proteins in mitochondria are essential for [4Fe-4S] cluster maturation (34). Plastids only have one A-type carrier protein, SUFA1 (previously known as CpISCA) (35,36). SUFA1 can bind a [2Fe-2S] cluster at the dimer interface upon cluster reconstitution *in vitro* (32,36). Although SUFA proteins can interact with the scaffold protein and promote the maturation of apo FDX, Δ*sufA1* mutants show no phenotype under standard growth conditions, which suggests SUFA1 might not be essential for SUF machinery (37). It is likely that SUFA1 acts as a backup carrier for [2Fe-2S] clusters under stress conditions. ISCA and IBA57 from yeast and human mitochondria form a complex, which is important for the maturation of homoaconitase, aconitase, biotin synthase,

lipoic acid synthase, and radical-S-adenosylmethionine (SAM) proteins (38,39). There are two isoforms of IBA57 in plants, IBA57.1 located in mitochondria and IBA57.2 located in plastids and both of them can complement the *E. coli* ortholog Δ*ygfZ* mutant (40,41). The exact function of IBA57, however, is still unknown.

HCF101 (high chlorophyll fluorescence 101) belongs to the ancient and ubiquitously distributed protein family of soluble, [4Fe-4S] cluster-containing, P-loop NTPases (42). There are four classes of P-loop NTPase family and they all play important roles in Fe-S cluster assembly pathways. Proteins of this family share a highly conserved p-loop NTPase sequence and are present in bacteria as well as eukaryotic plastids, mitochondria, and cytosol, see Figure 3.1 (42). HCF101 and eubacterial ApbC belong to class I of the P-loop NTPase family. *Salmonella enterica* ApbC, has C-terminal CXXC Fe-S cluster binding motif and is involved in the thiamine biosynthetic pathway for the maturation of Fe-S proteins (43-45). Ind1, a mitochondrial protein involved in the maturation of Fe-S centers in NADH dehydrogenase, is a member of class II, and has a C-terminal CXXCXXC Fe-S cluster binding motif (46). Class III member, *Sc* Nbp35 (nucleotide-binding protein 35) is in cytosolic protein that binds [4Fe-4S] clusters at both N- and C-termini using CXXCXXXXC and CXXC motifs, respectively (47). Class IV member, *Sc* Cfd1 (cytosolic iron-sulfur cluster deficient protein 1) binds a [4Fe-4S] cluster at the subunit interface of the homodimer using the first two cysteines of the C-terminal CXXCXXC motif (48,49). Cfd1 forms a stable complex with Nbp35 and Cfd1-Nbp35 complex acts as a novel scaffold in eukaryotic cytosolic Fe-S cluster assembly (50,51).

Based on the close analogy with other Fe-S cluster-containing nucleotide-binding proteins, such the nitrogenase Fe protein and the recent crystal structure of [4Fe-4S] cluster-bound Cfd1(49), it seems likely that members of P-loop NTPase family also bind exposed [4Fe-4S]

clusters at the subunit interface of homodimers or heterodimers using C-terminal CXXC motifs (44,46,51,52). However, HCF101 lacks the Fe-S cluster binding motif CXXC, which makes HCF101 very different type of Fe-S binding protein from other members of P-loop NTPase family. Nevertheless, the *Δhcf101* mutant is seedling lethal due to decreased amount of PS1 [4Fe-4S] proteins, PsaA, PsaB, PsaC and ferredoxin-thioredoxin reductase (FTR) which uses a [4Fe-4S] cluster to cleave disulfides in two sequential one-electron steps (42,53,54). However, amounts of [2Fe-2S] containing proteins Fdx and PetC are not affected in *Δhcf101* mutants; thus, HCF101 seems to be involved in the maturation of [4Fe-4S] clusters, not [2Fe-2S] clusters (53).

The ubiquitous NFU proteins bind [4Fe-4S] clusters and in some cases [2Fe-2S] clusters at the subunit interface of homodimers using CXXC motifs and are involved with Fe-S cluster trafficking and maturation of Fe-S clusters on target proteins. There are five NFU proteins in *Arabidopsis thaliana*: NFU1, NFU2, and NFU3 are present in plastid, whereas NFU4 and NFU5 are localized in mitochondria (55,56). Plastid NFU1/2/3 are composed of two domains with the cluster-binding CXXC motif in the N-terminal domain (55,57). NFU1 only binds [4Fe-4S] clusters and targets a specific subset of [4Fe-4S] cluster containing client proteins (58) . In contrast, NFU2 binds and traffics both [2Fe-2S] and [4Fe-4S] cluster, and the cluster-binding properties of NFU3 have yet to be fully explored. Mitochondrial NFU4/5 proteins are also bimodular proteins, but with the cluster-binding CXXC motif in the C-terminal domain (55,59), and they function exclusively in [4Fe-4S] trafficking and maturation of specific target proteins. The roles of the non-cluster binding domains have yet to fully explored but are most likely involved in determining the specificity of cluster transfers reactions.

Although NFU proteins are essential in human and in *Synechococcus,* they are only required under specific conditions in *Azotobacter vinelandii, E. coli,* and *Saccharomyces*

cerevisiae (60,61). For example, in oxygen-rich conditions, the *ΔnfuA* mutant in *A. vinelandii* is lethal (61-63). In *A. thaliana*, *Δnfu2* and *Δnfu3* mutants present a dwarf phenotype due to the impairment of PSI resulting in deficient photosynthesis (56,64). Deficient photosynthesis is further explained by defects in the maturation of the three PS1 [4Fe-4S] clusters assembled in PsaA, PsaB and PsaC subunits. Ultimately, NFU2 and NFU3 might have overlapping contributions as the double *Δnfu2-Δnfu3* mutant is lethal (65). In addition, NFU2 has been shown to rapidly transfer [2Fe-2S] clusters to plant ferredoxin(56,66) and dihydroxyacid dehydrogenase, a key enzyme in branched chain amino acid biosynthesis (67,68) to rapidly transfer [4Fe-4S] clusters to adenosine 5-phosphosulfate reductase, APR1, a key enzyme in sulfur assimilation mechanism in plants (57). Even though *Arabidopsis nfu2* and *nfu3* mutants have a PSI defect, plants show a much milder phenotype than *hcf101* mutant plants (69). In contrast. *Arabidopsis nfu1* mutants exhibited no phenotype when grown under standard conditions (58,69).

At NFU2 and *At* HCF101 are both required for the maturation of Fe-S clusters in PSI, but their potential connection has not been investigated *in vitro*. Our working model for the SUF machinery in plastids is that NFU2 accepts clusters from the $SUFBC_2D$ scaffold complex and then delivers them to HCF101 for the maturation of the three [4Fe-4S] clusters in PS1. Since relatively little has been reported about the properties of HCF101 in the literature, we first present spectroscopic characterization of HCF101, using UV-visible absorption/CD, resonance Raman and EPR, before demonstrating that NFU2 acts upstream of HCF101 for PSI [4Fe-4S] cluster assembly.

Experimental Procedures

All the chemicals and materials were purchased from commercial suppliers (Fisher Scientific, Sigma-Alrich Chemical Co, and GE Healthcare/Invitrogen) at Bio grade and were used

without any further treatment unless otherwise stated. Preparation and handling of anaerobic samples for spectroscopic studies and cluster transfer experiments were carried out inside a Vacuum Atmosphere glove box under argon atmosphere with an oxygen level lower than 2 ppm.

The plasmids for overexpression of *Arabidopsis thaliana* HCF101 and NFU2 were provided by Dr. Nicolas Rouhier (Université de Lorraine, Nancy, France). The plasmid for overexpression of *Synechococcus* sp PC 7002 was provided by Dr. John Golbeck (Penn State University, Pennsylvania). Nucleotide sequencing of these proteins was performed by the University of Georgia Genomics Facility. *At* NFU2 was heterologously expressed as a non-His-tagged protein in *E. coli*, and purified and reconstituted according to previously published procedures (57).

Overexpression and purification of His-tagged HCF101: Recombinant His-tagged HCF101 was expressed in *E. coli* BL21 (DE3) strain. Colonies containing HCF101 were grown in LB media at 37 °C and protein overexpression was induced at exponential phase with isopropyl 1-thio-β-D-galactopyranoside (IPTG) to a final concentration of 100 μg/mL. The bacterial culture was further allowed to cultivate at 37 °C for 4–5 hours. The brown cells were harvested by centrifugation at 6690 × g at 4 °C and stored at -80 °C for later use. 30 g of cell paste containing overexpressed HCF101 were thawed and resuspended in 50 mL of (100 mM Tris-HCl, pH 7.8) buffer A containing 150 μg/mL PMSF, 2 mU/mL DNase (Roche), and 0.5 μg/mL RNase (Roche) and lysed by intermittent anaerobic sonication on ice. After breaking the cells, soluble and insoluble fractions were separated by centrifugation at 39800 × g at 4 °C for 2.5 hours. The brown supernatant containing *At* HCF101 was loaded onto 5x5-mL His-Trap HP columns (GE Healthcare) previously equilibrated with binding buffer (100 mM Tris-HCl, pH 7.8, containing 0.5 M NaCl and 20 mM imidazole). The column was washed with 10 column volumes of binding

buffer before the protein of interest was eluted with a 20–500 mM imidazole gradient. Fractions containing HCF101, determined by sodium dodecyl sulfate polyacrylamide gel electrophoresis (SDS PAGE), were pooled and concentrated using Amicon ultrafiltration with a 30-kDa MW membrane. Excess imidazole was removed by loading concentrated HCF101 onto a 25 mL desalting column. estimated by SDS-PAGE. Apo HCF101 was prepared by incubating as isolated samples with a 50-fold excess of EDTA and a 20-fold excess of potassium ferricyanide for 90 minutes followed by anaerobic purification with desalting columns to remove residual iron and sulfide.

IscS mediated reconstitution of At HCF101: In order to enhance the cluster content, as purified HCF101 was chemically reconstituted by incubating it with 6-fold excess of ferrous ammonium sulfate (FAS), 12-fold excess of L-cysteine, and catalytic amount of IscS under strictly anaerobic conditions for approximately 3.5 hours. The reaction was monitored using UV-visible absorption and CD spectroscopy. The reconstitution mixture was loaded onto 3 in-line assembled 5 mL HiTrap Q Sepharose HP columns (GE Healthcare) and a single fraction containing predominantly [4Fe-4S] cluster-bound HCF101 was eluted under an increasing NaCl gradient.

Overexpression and aerobic purification of Syn PsaC: *Synechococcus* sp PC 7002, PsaC was overexpressed in *E.coli* strain BL21 (DE3) and purified from 6L grown according to the published procedure (70). Cells containing the overexpressed protein were broken by aerobic sonication, and the brown inclusion bodies were collected by centrifugation. The inclusion bodies were then washed by repetitive centrifugation with a 10% sucrose solution in TS buffer (50 mM Tris-HCl, pH = 8.0). Inclusion bodies were solubilized in TS buffer containing 6.5 M urea and 2 mM DTT for 1 hour at room temperature. The solubilized PsaC was purified using 3 in-line assembled 5 mL HiTrap Q Sepharose HP columns in TS buffer containing 6.5 M urea and 2 mM

DTT under aerobic conditions and the fractions containing PsaC were concentrated using an Amicon ultrafiltration unit equipped with a 5 kDa MW membrane.

Anaerobic reconstitution of Syn PsaC: Denatured PsaC was reconstituted anaerobically with the addition of $FeCl_3$ and Na_2S in the presence of 1% mercaptoethanol. After incubating the reconstitution mixture anaerobically in darkness for 16 hours, it was washed repetitively with 50 mM Tris-HCl buffer and concentrated using an Amicon ultrafiltration unit equipped with a 5 kDa MW membrane. For further purification of holo PsaC, the reconstitution mixture was applied to 2 in-line assembled 5 mL HiTrap Q Sepharose HP columns equilibrated with 25 mM sodium phosphate buffer, pH 7.92, with 0.1% mercaptoethanol, under anaerobic conditions. The yellow-brown protein solution was collected and concentrated to a volume of 2 mL. Holo PsaC was characterized using UV-vis absorption, CD, and EPR spectroscopy.

Analytical and spectroscopic methods: Protein concentrations were determined by the DC protein assay (Bio-Rad) using bovine serum albumin (Roche) as a standard (71). Iron concentrations were determined colorimetrically using bathophenanthroline under reducing conditions after digesting proteins in 0.8% KMnO4/0.2 M HCl (72). A standard curve was constructed from a series of dilutions of a 1000 ppm atomic absorption iron standard.

All spectroscopic studies and cluster transfer experiments were carried out inside a Vacuum Atmosphere glove box under argon atmosphere with an oxygen level lower than 2 ppm. UV-visible absorption spectra were recorded in sealed quartz cuvettes at room temperature using a Shimadzu-3101PC spectrophotometer. CD spectra were recorded in sealed quartz cuvettes using a Jasco J-715 spectropolarimeter. Resonance Raman samples were in the form of an 18-μL frozen droplet mounted on the cold finger of an Air Products Displex Model CSA-202E closed-cycle refrigerator (Air Products, Allentown, PA), and resonance Raman spectra were recorded using an

Instrument SA Ramanor U1000 scanning spectrometer coupled with a Coherent Sabre argon ion laser. The spectra were recorded with 0.5 cm^{-1} increments at 7 cm^{-1} resolution, and each spectrum consisted of 80–120 scans. X-band (~9.6 GHz) EPR spectra were recorded using a Bruker ESP-300E EPR spectrometer equipped with a dual-mode ER-4116 cavity and an Oxford Instruments ESR-9 flow cryostat. Spin quantifications of S = 1/2 resonances were carried out under non-saturating conditions using a 1 mM CuEDTA standard.

Cluster transfer from [4Fe-4S] cluster-bound At NFU2 to apo At HCF101: The cluster transfer reaction was initiated by the addition of DTT-pretreated apo HCF101 (140 µM) to NFU2 (70 µM in [4Fe-4S] clusters), under anaerobic conditions. As HCF101 is a member of P-loop NTPase family, we also repeated the cluster transfer experiment in the presence of 40 mM $MgCl_2$, 150 mM KCl, and 2 mM ADP. The time course for the cluster transfer was monitored by UV-visible absorption and CD spectroscopy at room temperature using a septum-sealed 1-cm cuvette. The reverse cluster transfer from [4Fe-4S]-HCF101 (70 µM in [4Fe-4S] clusters) to apo NFU2 (140 µM in monomer) was also monitored under anaerobic conditions using CD spectroscopy at room temperature using a 1-cm cuvette.

Cluster transfer from [4Fe-4S] cluster-bound At NFU2 to apo Syn PsaC: Apo PsaC was obtained by incubation with 50-fold excess of EDTA and 20-fold excess of potassium ferricyanide followed by repeated washes with 50 mM Tris-HCl buffer, pH 8.0, in the presence of 6.5 M urea. Apo PsaC was renatured by rapid dilution in 50 mM Tris-HCl buffer, pH 8.0, for cluster transfer experiment**s** in which apo PsaC **(**40 µM) was added to NFU2 (70 µM in [4Fe-4S] cluster) in 50 mM Tris-HCl buffer, pH 8.0, with 5 mM DTT and 1 M urea. The reaction was initiated by the addition of apo PsaC and the cluster transfer was monitored using UV-visible absorption and CD spectroscopy at room temperature using a 1-cm cuvette.

Results

Nature and properties of cluster-bound forms of A. thaliana HCF101: Anaerobically purified recombinant *At* HCF101 contained 1.6 ± 0.4 Fe/monomer and exhibited a UV-visible absorption spectrum with broad shoulders at 330, 420 and 600 nm, see Figure 3.2 (black lines). While the 330 and 420 nm bands are indicative of a $[4Fe\text{-}4S]^{2+}$ or $[2Fe\text{-}2S]^{2+}$ cluster, the 600 nm band is indicative of a linear $[3Fe\text{-}4S]^{1+}$ cluster (73). The presence of paramagnetic $S = 5/2$ linear $[3Fe\text{-}4S]^{1+}$ clusters was confirmed by EPR, which shows a rhombic ($E/D \sim 0.33$) S = 5/2 species with a near-isotropic resonance at $g = 4.30$ with a very broad absorption-shaped low-field resonance spanning $g = 9.6\text{-}6.2$, see Figure 3.3A. This type of broad low-field resonance is uniquely indicative of a $S = 5/2$ linear $[3Fe\text{-}4S]^{1+}$ cluster and has been attributed to distributed axial (D) and rhombic (E) zero-field splitting parameters resulting from inhomogeneity in the magnetic interactions in frozen solution(74-76). In addition to the $S = 5/2$ linear $[3Fe\text{-}4S]^{1+}$ cluster, as purified HCF101 also has a fast relaxing, nearly-isotropic $S = 1/2$ EPR $g = 2.02$ signal that is only observed without broadening below 30 K, see Figure 3.3A. This resonance is characteristic of a $S = 1/2$ cubane $[3Fe\text{-}4S]^{1+}$ cluster (77) and spin quantitation indicates that it is a minor component accounting for < 0.05 spins/monomer. It is not possible to reliably quantify the linear $[3Fe\text{-}4S]^{1+}$ cluster EPR signal, but the fact that is 600 nm band is clearly observable in the UV-visible spectrum indicates that it is significant component.

In order to enhance the cluster content, as purified HCF101 was chemically reconstituted by incubating with a 6-fold excess of ferrous ammonium sulfate (FAS), 12-fold excess of L-cysteine, and a catalytic amount of IscS under strictly anaerobic condition for approximately 3.5 hours. After repurifying using a Q Sepharose column, reconstituted HCF101 showed only broad shoulders 320 at 420 nm (Figure 3.2 blue lines) and the intensity relative to the protein band at 280

nm increased compared with the as purified protein (Figure 3.2). The loss of the band around 600 nm indicates the loss of the linear $[3Fe\text{-}4S]^{1+}$ cluster and the $\varepsilon_{420} = 14\ M^{-1}cm^{-1}$ coupled with the analytical data which indicate 3.6 ± 0.3 Fe/monomer indicate that reconstituted HCF101 contains approximately one $[4Fe\text{-}4S]^{2+}$ per monomer. Reconstituted HCF101 has a weak visible CD spectrum that is similar to the as purified sample, except in the 600 nm region, where the linear $[3Fe\text{-}4S]^{1+}$ dominates the absorption spectrum, suggesting that the linear $[3Fe\text{-}4S]^{1+}$ cluster is minor contributor to the CD spectrum of as purified sample in the 300-500 nm region. (Figure 3.2). Altogether, these results indicate HCF101 can bind one [4Fe-4S] cluster per monomer.

Reconstituted samples were also investigated by EPR and resonance Raman spectroscopy to investigate the ground state and vibrational properties of the $[4Fe\text{-}4S]^{2+,1+}$ cluster in HCF101. Reconstituted HCF101 has negligible EPR intensity indicative of $S = 0$ $[4Fe\text{-}4S]^{2+}$ cluster. Reduction with dithionite gives a broad axial $S = 1/2$ EPR signal, $g_{\|} = 2.02$ and $g_{\perp} = 1.93$ that accounts for 0.1 spins/monomer, see Figure 3.4, even though the absorption spectrum indicates complete reduction. Consequently, the low field region of the EPR spectrum was investigated, revealing a broad signal at $g = 5.3$, indicative of an $S = 3/2$ $[4Fe\text{-}4S]^{1+}$ cluster, see Figure 3.4. Hence, the $[4Fe\text{-}4S]^{1+}$ cluster ground state in dithionite-reduced reconstituted HCF101 is heterogeneous in frozen solution with a dominant $S = 3/2$ form and a minor $S = 1/2$ form. A similar situation is observed for many biological $[4Fe\text{-}4S]^{1+}$ clusters, and is particularly prevalent in clusters with one non-cysteinyl ligand (78).

Resonance Raman spectroscopy provides important information on cluster type and the nature of the coordination environment, because each type of cluster has a distinct spectrum and the vibrational frequencies are often depend on the nature of cluster ligands. The vibrational properties of the $[4Fe\text{-}4S]^{2+}$ cluster in HCF101 in the Fe-S stretching region (240-450 cm^{-1}) were

determined using 457.9 nm laser excitation, see Figure 3.5. The spectrum is uniquely indicative of a $[4Fe\text{-}4S]^{2+}$ cluster and the frequency of the intense totally symmetric breathing mode of the $[4Fe\text{-}4S]^{2+}$ core at 342 cm^{-1} is indicative of one oxygenic such as hydroxide, serinate or aspartate (observed range 340-343 cm^{-1}) rather complete cysteinyl ligation (observed range 333-339 cm^{-1}) (78). Hence both the EPR and RR data indicate that the [4Fe-4S] cluster in HCF is ligated by three cysteinyl and one oxygenic ligand.

Synthetic linear $[3Fe\text{-}4S]^{1+}$ clusters and linear $[3Fe\text{-}4S]^{1+}$ clusters generated under aerobic alkaline denaturing conditions in beef heart aconitase are converted into $[4Fe\text{-}4S]^{2+}$ clusters in the presence of Fe^{2+} ions (79,80). Since as purified HCF101 contains a mixture of linear $[3Fe\text{-}4S]^{1+}$ and $[4Fe\text{-}4S]^{2+}$ clusters, the possibility that Fe^{2+} alone could repair the $[4Fe\text{-}4S]^{2+}$ cluster on HCF101 was investigated using UV-visible absorption spectroscopy. As shown in Figure 3.6A, immediately after adding FAS the absorption band at around 600 nm disappeared, and a broad shoulder around 420 nm formed indicating the formation of a $[4Fe\text{-}4S]^{2+}$ cluster. The results clearly demonstrate that a Fe^{2+} ion alone is capable of enabling a linear $[3Fe\text{-}4S]^{1+}$ to $[4Fe\text{-}4S]^{2+}$ cluster conversion in HCF101. To investigate the possibility that linear $[3Fe\text{-}4S]^{1+}$ clusters are formed by O_2-induced degradation of $[4Fe\text{-}4S]^{2+}$ clusters in HCF101, the time course of aerial oxidative degradation of reconstituted HCF101 was monitored by UV-visible absorption spectroscopy, see Figure 3.6B. Complete O_2-induced degradation of $[4Fe\text{-}4S]^{2+}$ clusters in HCF101 required 5 h, but no bands in the 600 nm region indicative of formation of linear $[3Fe\text{-}4S]^{1+}$ clusters were observed at any time during the time course of the aerial oxidative degradation reaction. Consequently, the linear $[3Fe\text{-}4S]^{1+}$ clusters in as purified HCF101 do not appear to be the result aerial oxidative of $[4Fe\text{-}4S]^{2+}$ clusters.

Nature and properties of cluster-bound forms of Syn PsaC: PSAC is an 8Fe ferredoxin-like protein containing two [4Fe-4S]$^{2+,1+}$ clusters that forms a complex with the PSAAB heterodimer proximal to a subunit bridging [4Fe-4S] $^{2+,1+}$ cluster in PS1. *Synechococcus* PsaC rather than *At* PSAC was used as a potential cluster transfer target for *At* NFU2 and *At* HCF101. This is because recombinant *At* PSAC and *Syn* PsaC are both expressed as apo-protein inclusion bodies in *E. coli*, but only denatured apo *Syn* PsaC was successfully reconstituted and solubilized as an 8Fe ferredoxin. The UV-visible absorption spectrum of reconstituted PsaC prepared in this work, see Figure 3.7, has a broad maximum at 390 nm and a broad shoulder at 320 nm and is quantitatively very similar to spectra reported for other 8Fe ferredoxins (81). In the CD spectrum, four positive maxima are observed at 320 nm, 360 nm, 420 nm, and 570 nm (Figure 3.7). The EPR spectrum was recorded in the fully reduced state by adding 5 mM sodium dithionite at pH 10.0 (see *inset* in Figure 3.7). The complex EPR spectrum results from a spin-spin interaction between the two S = 1/2 [4Fe-4S]$^{1+}$ clusters and is identical to the spectrum previously published for reconstituted, dithionite-reduced *Syn* PsaC (70).

Cluster transfer from [4Fe-4S] cluster-bound At NFU2 to apo At HCF101: To investigate the interaction between NFU2 and HCF101, anaerobic cluster transfer studies from [4Fe-4S]-NFU2 to apo HCF101 were performed, see Figure 3.8. [4Fe-4S] cluster-bound NFU2 exhibits an intense CD spectrum with positive bands at ~315, 385 and 515 nm, and negative bands at 440, 580 and 620 nm, see Figure 3.8A. [4Fe-4S] cluster-bound HCF101 has a much weaker CD spectrum with positive bands around 315 and 430 nm and negative bands at 355 and 515 nm, see Figure 3.2. The intense CD spectrum of the [4Fe-4S] center on NFU2 is completely lost within the first few minutes of mixing with apo HCF101, but the parallel absorption spectrum shows no significant changes or loss in intensity. While the resulting CD spectrum is weak, it does not match

up well with the CD spectrum of [4Fe-4S]-HCF101 and continues to change with time until about 30 min. Moreover, the parallel absorption spectra show a progressive increase in the 600 nm band associated with linear $[3Fe\text{-}4S]^{1+}$ clusters, see Figure 3.8B. Since linear $[3Fe\text{-}4S]^{1+}$ clusters have only been characterized in HCF101, this indicates that cluster transfer has occurred. These results are tentatively interpreted in terms of rapid formation of a [4Fe-4S] cluster-containing HCF101-NFU2 complex with a dramatically altered cluster environment, followed by slower formation of a predominantly linear $[3Fe\text{-}4S]^{1+}$ cluster on HCF101 and complex dissociation. Similar results were observed in the presence of $MgCl_2$, KCl, and ADP or ATP (data not shown), suggesting cluster transfer is not significantly perturbed by nucleotide binding or hydrolysis

The possibility of a [4Fe-4S] cluster transfer from *At* HCF101 to apo NFU2 was also monitored by CD spectroscopy at room temperature. Over a 4-hour time period, the CD spectrum associated with [4Fe-4S] cluster-bound HCF101 did not change, showing that HCF101 is not the [4Fe-4S] cluster donor for NFU2. In addition, no changes in either the UV-visible absorption or CD spectra of [4Fe-4S]-NFU2 were observed in the control cluster transfer experiment where apo HCF101 was not added. The results indicate negligible degradation of the $[4Fe\text{-}4S]^{2+}$ cluster on NFU2 in the reaction mixture over the time course of the cluster transfer reaction.

Cluster transfer from [4Fe-4S] cluster-bound At NFU2 to apo Syn PsaC: *Δnfu2* and *Δnfu3* mutants have impaired PSI accumulation, which results in dwarf phenotypes (56,64,69). To investigate the involvement of NFU2 in PSI [4Fe-4S] cluster assembly, cluster transfer experiments from *At* [4Fe-4S]-NFU2 to *Syn* apo PsaC were attempted. The reaction mixture contained 1 M urea, which was required to keep apo PsaC in solution. [4Fe-4S] cluster-bound NFU2 exhibits an intense CD spectrum with positive bands at ~315, 385 and 515 nm, and negative bands at 440, 580 and 620 nm, see Figure 3.9. PsaC with two $[4Fe\text{-}4S]^{2+}$ clusters exhibits a strong

CD spectrum with four positive maxima at 320 nm, 360 nm, 420 nm, and 570 nm, see Figure 3.6. The CD bands associated with the NFU2 $[4Fe\text{-}4S]^{2+}$ center disappeared within 1 minute of adding apo PsaC to holo NFU2, and a new spectrum appears that is similar to that of holo PsaC, albeit with less that half the intensity and lacking a pronounced positive band at 570 nm. This spectrum continues to change and decrease in intensity with increasing time. After about 30 min the CD spectrum stabilizes with weak positive bands at 315, 367, 442, 490 and 540 nm and weak negative bands at 575 and 615 nm. Control experiments to assess the effect of 1 M urea on [4Fe-4S] cluster-bound NFU2 showed no change in the CD spectrum over the time course of the cluster transfer reaction. These results are tentatively interpreted in terms of rapid [4Fe-4S] cluster transfer from NFU2 to apo PsaC with concomitant slow degradation of the $[4Fe\text{-}4S]^{2+}$ clusters on PsaC due to the presence of 1 M urea in the reaction mixture. Analogous cluster transfer experiments using [4Fe-4S]-HCF101 as the cluster donor were not possible because [4Fe-4S]-HCF101 precipitates in the minimal concentration of urea that is required to keep apo PsaC in solution

Discussion

The HCF101 is a unique Fe-S cluster assembly protein that is found only in O_2-evolving chloroplasts and is essential for [4Fe-4S] cluster assembly in PS1 and FTR (53). Prior to this work, whole cell EPR studies showed that HCF101 contains $[4Fe\text{-}4S]^{2+}$ clusters *in vivo* (42). In addition, aerobically purified HCF101 was found to be largely depleted of Fe-S clusters and reconstituted HCF101 was reported to contain one $[4Fe\text{-}4S]^{2+,1+}$ cluster per monomer based on iron, sulfide and protein determinations, UV-visible absorption and EPR studies (42). The *in vitro* spectroscopic and analytical studies of HCF101 performed in this work are generally in agreement with the previous studies and extend these studies by incorporating RR and UV-visible CD studies and demonstrating that HCF101 can also accommodate linear $[3Fe\text{-}4S]^{1+}$ clusters. Indeed, the

previously published UV-visible absorption and EPR spectra for reconstituted HCF101 contains a significant amount of linear $[3Fe\text{-}4S]^{1+}$ clusters, based the absorption band at 600 nm and a distributed low field g-value for the rhombic $S = 5/2$ resonance which distinguishes adventitiously bound Fe^{3+} ions from linear $[3Fe\text{-}4S]^{1+}$ clusters. In contrast, the reconstituted HCF101 samples prepared in this work contain only [4Fe-4S] clusters as judged by the lack of a 600 nm band in the absorption spectrum and the absence of a significant the rhombic $S = 5/2$ resonance in the EPR spectrum.

Linear $[3Fe\text{-}4S]^{1+}$ clusters have yet to associated with any biological function. However, they can be formed in many proteins by degradation of $[2Fe\text{-}2S]^{2+}$, cubane $[3Fe\text{-}4S]^{+}$, and $[4Fe\text{-}4S]^{2+}$ clusters under oxidizing protein denaturing conditions (79,82-86). Linear $[3Fe\text{-}4S]^{1+}$ clusters are also bound and possibly recycled by one of the major classes of Fe-S cluster-carrier proteins. namely monothiol glutaredoxins (73). In common with synthetic linear $[3Fe\text{-}4S]^{1+}$ clusters and linear $[3Fe\text{-}4S]^{1+}$ clusters in alkaline-denatured aconitase, the linear $[3Fe\text{-}4S]^{1+}$ clusters in HCF101 are converted into $[4Fe\text{-}4S]^{2+}$ clusters by addition of Fe^{2+} ions. It is also important to note that $[4Fe\text{-}4S]^{2+}$ cluster transfer from NFU2 to HCF101 results predominantly in linear $[3Fe\text{-}4S]^{+}$ clusters, which highlights the stability of this type of cluster in HCF101. Taken together, these results suggest that HCF101 may assemble $[4Fe\text{-}4S]^{2+}$ clusters by scavenging linear $[3Fe\text{-}4S]^{1+}$ clusters formed by protein Fe-S protein denaturation in the O_2-rich environment of the chloroplast and using pools of Fe^{2+} ions to complete $[4Fe\text{-}4S]^{2+}$ clusters assembly *in situ.* In accord with this hypothesis, [4Fe-4S]-HCF101 is readily degraded by O_2 to form apo-HCF10, without the formation of a stable cubane- or linear-$[3Fe\text{-}4S]^{1+}$ intermediate.

HCF101 appears to be anomalous member of the soluble, [4Fe-4S] cluster-containing, P-loop NTPases in that it does not coordinate a solvent exposed [4Fe-4S] cluster at the subunit

interface of a homodimer using CXXC motifs, see Figure 3.1. Moreover, it is clear that HCF101 has one [4Fe-4S] cluster per monomer rather than one [4Fe-4S] cluster per dimer. Site-directed Cys-to-Ser mutagenesis studies involving each of the eight cysteine residues in HCF101 have found that three cysteine residues (Cys128, Cys347, and Cys419) are essential for binding the [4Fe-4S] cluster (42). This result is in accord with the EPR and RR studies presented in this work, which both suggest one non-cysteinyl ligand. Clearly crystallographic studies will be required to address the nature of non-cysteinyl ligation and the location of the cluster with respect to the nucleotide binding site.

The observation that *Δnfu2*, *Δnfu3,* and *Δhcf101* mutants in *At* have impaired photosystems provides strong evidence for the involvement of their gene products in the maturation of [4Fe-4S] proteins of PSI (53). More recent *in vivo* studies have shown that NFU2 and NFU3 have redundant functions in the maturation of PS1 [4Fe-4S] clusters and act upstream of HCF101 (68). This work focused on investigating cluster transfer interactions involving NFU2, HCF101, and PSAC, the 8Fe ferredoxin-like subunit in PS1 that functions as the terminal electron acceptor and electron donor for the mobile plant 2Fe ferredoxin. Bimolecular fluorescence complementation studies have shown interactions between NFU2 and HCF101 and between HCF101 and PSAC, but no interaction was observed between NFU2 and PSAC (68). *Syn* PsaC and *At* PSAC are both expressed as apo-protein inclusion bodies in *E. coli*, and *Syn* PsaC was used for *in vitro* cluster transfer studies because it can be successfully reconstituted and solubilized as an 8Fe ferredoxin.

The cluster transfer studies presented herein were only partially successful. Monitoring the time course of [4Fe-4S] cluster transfer from NFU2 to apo HCF101 revealed a rapid and unidirectional reaction in accord with HCF101 acting downstream of NFU2. However, the reaction appears to proceed via a semi-stable $[4Fe\text{-}4S]^{2+}$ NFU2-HCF101 complex that slowly degrades to

yield a predominantly linear $[3Fe\text{-}4S]^{1+}$ cluster-bound form of HCF101. As discussed above, [4Fe-4S]-HCF101 is readily obtained by incubating with Fe^{2+} ions under anaerobic conditions. Consequently, this could be a physiologically relevant mechanism for regulating the assembly of O_2-sensitive $[4Fe\text{-}4S]^{2+}$ clusters so that it occurs under more anaerobic dark conditions.

Unfortunately, it was not possible to perform *in vitro* cluster transfer reactions from [4Fe-4S]-HCF101 to apo PsaC, because control experiments revealed that the minimal urea concentration required to keep PsaC in solution resulted in degradation of the [4Fe-4S] cluster on HCF101. However, this was not the case for [4Fe-4S]-NFU2. [4Fe-4S] cluster transfer from NFU2 to apo PsaC appears to a very rapid reaction based on complete loss of the intense CD bands associated with [4Fe-4S]-NFU2 within 1 min of initiating the reaction by mixing [4Fe-4S]-NFU2 with apo PsaC. The resulting CD spectrum after 1 min is generally similar to that of holo PsaC, but less than half the intensity. Moreover, the intensity declines further, coupled with additional changes in CD for the next 30 min, suggesting gradual degradation of the clusters due the presence of 1 M urea. These qualitative results indicate that [4Fe-4S]-NFU2 has the potential to be a competent [4Fe-4S] donor for PsaC. However, it is not possible rule out other scenarios, such as [4Fe-4S]-HCF101 being the preferred donor or that both NFU2 and HCF101 bind and transfer clusters to apo PsaC. This appears to be the first attempt to assemble two clusters on one protein via intact cluster transfer and it possible that molecular chaperones are required to achieve the optimal conformational for cluster transfer or that binding of the apo protein to the PsaAB dimer is required to stabilize protein structure prior to intact cluster transfer. Clearly there is much to be learned about the assembly of multiple clusters in a single polypeptide.

Acknowledgements

This work was supported by grants from the National Institutes of Health (R37GM62524 to M.K.J).

References

1. Lill, R. (2009) Function and biogenesis of iron-sulphur proteins. *Nature* **460**, 831-838
2. Balk, J., and Pilon, M. (2011) Ancient and essential: The assembly of iron-sulfur clusters in plants. *Trends Plant Sci* **16**, 218-226
3. Balk, J., and Schaedler, T. A. (2014) Iron cofactor assembly in plants. *Annu. Rev. Plant Biol.* **65**, 125-153
4. Couturier, J., Touraine, B., Briat, J. F., Gaymard, F., and Rouhier, N. (2013) The iron-sulfur cluster assembly machineries in plants: Current knowledge and open questions. *Front Plant Sci* **4**, 259
5. Takahashi, Y., and Tokumoto, U. (2002) A third bacterial system for the assembly of iron-sulfur clusters with homologs in archaea and plastids. *J. Biol. Chem.* **277**, 28380-28383
6. Outten, F. W., Djaman, O., and Storz, G. (2004) A suf operon requirement for Fe-S cluster assembly during iron starvation in *Escherichia coli*. *Mol. Microbiol.* **52**, 861-872
7. Balk, J., and Lobreaux, S. (2005) Biogenesis of iron-sulfur proteins in plants. *Trends Plant Sci* **10**, 324-331
8. Fontecave, M., Choudens, S. O., Py, B., and Barras, F. (2005) Mechanisms of iron-sulfur cluster assembly: The SUF machinery. *J. Biol. Inorg. Chem.* **10**, 713-721

9. Hu, X., Kato, Y., Sumida, A., Tanaka, A., and Tanaka, R. (2017) The SUFBC$_2$D complex is required for the biogenesis of all major classes of plastid Fe-S proteins. *Plant J.* **90**, 235-248

10. Saini, A., Mapolelo, D. T., Chahal, H. K., Johnson, M. K., and Outten, F. W. (2010) SufD and SufC ATPase activity are required for iron acquisition during *in vivo* Fe-S cluster formation on SufB. *Biochemistry* **49**, 9402-9412

11. Van Hoewyk, D., Abdel-Ghany, S. E., Cohu, C. M., Herbert, S. K., Kugrens, P., Pilon, M., and Pilon-Smits, E. A. (2007) Chloroplast iron-sulfur cluster protein maturation requires the essential cysteine desulfurase CpNifS. *Proc. Natl. Acad. Sci. U. S. A.* **104**, 5686-5691

12. Pilon-Smits, E. A., Garifullina, G. F., Abdel-Ghany, S., Kato, S., Mihara, H., Hale, K. L., Burkhead, J. L., Esaki, N., Kurihara, T., and Pilon, M. (2002) Characterization of a NifS-like chloroplast protein from *Arabidopsis.* Implications for its role in sulfur and selenium metabolism. *Plant Physiol.* **130**, 1309-1318

13. Roret, T., Pegeot, H., Couturier, J., Mulliert, G., Rouhier, N., and Didierjean, C. (2014) X-ray structures of Nfs2, the plastidial cysteine desulfurase from *Arabidopsis thaliana*. *Acta Crystallogr F Struct Biol Commun* **70**, 1180-1185

14. Leon, S., Touraine, B., Briat, J. F., and Lobreaux, S. (2002) The *At* NFS2 gene from *Arabidopsis thaliana* encodes a NifS-like plastidial cysteine desulphurase. *Biochem. J.* **366**, 557-564

15. M, N. M., Ollagnier-de-Choudens, S., Sanakis, Y., Abdel-Ghany, S. E., Rousset, C., Ye, H., Fontecave, M., Pilon-Smits, E. A., and Pilon, M. (2007) Characterization of

Arabidopsis thaliana SufE2 and SufE3: Functions in chloroplast iron-sulfur cluster assembly and Nad synthesis. *J. Biol. Chem.* **282**, 18254-18264

16. Xu, X. M., and Moller, S. G. (2006) *At* SufE is an essential activator of plastidic and mitochondrial desulfurases in *Arabidopsis*. *EMBO J.* **25**, 900-909

17. Ye, H., Abdel-Ghany, S. E., Anderson, T. D., Pilon-Smits, E. A., and Pilon, M. (2006) CpSufE activates the cysteine desulfurase CpNifS for chloroplastic Fe-S cluster formation. *J. Biol. Chem.* **281**, 8958-8969

18. Couturier, J., Wu, H. C., Dhalleine, T., Pegeot, H., Sudre, D., Gualberto, J. M., Jacquot, J. P., Gaymard, F., Vignols, F., and Rouhier, N. (2014) Monothiol glutaredoxin-BolA interactions: Redox control of *Arabidopsis thaliana* BolA2 and SufE1. *Mol Plant* **7**, 187-205

19. Xu, X. M., Adams, S., Chua, N. H., and Moller, S. G. (2005) *At* NAP1 represents an atypical SufB protein in *Arabidopsis* plastids. *J. Biol. Chem.* **280**, 6648-6654

20. Nagane, T., Tanaka, A., and Tanaka, R. (2010) Involvement of *At* NAP1 in the regulation of chlorophyll degradation in *Arabidopsis thaliana*. *Planta* **231**, 939-949

21. Hjorth, E., Hadfi, K., Zauner, S., and Maier, U. G. (2005) Unique genetic compartmentalization of the SUF system in cryptophytes and characterization of a SufD mutant in *Arabidopsis thaliana*. *FEBS Lett.* **579**, 1129-1135

22. Wollers, S., Layer, G., Garcia-Serres, R., Signor, L., Clemancey, M., Latour, J. M., Fontecave, M., and Ollagnier de Choudens, S. (2010) Iron-sulfur (Fe-S) cluster assembly: the SufBCD complex is a new type of Fe-S scaffold with a flavin redox cofactor. *J. Biol. Chem.* **285**, 23331-23341

23. Ravet, K., Touraine, B., Boucherez, J., Briat, J. F., Gaymard, F., and Cellier, F. (2009) Ferritins control interaction between iron homeostasis and oxidative stress in *Arabidopsis*. *Plant J.* **57**, 400-412

24. Turowski, V. R., Aknin, C., Maliandi, M. V., Buchensky, C., Leaden, L., Peralta, D. A., Busi, M. V., Araya, A., and Gomez-Casati, D. F. (2015) Frataxin Is localized to both the chloroplast and mitochondrion and is involved in chloroplast Fe-S protein function in *Arabidopsis*. *PLoS One* **10**, e0141443

25. Soderberg, C., Gillam, M. E., Ahlgren, E. C., Hunter, G. A., Gakh, O., Isaya, G., Ferreira, G. C., and Al-Karadaghi, S. (2016) The structure of the complex between yeast frataxin and ferrochelatase: Characterization and pre-steady state reaction of ferrous iron delivery and heme synthesis. *J. Biol. Chem.* **291**, 11887-11898

26. Marinoni, E. N., de Oliveira, J. S., Nicolet, Y., Raulfs, E. C., Amara, P., Dean, D. R., and Fontecilla-Camps, J. C. (2012) $(IscS\text{-}IscU)_2$ complex structures provide insights into Fe_2S_2 biogenesis and transfer. *Angew. Chem. Int. Ed. Engl.* **51**, 5439-5442

27. Chahal, H. K., Dai, Y., Saini, A., Ayala-Castro, C., and Outten, F. W. (2009) The SufBCD Fe-S scaffold complex interacts with SufA for Fe-S cluster transfer. *Biochemistry* **48**, 10644-10653

28. Roche, B., Aussel, L., Ezraty, B., Mandin, P., Py, B., and Barras, F. (2013) Iron/sulfur proteins biogenesis in prokaryotes: Formation, regulation and diversity. *Biochim. Biophys. Acta* **1827**, 455-469

29. Shakamuri, P., Zhang, B., and Johnson, M. K. (2012) Monothiol glutaredoxins function in storing and transporting $[Fe_2S_2]$ clusters assembled on IscU scaffold proteins. *J. Am. Chem. Soc.* **134**, 15213-15216

30. Bandyopadhyay, S., Gama, F., Molina-Navarro, M. M., Gualberto, J. M., Claxton, R., Naik, S. G., Huynh, B. H., Herrero, E., Jacquot, J. P., Johnson, M. K., and Rouhier, N. (2008) Chloroplast monothiol glutaredoxins as scaffold proteins for the assembly and delivery of [2Fe-2S] clusters. *EMBO J.* **27**, 1122-1133

31. Rey, P., Becuwe, N., Tourrette, S., and Rouhier, N. (2017) Involvement of *Arabidopsis* glutaredoxin S14 in the maintenance of chlorophyll content. *Plant Cell Environ.* **40**, 2319-2332

32. Mapolelo, D. T., Zhang, B., Randeniya, S., Albetel, A. N., Li, H., Couturier, J., Outten, C. E., Rouhier, N., and Johnson, M. K. (2013) Monothiol glutaredoxins and A-type proteins: Partners in Fe-S cluster trafficking. *Dalton Trans* **42**, 3107-3115

33. Rouhier, N., Couturier, J., Johnson, M. K., and Jacquot, J. P. (2010) Glutaredoxins: Roles in iron homeostasis. *Trends Biochem. Sci.* **35**, 43-52

34. Mapolelo, D. T., Zhang, B., Naik, S. G., Huynh, B. H., and Johnson, M. K. (2012) Spectroscopic and functional characterization of iron-sulfur cluster-bound forms of *Azotobacter vinelandii* ^{Nif}IscA. *Biochemistry* **51**, 8071-8084

35. Yabe, T., and Nakai, M. (2006) *Arabidopsis At* IscA-I is affected by deficiency of Fe-S cluster biosynthetic scaffold *At*CnfU-V. *Biochem. Biophys. Res. Commun.* **340**, 1047-1052

36. Abdel-Ghany, S. E., Ye, H., Garifullina, G. F., Zhang, L., Pilon-Smits, E. A., and Pilon, M. (2005) Iron-sulfur cluster biogenesis in chloroplasts. Involvement of the scaffold protein CpIscA. *Plant Physiol.* **138**, 161-172

37. Lu, Y. (2018) Assembly and transfer of iron-sulfur clusters in the plastid. *Front Plant Sci* **9**, 336

38. Gelling, C., Dawes, I. W., Richhardt, N., Lill, R., and Mühlenhoff, U. (2008) Mitochondrial Iba57p is required for Fe/S cluster formation on aconitase and activation of radical SAM enzymes. *Mol. Cell. Biol.* **28**, 1851-1861

39. Sheftel, A. D., Wilbrecht, C., Stehling, O., Niggemeyer, B., Elsasser, H. P., Mühlenhoff, U., and Lill, R. (2012) The human mitochondrial ISCA1, ISCA2, and IBA57 proteins are required for [4Fe-4S] protein maturation. *Mol. Biol. Cell* **23**, 1157-1166

40. Waller, J. C., Alvarez, S., Naponelli, V., Lara-Nunez, A., Blaby, I. K., Da Silva, V., Ziemak, M. J., Vickers, T. J., Beverley, S. M., Edison, A. S., Rocca, J. R., Gregory, J. F., 3rd, de Crecy-Lagard, V., and Hanson, A. D. (2010) A role for tetrahydrofolates in the metabolism of iron-sulfur clusters in all domains of life. *Proc. Natl. Acad. Sci. U. S. A.* **107**, 10412-10417

41. Waller, J. C., Ellens, K. W., Alvarez, S., Loizeau, K., Ravanel, S., and Hanson, A. D. (2012) Mitochondrial and plastidial COG0354 proteins have folate-dependent functions in iron-sulphur cluster metabolism. *J Exp Bot* **63**, 403-411

42. Schwenkert, S., Netz, D. J., Frazzon, J., Pierik, A. J., Bill, E., Gross, J., Lill, R., and Meurer, J. (2009) Chloroplast HCF101 is a scaffold protein for [4Fe-4S] cluster assembly. *Biochem. J.* **425**, 207-214

43. Skovran, E., and Downs, D. M. (2003) Lack of the ApbC or ApbE protein results in a defect in Fe-S cluster metabolism in *Salmonella enterica* serovar Typhimurium. *J. Bacteriol.* **185**, 98-106

44. Boyd, J. M., Pierik, A. J., Netz, D. J., Lill, R., and Downs, D. M. (2008) Bacterial ApbC can bind and effectively transfer iron-sulfur clusters. *Biochemistry* **47**, 8195-8202

45. Boyd, J. M., Sondelski, J. L., and Downs, D. M. (2009) Bacterial ApbC protein has two biochemical activities that are required for *in vivo* function. *J. Biol. Chem.* **284**, 110-118

46. Bych, K., Kerscher, S., Netz, D. J., Pierik, A. J., Zwicker, K., Huynen, M. A., Lill, R., Brandt, U., and Balk, J. (2008) The iron-sulphur protein Ind1 is required for effective complex I assembly. *EMBO J.* **27**, 1736-1746

47. Bych, K., Netz, D. J., Vigani, G., Bill, E., Lill, R., Pierik, A. J., and Balk, J. (2008) The essential cytosolic iron-sulfur protein Nbp35 acts without Cfd1 partner in the green lineage. *J. Biol. Chem.* **283**, 35797-35804

48. Roy, A., Solodovnikova, N., Nicholson, T., Antholine, W., and Walden, W. E. (2003) A novel eukaryotic factor for cytosolic Fe-S cluster assembly. *EMBO J.* **22**, 4826-4835

49. Stehling, O., Jeoung, J. H., Freibert, S. A., Paul, V. D., Banfer, S., Niggemeyer, B., Rosser, R., Dobbek, H., and Lill, R. (2018) Function and crystal structure of the dimeric P-loop ATPase CFD1 coordinating an exposed [4Fe-4S] cluster for transfer to apoproteins. *Proc. Natl. Acad. Sci. U. S. A.* **115**, 9085-9094

50. Tsaousis, A. D., Gentekaki, E., Eme, L., Gaston, D., and Roger, A. J. (2014) Evolution of the cytosolic iron-sulfur cluster assembly machinery in Blastocystis species and other microbial eukaryotes. *Eukaryot Cell* **13**, 143-153

51. Netz, D. J., Pierik, A. J., Stumpfig, M., Mühlenhoff, U., and Lill, R. (2007) The Cfd1-Nbp35 complex acts as a scaffold for iron-sulfur protein assembly in the yeast cytosol. *Nat. Chem. Biol.* **3**, 278-286

52. Hausmann, A., Aguilar Netz, D. J., Balk, J., Pierik, A. J., Mühlenhoff, U., and Lill, R. (2005) The eukaryotic P loop NTPase Nbp35: An essential component of the cytosolic

and nuclear iron-sulfur protein assembly machinery. *Proc. Natl. Acad. Sci. U. S. A.* **102**, 3266-3271

53. Lezhneva, L., Amann, K., and Meurer, J. (2004) The universally conserved HCF101 protein is involved in assembly of [4Fe-4S]-cluster-containing complexes in *Arabidopsis thaliana* chloroplasts. *Plant J.* **37**, 174-185

54. Stockel, J., and Oelmuller, R. (2004) A novel protein for photosystem I biogenesis. *J. Biol. Chem.* **279**, 10243-10251

55. Leon, S., Touraine, B., Ribot, C., Briat, J. F., and Lobreaux, S. (2003) Iron-sulphur cluster assembly in plants: distinct NFU proteins in mitochondria and plastids from *Arabidopsis thaliana*. *Biochem. J.* **371**, 823-830

56. Yabe, T., Morimoto, K., Kikuchi, S., Nishio, K., Terashima, I., and Nakai, M. (2004) The *Arabidopsis* chloroplastic NifU-like protein CnfU, which can act as an iron-sulfur cluster scaffold protein, is required for biogenesis of ferredoxin and photosystem I. *Plant Cell* **16**, 993-1007

57. Gao, H., Subramanian, S., Couturier, J., Naik, S. G., Kim, S. K., Leustek, T., Knaff, D. B., Wu, H. C., Vignols, F., Huynh, B. H., Rouhier, N., and Johnson, M. K. (2013) *Arabidopsis thaliana* Nfu2 accommodates [2Fe-2S] or [4Fe-4S] clusters and is competent for *in vitro* maturation of chloroplast [2Fe-2S] and [4Fe-4S] cluster-containing proteins. *Biochemistry* **52**, 6633-6645

58. Roland, M., Przybyla-Toscano, J., Vignols, F., Berger, N., Azam, T., Christ, L., Santoni, V., Wu, H. C., Dhalleine, T., Johnson, M. K., Dubos, C., Couturier, J., and Rouhier, N. (2020) The plastidial *Arabidopsis thaliana* NFU1 protein binds and delivers [4Fe-4S] clusters to specific client proteins. *J. Biol. Chem.* **295**, 1727-1742

59. Py, B., Gerez, C., Angelini, S., Planel, R., Vinella, D., Loiseau, L., Talla, E., Brochier-Armanet, C., Garcia Serres, R., Latour, J. M., Ollagnier-de Choudens, S., Fontecave, M., and Barras, F. (2012) Molecular organization, biochemical function, cellular role and evolution of NfuA, an atypical Fe-S carrier. *Mol. Microbiol.* **86**, 155-171

60. Navarro-Sastre, A., Tort, F., Stehling, O., Uzarska, M. A., Arranz, J. A., Del Toro, M., Labayru, M. T., Landa, J., Font, A., Garcia-Villoria, J., Merinero, B., Ugarte, M., Gutierrez-Solana, L. G., Campistol, J., Garcia-Cazorla, A., Vaquerizo, J., Riudor, E., Briones, P., Elpeleg, O., Ribes, A., and Lill, R. (2011) A fatal mitochondrial disease is associated with defective NFU1 function in the maturation of a subset of mitochondrial Fe-S proteins. *Am. J. Hum. Genet.* **89**, 656-667

61. Bandyopadhyay, S., Naik, S. G., O'Carroll, I. P., Huynh, B. H., Dean, D. R., Johnson, M. K., and Dos Santos, P. C. (2008) A proposed role for the *Azotobacter vinelandii* NfuA protein as an intermediate iron-sulfur cluster carrier. *J. Biol. Chem.* **283**, 14092-14099

62. Angelini, S., Gerez, C., Ollagnier-de Choudens, S., Sanakis, Y., Fontecave, M., Barras, F., and Py, B. (2008) NfuA, a new factor required for maturing Fe/S proteins in *Escherichia coli* under oxidative stress and iron starvation conditions. *J. Biol. Chem.* **283**, 14084-14091

63. Melber, A., Na, U., Vashisht, A., Weiler, B. D., Lill, R., Wohlschlegel, J. A., and Winge, D. R. (2016) Role of Nfu1 and Bol3 in iron-sulfur cluster transfer to mitochondrial clients. *eLife* **5**, e15991

64. Nath, K., Wessendorf, R. L., and Lu, Y. (2016) A nitrogen-fixing subunit essential for accumulating 4Fe-4S-containing photosystem I core proteins. *Plant Physiol.* **172**, 2459-2470

65. Nath, K., O'Donnell, J. P., and Lu, Y. (2017) Chloroplastic iron-sulfur scaffold protein NFU3 is essential to overall plant fitness. *Plant Signal Behav* **12**, e1282023

66. Nishio, K., and Nakai, M. (2000) Transfer of iron-sulfur cluster from NifU to apoferredoxin. *J. Biol. Chem.* **275**, 22615-22618

67. Gao, H., Azam, T., Randeniya, S., Couturier, J., Rouhier, N., and Johnson, M. K. (2018) Function and maturation of the Fe-S center in dihydroxyacid dehydratase from *Arabidopsis*. *J. Biol. Chem.* **293**, 4422-4433

68. Touraine, B., Vignols, F., Przybyla-Toscano, J., Ischebeck, T., Dhalleine, T., Wu, H. C., Magno, C., Berger, N., Couturier, J., Dubos, C., Feussner, I., Caffarri, S., Havaux, M., Rouhier, N., and Gaymard, F. (2019) Iron-sulfur protein NFU2 is required for branched-chain amino acid synthesis in *Arabidopsis* roots. *J Exp Bot* **70**, 1875-1889

69. Touraine, B., Boutin, J. P., Marion-Poll, A., Briat, J. F., Peltier, G., and Lobreaux, S. (2004) Nfu2: A scaffold protein required for [4Fe-4S] and ferredoxin iron-sulphur cluster assembly in *Arabidopsis* chloroplasts. *Plant J.* **40**, 101-111

70. Bentrop, D., Bertini, I., Luchinat, C., Nitschke, W., and Mühlenhoff, U. (1997) Characterization of the unbound 2[Fe_4S_4]-ferredoxin-like photosystem I subunit PsaC from the cyanobacterium *Synechococcus elongatus*. *Biochemistry* **36**, 13629-13637

71. Brown, R. E., Jarvis, K. L., and Hyland, K. J. (1989) Protein measurement using bicinchoninic acid: elimination of interfering substances. *Anal. Biochem.* **180**, 136-139

72. Fish, W. W. (1988) Rapid colorimetric micromethod for the quantitation of complexed iron in biological samples. in *Methods Enzymol.*, Academic Press. pp 357-364

73. Zhang, B., Bandyopadhyay, S., Shakamuri, P., Naik, S. G., Huynh, B. H., Couturier, J., Rouhier, N., and Johnson, M. K. (2013) Monothiol glutaredoxins can bind linear [Fe_3S_4]$^+$

and $[Fe_4S_4]^{2+}$ clusters in addition to $[Fe_2S_2]^{2+}$ clusters: Spectroscopic characterization and functional implications. *J. Am. Chem. Soc.* **135**, 15153-15164

74. Kennedy, M. C., Kent, T. A., Emptage, M., Merkle, H., Beinert, H., and Münck, E. (1984) Evidence for the formation of a linear [3Fe-4S] cluster in partially unfolded aconitase. *J. Biol. Chem.* **259**, 14463-14471

75. Kittlesen, G. P., White, H. S., and Wrighton, M. S. (1984) Chemical derivatization of microelectrode arrays by oxidation of pyrrole and N-methylpyrrole: Fabrication of molecule-based electronic devices. *J. Am. Chem. Soc.* **106**, 7389-7396

76. Richards, A. J. M., Thomson, A. J., Holm, R. H., and Hagen, K. S. (1990) The magnetic circular dichroism spectra of the linear trinuclear clusters $[Fe_3S_4(SR)_4]^{3-}$ in purple aconitase and in a synthetic model. *Spectrochim Acta Part A: Molecular Spectroscopy* **46**, 987-993

77. Johnson, M. K., Duderstadt, R. E., and Duin, E. C. (1999) Biological and Synthetic $[Fe_3S_4]$ Clusters. in *Adv. Inorg. Chem.* (Sykes, A. G. ed.), Academic Press. pp 1-82

78. Brereton, P. S., Duderstadt, R. E., Staples, C. R., Johnson, M. K., and Adams, M. W. (1999) Effect of serinate ligation at each of the iron sites of the $[Fe_4S_4]$ cluster of *Pyrococcus furiosu*s ferredoxin on the redox, spectroscopic, and biological properties. *Biochemistry* **38**, 10594-10605

79. Kennedy, M. C., Kent, T. A., Emptage, M., Merkle, H., Beinert, H., and Munck, E. (1984) Evidence for the formation of a linear [3Fe-4S] cluster in partially unfolded aconitase. *J. Biol. Chem.* **259**, 14463-14471

80. Hagen, K. S., Watson, A. D., and Holm, R. H. (1983) Synthetic routes to iron sulfide (Fe_2S_2, Fe_3S_4, Fe_4S_4, and Fe_6S_9), clusters from the common precursor

tetrakis(ethanethiolate)ferrate(2-) ion ($[Fe(SC_2H_5)_4]^{2-}$): Structures and properties of $[Fe_3S_4(SR)_4]^{3-}$ and bis(ethanethiolate)nonathioxohexaferrate(4-) ion ($[Fe_6S_9(SC_2H_5)_2]^{4-}$), examples of the newest types of Fe-S-SR clusters. *J. Am. Chem. Soc.* **105**, 3905-3913

81. Armengaud, J., Gaillard, J., Forest, E., and Jouanneau, Y. (2008) Characterization of a 2[4Fe-4S] ferredoxin obtained by chemical insertion of the Fe-S clusters into the apoferredoxin II from *Rhodobacter Capsulatus*. *Eur J Biochem* **231**, 396-404

82. Griffin, S., Higgins, C. L., Soulimane, T., and Wittung-Stafshede, P. (2003) High thermal and chemical stability of *Thermus thermophilus* seven-iron ferredoxin. Linear clusters form at high pH on polypeptide unfolding. *Eur. J. Biochem.* **270**, 4736-4743

83. Leal, S. S., Teixeira, M., and Gomes, C. M. (2004) Studies on the degradation pathway of iron-sulfur centers during unfolding of a hyperstable ferredoxin: cluster dissociation, iron release and protein stability. *J. Biol. Inorg. Chem.* **9**, 987-996

84. Jones, K., Gomes, C. M., Huber, H., Teixeira, M., and Wittung-Stafshede, P. (2002) Formation of a linear [3Fe-4S] cluster in a seven-iron ferredoxin triggered by polypeptide unfolding. *J. Biol. Inorg. Chem.* **7**, 357-362

85. Higgins, C. L., and Wittung-Stafshede, P. (2004) Formation of linear three-iron clusters in *Aquifex aeolicus* two-iron ferredoxins: Effect of protein-unfolding speed. *Arch. Biochem. Biophys.* **427**, 154-163

86. Krebs, C., Henshaw, T. F., Cheek, J., Huynh, B. H., and Broderick, J. B. (2000) Conversion of 3Fe-4S to 4Fe-4S clusters in native pyruvate formate-lyase activating enzyme: Mössbauer characterization and implications for mechanism. *J. Am. Chem. Soc.* **122**, 12497-12506

Table 3.1: Plastidial proteins from *Arabidopsis thaliana* and their bacterial relatives

Plant protein names	**Bacterial relative**	**Function**
NFS2	SufS	Cysteine desulfurase. Sulfur donor for cluster assembly
SUFE1 SUFE2 SUFE3	SufE	Sulfurtransferase activator for cysteine desulfurase
SUFB SUFC SUFD	SufB SufC SufD	$SUFBC_2D$ scaffold complex for cluster assembly
SUFA1	SufA	Fe-S cluster trafficking and [4Fe-4S] cluster assembly
NFU1 NFU2 NFU3	NfuA	Fe-S cluster delivery to client proteins
HCF101	Mrp	Fe-S cluster delivery to client proteins
IBA57.2	Ygfz	Binding ATC proteins to a facilitate cluster transfer
GRXS14 GRXS16	Grx4	Fe-S cluster trafficking

Figure 3.1. Schematic alignment of cysteine residues in class I (plastidial *At* HCF101), class II (mitochondrial *At* Ind1), class III (cytosolic *Sc* Nbp35), class IV (cytosolic *Sc* Cfd1), members of the FSC-NTPase superfamily. Conserved cluster-binding CXXC residues are present in At Ind1, Sc Nbp35, Cfd1 but not in HCF101. TPc and TPm represents chloroplast and mitochondrial transit peptides respectively. *At*, *Arabidopsis thaliana*; *Sc*, *Saccharomyces cerevisiae*. Adapted from reference (42)

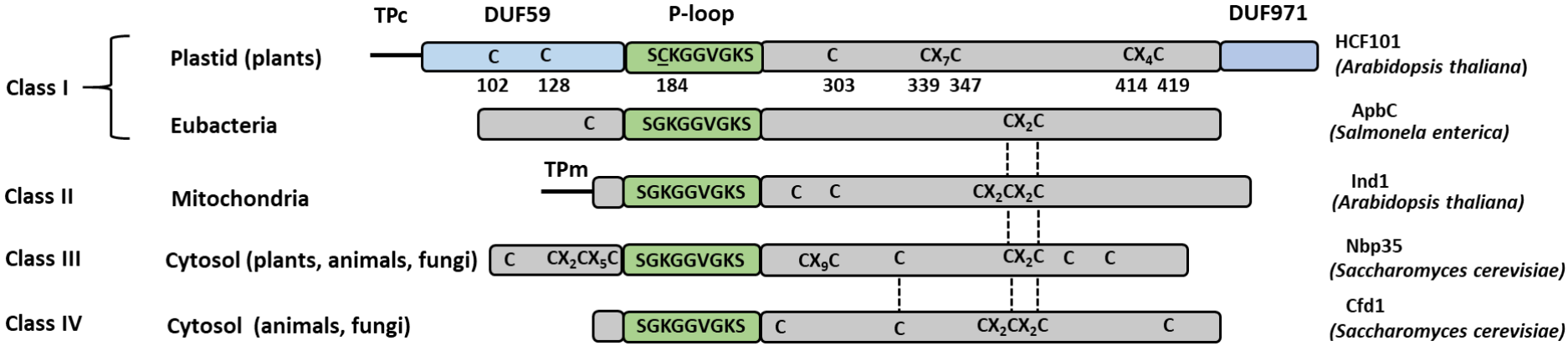
TPc
DUF59
P-loop
DUF971
Class I
Plastid (plants)
C C
SCKGGVGKS
C
CX7C
CX4C
102 128
184
303
339 347
414 419
HCF101
(Arabidopsis thaliana)
Eubacteria
C
SGKGGVGKS
CX2C
ApbC
(Salmonela enterica)
TPm
Class II
Mitochondria
SGKGGVGKS
C C
CX2CX2C
Ind1
(Arabidopsis thaliana)
Class III
Cytosol (plants, animals, fungi)
C CX2CX5C
SGKGGVGKS
CX9C
C
CX2C C C
Nbp35
(Saccharomyces cerevisiae)
Class IV
Cytosol (animals, fungi)
SGKGGVGKS
C
C
CX2CX2C
C
Cfd1
(Saccharomyces cerevisiae)

Figure 3.2. Room temperature UV-visible absorption and CD spectra of as isolated *At* HCF101 (black lines) and $[4Fe\text{-}4S]^{2+}$ cluster-bound reconstituted *At* HCF101 (blue lines). All ε and Δε values are expressed per HCF101 monomer.

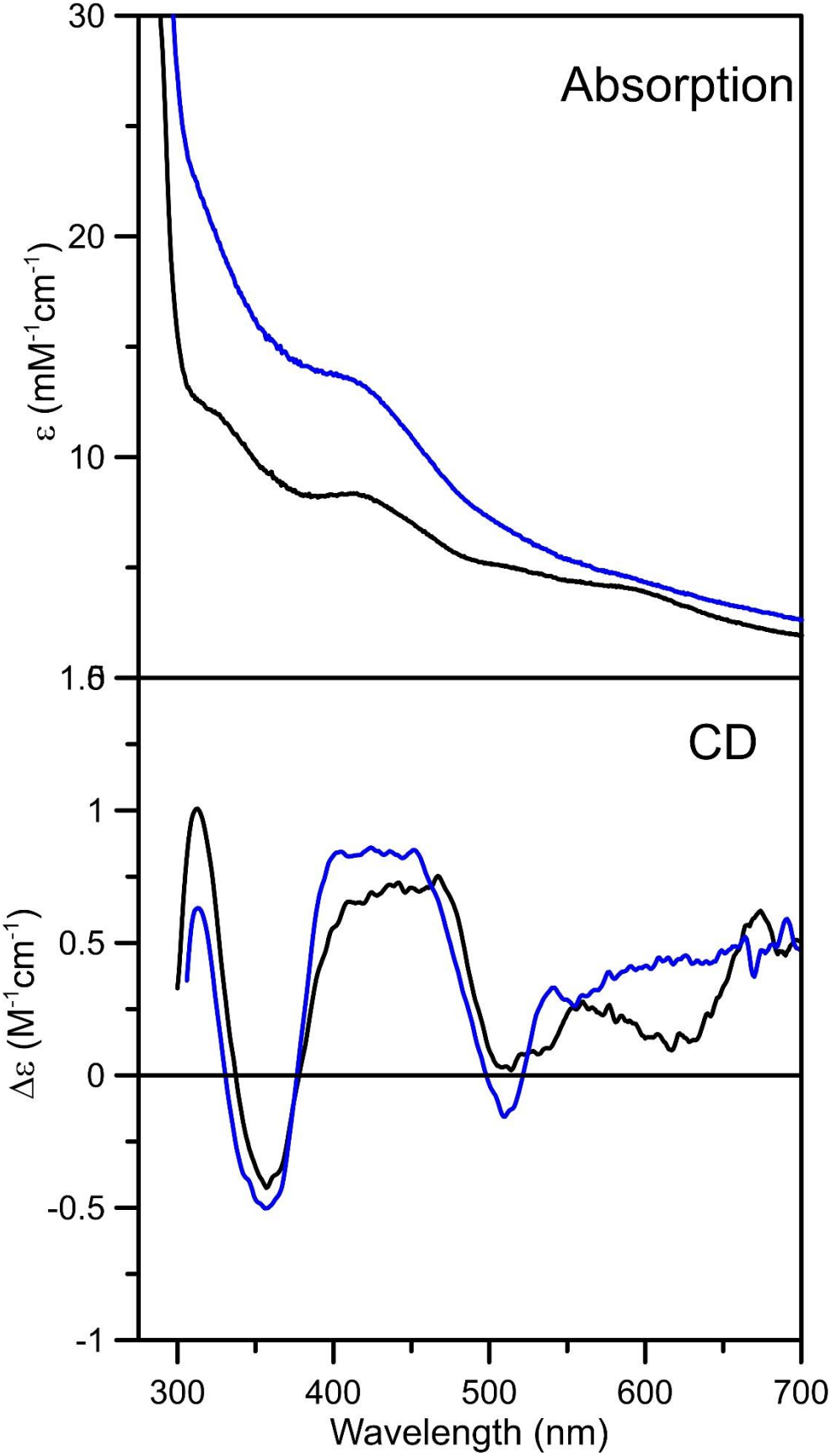
Absorption
ε (mM-1cm-1)
30
20
10
1.0
CD
Δε (M-1cm-1)
1
0.5
0
-0.5
-1
300
400
500
600
700
Wavelength (nm)

Figure 3.3. X-band EPR spectra of as purified HCF101 (A) and the final product of the cluster transfer reaction from [4Fe-4S]-NFU2 to apo HCF101 (B). The spectra were recorded at 10 K with a microwave frequency of 9.582 GHz, modulation amplitude of 6.477 G with microwave power of 10 mW.

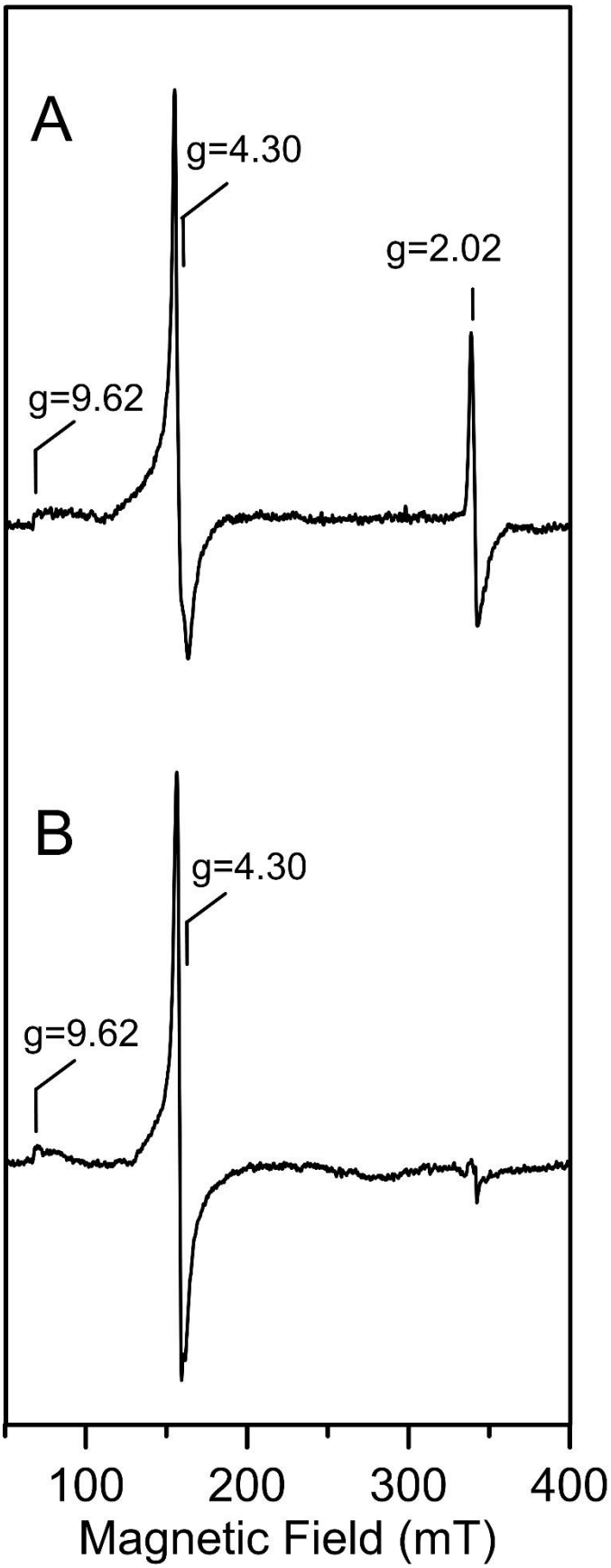
A
g=4.30
g=2.02
g=9.62
B
g=4.30
g=9.62
100
200
300
400
Magnetic Field (mT)

Figure 3.4. X-band EPR spectrum of dithionite-reduced reconstituted HCF101. The spectrum was recorded at 10 K with a microwave frequency of 9.582 GHz, modulation amplitude of 0.648 mT and microwave power of 4 mW.

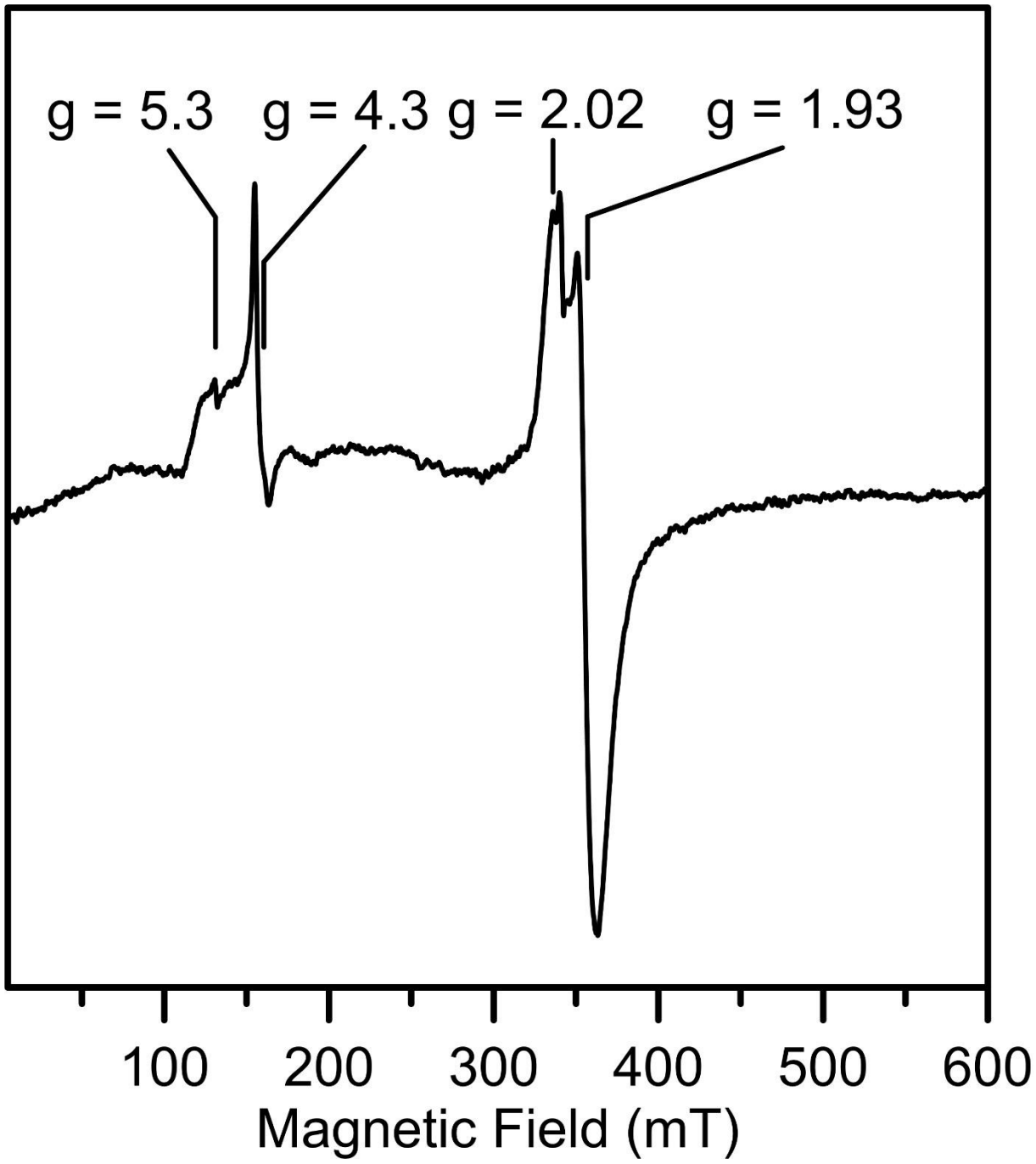
g = 5.3
g = 4.3
g = 2.02
g = 1.93
100
200
300
400
500
600
Magnetic Field (mT)

Figure 3.5. Resonance Raman spectra of reconstituted *At* HCF101 using 457.9-nm laser excitation. The sample (~2 mM in $[4Fe\text{-}4S]^{2+}$ clusters) was in 100 mM Tris-HCl buffer at pH 7.8 and was in the form of a frozen droplet at 17 K. The spectrum is the sum of 120 individual scans with each scan involving photon counting for 1 s at 0.5 cm^{-1} increment with 7 cm^{-1} spectral resolution. Bands due to lattice modes of ice have been subtracted.

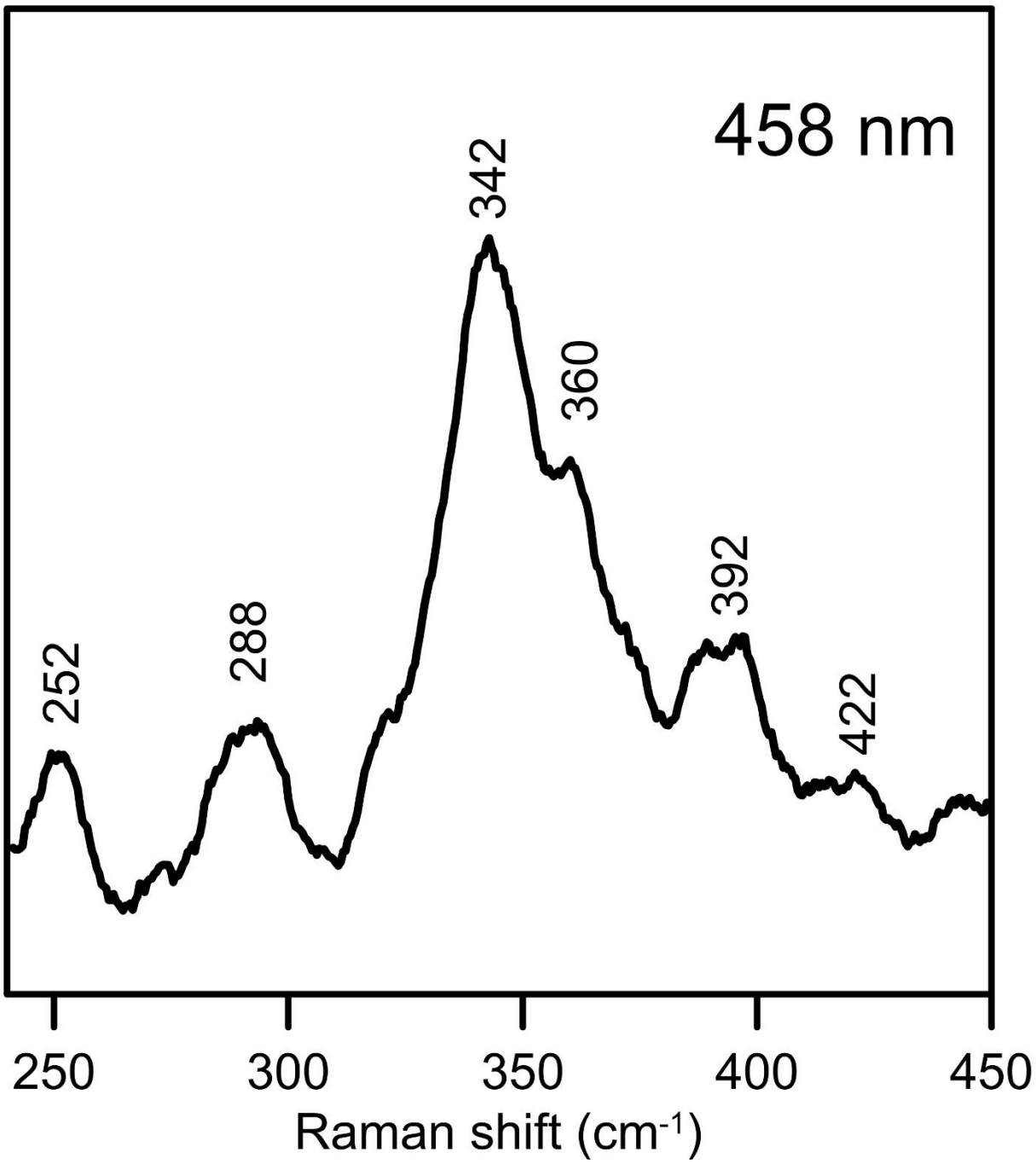
458 nm
342
360
392
422
288
252
250
300
350
400
450
Raman shift (cm-1)

Figure 3.6. (A) Room temperature UV-visible absorption spectra of as purified HCF101 (black line) and repurified HCF101 (red line) after anaerobic incubation with excess FAS. All ε values were calculated based on the protein concentrations. (B) UV-visible absorption spectra of reconstituted [4Fe-4S] cluster-bound *At* HCF101 before (thick blue line) and after exposing to O_2 for 300 min. Spectra recorded after 1, 7, 22, 33, 50, 60, and 205 min are shown as thin grey lines and the final spectra after 300 min is shown as a thick black thick line. All ε values were calculated based on the concentrations of $[4Fe\text{-}4S]^{2+}$ cluster in the sample before it was exposed to O_2.

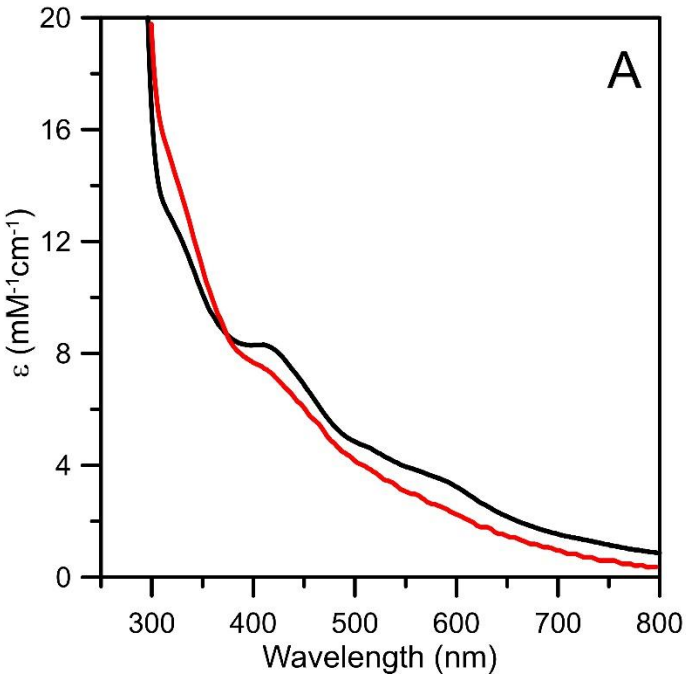
A
ε (mM-1cm-1)
Wavelength (nm)
0
4
8
12
16
20
300
400
500
600
700
800

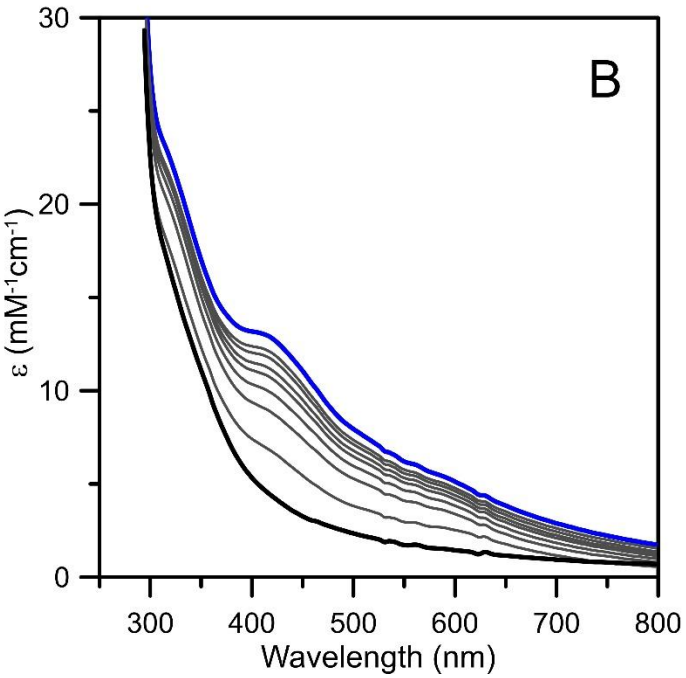
B
ε (mM-1cm-1)
Wavelength (nm)
0
10
20
30
300
400
500
600
700
800

Figure 3.7. Room temperature UV-visible absorption and CD spectra of reconstituted *Syn* PsaC. All ε and Δε values were calculated based on the cluster concentrations. The *inset* shows the X-band EPR spectrum of dithionite-reduced reconstituted *Syn* PsaC at pH 10. The sample was reduced under anaerobic conditions by the addition of 5 mM sodium dithionite and frozen immediately in liquid nitrogen. The spectrum was recorded at 10 K with a microwave frequency of 9.60 GHz, modulation amplitude of 0.63 mT and microwave power of 4 mW.

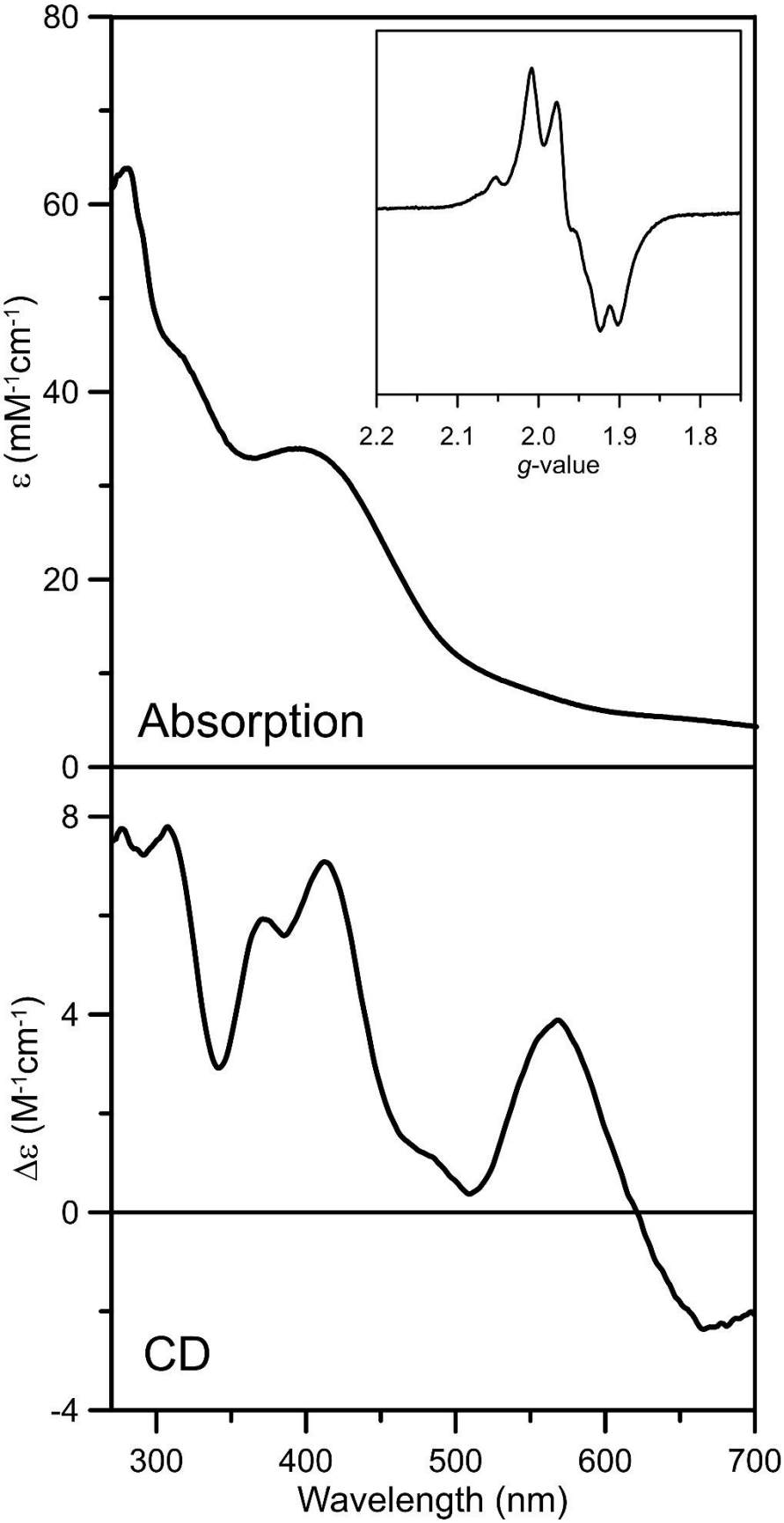
80
60
40
20
0
ε (mM-1cm-1)
Absorption
2.2
2.1
2.0
1.9
1.8
g-value
8
4
0
-4
Δε (M-1cm-1)
CD
300
400
500
600
700
Wavelength (nm)

Figure 3.8. Cluster transfer from *A. thaliana* [4Fe-4S]-NFU2 to apo HCF101 monitored by CD (A) and UV-vis absorption (B) spectroscopy as a function of time. CD spectra of the cluster transfer reaction mixture that was initially 70 µM in NFU2 [4Fe-4S] clusters and 140 µM in apo HCF101. The cluster transfer reaction was carried out under anaerobic conditions at room temperature in 100 mM Tris-HCl buffer at pH 7.8. The thick red lines correspond to [4Fe-4S]-NFU2 recorded before addition of apo HCF101 and the thick blue lines corresponds to the final product of the cluster transfer from NFU2 to HCF101 after 70 min. (A) Thin grey lines correspond to the CD spectra recorded at 3, 9, 12, 20, 27, 32, 38 and 56 min after the addition of apo HCF101. (B) Thin grey lines correspond to the UV spectra recorded at 7, 17, 25, 36, 44, 54 and 65 min after the addition of apo HCF101. The arrows indicate the direction of intensity change with increasing amount of time at selected wavelengths. All ε and $\Delta\varepsilon$ values are based on the concentrations of [4Fe-4S] clusters on NFU2.

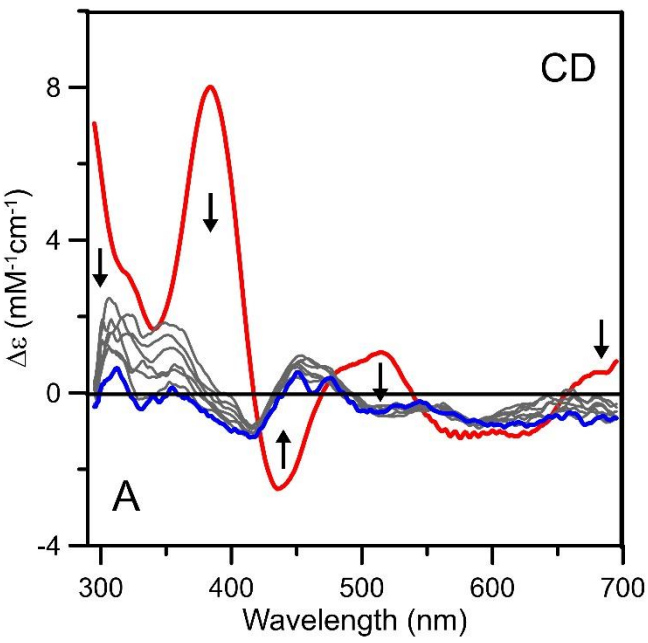
CD
A
Δε (mM-1cm-1)
Wavelength (nm)
8
4
0
-4
300
400
500
600
700

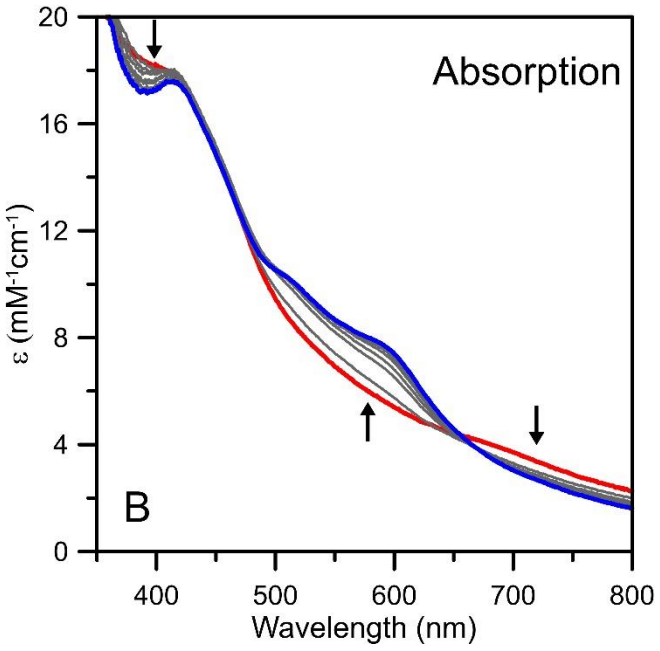
Absorption
B
ε (mM-1cm-1)
Wavelength (nm)
20
16
12
8
4
0
400
500
600
700
800

Figure 3.9: Attempted cluster transfer from *A. thaliana* [4Fe-4S]-NFU2 to apo PsaC monitored by CD spectroscopy as a function of time. CD spectra of the cluster transfer reaction mixture that was initially 70 µM in NFU2 [4Fe-4S] clusters and 40 µM in apo PsaC. The cluster transfer reaction was carried out under anaerobic conditions at room temperature in 100 mM Tris-HCl buffer at pH 7.8 with 1 M urea (required to keep PsaC in solution). The thick red line corresponds to [4Fe-4S]-NFU2 recorded before addition of apo PsaC and thin grey lines correspond to CD spectra recorded at 1, 4, 7, 10, 13, 21, 24 and 34 min after the addition of apo PsaC. Thick blue line corresponds to the final product of the cluster transfer from NFU2 to PsaC. The arrows indicate the direction of intensity change with increasing amount of time at selected wavelengths. The cluster transfer reaction was carried out under anaerobic conditions at room temperature in 50 mM Tris-HCl buffer at pH 8.

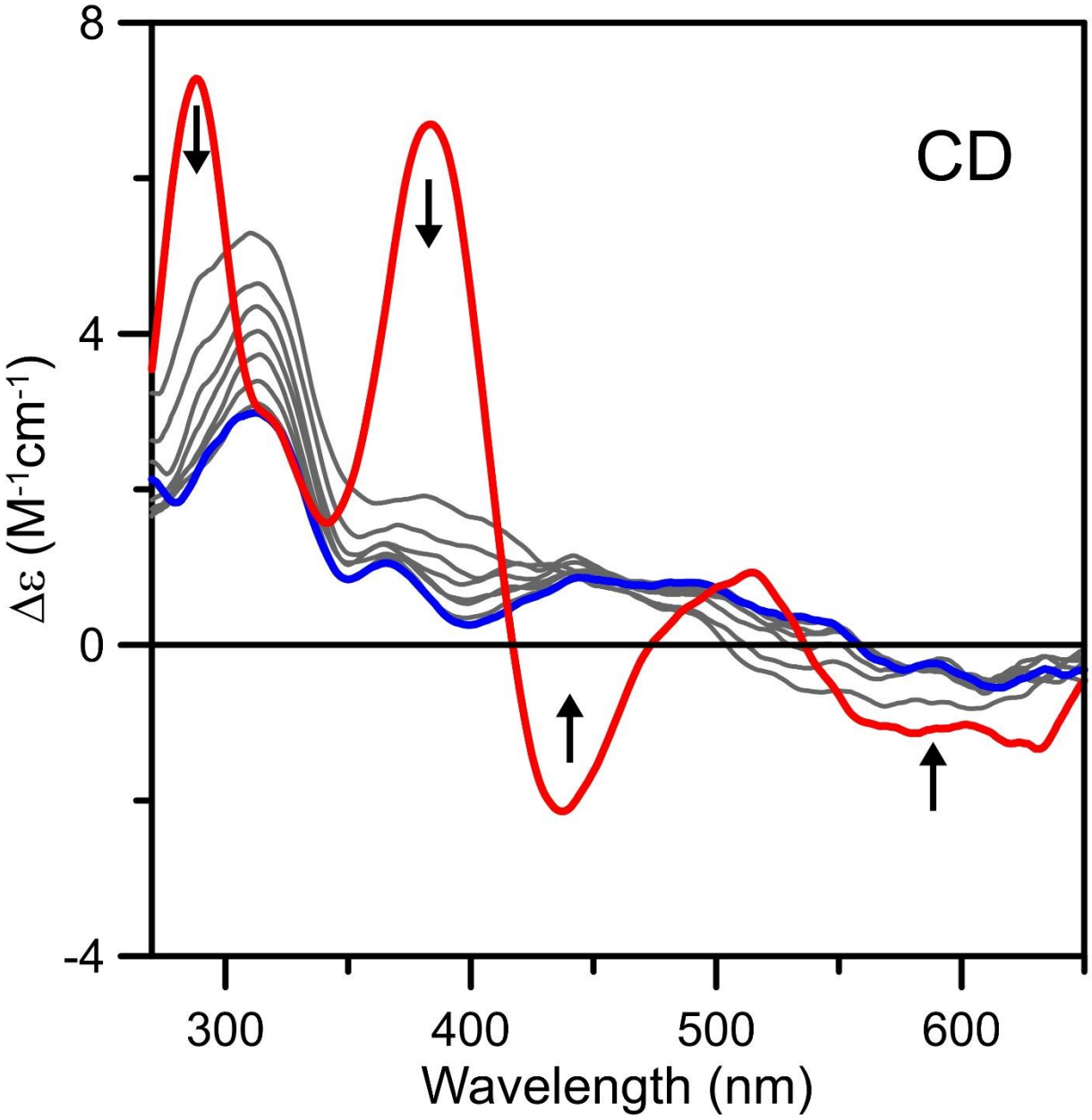
CD
8
4
0
-4
Δε (M-1cm-1)
300
400
500
600
Wavelength (nm)

CHAPTER 4

CONCLUSIONS AND FUTURE STUDIES

The overall objectives of this research project were to provide new insights into the function and properties of late-acting mitochondrial Fe-S cluster carrier proteins from *Arabidopsis thaliana* (*At*), GRXS15, ISCA1a/2 and NFU4/5 and to understand the potential roles of plastidial proteins, HCF101 and NFU2 in the maturation of plant Fe-S proteins.

Based on yeast and human studies, a basic model of the mitochondrial ISC machinery has been proposed in the literature, but uncertainties concerning the mechanistic pathways of late-acting steps still persist. The molecular mechanism of $[4Fe\text{-}4S]^{2+}$ cluster assembly and insertion into target proteins by late-acting mitochondrial Fe-S cluster assembly proteins is not well understood. Moreover, the proteins involved with late-acting plant mitochondrial ISC machinery have yet to be purified and characterized *in vitro*. In order to understand the late steps of mitochondrial Fe-S machinery in *Arabidopsis thaliana,* we studied three classes of recombinant proteins namely GRXS15, ISCA-type, and NFU-type proteins. *Arabidopsis* has four ATC proteins: SUFA1 is localized in plastids (1), while the other three are predicted to be present in mitochondria. Three mitochondrial ATC proteins, i.e., ISCA1a, ISCA1b, and ISCA2 are present in *At*, but they have yet to be investigated *in vitro*. These three are named based on their homologs in eukaryotic model organisms(2). For example, *At* ISCA1a and *At* ISCA1b are grouped with yeast Isa1 and human ISCA1 (3), and *At* ISCA2 is grouped with yeast Isa2 and human ISCA2. Chapter 2 presents the spectroscopic characterization of co-expressed ISCA1a/2 and their involvement in the maturation of [4Fe-4S] clusters in mitochondria. There are five NFU-type proteins in

Arabidopsis, and based on their localization, they are divided into two classes (4). NFU1-3 are located in plastids and share a similar sequence identity with cyanobacterial *Sy* Nfu. NFU4 and NFU5 are predicted to be in mitochondria and have a similar sequence and structural organization to *Hs* NFU1 and *Sc* Nfu1 (4). All Nfu-type proteins have a conserved CXXC motif; however, NFU4 and NFU5 have a unique N-terminal domain, which is specific to eukaryotic mitochondrial, cytosolic, and nuclear Nfu proteins (5). In this chapter, we also characterized the properties and coordination environment of the cluster assembled on NFU4 and NFU5 proteins. Protein heterologous expression, chromatography purification, protein/Fe determination, and different spectroscopic techniques-absorption, circular dichroism (CD), resonance Raman (RR), and electron paramagnetic resonance (EPR) have been employed to understand the electronic, vibrational, and magnetic properties of the clusters assembled on these proteins.

In vivo and *in vitro* studies have identified mitochondrial and bacterial monothiol glutaredoxins as primary or sole acceptors of $[2Fe\text{-}2S]^{2+}$ clusters assembled on U-type scaffold proteins (6-8). In accord with this hypothesis, *At* GRXS15 plays a central role in plant mitochondrial Fe-S cluster biogenesis and has recently been shown to be essential for plant growth (9). We have demonstrated that GRXS15 can assemble a $[2Fe\text{-}2S]^{2+}$ cluster and effective in [2Fe-2S] cluster trafficking and the maturation of [2Fe-2S] cluster-containing proteins.

In chapter 2, we presented a comprehensive investigation of the cluster bound forms of [ISCA1a.ISCA2] heterodimer complex using different spectroscopic techniques in combination with analytical studies. Co-expression of ISCA1a/2 resulted in samples with one $[2Fe\text{-}2S]^{2+}$ cluster per heterodimer, which can be converted to a form containing one $[4Fe\text{-}4S]^{2+}$ cluster per heterodimer by anaerobic Fe-S cluster reconstitution. Moreover, the $[4Fe\text{-}4S]^{2+}$ cluster-bound *At* ISCA1a/2 heterodimer was also formed via rapid $[2Fe\text{-}2S]^{2+}$ cluster transfer from *At* [2Fe-2S]-

GRXS15 to apo *At* ISCA1a/2, in the absence of exogenous GSH or DTT. Since GRXS15 cannot bind a $[4Fe\text{-}4S]^{2+}$ cluster, $[4Fe\text{-}4S]^{2+}$ cluster formation must involve the ISCA1a/2 heterodimer acting as a $[4Fe\text{-}4S]^{2+}$ cluster assembler complex. The observation that cluster transfer product is a 80:20 mixture of [4Fe-4S]-ISCA1a/2 and [2Fe-2S]-ISCA1a/2 heterodimers suggests that the first step involves intact $[2Fe\text{-}2S]^{2+}$ cluster transfer from GRXS15 to form a [2Fe-2S]-ISCA1a/2 heterodimer. The second step is likely to involve binding of [2Fe-2S]-GRXS15 to [2Fe-2S]-ISCA1a/2 resulting in two $[2Fe\text{-}2S]^{2+}$ clusters in close enough proximity for two-electron reductive coupling, mediated by disulfide formation involving released cysteine or GSH ligands. Two-electron reductive coupling of two $[2Fe\text{-}2S]^{2+}$ clusters to form a $[4Fe\text{-}4S]^{2+}$ has been well established and rationalized for bacterial ^{Nif}IscA and IscU proteins using DTT and dithionite, respectively as exogenous reducing agents (10,11). In addition, cluster transfer from human [2Fe-2S]-GRX5 to the apo human ISCA1/2 heterodimer also resulted in the formation of [4Fe-4S]-ISCA1/2 in the presence of excess DTT and/or GSH, as assessed by the combination NMR, MS and UV-visible absorption data (12). Hence, the results presented in this work add further support to the proposed role of ISCA1/2 heterodimers as effectors of $[2Fe\text{-}2S]^{2+}$ to $[4Fe\text{-}4S]^{2+}$ cluster conversions in mitochondrial Fe-S cluster biosynthesis.

ISC targeting factors (e.g., Nfu1, INDH, and Bol1/3) help to transfer the assembled clusters to target apo proteins (13). In yeast and human cells, the deletion of Nfu1 only partially affects aconitase, lipoic acid synthase, and succinate dehydrogenase activity, suggesting a non-essential role for Nfu1 as a $[4Fe\text{-}4S]^{2+}$ cluster targeting protein (14,15). NFU4 and NFU5 are predicted to be in mitochondria and have a similar sequence and structural organization to *Hs* NFU1 and *Sc* Nfu1 (4). NFU4 and NFU5 were both purified as apo proteins but assembled one $[4Fe\text{-}4S]^{2+}$ cluster per homodimer after cluster reconstitution. Cluster transfer studies also implicate [4Fe-4S]-

ISCA1a/2 as a viable and unidirectional donor for incorporating [4Fe-4S]$^{2+}$ clusters on NFU4 and NFU5. The *in vitro* cluster transfer results presented in this work suggest that [4Fe-4S]-ISCA1a/2 is competent for the rapid maturation of *At* ACO2 via intact cluster transfer even in the absence of IBA57.1. In addition, [4Fe-4S]-NFU4 and [4Fe-4S]-NFU5 are shown to be viable alternative [4Fe-4S]$^{2+}$ cluster donors for *At* ACO2, albeit with slightly lower rates of cluster transfer. This is consistent with the non-essential role of NFU1 in yeast and human mitochondria, as evidenced by partially defective Fe-S enzymes aconitase, and succinate dehydrogenase, in cells lacking NFU1 (14-16).

There are still some uncertainties concerning the late ISC machinery of plants which need to be addressed. For example, the role of mitochondrial *At* IBA57.1 in the late steps of mitochondrial ISC machinery is still unknown. Recently, there has been a debate about the molecular relationship between Iba57 and IscA proteins. *In vivo* and *in vitro* studies have shown that *Hs* ISCA2 reacts with *Hs* IBA57, but not with *Hs* ISCA1(17,18); whereas in yeast both ATC proteins interact with Iba57 (19). However, the deletion of IBA57, *Hs* ISCA1 (*Sc* Isa1), or *Hs* ISCA2 (*Sc* Isa2) from yeast and human cell lines causes defects in the assembly of the respiratory complex, the biosynthesis of lipoic acid, and the maturation of aconitase, homoaconitase, and glutamate synthase (19-22).Therefore, *At* IBA57.1 needs to be characterized and studied *in vitro* to understand the molecular picture on how the ISCA1, ISCA2, and IBA57.1 proteins cooperate in the mitochondrial ISC machinery. *In vivo*, yeast Nfu1 has been shown to be important for the maturation of mitochondrial lipoic acid synthase, an enzyme containing 2[4Fe-4S] clusters(23,24). As NFU4/5 can complement *Δnfu1* mutant and interact with physiological partners of Nfu1 (15,24,25), it would be very interesting to see if NFU4/5 could incorporate 2[4Fe-4S] cluster on lipoic acid synthase *in vitro*.

Chapter 3 focused on investigating cluster transfer interactions involving NFU2, HCF101, and PSAC, the 8Fe ferredoxin-like subunit in PS1 that functions as the terminal electron acceptor and electron donor for the mobile plant 2Fe ferredoxin. Our working model for the SUF machinery in plastids is that NFU2 accepts clusters from the $SUFBC_2D$ scaffold complex and then delivers them to HCF101 for the maturation of the three [4Fe-4S] clusters in PS1. The observation that *Δnfu2*, *Δnfu3,* and *Δhcf101* mutants in *At* have impaired photosystems provides strong evidence for the involvement of their gene products in the maturation of [4Fe-4S] proteins of PSI (26). The *in vitro* spectroscopic and analytical studies of HCF101 performed in this work are generally in agreement with the previous studies and extend these studies by incorporating RR and UV-visible CD studies and demonstrating that HCF101 can also accommodate linear $[3Fe\text{-}4S]^{1+}$ clusters. The cluster transfer studies presented herein were only partially successful. Monitoring the time course of [4Fe-4S] cluster transfer from NFU2 to apo HCF101 revealed a rapid and unidirectional reaction in accord with HCF101 acting downstream of NFU2. However, the reaction appears to proceed via a semi-stable $[4Fe\text{-}4S]^{2+}$ NFU2-HCF101 complex that slowly degrades to yield a predominantly linear $[3Fe\text{-}4S]^{1+}$ cluster-bound form of HCF101. Taken together, these results suggest that HCF101 may assemble $[4Fe\text{-}4S]^{2+}$ clusters by scavenging linear $[3Fe\text{-}4S]^{1+}$ clusters formed by protein Fe-S protein denaturation in the O_2-rich environment of the chloroplast and using pools of Fe^{2+} ions to complete $[4Fe\text{-}4S]^{2+}$ clusters assembly *in situ.*

[4Fe-4S] cluster transfer from NFU2 to apo PsaC appears to a very rapid reaction based on complete loss of the intense CD bands associated with [4Fe-4S]-NFU2 within 1 min of initiating the reaction by mixing [4Fe-4S]-NFU2 with apo PsaC. The resulting CD spectrum after 1 min is generally similar to that of holo PsaC, but less than half the intensity. Moreover, the intensity declines further, coupled with additional changes in CD for the next 30 min, suggesting gradual

degradation of the clusters due the presence of 1 M urea. These qualitative results indicate that [4Fe-4S]-NFU2 has the potential to be a competent [4Fe-4S] donor for PsaC. To understand the roles of NFU2, NFU3 and HCF101 for the maturation of [4Fe-4S] cluster containing photosystem I subunits, a stable form of $[4Fe\text{-}4S]^{2+}$ cluster-bound NFU3 needs to be characterized and studied. Considering both the *Δnfu2* and *Δnfu3* mutants show impaired PSI development, the cluster transfer from both NFU2 and NFU3 to PsaC needs to be studied. However, it is not possible to rule out other scenarios, such as [4Fe-4S]-HCF101 being the preferred donor or that both NFU2 and HCF101 bind and transfer clusters to apo PsaC. This appears to be the first attempt to assemble two clusters on one protein via intact cluster transfer and it possible that molecular chaperones are required to achieve the optimal conformational for cluster transfer or that binding of the apo protein to the PsaAB dimer is required to stabilize protein structure prior to intact cluster transfer. Clearly there is much to be learned about the assembly of multiple clusters in a single polypeptide.

Abbreviations:

Fe-S clusters, iron-sulfur clusters; *At*, *Arabidopsis thaliana*; PSI; photosystem I, ferredoxin; FDX, CD, circular dichroism; RR, resonance Raman; EPR, electron paramagnetic resonance; DTT, dithiothreitol.

References

1. Abdel-Ghany, S. E., Ye, H., Garifullina, G. F., Zhang, L., Pilon-Smits, E. A., and Pilon, M. (2005) Iron-sulfur cluster biogenesis in chloroplasts. Involvement of the scaffold protein CpIscA. *Plant Physiol* **138**, 161-172
2. Vinella, D., Brochier-Armanet, C., Loiseau, L., Talla, E., and Barras, F. (2009) Iron-sulfur (Fe/S) protein biogenesis: Phylogenomic and genetic studies of A-type carriers. *PLoS Genet* **5**, e1000497
3. Uzarska, M. A., Przybyla-Toscano, J., Spantgar, F., Zannini, F., Lill, R., Mühlenhoff, U., and Rouhier, N. (2018) Conserved functions of *Arabidopsis* mitochondrial late-acting maturation factors in the trafficking of iron-sulfur clusters. *Biochimica et biophysica acta* **1865**, 1250-1259
4. Leon, S., Touraine, B., Ribot, C., Briat, J. F., and Lobreaux, S. (2003) Iron-sulphur cluster assembly in plants: distinct NFU proteins in mitochondria and plastids from *Arabidopsis thaliana*. *Biochem J* **371**, 823-830
5. Cai, K., Liu, G., Frederick, R. O., Xiao, R., Montelione, G. T., and Markley, J. L. (2016) Structural/functional properties of human NFU1, an intermediate [4Fe-4S] carrier in human mitochondrial iron-sulfur cluster biogenesis. *Structure* **24**, 2080-2091
6. Shakamuri, P., Zhang, B., and Johnson, M. K. (2012) Monothiol glutaredoxins function in storing and transporting [Fe_2S_2] clusters assembled on IscU scaffold proteins. *J Am Chem Soc* **134**, 15213-15216

7. Uzarska, M. A., Dutkiewicz, R., Freibert, S. A., Lill, R., and Mühlenhoff, U. (2013) The mitochondrial Hsp70 chaperone Ssq1 facilitates Fe/S cluster transfer from Isu1 to Grx5 by complex formation. *Mol Biol Cell* **24**, 1830-1841

8. Mühlenhoff, U., Gerber, J., Richhardt, N., and Lill, R. (2003) Components involved in assembly and dislocation of iron-sulfur clusters on the scaffold protein Isu1p. *EMBO J* **22**, 4815-4825

9. Moseler, A., Aller, I., Wagner, S., Nietzel, T., Przybyla-Toscano, J., Mühlenhoff, U., Lill, R., Berndt, C., Rouhier, N., Schwarzlander, M., and Meyer, A. J. (2015) The mitochondrial monothiol glutaredoxin S15 is essential for iron-sulfur protein maturation in *Arabidopsis thaliana*. *Proc Natl Acad Sci U S A* **112**, 13735-13740

10. Mapolelo, D. T., Zhang, B., Naik, S. G., Huynh, B. H., and Johnson, M. K. (2012) Spectroscopic and functional characterization of iron-sulfur cluster-bound forms of *Azotobacter vinelandii* ^{Nif}IscA. *Biochemistry* **51**, 8071-8084

11. Chandramouli, K., Unciuleac, M. C., Naik, S., Dean, D. R., Huynh, B. H., and Johnson, M. K. (2007) Formation and properties of [4Fe-4S] clusters on the IscU scaffold protein. *Biochemistry* **46**, 6804-6811

12. Brancaccio, D., Gallo, A., Mikolajczyk, M., Zovo, K., Palumaa, P., Novellino, E., Piccioli, M., Ciofi-Baffoni, S., and Banci, L. (2014) Formation of [4Fe-4S] clusters in the mitochondrial iron-sulfur cluster assembly machinery. *J Am Chem Soc* **136**, 16240-16250

13. Sheftel, A. D., Stehling, O., Pierik, A. J., Netz, D. J., Kerscher, S., Elsasser, H. P., Wittig, I., Balk, J., Brandt, U., and Lill, R. (2009) Human ind1, an iron-sulfur cluster assembly factor for respiratory complex I. *Mol Cell Biol* **29**, 6059-6073

14. Navarro-Sastre, A., Tort, F., Stehling, O., Uzarska, M. A., Arranz, J. A., Del Toro, M., Labayru, M. T., Landa, J., Font, A., Garcia-Villoria, J., Merinero, B., Ugarte, M., Gutierrez-Solana, L. G., Campistol, J., Garcia-Cazorla, A., Vaquerizo, J., Riudor, E., Briones, P., Elpeleg, O., Ribes, A., and Lill, R. (2011) A fatal mitochondrial disease is associated with defective NFU1 function in the maturation of a subset of mitochondrial Fe-S proteins. *Am J Hum Genet* **89**, 656-667

15. Melber, A., Na, U., Vashisht, A., Weiler, B. D., Lill, R., Wohlschlegel, J. A., and Winge, D. R. (2016) Role of Nfu1 and Bol3 in iron-sulfur cluster transfer to mitochondrial clients. *eLife* **5**, e15991

16. Uzarska, M. A., Nasta, V., Weiler, B. D., Spantgar, F., Ciofi-Baffoni, S., Saviello, M. R., Gonnelli, L., Mühlenhoff, U., Banci, L., and Lill, R. (2016) Mitochondrial Bol1 and Bol3 function as assembly factors for specific iron-sulfur proteins. *eLife* **5**, e16673

17. Gourdoupis, S., Nasta, V., Calderone, V., Ciofi-Baffoni, S., and Banci, L. (2018) IBA57 Recruits ISCA2 to Form a [2Fe-2S] Cluster-Mediated Complex. *J. Am. Chem. Soc.* **140**, 14401-14412

18. Nasta, V., Da Vela, S., Gourdoupis, S., Ciofi-Baffoni, S., Svergun, D. I., and Banci, L. (2019) Structural properties of [2Fe-2S] ISCA2-IBA57: a complex of the mitochondrial iron-sulfur cluster assembly machinery. *Sci. Rep.* **9**, 18986

19. Mühlenhoff, U., Richter, N., Pines, O., Pierik, A. J., and Lill, R. (2011) Specialized function of yeast Isa1 and Isa2 proteins in the maturation of mitochondrial [4Fe-4S] proteins. *J Biol Chem* **286**, 41205-41216

20. Beilschmidt, L. K., Ollagnier de Choudens, S., Fournier, M., Sanakis, I., Hograindleur, M. A., Clemancey, M., Blondin, G., Schmucker, S., Eisenmann, A., Weiss, A., Koebel,

P., Messaddeq, N., Puccio, H., and Martelli, A. (2017) ISCA1 is essential for mitochondrial Fe_4S_4 biogenesis *in vivo*. *Nat Commun* **8**, 15124

21. Gelling, C., Dawes, I. W., Richhardt, N., Lill, R., and Mühlenhoff, U. (2008) Mitochondrial Iba57p is required for Fe/S cluster formation on aconitase and activation of radical SAM enzymes. *Mol Cell Biol* **28**, 1851-1861

22. Sheftel, A. D., Wilbrecht, C., Stehling, O., Niggemeyer, B., Elsasser, H. P., Mühlenhoff, U., and Lill, R. (2012) The human mitochondrial ISCA1, ISCA2, and IBA57 proteins are required for [4Fe-4S] protein maturation. *Mol Biol Cell* **23**, 1157-1166

23. McCarthy, E. L., and Booker, S. J. (2017) Destruction and reformation of an iron-sulfur cluster during catalysis by lipoyl synthase. *Science* **358**, 373-377

24. Uzarska, M. A., Przybyla-Toscano, J., Spantgar, F., Zannini, F., Lill, R., Mühlenhoff, U., and Rouhier, N. (2018) Conserved functions of *Arabidopsis* mitochondrial late-acting maturation factors in the trafficking of ironsulfur clusters. *Biochim Biophys Acta Mol Cell Res* **1865**, 1250-1259

25. Benz, C., Kovarova, J., Kralova-Hromadova, I., Pierik, A. J., and Lukes, J. (2016) Roles of the Nfu Fe-S targeting factors in the trypanosome mitochondrion. *Int J Parasitol* **46**, 641-651

26. Lezhneva, L., Amann, K., and Meurer, J. (2004) The universally conserved HCF101 protein is involved in assembly of [4Fe-4S]-cluster-containing complexes in *Arabidopsis thaliana* chloroplasts. *Plant J* **37**, 174-185